ENERGY TRANSDUCTION BY RESPIRATORY COMPLEX I

Ana Paula Gonçalves Batista

Dissertation presented to obtain a PhD degree in Biochemistry at the Instituto de Tecnologia Química e Biológica, Universidade Nova de Lisboa

Supervisors

Prof. Miguel Teixeira & Dr. Manuela M. Pereira

Opponents

Prof. Ulrich Brandt & Prof. Carlos Salgueiro

Instituto de Tecnologia Química e Biológica
Universidade Nova de Lisboa

FCT Fundação para a Ciência e a Tecnologia
MINISTÉRIO DA CIÊNCIA, TECNOLOGIA E ENSINO SUPERIOR

Second Edition, September 2010

Prof. Miguel Teixeira, Dr. Ricardo O. Louro, Prof. Graça Soveral, Prof. Ulrich Brandt, Ana P. Batista, Dr. Manuela M. Pereira, Prof. Carlos Salgueiro, Prof. Carlos Romão.

Metalloproteins and Bioenergetic Unit
Biological Energy Transduction Laboratory
Instituto de Tecnologia Química e Biológica
Av. da República
Estação Agronómica Nacional
2780-157 Oeiras
Portugal
Tel. +351-214469323

FOREWORD

This dissertation comprises research work performed under the supervision of Prof. Miguel Teixeira and Dr. Manuela M. Pereira, in the Metalloproteins and Bioenergetics Unit from the Instituto de Tecnologia Química e Biológica, Universidade Nova de Lisboa.

The studies presented in this dissertation were to provide a contribution to the understanding of the energy transducing mechanism of respiratory complex I.

The thesis is organized in three parts. The introduction part is divided in three sections describing the energy transduction process, the NADH:quinone oxidoreductases and the sodium/proton antiporters. The second part comprises the experimental results obtained during this work, and is divided in four chapters. Three of the chapters describe the structural and functional studies performed on *Rhodothermus marinus* complex I, whereas the other describes the studies performed on complexes I from *Escherichia coli* and *Paracoccus denitrificans*. The last part consists of a general discussion integrating the described results.

ACKNOWLEDGMENTS

I would like to thank all the people that supported and helped me during these last years:

Prof. Miguel Teixeira and Dr. Manuela M. Pereira, my supervisors, for their enormous support, enthusiasm, dedication, advices and scientific discussions. A special thank to Manuela for her friendship, critical sense, and for giving me strength and confidence during these years.

Dr. Ana Coelho and co-workers, especially Catarina Franco, for their advices, help and discussions on the mass spectrometry studies.

Prof. Hartmut Michel, Dr. Guohong Peng and co-workers (especially Marco Marcia), and Dr. Janet Vonck from the Max-Planck Institute for Biophysics, Frankfurt am Main, for the structural studies of the *Rhodothermus marinus* complex I.

Prof. Bernhard Brutschy and Lucie Sokova from the Institute of Physical and Theoretical Chemistry, Johann Wolfgang Goethe-Universitat, Frankfurt am Main, for the LILBID MS studies of *Rhodothermus marinus* complex I.

Dr. Andreia S. Fernandes, for helping and teaching me so much during the period that we worked together and, especially for her friendship.

Dr. Ricardo O. Louro, for the helpful scientific discussions, innumerous advices and support.

João Carita, for the friendship and for growing the cells.

Manuela Regalla, for the N-terminal sequence determination and HPLC analysis.

All my colleagues and friends at the Metalloproteins and Bioenergetics Unit, for providing a stimulating and friendly environment: Célia Romão, João Vicente, Filipa Sousa, Patrícia Refojo, Vera Gonçalves, Ana Filipa Pinto, Sandra Santos, Lara Paulo, Ana Teresa Bernardo, Liliana Pinto, Carolina Júlio, Miguel Ribeiro and Bruno Marreiros. And previous members of the group, especially Smilja Todorovic, João Rodrigues, Andreia Veríssimo and Pedro Almeida.

Everyone in the groups of Dr. Cláudio Gomes, Dr. Lígia Saraiva, Dr. Ricardo Louro and Dr. Inês Pereira for the helpful and friendly environment in the "3rd floor" of ITQB.

Bárbara, Lígia, Patrícia, Raquel, Sofia and Vera, my friends with whom I shared the good and the bad moments during these years. I am deeply grateful to my "girls" for the massive encouragement, friendship and support. Special thanks also to Jota, Sandra, Hugo and Gabriel for all the great moments, in and out of the lab.

All my friends outside the "ITQB world".

My family, especially my parents, brothers and grandparents.

Miguel for his love, unconditional support, and for always being there.

Fundação para a Ciência e Tecnologia is acknowledgment for financial support, by awarding a PhD Grand SFRH/BD/25288/2005 and for funding POCI/BIA-PRO/58374/2004, REDE/1517/RMN/2005, REEQ/336/BIO/2005 and POCI/QUI-BIQ/100302/2008.

THESIS PUBLICATIONS

The work presented in this dissertation is based on the following publications:

1. **A.P. Batista***, A.S. Fernandes*, R.O. Louro, J. Steuber, M.M. Pereira, "Energy conservation by *Rhodothermus marinus* respiratory complex I", Biochim Biophys Acta 1797 (2010) 509-515.

2. **A.P. Batista**, C. Franco, M. Mendes, A.V. Coelho, M.M. Pereira, "Subunit composition of *Rhodothermus marinus* respiratory complex I", Analytical Biochemistry 407 (2010) 104-110.

3. **A.P. Batista** and M.M. Pereira, "Decoupling of the catalytic and transport activities of complex I from *Rhodothermus marinus* by a sodium/proton antiporter inhibitor", (2010), submitted.

4. **A.P. Batista** and M.M. Pereira, "Sodium influence on energy transduction by complexes I from *Escherichia coli* and *Paracoccus denitrificans*", (2010), submitted.

Publications not included in this thesis:

5. **A.P. Batista**, A. Kletzin and M.M. Pereira, "The dihydrolipoamide dehydrogenase from the crenarchaeon *Acidianus ambivalens*", FEMS Microbiol Lett 281 (2008) 147-154.

* Equally contributing authors.

SUMMARY

The aim of the work presented in this dissertation was to provide a contribution to the understanding of the energy transducing mechanism of respiratory complex I. This enzyme is present in most bacteria and in all mitochondrial systems and it is characterized by its large number of subunits, its prosthetic groups (flavin and iron-sulfur centers), and its NADH:quinone oxidoreductase activity sensitive to specific inhibitors and coupled with charge translocation across the membrane.

Complex I from the halothermophilic bacterium *Rhodothermus marinus* was the main model system used and its detailed structural and functional characterization were performed. Electron microscopy studies, suggested that the enzyme has the typical L-shaped structure. Further studies were performed to clarify the possible presence (and function) of two non-canonical subunits in *R. marinus* enzyme, since two additional genes were previously found among the canonical complex I genes, a gene encoding for a pterin-4α-carbinolamine dehydratase (PCD) and a gene encoding for a Nha-type Na^+/H^+ antiporter, suggesting that their products could be part of the complex. Using an original approach that combined several protein separation strategies with different identification methods (ESI-MS/MS, MALDI-TOF MS and Edman degradation analysis), the identification of the canonical proteins and also of the PCD was possible. On the contrary, the Nha-type Na^+/H^+ antiporter was not identified indicating its absence in the composition of complex I. Studies performed to determine the total mass of the enzyme, that included LILBID MS and native gel electrophoresis suggested an apparent molecular mass of ≈ 550 kDa, compatible with the sum of the molecular masses of the fifteen subunits (canonical *plus* PCD), reinforcing that

the Nha-type Na^+/H^+ antiporter is not part of the *R. marinus* complex. The identification of the PCD, a protein proposed to have an auxiliary role in the metabolism of molybdopterin cofactors, as a novel complex I subunit may suggest the existence of a possible regulatory mechanism of complex I involving the PCD and pterin like compounds.

The nature of the coupling charge of *R. marinus* complex I was investigated using inside-out membrane vesicles, which were active with respect to NADH oxidation and capable of creating and maintaining an NADH-driven membrane potential ($\Delta\Psi$) positive inside. It was observed that this prokaryotic complex I is able of H^+ and Na^+ transport, although to opposite directions. The coupling ion of the system was shown to be the H^+ being transported to the periplasm, contributing in this way to the establishment of the electrochemical potential difference, while Na^+ is translocated to the cytoplasm. Proton transport was monitored using pH dependent fluorescence probes and Na^+ transport was measured by ^{23}Na-NMR spectroscopy. This was the first time that such a technique was used to monitor substrate-driven Na^+ transport by membrane vesicles. Additional studies have shown that although neither the catalytic reaction nor the establishment of the ΔpH required the presence of Na^+, the presence of this ion increased the proton transport. Combining all these results, a model for the coupling mechanism of complex I was proposed, suggesting the presence of two different energy coupling sites, one that works only as a proton pump (Na^+ independent), and the other functioning as a Na^+/H^+ antiporter (Na^+ dependent). This model was further supported by studies performed in the presence of the Na^+/H^+ antiporter inhibitor, 5-(*N*-ethyl-*N*-isopropyl)-amiloride (EIPA). In these conditions both H^+ and Na^+ transports are inhibited but show different inhibitory profiles. In the presence of 10 μM of EIPA, decreases of ≈ 30% and ≈ 50% are observed for H^+ and Na^+ transports, respectively, excluding the exis-

tence of only a common transport site. Moreover, the H^+ transport exhibited different inhibition behaviors in the presence and absence of Na^+, which also reinforce the hypothesis for the presence of two H^+ translocating sites. A half maximal inhibition (IC_{50}) value of ≈ 22 μM was estimated for the Na^+ independent H^+ translocating site and a IC_{50} value of ≈ 10 μM for the Na^+ dependent H^+ translocating site. More interestingly, the NADH:quinone oxidoreductase activity is also inhibited by EIPA (IC_{50}= 230 μM); however the H^+ and Na^+ transports are inhibited at concentrations of EIPA at which the catalytic activity is not affected, meaning that the catalytic and transports activities can be decoupled. Strictly indirect coupling mechanisms, possible through conformational changes, are thus suggested to be operating on respiratory complex I.

A deeper insight into the coupling mechanism of this enzyme was provided by studying the influence of sodium ions on energy transduction by complexes I from *Escherichia coli* and *Paracoccus denitrificans*. Using the same approaches as before, it was observed that the Na^+/H^+ antiport activity is not exclusive of *Rhodothermus* complex I, since the *E. coli* enzyme is also capable of such a transport, but is not a general property given that the *P. denitrificans* enzyme does not perform sodium translocation. Due to the fact that *R. marinus* and *E. coli* enzymes reduce menaquinone while *P. denitrificans* complex I reduces ubiquinone, it was suggested that the Na^+/H^+ antiport activity may be correlated with the type of quinone used as substrate. Although the full mechanistic details remain to be clarified by atomic structures of the entire complex I, the results here reported open new perspectives in the studies of the process of energy transduction by this respiratory enzyme, which may be more versatile than one could anticipate.

SUMÁRIO

O objectivo do trabalho descrito nesta dissertação foi contribuir para a compreensão do mecanismo de transdução de energia do complexo I respiratório. Este enzima está presente na maioria das bactérias e em todos os sistemas mitocondriais e é caracterizado pelo seu grande número de subunidades, os seus grupos prostéticos (flavina e centros de ferro-enxofre), e pela actividade NADH: quinona oxidoredutase sensível a inibidores específicos e acoplada à translocação de iões através da membrana.

O principal sistema modelo utilizado neste trabalho foi o complexo I da bactéria termohalófila *Rhodothermus marinus* tendo-se efectuado uma caracterização estrutural e funcional detalhada do mesmo. Estudos de microscopia eletrónica, sugerem que o enzima tem a estrutura típica em forma de L. A determinação da composição em subunidades do complexo teve como base esclarecer a eventual presença (e função) de duas subunidades não canónicas no enzima de *R. marinus*, uma vez que dois genes adicionais foram previamente encontrados entre os genes canónicos do complexo I; um deles codifica para uma pterina-4α-carbinolamina desidratase (PCD) e o outro codifica para um antiporte de Na^+/H^+ do tipo Nha, sugerindo que os respectivos produtos possam fazer parte do complexo. A utilização de uma abordagem original que combinou diferentes estratégias de separação de proteínas com diferentes métodos de identificação (ESI-MS/MS, MALDI-TOF MS e degradação de Edman), permitiu a identificação das subunidades canónicas do complexo I e também do PCD. Contrariamente, o antiporte de Na^+/H^+ do tipo Nha não foi identificado, sugerindo a sua ausência na composição do complexo I. A ausência desta proteína foi reforçada pela determinação da massa total do enzima por LILBID MS e electroforese em

gel nativo. O valor obtido de ≈ 550 kDa é compatível com a soma das massas moleculares das quinze subunidades (as canónicas mais o PCD). A identificacão do PCD, uma proteína sugerida como tendo um papel auxiliar no metabolismo do cofactor molibdopterina, como uma nova subunidade do complexo I sugere a existência de um possivel mecanismo de regulação do complexo I envolvendo o PCD e compostos pterinicos.

A natureza da carga que está acoplada à actividade NADH: quinona oxidoredutase, catalisada pelo complexo I de *R. marinus*, foi investigada utilizando vesiculas membranares invertidas, sendo estas activas em relação à oxidação do NADH e capazes de criar e manter um potencial de membrana ($\Delta\Psi$) positivo dentro. Foi demonstrado que este complexo procariota é capaz de transportar H^+ e Na^+, embora em direcções opostas. O ião de acoplamento do sistema é o H^+ sendo transportado para o periplasma, contribuindo desta forma para o estabelecimento da diferença de potencial electroquímico, enquanto o Na^+ é translocado para o citoplasma. O transporte protónico foi monotorizado utilizando-se sondas de fluorescência dependentes de pH, enquanto o transporte de Na^+ foi medido por espectroscopia ^{23}Na-RMN, sendo a primeira vez que esta técnica foi utilizada para monitorizar o transporte de Na^+ através de vesículas membranares. Estudos adicionais mostraram que, embora nem a reacção catalítica, nem o estabelecimento do ΔpH necessitem de Na^+, a presença deste ião aumenta o transporte de protões. Combinando todos estes resultados, um modelo para o mecanismo de acoplamento do complexo I foi proposto, sugerindo a presença de dois locais diferentes de transdução de energia, um que funciona apenas como uma bomba protónica (independente de Na^+), e o outro funcionando como um antiporte de Na^+/H^+ (dependente de Na^+). Este modelo foi suportado por estudos realizados na presença do inibidor de antiportes de Na^+/H^+, 5-(*N*-etil-*N*-isopropil)-amilorida (EIPA). Foi

observado que tanto o transporte de H^+ como o de Na^+ são inibidos por este composto, mas apresentam diferentes perfis de inibição. Na presença de 10 μM de EIPA, diminuções de ≈ 30% e ≈ 50% foram observadas para o transporte de H^+ e Na^+, respectivamente, o que exclui a existência de apenas um local de transporte comum. Além disso, o transporte de H^+ apresenta diferentes perfis de inibição na presença e na ausência de Na^+, o que também reforça a hipótese da presença de dois locais diferentes de transporte protónico. O valor ao qual o transporte se encontra inibido em 50% (IC_{50}), foi estimado como sendo ≈ 22 μM para o local de transporte protónico independente de Na^+, enquanto um valor de IC_{50} ≈ 10 μM foi estimado para o local de transporte protónico dependente de Na^+. Mais interessante ainda é o facto da actividade NADH:quinona oxidoredutase ser também inibida pelo EIPA (IC_{50}=230 μM), embora os transportes de H^+ e Na^+ sejam inibidos a concentrações de EIPA em que a actividade catalítica não está afectada. Estes dados significam que as actividades catalítica e de transporte podem ser desacopladas. Um mecanismo de acoplamento indirecto, possivelmente através de alterações conformacionais, foi assim sugerido para o funcionamento do complexo I respiratório.

Um maior conhecimento sobre o mecanismo de acoplamento deste enzima foi obtido através do estudo da influência dos iões sódio na transdução de energia dos complexos I de *Escherichia coli* e *Paracoccus denitrificans*. Seguindo a mesma linha de pensamento e aplicando as mesmas técnicas espectroscópicas, observou-se que a actividade de antiporte Na^+/H^+ não é exclusiva do complexo de *Rhodothermus*, uma vez que o enzima de *E. coli* também é capaz de tal transporte; contudo, não é uma propriedade geral dado que o enzima de *Paracoccus* não transporta sódio. Devido ao facto dos enzimas de *R. marinus* e *E. coli* reduzirem menaquinona enquanto o complexo I de *P. denitrificans* reduz a ubiquinona, é sugerido que a actividade de antiporte

Na^+/H^+ possa estar correlacionada com o tipo de quinona utilizada como substrato. Embora o mecanismo do complexo I continue por esclarecer, os resultados aqui reportados abrem novas perspectivas no estudo do processo de transdução de energia por este enzima respiratório, que poderá ser mais versátil do que se poderia antecipar.

TABLE OF CONTENTS

PART I - INTRODUCTION

CHAPTER 1 | **ENERGY TRANSDUCTION IN BIOLOGICAL MEMBRANES**

PART II - RESULTS

CHAPTER 2 | STRUCTURAL STUDIES OF *Rhodothermus marinus* COMPLEX I

PART I

INTRODUCTION

Chapter 1

Energy Transduction in Biological Membranes

Abbreviations

A.: *Aquifex*; *B.*: *Bacillus*; *E.*: *Escherichia*; *K.*: *Klebsiella*; *P.*: *Paracoccus*; R.: *Rhodothermus*; *T.*: *Thermus*; *T.*: *Thermosynechococcus*; *V.*: *Vibrio*; *Y.*: *Yarrowia*.

ΔG: Gibbs energy change; ΔG°: standard Gibbs energy change (kJ. mol^{-1}); *R*: gas constant (8.3 J mol^{-1} K^{-1}); ΔE: reduction potential difference (mV); $\Delta E_{m,7}$: standard reduction potential difference at pH 7 (mV); E: reduction potential (mV); $E_{m,7}$: standard reduction potential at pH 7 (mV); *F*: Faraday constant (96 485 J V^{-1} mol^{-1}); *n*: number of electrons transferred; $\Delta\tilde{\mu}_{X^{m+}}$: ion electrochemical potential difference (J.mol^{-1}); ΔΨ: membrane potential (mV); *m*: valence of an ion; *pmf*: proton-motive force (mV); *smf*: sodium-motive force (mV).

b_L heme: low potential heme *b*; b_H heme: high potential heme *b*; cyt. *c*: cytochrome *c*; complex I: NADH:quinone oxidoreductase type I; complex II: succinate:quinone oxidoreductase; complex III: quinol:cytochrome *c* oxidoreductase; complex IV: cytochrome *c*:oxygen oxidoreductase; Ech: energy-converting hydrogenase; EPR: electron paramagnetic resonance; HIPIP: high potential iron-sulfur protein; Mrp: multiple resistance and pH related antiporter; NDH-II: alternative NAD(P)H dehydrogenase; Na^+-NQR: Na^+ translocating NADH:quinone oxidoreductase; Nqo/Nuo/Ndh/Fpo: complex I subunits; Nqr: Na^+-NQR subunits; PCD: pterin-4α-carbinolamine dehydratase; Q: quinone; QH_2: quinol; SQ_{Nf}: fast relaxing semiquinone; SQ_{Ns}: slow relaxing semiquinone; SQ_{Nx}: very fast relaxing semiquinone.

Chapter 1: Energy Transduction in Biological Membranes

1.1

Energy Transduction: an overview

Chapter 1: Energy Transduction in Biological Membranes

Section 1.1 – Energy transduction: an overview

1.1.1–LIFE AND ENERGY

Life depends on continuous flow of energy and on mechanisms that control this energy flow. In biological systems the main form of chemical energy is adenosine triphosphate (ATP). The synthesis of this nucleotide is mainly associated with membrane-bound enzymes, the so-called electron transfer or respiratory complexes, which are located in the cytoplasmatic membrane of prokaryotic cells, in the inner membrane of mitochondria and in the thylakoid membranes of chloroplasts [6]. The endergonic synthesis of ATP is indirectly driven by the flow of electrons through the electron transfer chain which is essentially conserved among the three domains of life, despite the different nature of their primary energy sources (substrate oxidation, absorption of light). The energy release by the electron transfer must be transduced to a form that can be used for the ATP synthesis (Figure 1.1.1).

Figure 1.1.1 – The energy released by electron transport is transduced in a different form of energy that is used for ATP synthesis.

This section will address the biological mechanisms for energy transduction and ATP synthesis. It starts by a brief description of the thermodynamic principles of biological energy changes and ends with the description of the coupling process of electron transfer and ATP synthesis - the Chemiosmotic Theory – and the different ion/electron coupling mechanisms of respiratory complexes.

1.1.2–THERMODYNAMICS IN BIOENERGETICS [6-8]

Biological energy changes obey the laws of thermodynamics, meaning that energy is conserved and spontaneous changes occur in directions that increase the overall disorder of the universe (system *plus* surrounding).

Gibbs energy indicates the spontaneity of a process and can be described by the following expression:

$$\Delta G = \Delta G^{o} + RT \ln \frac{\Pi(\text{Products})}{\Pi(\text{Reactants})} \qquad \text{(eq.1)}$$

through which the maximum energy that can be obtained from a process (the energy available to perform work) can be calculated. If ΔG is zero, the system is at equilibrium, which means that it cannot obtain energy from the process. If ΔG<0, the process can release energy (exergonic process) as the system proceeds spontaneously to the equilibrium. If ΔG>0, the process is headed way from the equilibrium, and it will have to acquire energy (performed work) in order to occur. The latter process is endergonic and is thermodynamically unfavorable, however it will take place if associated to another process with a ΔG<<0, which will reverse the overall sign of ΔG. An example of such a process is the phosphorylation of glucose, a reaction from the glycolytic pathway [9]. This reaction is unfavorable and does not occur spontaneously. However, when coupled to ATP hydrolysis the combined reaction is thermodynamically favorable (Figure 1.1.2).

To take advantage of the thermodynamic combination of favorable and unfavorable processes, the system must have a mechanism of associating the two reactions. In the particular case described above, the two reactions share a common intermediate (P_i) and are catalyzed by the same enzyme (hexokinase). It is described that after glucose binding, conformational changes occur in the hexokinase having the new conformation a higher

affinity to ATP, which will allow the transfer of phosphate from ATP directly to glucose.

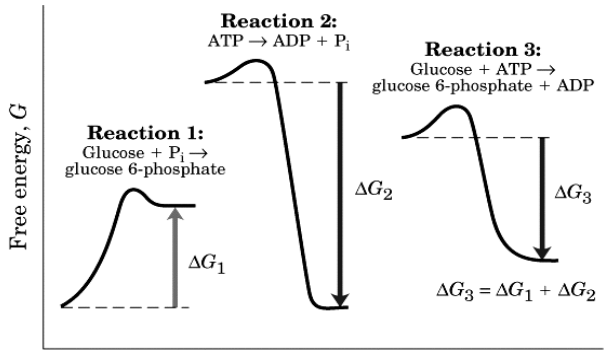

Figure 1.1.2 – Example of an unfavorable reaction (R1) that takes place when associated with a more favorable one (R2). Reaction 1: ΔG^{o}=+13.8 kJ.mol^{-1}; Reaction 2: ΔG^{o}=-30.5 kJ.mol^{-1}, Reaction 3: ΔG^{o}=-17.2 kJ.mol^{-1} (Adapted from[2]).

Besides this example, there are other coupling mechanisms in biological systems such as: sequential reaction coupling, in which metabolites works as a product in one reaction and as a reactant in other reaction (both reactions catalyzed by a different enzyme); mechano-chemical coupling, as in the case of muscle contraction; reduction-oxidation (redox) coupling, in which electrons act effectively as common intermediates; ion gradient coupling, where reactions are coupled through a shared gradient of molecules across the membrane. The mechanisms describing the coupling of the electron transfer and ATP synthesis will be further discussed below.

1.1.3–ENERGY TRANSDUCTION IN BIOLOGICAL MEMBRANES

The mitochondrial respiratory chain has NADH (or succinate) as the initial electron donor and O_2 as the final electron acceptor. Electron transfer does not occur by a direct reaction between NADH (or succinate) and O_2 but

rather by a stepwise flow of electrons through the electron transfer (respiratory) complexes.

The canonical description of the aerobic respiratory chain considers the existence of four transmembranar complexes: complex I (NADH:quinone oxidoreductase); complex II (succinate:quinone oxidoreductase); complex III (quinol:cytochrome *c* oxidoreductase) and complex IV (cytochrome *c*:oxygen oxidoreductase) (Figure 1.1.3). Complexes I and II are the entry point for electrons while complex IV is the terminal oxidase, since it is the last complex involved in the electron transfer, reducing O_2 to water. Electrons flow from complexes I and II to complex III and from complex III to IV via electron carriers, a hydrophobic quinone (Q) and a soluble cytochrome *c* (cyt. *c*), respectively.

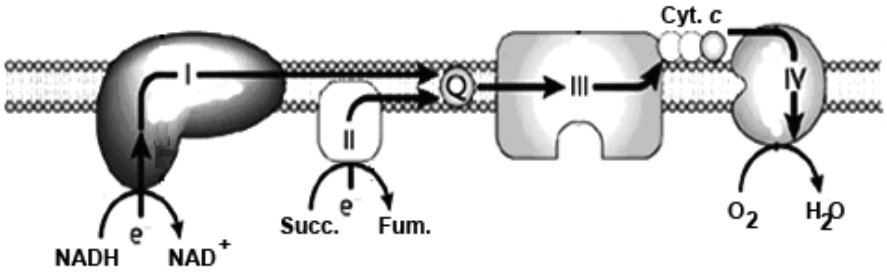

Figure 1.1.3 – Schematic representation of canonical aerobic respiratory chains. I, complex I (NADH:quinone oxidoreductase); II, complex II (succinate:quinone oxidoreductase); III, complex III (quinol:cytochrome *c* oxidoreductase); IV, complex IV (cytochrome *c*:oxygen oxidoreductase); Q, quinone; Cyt. *c*, cytochrome *c*.

Prokaryotes may have branched respiratory chains with alternative pathways [10]. The fact that many prokaryotes are facultative aerobes allows them to reduce besides oxygen a large set of compounds, such as nitrate, sulfate, fumarate [11]. NADH oxidation can be performed by two other enzymes besides complex I, the so-called alternative NADH dehydrogenase (NDH-II) and sodium-translocating NADH:quinone oxidoreductase (Na^+-

NQR) (see section 1.2 – NADH:quinone oxidoreductases) [12]. Quinol:oxygen oxidoreductases, which are directly reduced by quinol bypassing complex III, define another variant electron pathway [11]. The diversity of terminal oxygen reductases is also a clear example of the flexibility of prokaryotic respiratory chains. Typical cases are *Paracoccus (P.) denitrificans* and *Rhodothermus (R.) marinus* respiratory chains which possesses at least three different oxygen reductases [13-16]. Several electron carriers can also intervene in these respiratory chains. Apart from three different types of quinones which differ in physical and functional proprieties, also the electron carrier between complex III and IV can vary, being the usual cytochrome *c*, a high potential iron-sulfur protein (HiPIP) [17] or small copper proteins (e.g. halocyanin) [18].

It is possible to estimate the thermodynamic efficiency of electron transfer but it is necessary first to take into account some considerations. Biological systems are open systems (not at equilibrium) exchanging both energy and matter with the surrounding, which require a non-equilibrium thermodynamic treatment. However, considering individual reactions or group of reactions as closed systems it is possible to apply equilibrium thermodynamics. Thus, it is possible to estimate the efficiency of each of the respiratory chain complexes individually, as well as, the efficiency of the overall respiratory chain. To simplify, the process of energy transduction will be described for a canonical aerobic respiratory chain.

1.1.3.1–Thermodynamics of electron transfer [1, 6, 7]

Respiratory chains operate as a sequence of oxidation-reduction reactions in which electrons are transferred from one component (enzymatic complex or electron carrier) to another. The energy that is available from a

redox reaction is a function of the difference in reduction potential (ΔE) between the oxidant and the reductant couples. In general,

$$\Delta G = -nF\Delta E \qquad \text{(eq.2)}$$

where *n* is the number of electrons transferred and *F* is the Faraday constant (96 485 $J.V^{-1}.mol^{-1}$). As with Gibbs energy changes (eq.1), the ΔE obtained under conditions other than the standard ones ($\Delta E_{m,7}$[1], where all the components are present at a concentration of 1M) depends on the concentrations of the oxidized and reduced species. Considering eq.1 and eq.2, the actual ΔE for a redox reaction is given by,

$$\Delta E = \Delta E_{m,7} - \frac{RT}{nF} \ln \frac{[\text{Reduced}]}{[\text{Oxidized}]} \qquad \text{(eq.3)}$$

and each of the redox couples can be described as

$$E = E_{m,7} - \frac{RT}{nF} \ln \frac{[\text{Reduced}]}{[\text{Oxidized}]} \qquad \text{(eq.4)}$$

Appling these equations, it is possible to estimate the efficiency of the electron transfer process (Figure 1.1.4). The oxidation of NADH to NAD^+, the reaction with the lowest reduction potential in the chain, occurs at a reduction potential of -320 mV, while the reduction of O_2 to water has a reduction potential of +815 mV, the highest value. The net reaction has a $\Delta E_{m,7}$ of ≈ 1,14 V, which corresponds to a ΔG^o of ≈ -219 $kJ.mol^{-1}$. If NADH oxidation and O_2 reduction occurred in a single step the amount of energy released would be so large that the cell would no longer be viable. This problem is overcome by a stepwise electron transfer process in which the energy is released in a stepwise manner. As a consequence, in the respiratory chain, the electron transfer is not simply determined by reduction potentials.

[1] Standard reduction potential can be designated as $\Delta E^{o\prime}$ or as $\Delta E_{m,7}$. The usual convention is to define the reduction potential for pH 7.

Specificity of interaction between the redox components must be present in order to avoid short-circuiting reactions.

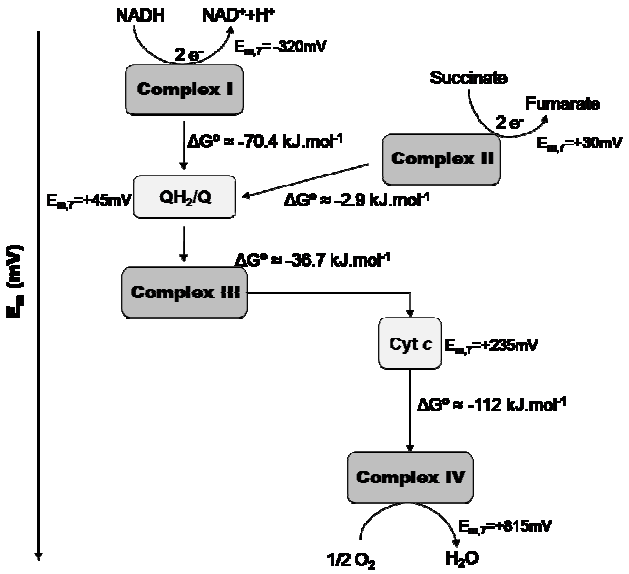

Figure 1.1.4 – Diagram of the respiratory complexes according to their subtract reduction potentials (in mV). For $E_{m,7}$ values see reference [1]. ΔG^{o} are calculated using eq.2.

1.1.3.2 – Thermodynamics of ATP synthesis [6, 7]

The phosphorylation of ADP to ATP is catalyzed by the enzyme ATP synthase and the energy associated with this reaction can be determined by the following equation (based on eq.1)

$$\Delta G_{ATP} = \Delta G^{o}{}_{ATP} + RT \ln \frac{[ATP]}{[ADP][P_i]} \qquad \text{(eq.5)}$$

The $\Delta G^{0}{}_{ATP}$ is ≈ +30.5 kJ.mol^{-1}. This means that the synthesis of ATP is an unfavorable reaction and that energy has to be supplied for it to occur. This energy is obtained from the electron transfer process, which is thermodynamically very efficient (ΔG^{o}≈ -219 kJ.mol^{-1}). The energy released by complexes I, III and IV reactions is sufficient to the synthesis of ATP

molecules (Figure 1.1.4). On the contrary, the redox reaction performed by complex II does not release enough energy and it functions only to inject electrons into the respiratory chain.

1.1.3.3 – Electron transfer and ATP synthesis coupling mechanism – The Chemiosmotic Theory

Thermodynamics describes energetically how respiratory electron transfer reactions can allow the synthesis of ATP but does not explain how the exergonic and endergonic processes are coupled. Peter Mitchell suggested an indirect mechanism that couples the two processes – the chemiosmotic theory [19]. This hypothesis postulates that the electron transfer and phosphorylation are not chemically linked; instead they are coupled by a transmembrane current of ions. Since the membrane has a low intrinsic conductance for ions, a difference of ion concentration and of electric potential is able to develop between the two sides of the membrane. The energy released by the electron transfer is thus transduced into and stored as the electrochemical potential of ions. Dissipation of this potential releases the stored energy, which in turn is used, by ATP synthase, to drive the phosphorylation of ATP. It was shown that ions move back across the membrane through specific ion channels in ATP synthase (Figure 1.1.5).

In developing and improving his theory, Mitchell has suggested that the electrochemical potential is also needed to power other membrane processes such as flagellum rotation and/or solute transports [3].

The basic principles of the chemiosmotic theory are accepted nowadays, although the model proposed by Mitchell was to some extent different from the one considered today. Some of the main differences are related with: 1. the ion/electron coupling mechanisms by respiratory complexes (see below section 1.1.3.4); and 2. the ATP phophorylation

mechanism (see below part B. Electrochemical potential as the driving force for ATP synthesis).

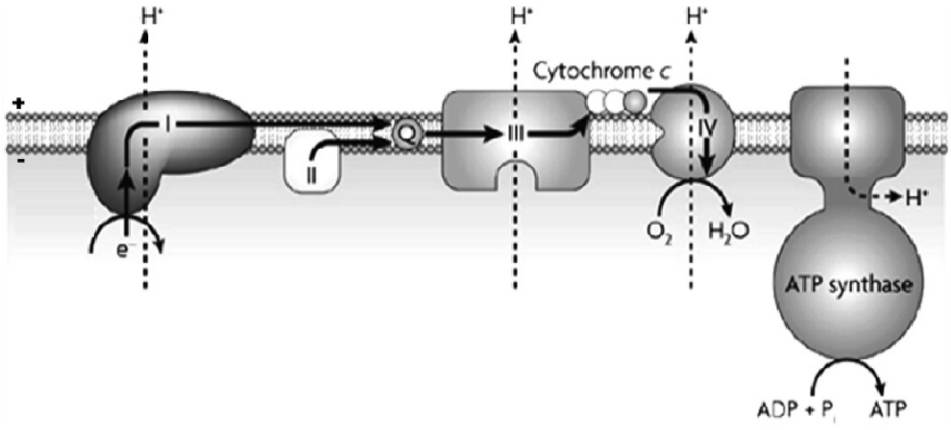

Figure 1.1.5 – Schematic representation of the flow of electrons through the respiratory complexes highlighting proton translocation across the membrane. Ions flow back through a channel in the ATP synthase and this flow drives the formation of ATP.

A. Thermodynamics of ion electrochemical potential [6, 7]

The energy available in an ion electrochemical potential can be determined taking into account the two forces acting on it: the ion concentration difference and the electrical potential difference between the two sides of the membrane (the membrane potential, $\Delta\Psi$). The ΔG involved in the transport of a cation (X) of valence *m* from compartment A to compartment B, against both a concentration gradient ($C_B > C_A$) and a difference of electrical potential (compartment B is electropositive relative to compartment A) can be described by,

$$\Delta\tilde{\mu}_{X^{m+}} = \Delta G = RT \ln \left[\frac{X^{m+}}{X^{m+}}\right]_A^B + mF\Delta\Psi \qquad \text{(eq.6)}$$

where $\Delta\tilde{\mu}_{X^{m+}}$ is the ion electrochemical potential difference and is numerically equal to ΔG. It is usual to express eq.6 in units of electric potential, volts or millivolts (instead of J.mol^{-1}):

$$\frac{\Delta\tilde{\mu}_{X^{m+}}}{F} = \frac{\Delta G}{F} = \frac{RT}{F}\ln\frac{[X^{m+}]_B}{[X^{m+}]_A} + m\Delta\Psi \qquad \text{(eq.7)}$$

At equilibrium (ΔG=0), equation 6 can be rearranged, relating the equilibrium distribution of an ion to the membrane potential:

$$\Delta\Psi = \frac{-RT}{mF}\ln\frac{[X^{m+}]_B}{[X^{m+}]_A} \qquad \text{(eq.8)}$$

Protons and sodium ions are coupling ions in membrane associated bioenergetics processes. From a thermodynamic point of view the proton electrochemical potential difference and the sodium electrochemical potential difference are equivalent, and composed of both a chemical and an electrical component. Based on eq.6 the proton electrochemical potential difference is described by

$$\Delta\tilde{\mu}_{H^+} = \Delta G = RT\ln\frac{[H^+]_B}{[H^+]_A} + F\Delta\Psi \qquad \text{(eq.9)}$$

Considering pH=- $\log_{10}[H^+]$

$$\Delta\tilde{\mu}_{H^+} = \Delta G = -2.3RT\Delta pH + F\Delta\Psi \qquad \text{(eq.10)}$$

In units of electrical potential, the proton electrochemical potential difference is designated as proton-motive force (pmf) and eq. 10 can be rearranged as

$$pmf = \frac{\Delta\tilde{\mu}_{H^+}}{F} = \frac{\Delta G}{F} = -\frac{2.3RT}{F}\Delta pH + \Delta\Psi \qquad \text{(eq.11)}$$

For an analogous electrochemical difference involving the translocation of Na^+ from its initial, A, to its final state, B,

$$\Delta\tilde{\mu}_{Na^+} = \Delta G = RT \ln \frac{[Na^+]_B}{[Na^+]_A} + F\Delta\Psi \qquad \text{(eq.12)}$$

and sodium-motive force (smf)

$$smf = \frac{\Delta\tilde{\mu}_{Na^+}}{F} = \frac{\Delta G}{F} = -\frac{2.3RT}{F}\Delta pNa + \Delta\Psi \qquad \text{(eq.13)}$$

Most of the known biological systems are proton-motive systems, however some microorganisms (such as thermophilic anaerobes, marine bacteria and some bacterial pathogens) use sodium as a coupling ion in addition to proton or even instead of it [20]. In the latter type of systems (sodium dependent), sodium-specific versions of proton-translocating enzymes are present in addition to sodium-translocating pumps which are absent in proton-motive systems. Examples of these pumps are: sodium-translocating decarboxylases; sodium-translocating NADH:quinone oxidoreductase and sodium-translocating ferredoxin:NAD^+ oxidoreductase [21].

The use of the proton or the sodium as the coupling ion is suggested to be a consequence of the adaptation of the organism to a changing environment [20, 22]. Inter-conversion of the different ion motive forces is achieved by secondary transport mechanisms, such as sodium/proton antiporters.

B. Electrochemical potential difference as the driving force for ATP synthesis [6]

ATP synthases can be divided into two main types: F-type (F_0F_1-ATP synthase) and V-type (vacuolar ATP synthase). F-type comprises F_0F_1-ATP synthase of bacteria, chloroplasts and mitochondria and is composed of two functional units F_0 and F_1 (Figure 1.1.6). F_0 is the transmembranar ion translocation part of the enzyme and its composition depends on the

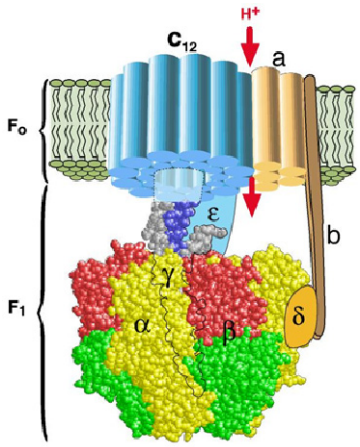

Figure 1.1.6 - Schematic representation of the structure of the ATP synthase. It has a membranar part (F_0) and a peripheral part (F_1). The ion channel is located at the F_0 and the three catalytic sites at the F_1 (Adapted from [5]).

organism. For example, *Escherichia* (*E.*) *coli* F_0 contains a large subunit *a*, two copies of subunits *b* and probably 12 copies of a smaller subunit *c*. F_1 is the peripheral part of the complex, composed of five different subunits (α_3, β_3, γ, δ, ε) that are easily dissociated from F_0. The subunits α and β are arranged alternately around the γ subunit. The enzyme has three catalytic sites located at the interface of α and β subunits [23].

The way how ATP synthase uses the electrochemical potential to synthesize ATP has been the subject of enormous discussions over the past years. Paul D. Boyer was one of the most enthusiastic researchers in this field and his work helped to open new perspectives concerning biological coupling mechanisms. After his suggestion that "the energy from oxidations was not used to *make* the ATP molecule, but instead was used to bring about the *release* of the tightly bound ATP" [24], the possibility of indirect coupling mechanisms operating in biological systems was put forward.

During ATP synthesis the three catalytic sites act in sequence, changing conformation and affinity towards substrates and products. First ADP and P_i bind, then a conformational change takes place and a tightly bound ATP is produced; finally an additional conformational change occurs to release this ATP. The conformational changes are accomplished by the mechanical process of rotation of the F_0 portion of the enzyme, which is driven by the ion (proton or sodium) movement across the membrane (from

the positive side to the negative side) by dissipation of the electrochemical potential (Figure 1.1.6) [23]. ATP synthase may also operates in reverse, acting as an ion pump, thereby using the energy derived from the hydrolysis of ATP to establish an ion concentration difference.

The coupled rotation between the F_1 and F_0 parts was proven by the connection of a fluorescent-labeled actin filament to the F_0 part (*c* subunit), which was able to rotate by using the energy of ATP hydrolysis [25]. This experiment demonstrated that the mechanical rotation is an essential feature for the energy coupling between ion transport through the F_0 sector and ATP hydrolysis and synthesis at the F_1 sector.

The coupling mechanism of the ion transport and the rotation of the *c*-subunits is not completely known. Ion specificity (proton *versus* sodium) is determined by the structure of the ion-binding site; sodium binding usually requires up to six ligands while protons just need, in principle, a single ionisable group [26]. This may explain the observation that in the absence of sodium, a sodium ATP synthase can translocate protons, while a proton ATP synthase is apparently unable of sodium translocation [26].

1.1.3.4 – Ion/electron coupling mechanisms of respiratory complexes

The coupling mechanisms of the three respiratory complexes involved in energy transduction (complexes I, III and IV) are not completely known. However, it is recognized that they have different mechanisms of action.

In the original formulation of the chemiosmotic theory, Mitchell envisaged oxidation chains as vectorial pathways so arranged that at each respiratory complex an electron/ion carrier is reduced at the membrane surface. It then diffuses to the other side of the membrane surface, where protons and electrons become separated: the electrons pass back across the

membrane by an electron carrier while protons are released. This was known as Mitchell´s redox loops and shows the direct coupling between a redox reaction and ion concentration differences across the membrane (Figure 1.1.7-A) [3].

Based on the redox loop mechanism, Mitchell formulated a first proposal for the coupling mechanism that operates on canonical complex III, the Q-cycle [27-29]. Taking into account the X-ray structure of complex III, together with physical and chemical characterization of its cofactors, this mechanism was later re-formulated giving origin to the mechanism recognized nowadays (Figure 1.1.7-B).

Complex III (that comprises a 2Fe-2S center, two *b*-type hemes, one *c*-type heme and two quinone binding sites) catalyses the oxidation of two quinol molecules (QH_2) with the reduction of two soluble cytochromes *c* and one quinone (Q). This redox reaction is directly coupled to proton uptake from the negative side of the membrane (N-side) and to proton release in the positive side of the membrane (P-side) (Figure 1.1.7-B). Briefly, a molecule of

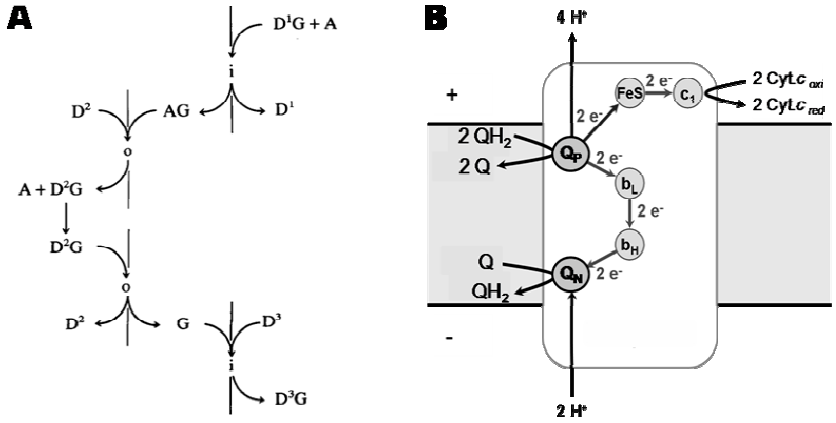

Figure 1.1.7- Scheme of the ion/electron coupling mechanism operating in complex III. A) Mitchell´s redox loop, where *i* and *o* represent the two sides of the membrane and A, G, AG and $D^{1,2,3}$ represent a proton, an electron, a hydrogen atom and donor/acceptor group, respectively (Adapted from [3]). B) Current view of the Q-cycle mechanism (see text for details).

QH_2 diffuses to the binding site Q_p, close to the P-side, and is oxidized to quinone. The two protons from the quinol molecule are released to the P-side. One of the QH_2 electrons is transferred to the *c*-type heme (c_1), via 2Fe-2S center (FeS) and then to the soluble electron carrier cytochrome *c* (Cyt. *c*). The other electron is transferred to the b_L heme (low potential heme *b*), passes to the b_H heme (high potential heme *b*) and reduces a quinone, located close to the N-side, to a semiquinone species. When a second molecule of QH_2 is oxidized at the Q_p site, two protons are again released to the P-side and one of the electrons follows the first pathway reaching the Cyt. *c*. The second electron is transferred again through the *b*-type hemes to the semiquinone species which is reduced to quinol, with the two protons required for this being taken up from the N-side [30].

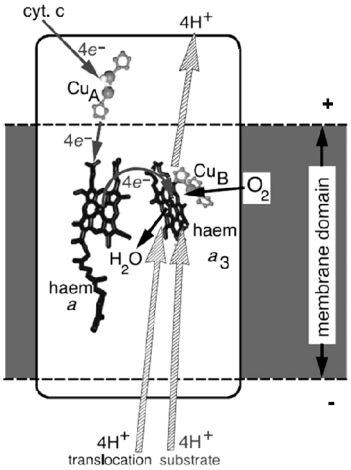

Figure 1.1.8 – Scheme of the overall function of O_2 reductases (Adapted from [4]). The enzyme promotes energy conservation by charge separation, in which electrons and protons for the catalytic reaction come from opposite sides of the membrane, and by proton pumping.

Mitchell had proposed a similar type of mechanism for complex IV, the redox zoop, which is an extension of the redox loop by the addition of a second electron-conducting arm. In this respiratory complex the proton carrier would be oxygen (or oxygen species) instead of quinone [3]. Although the proton/electron coupling mechanism of complex IV remains unsolved, a redox zoop mechanism can be excluded since it was determined that for each full catalytic cycle, four electrons are transferred and up to eight protons are taken up from the negative side of the membrane, four of which are used in

substrate reduction and up to additional four are transported across the membrane (Figure 1.1.8) [4]. Proton transport excludes the operation of a redox loop mechanism in complex IV. In alternative it is suggested that this respiratory complex works as a redox-driven proton pump.

As in the case of complex IV, the ion/electron coupling mechanism of complex I is not known. Different types of mechanisms, based on the redox loops and on the redox-driven proton pumps, have been proposed and will be revised in the next section (see section 1.2-NADH:quinone oxidoreductases).

1.1.4 – REFERENCES

[1] D. Voet, J.G. Voet, Biochemistry, Second ed., John Wiley and Sons, INC, New York, 1995.

[2] D.L. Nelson, M.M. Cox, Lehninger Principles of Biochemistry, Third ed., Worth Publishers, New York, 2000.

[3] P. Mitchell, Foundations of vectorial metabolism and osmochemistry, Biosci Rep 11 (1991) 297-344; discussion 345-296.

[4] M. Wikstrom, Cytochrome *c* oxidase: 25 years of the elusive proton pump, Biochim Biophys Acta 1655 (2004) 241-247.

[5] H. Wang, G. Oster, Energy transduction in the F_1 motor of ATP synthase, Nature 396 (1998) 279-282.

[6] D.G. Nicholls, S.J. Ferguson, Bioenergetics 3, Academic Press, London, 2002.

[7] F.M. Harold, The Vital Force: A study of bioenergetics, W.H.Freeman and Company, New York, 1986.

[8] J. Wrigglesworth, Energy and Life, Taylor and Francis, London, 1997.

[9] G.L. Zubay, Biochemistry, Fourth ed., Wm. C. Brown Publishers, Dubuque, 1998.

[10] S. Berry, Endosymbiosis and the design of eukaryotic electron transport, Biochim Biophys Acta 1606 (2003) 57-72.

[11] G. Unden, J. Bongaerts, Alternative respiratory pathways of *Escherichia coli*: energetics and transcriptional regulation in response to electron acceptors, Biochim Biophys Acta 1320 (1997) 217-234.

[12] S. Kerscher, S. Drose, V. Zickermann, U. Brandt, The three families of respiratory NADH dehydrogenases, Results Probl Cell Differ 45 (2008) 185-222.

[13] B. Ludwig, Terminal oxidases in *Paracoccus denitrificans*, Biochim Biophys Acta 1101 (1992) 195-197.

[14] M.M. Pereira, J.N. Carita, R. Anglin, M. Saraste, M. Teixeira, Heme centers of *Rhodothermus marinus* respiratory chain. Characterization of its cbb_3 oxidase, J Bioenerg Biomembr 32 (2000) 143-152.

[15] M.M. Pereira, M. Santana, C.M. Soares, J. Mendes, J.N. Carita, A.S. Fernandes, M. Saraste, M.A. Carrondo, M. Teixeira, The caa_3 terminal oxidase of the thermohalophilic bacterium *Rhodothermus marinus*: a HiPIP:oxygen oxidoreductase lacking the key glutamate of the D-channel, Biochim Biophys Acta 1413 (1999) 1-13.

[16] A.F. Verissimo, M.M. Pereira, A.M. Melo, G.O. Hreggvidsson, J.K. Kristjansson, M. Teixeira, A ba_3 oxygen reductase from the thermohalophilic bacterium *Rhodothermus marinus*, FEMS Microbiol Lett 269 (2007) 41-47.

[17] M.M. Pereira, A.M. Antunes, O.C. Nunes, M.S. da Costa, M. Teixeira, A membrane-bound HIPIP type center in the thermohalophile *Rhodothermus marinus*, FEBS Lett 352 (1994) 327-330.

[18] G. Schafer, M. Engelhard, V. Muller, Bioenergetics of the Archaea, Microbiol Mol Biol Rev 63 (1999) 570-620.

[19] P. Mitchell, Coupling of phosphorylation to electron and hydrogen transfer by a chemi-osmotic type of mechanism, Nature 191 (1961) 144-148.

[20] G. Speelmans, Na^+ and energy transduction in the thermophile *Clostridium fervidus*, vol. Ph. D. thesis, University of Groningen, 1993, pp. 3-38.

[21] P. Dimroth, Primary sodium ion translocating enzymes, Biochim Biophys Acta 1318 (1997) 11-51.

[22] J.S. Lolkema, G. Speelmans, W.N. Konings, Na(+)-coupled versus H(+)-coupled energy transduction in bacteria, Biochim Biophys Acta 1187 (1994) 211-215.

[23] P.D. Boyer, Energy, life, and ATP, Biosci Rep 18 (1998) 97-117.

[24] P.D. Boyer, R.L. Cross, W. Momsen, A new concept for energy coupling in oxidative phosphorylation based on a molecular explanation of the oxygen exchange reactions, Proc Natl Acad Sci U S A 70 (1973) 2837-2839.

[25] Y. Sambongi, Y. Iko, M. Tanabe, H. Omote, A. Iwamoto-Kihara, I. Ueda, T. Yanagida, Y. Wada, M. Futai, Mechanical rotation of the *c* subunit oligomer in ATP synthase (F_0F_1): direct observation, Science 286 (1999) 1722-1724.

[26] A.Y. Mulkidjanian, M.Y. Galperin, E.V. Koonin, Co-evolution of primordial membranes and membrane proteins, Trends Biochem Sci 34 (2009) 206-215.

[27] P. Mitchell, The protonmotive Q cycle: a general formulation, FEBS Lett 59 (1975) 137-139.

[28] P. Mitchell, Protonmotive redox mechanism of the cytochrome *b-c*1 complex in the respiratory chain: protonmotive ubiquinone cycle, FEBS Lett 56 (1975) 1-6.

[29] P. Mitchell, Possible molecular mechanisms of the protonmotive function of cytochrome systems, J Theor Biol 62 (1976) 327-367.

[30] B.L. Trumpower, The protonmotive Q cycle. Energy transduction by coupling of proton translocation to electron transfer by the cytochrome bc_1 complex, J Biol Chem 265 (1990) 11409-11412.

1.2

NADH:quinone oxidoreductases

Chapter 1: Energy Transduction in Biological Membranes

Section 1.2 – NADH:quinone oxidoreductases

1.2.1 - INTRODUCTION

As previously described in section 1.1, the oxidation of NADH and the reduction of quinone is a highly exergonic reaction ($\Delta G^{o} \approx -70.4$ kJ.mol^{-1}, considering ubiquinone as the electron acceptor). The energy released by this redox reaction may be used to transport ions across the membrane and thus contribute to the $\Delta\tilde{\mu}_{X^{m+}}$. The redox reaction can be performed by three different types of NADH:quinone oxidoreductases (Figure 1.2.1): complex I (NDH-I), a multisubunit transmembrane enzyme coupling quinone reduction to charge translocation across the membrane; a multisubunit sodium-translocating NADH:quinone oxidoreductase (Na^+-NQR) that couples quinone reduction to sodium transport; and an alternative NAD(P)H dehydrogenase (NDH-II) which does not perform energy conservation. No homologies regarding subunits and prosthetic groups composition, inhibitors and mechanism exist between the three types of enzymes. This section will introduce the three enzymes with special focus on complex I and its ion/electron coupling mechanism.

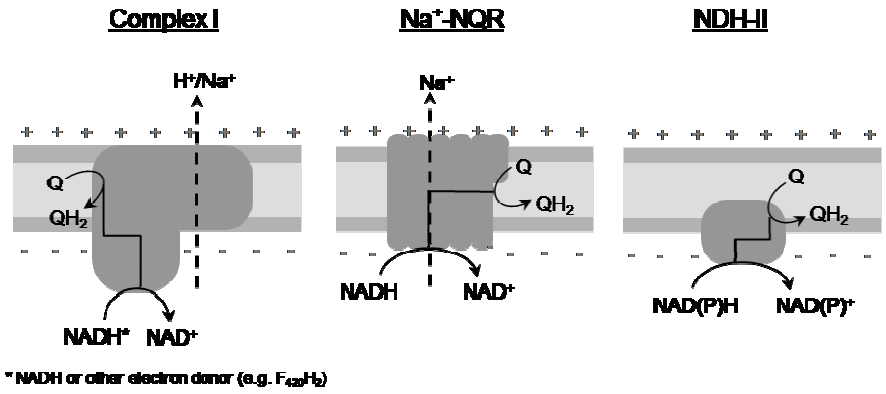

Figure 1.2.1 – Schematic representation of the three types of respiratory NADH:quinone oxidoreductases. The three enzymes are capable of quinone reduction. Complex I and Na^+-NQR couple the quinone reduction to charge translocation across the membrane. NDH-II does not perform energy conservation.

1.2.2 - COMPLEX I[1]

Complex I couples the electron transfer from NADH to quinone with charge translocation across the membrane, contributing for the establishment of the $\Delta\tilde{\mu}_{X^+\ (X=H^+;Na^+)}$. Homologues of complex I exist in bacteria, archaea and eukarya (mitochondria and chloroplasts). This enzyme is characterized by its large number of subunits, its prosthetic groups (flavin and iron-sulfur centers) and its sensitivity to specific inhibitors, such as rotenone. The electron donor of most bacterial and mitochondrial complexes is NADH, while the archaeal complex I works apparently as a $F_{420}H_2$ dehydrogenase [11]. The electron donor of cyanobacterial and chloroplastidal complexes is not known, yet [11]. Common to the three domains of life are 11 subunits suggested to be responsible for the charge translocation and the quinone binding.

1.2.2.1 – Structure and subunit composition

Bacterial complex I is generally composed by 14 subunits designated as Nqo1-14 (from NADH:quinone oxidoreductase – *P. denitrificans* nomenclature [13]) or as NuoA-N (from NADH:ubiquinone oxidoreductase – *E. coli* nomenclature [14, 15]). This enzyme has a molecular mass of ≈500 kDa. The genes coding for its subunits may be organized in a single operon [13, 14, 16-18] or may be disperse throughout the genome (ordered in more than one operon [7, 19] and/or as isolated genes [7]). In several organisms, unknown reading frames (URFs) are observed between the genes coding for complex I subunits [7, 13, 18]. More than one gene coding for a specific

[1] Throughout the text, and unless otherwise stated, the subunit nomenclature of *Paracoccus denitrificans* complex I, is used.

subunit can be found in some organisms [19] and there are also cases in which two genes are fused [20, 21].

The canonical 14 subunits are organized in two different segments, a peripheral and a membranar arm, in an L-shaped structure. The peripheral part is composed by 7 subunits (Nqo1-6 and 9) and contains the binding site for the electron donor and all known prosthetic groups [10]. The remaining 7 subunits (Nqo7-8 and 10-14) compose the membrane part and are most likely involved in quinone reduction and charge translocation. The L-shaped structure of bacterial complex I has been determined by electron microscopy for *E. coli* [22] and *Aquifex (A.) aeolicus* enzymes (Figure 1.2.3) [19]. A horseshoe shape was also reported for the *E. coli* enzyme [23], however this result could not be reproduced and was interpreted as a possible artifact [24].

Only recently, progresses toward a X-ray structure were successful and the structure of the entire complex I from *Thermus (T.) thermophilus* was determined at a 4.5 Å resolution [2]. The structure of the membrane part from *E. coli* complex I and the hydrophilic domain from *T. thermophilus* enzyme have also been solved to 3.9 Å and 3.3 Å resolution, respectively [2, 10]. The current model for *T. thermophilus* complex I consists of an atomic model for the hydrophilic domain and an α-helical model for the membrane domain (Figure 1.2.2). The peripheral arm has an Y shape with a length of 130 Å [2, 10]. One of the Y arms is formed by the subunits Nqo1 and Nqo2 and the other by the C-terminal domain of Nqo3. The central part is formed by the N-terminal domain of Nqo3 and by the subunits Nqo5 and Nqo9. An additional subunit, named Nqo15, was also observed in *T. thermophilus* enzyme, which is not conserved in other complexes I. At the Y end are the subunits Nqo4 and Nqo6, forming an interface with the membrane domain [10]. Nine iron-sulfur centers were identified and from the distance between them, it can be concluded that seven of the centers form an electron "wire"

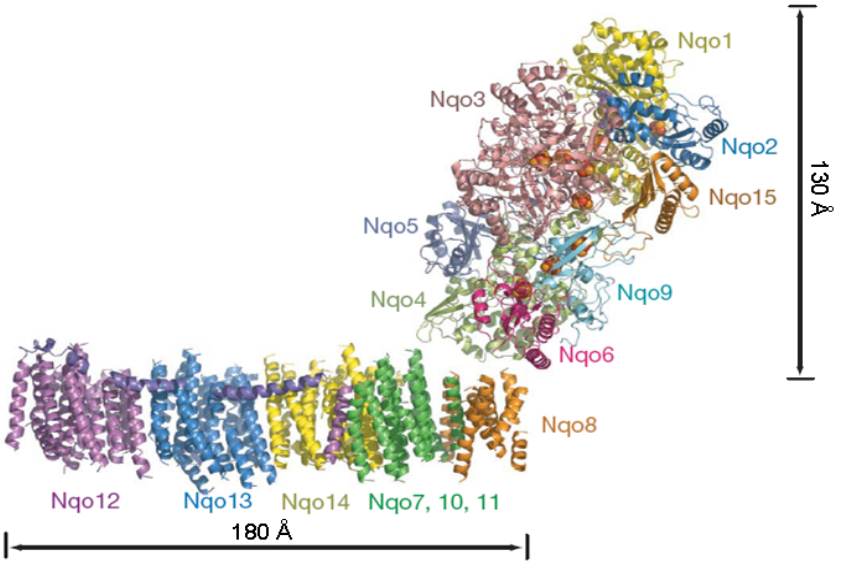

Figure 1.2.2 – Structural model of the entire complex I from *T. thermophilus*. The structure consists of the atomic model of the peripheral arm and the α-helical model of the membrane part. Each subunit is colored differently. FMN is shown as magenta spheres. Fe atoms are shown as red spheres and S atoms as yellow spheres. The amphipathic α-helice from Nqo12, spanning almost the entire length of the membrane domain, is in a darker colour (Adapted from [2]).

that bridges a distance of 84 Å (see below section 1.2.2.3 – Prosthetic groups) [10]. The last center of the chain (center N2) is about 20-25 Å from the surface of lipid bilayer [2]. An atomic model of the membrane part is still not available; however, the electron density of *E. coli* and *T. termophilus* enzyme crystals were of sufficient quality to allow the built up of an α-helical model for the membrane arm. It consists of up to 63 transmembrane (TM) helices presenting a curve shape with a total length of 180 Å. The model has also revealed a three times repetitive pattern of 14 TM helices, which were assigned to the subunits Nqo12, 13 and 14. Interestingly, two of these TM helices are discontinuous, as in some transporters and channels [25]. Unexpectedly, the subunit Nqo12 also contains a 110 Å long amphipathic α-helice, spanning almost the entire length of the membrane domain (Figure 1.2.2). The assignment of the individual membrane subunits within the

domain was based on fragmentation studies in which the *E. coli* complex was dissociated into sub-complexes [26]. The subunits Nqo12 and Nqo13 are located in a distal part of the membrane arm and as so separated from the redox centers of the hydrophilic domain. These subunits can be individually removed from the entire complex without affecting the other subunits, demonstrating that neither subunit is involved in contacts between the membrane and the peripheral arms [26]. Two additional sub-complexes were detected. One of them was composed by the subunits Nqo7, 11 and 14, and the other by the subunits Nqo8 and 10. The presence of a transient sub-complex formed by Nqo12, 13 and 14 places the one composed by Nqo7, 11 and 14 between the subunit Nqo13 and the Nqo8, Nqo10 sub-complex [26]. The assignment of the membrane subunits was also supported by other experimental studies such as cross-linking experiments that have shown a direct interaction between subunits Nqo6 and Nqo7 [27]; site-directed mutagenesis which indicated the involvement of Nqo8 in connecting the membrane and the peripheral arms, presumably by interacting with Nqo6 and/or Nqo4 [28, 29]; and photoaffinity labeling studies with a specific complex I inhibitor that suggested that the Nqo6 and Nqo8 subunits work together in the coupling reaction between electron transfer and ion transfer [29]. The absence of the Nqo8 subunit in the structure of *E. coli* membrane bound subunits also supports the close association between this subunit and Nqo6 and/or Nqo4 [2]. The distal position of the subunits Nqo12 and Nqo13 (≈100 Å away from the redox centers) was corroborated by electron microscopy, whereas a shorter membrane domain was observed when the two subunits were absent [30, 31].

Mitochondrial complex I is composed of more than 40 subunits and has a molecular mass of ≈1000 kDa [32]. The nomenclature of the subunits is based both on their N-terminal amino acid sequence (e.g. PSST) and on their

molecular mass (e.g. 51 kDa). Some subunits are also designated as ND [32]. Fourteen of the subunits are homologues to the bacterial ones and are sufficient to perform all the bioenergetics functions; thus they are called the minimal functional unit [11]. The homologous seven membrane subunits are mitochondria-encoded (homologues to Nqo7-8 and 10-14) whereas the peripheral subunits are, predominantly, nuclear-encoded (homologues to Nqo1-6 and 9) [11]. The function of most of the extra subunits, all nuclear-encoded, is unknown [32]. As bacterial complex I, the mitochondrial complex has an L-shaped structure as observed for *Yarrowia (Y.) lipolytica* [33] and bovine [34] complexes I (Figure 1.2.3).

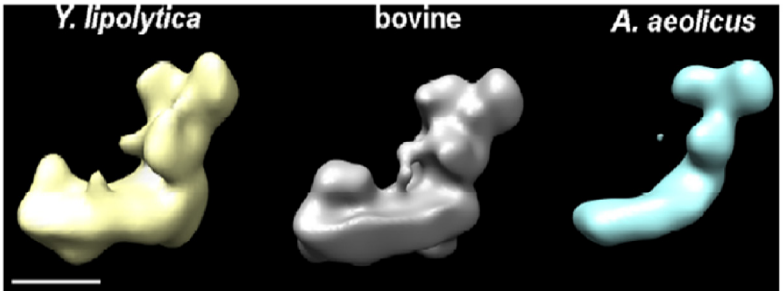

Figure 1.2.3 – 3D electron microscopy structures of *Y. lipolytica*, bovine and *A. aeolicus* complexes I. Resolution from the left to the right: 24, 27 and 45Å. Scale bar 10nm (Taken from [4]).

Archaea, cyanobacteria and chloroplasts contains homologues of 11 bacterial *nqo* genes, whereas the three genes encoding the electron input module (Nqo1-3) are missing [11]. In the case of the archaeal complex I a $F_{420}H_2$ dehydrogenase module was suggested [11, 35, 36], while in cyanobacteria and plastids the electron input module is still unknown. However, it is predicted that they display ferredoxin or NAD(P)H:quinone oxidoreductase activity [37]. Single particle electron microscopy analysis has shown that the complete complex I from the cyanobacterium *Thermosynechococcus (T.) elongatus* is also L-shaped [31]. The presence of a

structure with a shorter membrane domain, whereas the subunits NhdF and NdhD (Nqo12 and Nqo13 homologues, respectively) were missing reinforces the similar basic shape and assembly of prokaryotic and eukaryotic complexes I. Table 1.2.1 presents examples of homologous subunits in the three domains of life and respective localization.

Table 1.2.1 – Nomenclature and localization of homologous subunits of bacterial (*Paracoccus denitrificans* [13], *Escherichia coli* [15] and *Synechocystis*), eukaryal (*Bos taurus)* and archaeal (*Methanosarcina mazei* [35]) complexes I.

Subunits					**Localization**
Bacteria			Eukarya	Archaea	
P. denitrificans	*E. coli*	*Synechocystis*[b]	*B. taurus*	*M. mazei*[c]	
Nqo1	NuoF	-	51	-	peripheral
Nqo2	NuoE	-	24	-	peripheral
Nqo3	NuoG	-	75	-	peripheral
Nqo4	NuoD[a]	NdhH	49	FpoD	peripheral
Nqo5	NuoC[a]	NdhJ	30	FpoC	peripheral
Nqo6	NuoB	NdhK	PSST	FpoB	peripheral
Nqo7	NuoA	NdhC	ND3	FpoA	membranar
Nqo8	NuoH	NdhA	ND1	FpoH	membranar
Nqo9	NuoI	NdhI	TYKY	FpoI	peripheral
Nqo10	NuoJ	NdhG	ND6	FpoJ	membranar
Nqo11	NuoK	NdhE	ND4L	FpoK	membranar
Nqo12	NuoL	NdhF	ND5	FpoL	membranar
Nqo13	NuoM	NdhD	ND4	FpoM	membranar
Nqo14	NuoN	NdhB	ND2	FpoN	membranar
-	-	-	-	FpoO	peripheral
-	-	-	-	FpoF	peripheral

[a]The genes of NuoC and NuoD are fused to one gene.
[b]Ndh from NADH dehydrogenase.
[c]Fpo from $F_{420}H_2$:phenazine oxidoreductase.

1.2.2.2 – Evolution

Amino acid sequence analysis revealed that most of the complex I subunits have evolved from the same ancestors of other existing proteins

which are related with electron transfer and proton translocation processes. Depending on their homologies the subunits can be grouped into three functional modules: the electron input module, the hydrogenase module and the transporter module.

The subunits Nqo4, 5, 6, 8 and 9 are homologous to subunits of the membrane-bound NiFe-hydrogenases [11, 38] and so are known as the hydrogenase module. This NiFe-hydrogenase catalyzes the reaction $H_2 \leftrightarrow 2H^+ + 2e$, and this reaction is most likely coupled with ion translocation across the membrane [38, 39]. The hydrogenase complex is composed by six subunits (Ech A to F from energy-converting hydrogenase – *Methanosarcina barkeri* nomenclature) [38], four hydrophilic proteins and two integral membrane proteins. Nqo6 is closely related to a soluble small subunit that displays a conserved amino acid sequence characteristic for the binding of a tetranuclear iron-sulfur center. The Nqo9 is homologous to a two [4Fe-4S]$^{2+/1+}$ ferredoxin [40] while Nqo8 is homologous to one of the membrane proteins.

Subunit Nqo12 was assigned as an hydrogenase homologue [11, 40] but it was observed that this subunit is also related to one particular class of Na^+/H^+ antiporters, the multiple resistance and pH (Mrp) antiporters (see section 1.3 – Sodium/proton antiporters) [41]. Also subunits Nqo 11, 13 and 14 are related with these antiporters [5, 41]. The Mrp antiporters are encoded by an operon that contains seven genes (*mrpA* to *G*). Nqo12 is closely related to MrpA and Nqo13 and 14 are related to MrpD [41]. Nqo11 has been proposed to be homologous to MrpC [5]. Nqo11, 12, 13 and 14 should thus constitute the transporter module.

The electron input module is not conserved within the complex I family, which most probably is related to the different nature of the electron donors. NADH is the only well established electron donor and in this case

the electron input module is formed by the subunits Nqo1, 2 and 3. These subunits (excepting the C-terminal part of Nqo3) are homologues to the diaphorase part of the soluble NAD^+- reducing hydrogenases [40], which contains a non-covalently bound FMN and Fe-S centers (binuclear and tetranuclear). The C-terminal part of Nqo3 is homologous to molybdopterin enzymes [10].

The only subunits with unknown homologies to other proteins are Nqo7 and Nqo10. Table 1.2.2 summarizes the homologies between bacterial (and mitochondrial) complex I subunits and other proteins. The function, modular localization and prosthetic group content, based on the amino acid sequence [5, 11, 40, 41] and on the *T. thermophilus* X-ray structural model [10], are also included.

Table 1.2.2 – Subunits homologies of bacterial complex I, predicted function, modular localization and prosthetic groups content.

Subuni	Homology	Prosthetic groups/Function	M[a]
Nqo1	N-ter NAD^+ hydrogenase(α)	NADH oxidation, FMN, 4Fe-4S	E
Nqo2	C-ter NAD^+ hydrogenase(α)	2Fe-2S	E
Nqo3	NAD^+ hydrogrogenase(γ) Molybdopterin enzymes	2Fe-2S; 2x or 3x 4Fe-4S	E
Nqo4	NiFe hydrogenase (EchE)	-	H
Nqo5	NiFe hydrogenase (EchD)	-	H
Nqo6	NiFe hydrogenase (EchC)	4Fe-4S	H
Nqo7	-	-	-
Nqo8	NiFe hydrogenase (EchB)	H^+ transport	H
Nqo9	NiFe hydrogenase (EchF)	2x 4Fe-4S	H
Nqo10	-	-	-
Nqo11	Na^+/H^+ antiporter (MrpC)	H^+/Na^+ transport	T
Nqo12	NiFe hydrogenase (EchA) Na^+/H^+ antiporter (MrpA)	H^+ transport H^+/Na^+ transport	H/ T
Nqo13	Na^+/H^+ antiporter (MrpD)	H^+/Na^+ transport	T
Nqo14	Na^+/H^+ antiporter (MrpD)	H^+/Na^+ transport	T

[a]E-electron input module; H-hydrogenase module, T-transporter module. N-ter: N-terminal; C-ter: C-terminal

In an earlier modular evolution scenario for complex I, proposed by Friedrich and Scheide [11], the subunits Nqo4 and 6 combined with Nqo5, 8, 9 and 12 to form a membrane bound hydrogenase module. Then after a triplication of Nqo12 (in Nqo13 and Nqo14), and recruitment of Nqo7, 10 and 11 the common ancestor of complex I was formed. Different electron input modules were then recruited.

This scenario was contested by Mathiesen and Hagerhall after having recognized the homologies between the Mrp systems and complex I subunits [5, 41]. Mathiesen and Hagerhall have suggested that a multisubunit antiporter module consisting of MrpA, C and D was present in the last common ancestor of complex I and that this module was most likely recruited in one

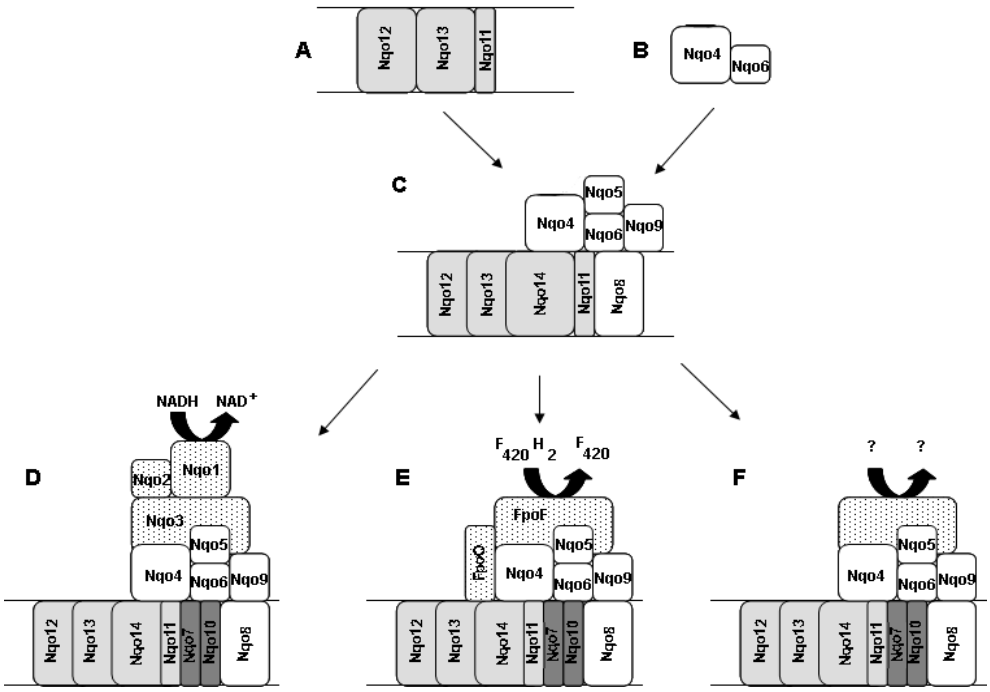

Figure 1.2.4 – Evolutionary scheme for complex I based on Mathiesen and Hagerhall proposal [5]. A-Ancestral Mrp antiporter subunits; B-Ancestral hydrogenase subunits; C-Last common ancestor of complex I; D-Bacterial and mitochondrial complex I; E-Archaeal complex I; F- Cyanobacterial and plastidial complex I.

step rather than in three successive events (Figure 1.2.4-A). The same authors suggested that besides the subunits Nqo11, 12, 13 and 14 (the latter resulting from a gene duplication of Nqo13) the last common ancestor contained the subunits Nqo4 and 6 (Figure 1.2.4-B) and the subunits Nqo5, 8 and 9 (Figure 1.2.4-C). Different electron input modules were then recruited giving origin to the complexes I, known nowadays (Figure 1.2.4-D, E, F). Due to no obvious homologues of Nqo7 and 10 with other known proteins, it is not possible to conclude whether these subunits were present in the last common ancestor.

1.2.2.3 – Prosthetic groups

Complex I contains as prosthetic groups one non-covalently bound flavin and up to nine iron-sulfur centers (Figure 1.2.5 and Table 1.2.3) [10].

FMN, located in the Nqo1 subunit, is the characteristic flavin of complex I. However, instead of FMN, an FAD molecule was detected in archaeal complex I [35, 36]. Albracht and Hedderich had proposed a second FMN group in bovine complex I, located in Nqo6 subunit [42], but this has never been observed and is not sustained by the X-ray structure of *T. thermophilus* enzyme [10].

The iron-sulfur centers of complex I include binuclear and tetranuclear centers. They were predicted by amino acid sequence analysis and have been studied by electron paramagnetic resonance (EPR) spectroscopy. Later the X-ray structure of the peripheral part of *T. thermophilus* complex I confirmed the presence and arrangement of the centers [10, 43]. The nomenclature of the clusters is not consensual. The first nomenclature was proposed by Ohnishi and is based on the spin relaxation of the centers of the bovine enzyme: the higher the center numbering, the faster its spin relaxation and consequently the lower optimal temperature for its observation by EPR

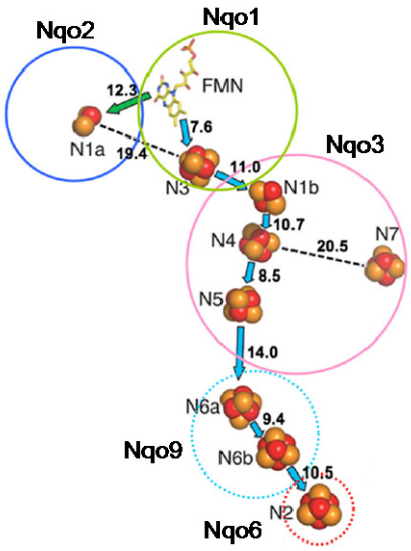

Figure 1.2.5 – Arrangement of prosthetic groups and respective subunit localization, according to Ohnishi [6]. Fe atoms are shown as red spheres and the S atoms as yellow spheres. The main pathway of electron transfer is denoted with blue arrows. The distances between the centers given in angstroms were calculated from edge to edge [10]. (Adapted from [6])

spectroscopy [43]. Ohnishi has named the binuclear centers as N1a and N1b, and the tetranuclear ones as N2, N3, N4 and N5. [43]. The two missing tetranuclear centers, not observed by EPR spectroscopy on the intact enzyme, are referred as N6a and N6b [44]. An additional center is observed in some bacterial complexes [10, 45, 46]. This center was mistakenly assigned as a binuclear center (N1c) [46] and afterwards correctly assigned as a [4Fe-4S]$^{2+/1+}$ center and referred as N7 [45]. Excepting the centers N1a and N2, all the others are isopotential at about -250 mV (pH 7) [43]. The center N1a has a lower reduction potential ($E_{m,7}$≈ -370 mV) and its functional significance remains unclear [43]. Although the center can accept electrons directly from FMN, it may have a role unrelated to the main electron transfer pathway since it cannot conduct electrons to the other centers (N3 is the nearest one and it is 19Å away – Figure 1.2.5) [10]. It has been proposed that it may act as an anti-oxidant [47]. Center N2 has a more positive and pH-dependent reduction potential ($E_{m,7}$≈-50 to -150 mV) [43]. The function of N7 is unknown and its distance from the other centers is too long to allow effective electron transfer [10]. Therefore, the electron "wire" is composed by the centers N1b, N3, N4, N5, N6a, N6b and N2 (Figure 1.2.5).

It is likely that center N3 accepts electrons from FMN which are transferred through the other isopotential centers to center N2 by which the quinone is reduced. The assignment of the centers N4, N5 and N6b to the X-ray data is not consensual and is still under debate [6, 48, 49]. A different nomenclature for the iron-sulfur centers was proposed by Hirst, in which the centers are named according to their nuclearity (2Fe or 4Fe), their subunit location and by the number and type of ligands (cysteine or hystidine) [48].

Endogenous quinones have also been suggested to function as prosthetic groups being involved in the electron transfer pathway [50-52]. However, this is still under discussion (see section 1.2.2.4 - Quinones and section 1.2.2.7 – Reaction mechanism).

Table 1.2.3 – Localization of the predicted prosthetic groups (and respective reduction potential) of bacterial and mitochondrial complex I [10, 42-44].

Subunit	Prosthetic groups[a]	$E_{m,7}$ (mV)
Nqo1	FMN, $[4Fe\text{-}4S]^{2+/1+}$ (N3)	-340 -250
Nqo2	$[2Fe\text{-}2S]^{2+/1+}$ (N1a)	-370
Nqo3	$[2Fe\text{-}2S]^{2+/1+}$ (N1b), 2x or 3x $[4Fe\text{-}4S]^{2+/1+}$ (N4, N5, N7)	-250 -250, -250, -250
Nqo6	FMN (?) $[4Fe\text{-}4S]^{2+/1+}$ (N2)	- -50 to -150
Nqo9	2x $[4Fe\text{-}4S]^{2+/1+}$ (N6a, N6b)	-270, -270

[a]N4, N5 and N6b are assigned based on Ohnishi´s studies.

1.2.2.4 – Quinones

Quinones play an important role in the overall bioenergetic function of complex I. These lipophilic compounds can move freely between partner reductants and oxidants in the membranes and can be divided into three major groups: naphtoquinones, benzoquinones and benzothiophenquinones (Figure 1.2.6). Their different structures reflect different physical and

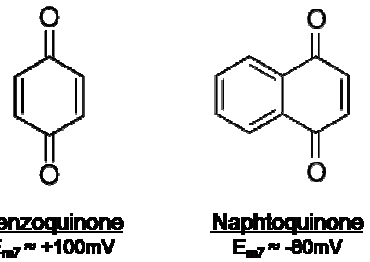

Figure 1.2.6 – Chemical structure of benzoquinone and naphoquinone. $E_{m,7}$ of ubiquinone (benzoquinone) and menaquinone (naphtoquinone).

functional proprieties [53]. One of the differences is the reduction potential which is usually lower for naphtoquinones [54]. The type of quinone synthesized by an organism is determined by growth conditions. Organisms which can switch between aerobic and anaerobic modes usually can synthesize benzoquinones and naphtoquinones. An example is *E. coli* that can contain menaquinone (naphoquinones) or ubiquinone (benzoquinone) depending whether it is grown anaerobic or aerobically [54].

It is still not clear if the quinone acts in complex I simply as one of the substrates or also as a prosthetic group. The number of quinones that are associated with complex I, as well as, the number of quinone binding sites and respective subunit localization are not known.

Up to three complex I-associated semiquinone species, showing different behaviors in the presence of $\Delta\tilde{\mu}_{X^+}$ or specific complex I inhibitors, were detected by EPR spectroscopy in sub-mitochondrial particles [43, 51, 55-57]. These species are distinguishable by their different spin-relaxation behaviors: a fast relaxing (SQ_{Nf}), a slow relaxing (SQ_{Ns}) and in some situations a very slow relaxing one (SQ_{Nx}). After reanalysis of the EPR data the latter species was excluded as an intrinsic complex I component (most likely corresponds to a semiquinone from another respiratory complex – complex III) [8]. The SQ_{Nf} was only detected in coupled membranes, not in isolated complex I, and interacts magnetically with one paramagnetic center nearby, probably the center N2 [56]. The SQ_{Ns} was not sensitive to the uncoupler carbonyl cyanide *m*-chlorophenyl hydrazone (CCCP) and was weakly spin-

coupled with N2 [56]. These semiquinone species are differently affected by complex I inhibitors. Although the two species are affected by piericidin A in the same manner, the SQ_{Nf} is highly rotenone-sensitive while the other species has low rotenone sensitivity [56]. Another difference is the pH dependency. The signal amplitude of SQ_{Nf} is not significantly affected by pH between 7 and 8.5, whereas the SQ_{Ns} intensity is pH dependent between 6.5 and 9 [51]. Both species were shown to be anionic forms (SQ^{-}) at a pH close to neutral [52]. It has been proposed that the SQ_{Nf} works as a prosthetic group being the first electron acceptor, which receives electrons directly from the center N2. The SQ_{Ns} may function as a second electron acceptor being the converter between one and two electron transfer pathways [8, 50, 52]. In spite of the distinct properties observed for the semiquinones, there is still some controversy whether these reflect two quinones or two forms of the same quinone.

Which complex I subunit(s) harbour the quinone binding site(s) is still an open question. A large and unique binding pocket for quinone, acting as a substrate, has been proposed in recent years [58, 59]. It was suggested that this pocket is located at the interface of the Nqo6 and Nqo4 subunits. This suggestion was based on mutagenesis studies [59, 60], on photoaffinity labelling studies with rotenone analogues [61] and on the crystal structure of the hydrophilic domain of complex I, which revealed a broad cavity at the interface of these two subunits [10]. A conserved tyrosine residue, in the Nqo4 subunit, was shown to be critical for quinone binding [59]. Photoaffinity labelling studies also suggested that Nqo8 subunit is involved in quinone interaction [29, 61]. This hypothesis was also considered based on topology models of Nqo8 [62]. The amino acid sequence LxxxHxxx(S/L/T), described as a "consensus quinone-binding motif", was identified in a well conserved region of a diverse range of Nqo13 sequences and a variant of that

motif was identified in Nqo12 sequences [63]. Given these observations, it was proposed that the Nqo13/Nqo12 pair might harbour two separate quinone sites or a single site could be formed from elements of both subunits [63]. Although this seems rather unlikely because of the distal position of these two subunits, which are ≈ 100 Å away from the known redox centers, it was suggested that in the absence of these two subunits or even of only one, complex I was no longer able to perform quinone reduction [26, 64]. If this was due to the fact that these two subunits really contain at least a quinone binding site or due to some drastic conformational change resulting from their absence so that the quinone binding site was no longer accessible to quinone is still unknown. Furthermore, there is no clear evidence for the presence of the quinone(s) within these subunits in the *T. termophilus* complex I structure, although it cannot be excluded that the quinone(s) binds at the surface of these subunits [2].

1.2.2.5 – Inhibitors

A plethora of inhibitors that interfere with quinone reduction have been characterized over the years. The inhibitors have been divided in at least three groups. Piericidin A is a typical example of a type A inhibitor which is antagonist of the quinone. Rotenone represents the type B, antagonist of the semiquinone intermediate, whereas capsaicin represents the type C which is antagonist of the quinol [65]. It has been suggested that the various groups of inhibitors would bind to at least two different sites in the enzyme [66]. On the contrary, a unique binding domain has also been suggested. Direct competition experiments and mutagenesis studies, have suggested that the three classes of inhibitors share a common binding domain with partially overlapping sites. Type B site overlaps with both type A and C sites, but

binding of the latter two types of inhibitors does not interfere with each other [58, 59, 67].

1.2.2.6 – Coupling ion: Proton *versus* Sodium

The nature of the charge that is translocated by complex I is still under debate. It was for long assumed that the coupling ion was the proton. However, Steuber and colleagues have proposed that instead of proton, the coupling ion of complex I is sodium. The H^+(or Na^+)/e stoichiometry is not completely established although a ratio of 2 has been described as "universally accepted" in the case of the proton.

Most of the studies of proton translocation by complex I were performed using the entire respiratory chain combining exogenous substrates with various respiratory inhibitors. Measurements of the H^+/O stoichiometry of rat liver and heart mitochondria, respiring in steady-state, have given H^+/e values from 1 to 2 [68-70]. A ratio of 2 was also determined by measurements with the pH indicators neutral red and/or phenol red in rat liver mitochondria, bovine heart sub-mitochondrial particles and intact mitochondria from the yeast *Y. lipolytica* [71-74]. Purified *Y. lipolytica* complex I reconstituted into liposomes also showed a H^+/e stoichiometry of 2 [74]. A ratio of 1.5 was found for *E. coli* cells [75]. Archaeal complex I is also described as a proton translocator and a H^+/e ratio of 0.9 was determined for *M. mazei* inverted vesicles [35].

Translocation of sodium ions, measured by atomic absorption spectroscopy, has been reported for complex I from *Klebsiella (K.) pneumoniae* [76, 77], *E. coli* [78] and *Y. lipolytica* [79]. It has been demonstrated that *K. pneumoniae* and *Y. lipolytica* complexes I, reconstituted into liposomes, act as sodium translocator with a stoichiometry of 1 Na^+/e [77, 79]. *E. coli* inverted membrane vesicles catalyzed NADH-driven Na^+ uptake, which was

prevented by complex I inhibitors but not by protonophores [78]. It was also shown that subunit NuoL (Nqo12) of *E. coli* complex I mediates Na^+ uptake when reconstituted into liposomes or when produced in *Saccharomyces cerevisiae*, being this transport prevented by an inhibitor of Na^+/H^+ antiporters [80, 81]. These sodium translocation studies have been contested by other authors claiming that the observed sodium transport was probably due to contamination with Na^+-NQR, in the case of *K. pneumoniea* complex I, or to a secondary Na^+/H^+ antiport activity performed by complex I, in the case of *E. coli* [82, 83].

1.2.2.7 – Reaction mechanisms

A. Electron transfer pathway

The electron transfer pathway between NADH and the center N2 occurs totally in the peripheral arm of complex I [10]. NADH ($E_{m,7}$=-320 mV) binds to the Nqo1 subunit and donates the electrons directly to the FMN group ($E_{m,7}$≈-340 mV) located in the same subunit. The electrons are then transferred, one at a time, through the isopotential iron-sulfur centers (N3, N1b, N4, N5, N6a, N6b; $E_{m,7}$=-250 mV) until the N2 center ($E_{m,7}$=-50 to -150 mV). Two different mechanisms have been proposed for the electron transfer between the N2 center and the quinone. In one of those mechanisms, the electrons are directly transferred to the quinone that acts simply as one of the substrates. In the other hypothesis, the electrons are transferred from the iron-sulfur center to the bound-semiquinone species (acting as prosthetic groups) and finally to a second quinone within the membrane (acting as a substrate) (Figure 1.2.7) [52].

Ultrafast freeze-quench studies of the electron transfer have shown that after NADH binding, electrons move via FMN to the iron-sulfur center N2 with an apparent time constant of ≈ 90 μs [47]. These results are in

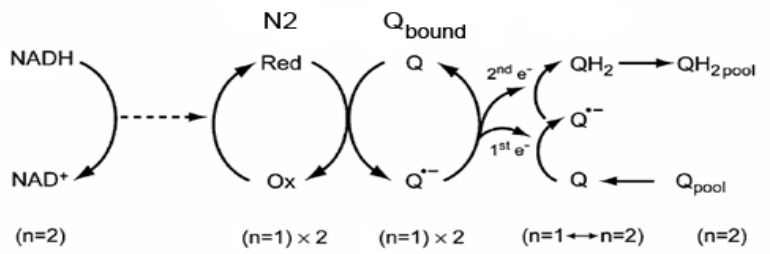

Figure 1.2.7 – A proposed electron transfer pathway from N2 to quinone. Quinones functioning as prosthetic groups and as substrate (Adapted from [8]).

agreement to those predicted by electron transfer theory. Tunneling simulations have shown that there is probably no barrier between NADH and the iron-sulfur center N2 and that the electrons arrive rapidly at center N2 (τ = 100 μs) [84]. Based on the theoretical and experimental rates of N2 reduction, the electron transfer between NADH and N2 is unlikely to be coupled to other reactions, such as proton transfer [47]. Although center N2 was totally reduced and a bound quinone per *E. coli* complex I was observed, no semiquinone species was detected by the ultrafast freeze-quench approach [47].

B. Ion/electron coupling mechanism

The coupling process of electron transfer between NADH and quinones and charge translocation across the membrane is poorly understood. Over the past decades different mechanisms have been proposed for that process. Three types of mechanisms have been discussed: direct coupling, indirect coupling and a combination of these two types. The "direct mechanism" implies that the electron carrier(s) is directly involved in the charge translocation, whereas in the "indirect mechanism" there is only conformational coupling between the redox centers and the polypeptide(s) responsible for the charge translocation.

Taking into account the current structural knowledge of complex I, several mechanisms may be excluded, as for example models suggesting the direct involvement of FMN in the coupling mechanism [85]. Most likely these models were based on Peter Mitchell´s theories of strictly direct coupling mechanisms. By the same reason and in analogy with the mechanism proposed for complex III (Q-cycle), models describing proton translocation directly linked to the quinone/quinol couple were proposed. These hypotheses became more attractive when more than one semiquinone species were detected by EPR spectroscopy. Esposti and Ghelli constructed their model (dual Q-gated pump) based in this latter assumption (Figure 1.2.8-A) [3]. The authors suggested that proton translocation was linked to the sequential formation of two types of semiquinones, localized in two different quinone binding sites (sites A and B). A protein-bound quinone would be at the site A, promoting proton translocation during its reduction/oxidation, while site B could also harbor a protein-bound quinone and/or could only interact with an external quinone, being this site also involved in proton translocation. It was suggested that after two semiquinones have been formed in site B, they were supposed to dismutate resulting in the formation of one quinol molecule that was released from the complex. Against this hypothesis is the fact that two semiquinone anionic species have to exist at the same time at the same binding site (site B) to allow dismutation which would be very unlikely due to electrostatic repulsion. This repulsion effect was overcome in the model proposed by Dutton *et al* in which it was suggested that complex I operates in a symmetric and expanded Q-cycle way [9]. This model combines a direct reversal of a Q-cycle mechanism with an additional protein-bound quinone (Q_{NY}) which acts as an electron carrier and as a proton translocator element. This bound-quinone gates a proton channel, which would allow unrestricted proton movement in either direction (Figure 1.2.8-B). The

"extra" quinone was invoked in order to explain the $4H^+/2e$ stoichiometry calculated for some complexes I, which was not compatible with the canonical Q-cycle stroichiometry ($2H^+/2e$). Sherwood and Hirst also investigated the possibility of this enzyme to operate through a Q-cycle mechanism but no evidences of the oxidation of quinol induced by the reduction of complex I by NADH could be detected [64]. As Dutton *et al*, Ulrich Brandt proposed a mechanism involving the presence of three quinone binding sites, one quinol oxidation site (P_i) and two quinone reduction sites (N_A and N_B); but in his model also the iron-sulfur center N2 directly contributes to the proton translocation (Figure 1.2.8-C) [12]. The involvement of the centre N2 in the process was suggested due to its redox-Bohr proprieties. However, it was observed later that replacing histidine-226 (*Y.*

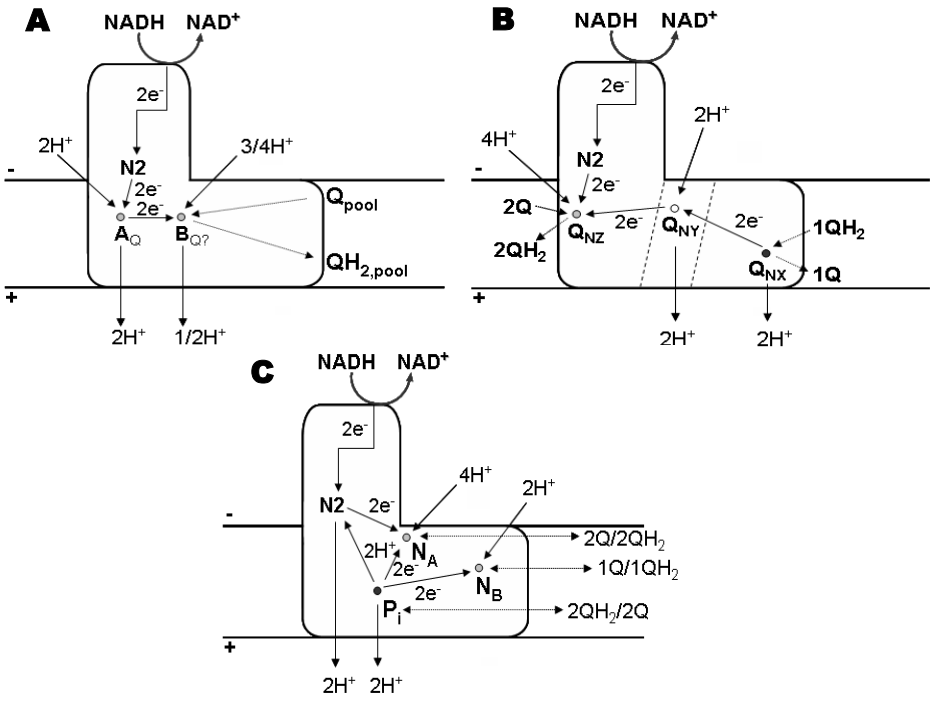

Figure 1.2.8 – Direct coupling mechanisms proposed by Esposti and Ghelli (A) [3], Dutton *et al* (B) [9] and Brandt (C) [12]. For mechanistic details see respective references.

lipolytica numbering), which is located in the vicinity of cluster N2, by a methionine residue completely abolished the redox-Bohr effect and shifted the reduction potential of the cluster from -140mV to -220mV (at pH 7) [86]. Nevertheless, the mutation did not affect the catalytic activity or the ion translocation stoichiometry, excluding a role of this center in the translocation process due to its redox-Bohr proprieties [86]. Recently, a model based on electrostatic and cooperative interactions between conserved lysine residues in subunits Nqo8, Nqo12, Nqo13 and Nqo14 triggered by formation of the semiquinone anion was suggested. In this model the energy of quinone reduction is sequentially transmitted to the distal membrane subunits [87]. Briefly, the energy transduction process can be divided in two phases. The first phase of electrostatic polarization includes the formation of a semiquinone anion (or quinol anion), in the coupling domain formed by the subunits Nqo7, 8, 10 and 11, and shifts of the pK_a value of conserved lysine residues in the membrane domain. This phase may include partial proton transfer. Assuming that the subunits Nqo8, 12, 13 and 14 interact electrostatically with their closer subunits by means of conservative lysine residues, this would allow the transfer of energy between the subunits. The second phase of the process is then initiated by Nqo12 subunit (the distal one) and proceeds in the reverse direction towards the "coupling domain". This phase would complete the pumping process and the quinone neutralisation by proton uptake. This mechanism is compatible with a H^+/e ratio of 2, since it can be assumed that each subunit (Nqo8, 12, 13 and 14) pumps one proton.

Most of these "strictly direct" models were contested after Steuber *et al* proposed that the coupling ion of complex I could be the sodium ion instead of the proton [76, 78-80, 88], since a Q-cycle with Na^+ is not possible. As an alternative, a combination of a direct mechanism, with a quinone or N2

center involvement, and an indirect mechanism, with the antiporter-like subunits involvement, started to be considered in recent years [89, 90]. One of the most detailed and sustained model was proposed by Berrisford and Sazanov [1] and it is based on the unique coordination of the center N2 by two consecutive cysteines of Nqo6 subunit. The unique coordination is central for direct coupling via cysteines protonation and for conformational coupling allowing movements of helices of Nqo6 and Nqo4 subunits (Figure 1.2.9). Briefly, when N2 center is reduced, one of the conserved cysteines (Cys 1) disconnects from the iron; the helices H1/H2 (H1) of Nqo6 subunit shift and a proton is delivered to Cys 1 (Figure 1.2.9-B). As soon as the second electron arrives to the center N6b (electron donor to the center N2), Cys 1 is deprotonated, being the proton transferred to one residue nearby (X_1-OH), and reconnects to the center N2. At this stage the other cysteine (Cys 2) is disconnected (and protonated) and a four-helix bundle (4HB) of Nqo4 subunit is shifted (Figure 1.2.9-C). The N2 center is now able to donate the first electron to a quinone, creating a semiquinone radical, and receive the second electron via N6b center. The cysteine cycle of disconnection/reconnection restarts. Cys 1 is disconnected and so protonated again, whereas the Cys 2, after releasing the proton to one residue nearby (X_2-OH), is reconnected to N2 center (Figure 1.2.9-D). This center donates the second electron to the semiquinone radical, which is protonated by the X_1-OH and X_2-OH groups, so that the quinol is produced. The center N2 is now fully oxidized allowing the helices H1/H2 (and the four-helix bundle) to return to their starting positions and the pumping of three protons through antiporter-like membrane subunits via conformational changes. The full coordination of the two cysteines to the center N2 occurs after deprotonation of Cys 1. The proton can be ejected into the periplasm, being the exit pathway most likely located in Nqo6/Nqo4 adjacent membrane subunits

(Figure 1.2.9-D). This mechanistic model is compatible with the X-ray structure of the entire complex I from *T. termophilus* [2]. It was observed in the structure that the four-helix bundle and the helix H1 are most likely in direct contact with the Nqo8 subunit. Thus, the Nqo4/Nqo6 helices are well positioned to transmit conformational changes to Nqo8 and Nqo7, 10 and 11. Additionally, the long amphipathic helix (HL) of Nqo12, also observed on the structure, can act as a mechanical link transmitting conformational changes from the near quinone-site to the antiporter-like subunits. Against this model is the elevated position of the center N2 over the membrane (20-

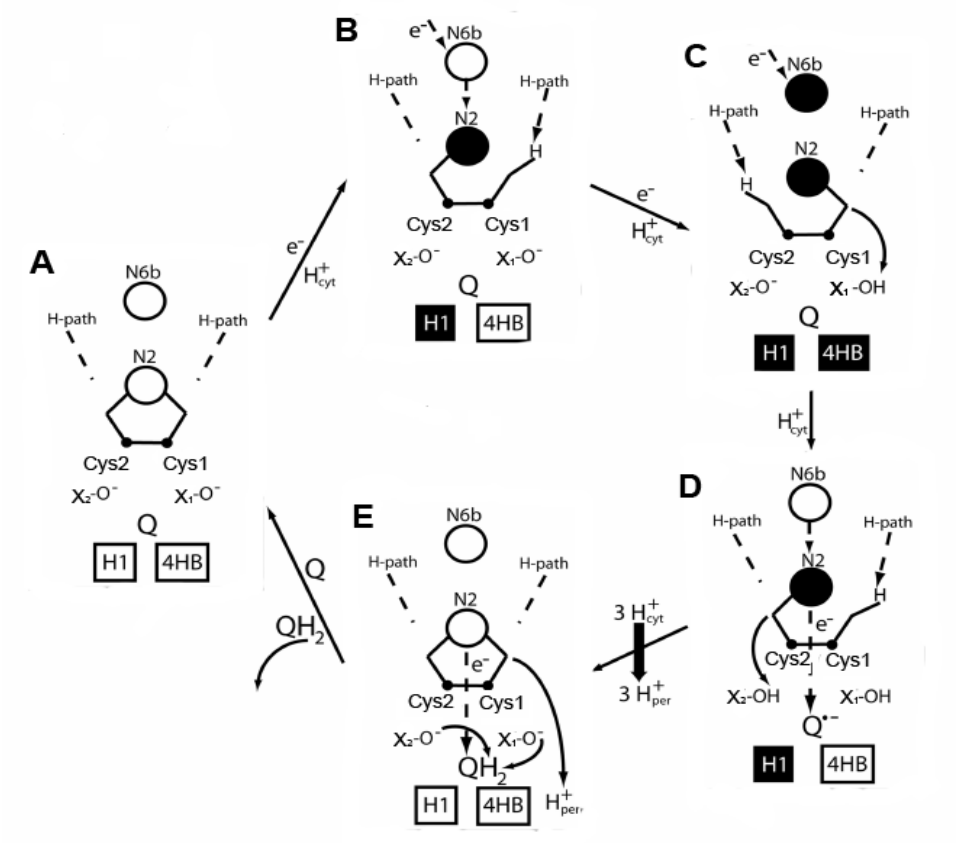

Figure 1.2.9 - Model proposed by Berrisford and Sazanov based on conformational changes and protonation/deprotonation events (Adapted from [1]).

25 Å), suggesting that the translocation of the proton, previously proposed to be via cluster N2, may also be conformation-driven via subunits Nqo8 or Nqo7, 10 and 11 [2].

Strictly indirect coupling mechanisms may thus be considered the most probable type of mechanism operating on complex I. Based on the *T. termophilus* structure, Efremov *et al* proposed a model in which conformational changes in Nqo8 and in Nqo7, 10 and 11 affect the nearby C-terminal helix of Nqo12 which leads to a piston-like motion of the HL along the membrane domain (Figure 1.2.10). This movement synchronously tilts the three nearby discontinuous helices, resulting in proton translocation. A net result of three translocated protons (one per antiporter-like subunit) would be achieved. The

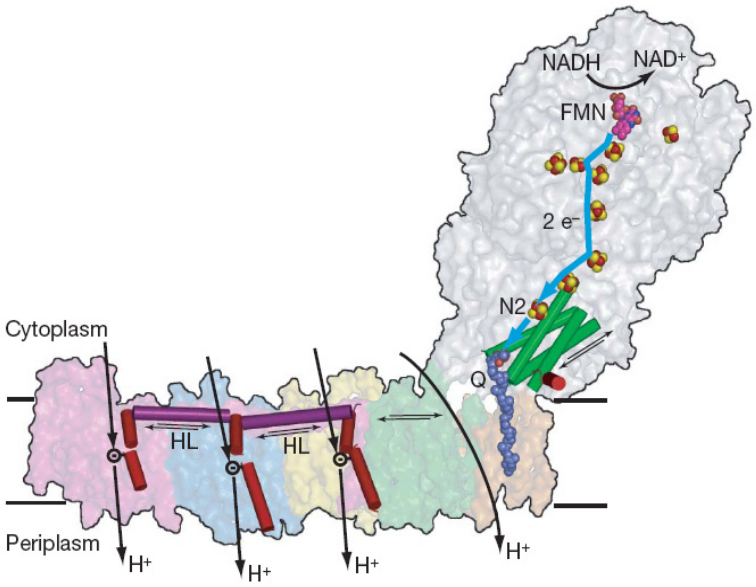

Figure 1.2.10 – Ion/electron coupling model proposed by Efremov *et al* based on the *T. termophilus* complex I structure [2]. Electrons move from NADH to the quinone (dark blue) via FMN (magenta) and the chain of iron-sulfur centers (red and yellow spheres). Electron transfer is coupled to conformational changes (indicated by arrows) in the hydrophilic domain which are transmitted to the amphipathic helix HL (magenta), which tilts three discontinuous helices (red) in the antiporter-like subunits resulting in translocation of three protons. The fourth proton is translocated at the interface of the two main domains.

fourth proton is suggested to be translocated at the interface of the peripheral and membrane domain (via Nqo7, 10 and 11 or Nqo8) and may also be driven by conformational changes [2].

An indirect mechanism is also supported by the possible different nature of the coupling ion, conformational changes detected after NADH binding and/or quinone reduction [91, 92] and different classes of inhibitors binding to the same large binding pocket [58].

1.2.2.8 – *Rhodothermus marinus* Complex I

R. marinus complex I is one of the few examples of bacterial complexes I so far purified (in its intact form). This complex was isolated with the canonical prosthetic groups (FMN and iron-sulfur centers) [93]. An extensive analysis of the iron-sulfur centers of purified complex I was performed by EPR spectroscopy allowing the identification of a minimum of two $[2Fe\text{-}2S]^{2+/1+}$ and four $[4Fe\text{-}4S]^{2+/1+}$ centers [94]. Redox titrations have showed that five of the six identified centers are isopotential, having a reduction potential of -240 mV (pH 7.5) [94]. The other center (one $[4Fe\text{-}4S]^{2+/1+}$) has a much lower reduction potential [94]. The possible presence of two additional $[2Fe\text{-}2S]^{2+/1+}$ centers was considered [94]. Additionally to the canonical prosthetic groups, the presence of three menaquinone molecules per complex was also suggested [93]. This enzyme displays NADH:menaquinone oxidoreductase activity which is sensitive to the complex I specific inhibitor rotenone and its reconstitution in liposomes showed proton translocation coupled to the catalytic activity [93]. The genes coding for *R. marinus* Nqo subunits are organized in two clusters, *nqo*1-7 (nqoA) and *nqo*10-14 (nqoB) and two independent genes, *nqo*8 and *nqo*9. Among complex I genes, and co-transcribed with them, two additional genes

encoding a pterin-4α-carbinolamine dehydratase (PCD) and a putative Na^+/H^+ antiporter were identified in nqoB (Figure 1.2.11). This putative antiporter exhibits higher similarity to a Nha-type Na^+/H^+ antiporters than to

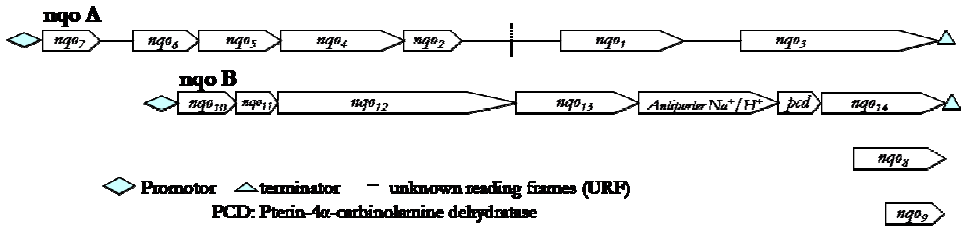

Figure 1.2.11 – Genetic organization of *Rhodothermus marinus* complex I [7].

Mrp type antiporters or to other complex I subunits [7].

1.2.3 – ALTERNATIVE NAD(P)H DEHYDROGENASE (NDH-II)

NDH-II is usually constituted by a single polypeptide chain, of ≈ 50 kDa, containing a non-covalently bound flavin (FAD or FMN) as the only prosthetic group [95]. NADH is the preferential substrate but NDH-II are also able to oxidize NADPH [96-98]. The electron transfer from NAD(P)H to quinones is suggested to occur by a ping-pong mechanism [99-102] and is not coupled to ion translocation across the membrane. In this sense this enzyme does not contribute directly to the formation of $\Delta\tilde{\mu}_{X^+}$. The mode of interaction of the enzyme with the quinone and the nature and localization of the quinone binding site are unknown [95]. Also the nature of membrane-protein interactions is not known, being possible a membrane association via amphipathic α-helices and/or via electrostatic interactions [103]. So far no general specific inhibitor was assigned to this enzyme [104], but there are compounds that can prevent its activity, such as flavone [100, 105], diphenyliodonium chloride [105], dibenziodolium chloride, 1-hydroxy-2-dodecyl-4(1*H*)quinolone [99, 102], scopanfungin [106] and gramicidin S [106].

In the absence of a crystal structure of this enzyme, the structure-function information is restricted to modeling studies based on sequence similarity with other flavoenzymes, such as dihydrolipoamide dehydrogenase [95]. These comparative studies suggested that the amino acid sequences of NDH-II contain two typical dinucleotide binding domains, both in the N-terminus region of the protein and both harboring a conserved GxGxxG motif. It is proposed that the first GxGxxG motif binds the flavin and the second NAD(P)H [103]. NDH-II is found in respiratory chain of plants, yeast and fungi, as well as, in bacteria and protozoa [104]. While most bacteria seem to have only one, two or more NDH-II enzymes co-exist in some eukaryotic species facing either the mitochondrial matrix (internal enzymes), or the cytoplasm (external enzymes) [107]. In most cases, this enzyme is found together with NDH-I but in organisms lacking NDH-I, NDH-II is the only component of the respiratory chain responsible for the oxidation of NAD(P)H [107]. A common physiological role for this enzyme remains unclear. Besides its role in keeping the [NADH]/[NAD^+] balance, NDH-II has been suggested to be involved in the protection of nitrogenase from O_2 inhibition [108]; in the electron transfer to the membrane-bound methane monooxygenase; in oxidative protection and in copper homeostasis [109]; in non-photochemical reduction of plastoquinones [98]; and in regulation responding to the redox state of the quinone pool [110].

1.2.4–Na^+ - TRANSLOCATING NADH:QUINONE OXIDOREDUCTASE

Na^+-NQR is composed by six subunits (NqrA to F) encoded by the *nqr* operon and has an approximate molecular mass of 210 kDa. Three of the subunits are very hydrophobic (NqrB, D and E) whereas the others are relatively hydrophilic (NqrA, C and F) [111]. This enzyme has as prosthetic groups one [2Fe-2S]$^{2+/1+}$ center (in NqrF) and three flavins, a non-covalently

bound FAD (in NqrF) and two covalently bound FMN (in NqrB and C) [111]. The presence of a non-covalently bound riboflavin was also observed but its localization is unknown [112]. Additionally to flavins and the [2Fe-2S]$^{2+/1+}$center, Na^+-NQR can also hold a molecule of quinone [113, 114]. Na^+-NQRs are found in bacteria, including many marine species [111, 113-115]. This enzyme is a primary (and specific) sodium pump that couples the electron transfer from NADH to quinone to sodium translocation across the membrane, contributing to the establishment of the $\Delta\tilde{\mu}_{X^+}$ [113, 114]. The quinone reduction by NADH is dependent on sodium [115], but the NADH oxidation by artificial electron acceptors is not [111, 114]. The mechanism of energy transduction by Na^+-NQR is still unknown. It has been proposed that it can have more than one phase showing different sodium dependencies. In the first phase of the process (before the coupling site), a sodium independent reaction generates a highly reactive intermediate which is then utilized by the sodium dependent process(es) to drive sodium translocation across the membrane [111, 115, 116]. Studies showing that the affinity of the protein to sodium ions was dependent on the redox state of the enzyme corroborate this hypothesis [117]. However, no sodium dependence of the reduction potential of any of the Na^+-NQR prosthetic groups was detected [107, 118]. Novel prosthetic groups, not detected so far, have been suggested in order to explain the sodium dependency [117]. A ratio of 1 Na^+/e for *Vibrio alginolyticus* Na^+-NQR has been determined [119]. Known activity inhibitors are the antibiotic korormicin [111] and silver ions [114].

1.2.5 - REFERENCES

[1] J.M. Berrisford and L.A. Sazanov, Structural basis for the mechanism of respiratory complex I, J Biol Chem 284 (2009) 29773-83.

[2] R.G. Efremov, R. Baradaran and L.A. Sazanov, The architecture of respiratory complex I, Nature 465 (2010) 441-5.

[3] M. Degli Esposti and A. Ghelli, The mechanism of proton and electron transport in mitochondrial complex I, Biochim Biophys Acta 1187 (1994) 116-20.

[4] T. Clason, T. Ruiz, H. Schagger, G. Peng, V. Zickermann, U. Brandt, H. Michel and M. Radermacher, The structure of eukaryotic and prokaryotic complex I, J Struct Biol 169 81-8.

[5] C. Mathiesen and C. Hagerhall, The 'antiporter module' of respiratory chain complex I includes the MrpC/NuoK subunit -- a revision of the modular evolution scheme, FEBS Lett 549 (2003) 7-13.

[6] T. Ohnishi and E. Nakamaru-Ogiso, Were there any "misassignments" among iron-sulfur clusters N4, N5 and N6b in NADH-quinone oxidoreductase (complex I)?, Biochim Biophys Acta 1777 (2008) 703-10.

[7] A.M. Melo, S.A. Lobo, F.L. Sousa, A.S. Fernandes, M.M. Pereira, G.O. Hreggvidsson, J.K. Kristjansson, L.M. Saraiva and M. Teixeira, A nhaD Na^+/H^+ antiporter and a pcd homologues are among the *Rhodothermus marinus* complex I genes, Biochim Biophys Acta 1709 (2005) 95-103.

[8] T. Ohnishi, J.E. Johnson, Jr., T. Yano, R. Lobrutto and W.R. Widger, Thermodynamic and EPR studies of slowly relaxing ubisemiquinone species in the isolated bovine heart complex I, FEBS Lett 579 (2005) 500-6.

[9] P.L. Dutton, C.C. Moser, V.D. Sled, F. Daldal and T. Ohnishi, A reductant-induced oxidation mechanism for complex I, Biochim Biophys Acta 1364 (1998) 245-57.

[10] L.A. Sazanov and P. Hinchliffe, Structure of the hydrophilic domain of respiratory complex I from *Thermus thermophilus*, Science 311 (2006) 1430-6.

[11] T. Friedrich and D. Scheide, The respiratory complex I of bacteria, archaea and eukarya and its module common with membrane-bound multisubunit hydrogenases, FEBS Lett 479 (2000) 1-5.

[12] U. Brandt, Proton-translocation by membrane-bound NADH:ubiquinone-oxidoreductase (complex I) through redox-gated ligand conduction, Biochim Biophys Acta 1318 (1997) 79-91.

[13] T. Yagi, X. Xu and A. Matsuno-Yagi, The energy-transducing NADH-quinone oxidoreductase (NDH-1) of *Paracoccus denitrificans*, Biochim Biophys Acta 1101 (1992) 181-3.

[14] U. Weidner, S. Geier, A. Ptock, T. Friedrich, H. Leif and H. Weiss, The gene locus of the proton-translocating NADH: ubiquinone oxidoreductase in *Escherichia coli*. Organization of the 14 genes and relationship between the derived proteins and subunits of mitochondrial complex I, J Mol Biol 233 (1993) 109-22.

[15] T. Friedrich, The NADH:ubiquinone oxidoreductase (complex I) from *Escherichia coli*, Biochim Biophys Acta 1364 (1998) 134-46.

[16] T. Yano, S.S. Chu, V.D. Sled, T. Ohnishi and T. Yagi, The proton-translocating NADH-quinone oxidoreductase (NDH-1) of thermophilic bacterium *Thermus thermophilus* HB-8. Complete DNA sequence of the gene cluster and thermostable properties of the expressed NQO2 subunit, J Biol Chem 272 (1997) 4201-11.

[17] C.D. Archer and T. Elliott, Transcriptional control of the nuo operon which encodes the energy-conserving NADH dehydrogenase of *Salmonella typhimurium*, J Bacteriol 177 (1995) 2335-42.

[18] A. Dupuis, M. Chevallet, E. Darrouzet, H. Duborjal, J. Lunardi and J.P. Issartel, The complex I from *Rhodobacter capsulatus*, Biochim Biophys Acta 1364 (1998) 147-65.

[19] G. Peng, G. Fritzsch, V. Zickermann, H. Schagger, R. Mentele, F. Lottspeich, M. Bostina, M. Radermacher, R. Huber, K.O. Stetter and H. Michel, Isolation, characterization and electron microscopic single particle analysis of the NADH:ubiquinone oxidoreductase (complex I) from the hyperthermophilic eubacterium *Aquifex aeolicus*, Biochemistry 42 (2003) 3032-9.

[20] M. Braun, S. Bungert and T. Friedrich, Characterization of the overproduced NADH dehydrogenase fragment of the NADH:ubiquinone oxidoreductase (complex I) from *Escherichia coli*, Biochemistry 37 (1998) 1861-7.

[21] M.A. Clark, L. Baumann and P. Baumann, *Buchnera aphidicola* (endosymbiont of aphids) contains nuoC(D) genes that encode subunits of NADH dehydrogenase, Curr Microbiol 35 (1997) 122-3.

[22] V. Guenebaut, A. Schlitt, H. Weiss, K. Leonard and T. Friedrich, Consistent structure between bacterial and mitochondrial NADH:ubiquinone oxidoreductase (complex I), J Mol Biol 276 (1998) 105-12.

[23] B. Bottcher, D. Scheide, M. Hesterberg, L. Nagel-Steger and T. Friedrich, A novel, enzymatically active conformation of the *Escherichia coli* NADH:ubiquinone oxidoreductase (complex I), J Biol Chem 277 (2002) 17970-7.

[24] L.A. Sazanov, J. Carroll, P. Holt, L. Toime and I.M. Fearnley, A role for native lipids in the stabilization and two-dimensional crystallization of the *Escherichia coli* NADH-ubiquinone oxidoreductase (complex I), J Biol Chem 278 (2003) 19483-91.

[25] E. Screpanti and C. Hunte, Discontinuous membrane helices in transport proteins and their correlation with function, J Struct Biol 159 (2007) 261-7.

[26] P.J. Holt, D.J. Morgan and L.A. Sazanov, The location of NuoL and NuoM subunits in the membrane domain of the *Escherichia coli* complex I: implications for the mechanism of proton pumping, J Biol Chem 278 (2003) 43114-20.

[27] S. Di Bernardo and T. Yagi, Direct interaction between a membrane domain subunit and a connector subunit in the H(+)-translocating NADH-quinone oxidoreductase, FEBS Lett 508 (2001) 385-8.

[28] P.K. Sinha, J. Torres-Bacete, E. Nakamaru-Ogiso, N. Castro-Guerrero, A. Matsuno-Yagi and T. Yagi, Critical roles of subunit NuoH (ND1) in the assembly of peripheral subunits with the membrane domain of *Escherichia coli* NDH-1, J Biol Chem 284 (2009) 9814-23.

[29] F. Schuler and J.E. Casida, Functional coupling of PSST and ND1 subunits in NADH:ubiquinone oxidoreductase established by photoaffinity labeling, Biochim Biophys Acta 1506 (2001) 79-87.

[30] E.A. Baranova, D.J. Morgan and L.A. Sazanov, Single particle analysis confirms distal location of subunits NuoL and NuoM in *Escherichia coli* complex I, J Struct Biol 159 (2007) 238-42.

[31] A.A. Arteni, P. Zhang, N. Battchikova, T. Ogawa, E.M. Aro and E.J. Boekema, Structural characterization of NDH-1 complexes of *Thermosynechococcus elongatus* by single particle electron microscopy, Biochim Biophys Acta 1757 (2006) 1469-75.

[32] U. Brandt, Energy converting NADH:quinone oxidoreductase (complex I), Annu Rev Biochem 75 (2006) 69-92.

[33] M. Radermacher, T. Ruiz, T. Clason, S. Benjamin, U. Brandt and V. Zickermann, The three-dimensional structure of complex I from *Yarrowia lipolytica*: a highly dynamic enzyme, J Struct Biol 154 (2006) 269-79.

[34] N. Grigorieff, Three-dimensional structure of bovine NADH:ubiquinone oxidoreductase (complex I) at 22 A in ice, J Mol Biol 277 (1998) 1033-46.

[35] S. Baumer, T. Ide, C. Jacobi, A. Johann, G. Gottschalk and U. Deppenmeier, The $F_{420}H_2$ dehydrogenase from *Methanosarcina mazei* is a Redox-driven proton pump closely related to NADH dehydrogenases, J Biol Chem 275 (2000) 17968-73.

[36] J. Kunow, D. Linder, K.O. Stetter and R.K. Thauer, $F_{420}H_2$: quinone oxidoreductase from *Archaeoglobus fulgidus*. Characterization of a membrane-bound multisubunit complex containing FAD and iron-sulfur clusters, Eur J Biochem 223 (1994) 503-11.

[37] L.A. Sazanov, P.A. Burrows and P.J. Nixon, The plastid ndh genes code for an NADH-specific dehydrogenase: isolation of a complex I analogue from pea thylakoid membranes, Proc Natl Acad Sci U S A 95 (1998) 1319-24.

[38] R. Hedderich, Energy-converting [NiFe] hydrogenases from archaea and extremophiles: ancestors of complex I, J Bioenerg Biomembr 36 (2004) 65-75.

[39] R. Sapra, K. Bagramyan and M.W. Adams, A simple energy-conserving system: proton reduction coupled to proton translocation, Proc Natl Acad Sci U S A 100 (2003) 7545-50.

[40] T. Friedrich and H. Weiss, Modular evolution of the respiratory NADH:ubiquinone oxidoreductase and the origin of its modules, J Theor Biol 187 (1997) 529-40.

[41] C. Mathiesen and C. Hagerhall, Transmembrane topology of the NuoL, M and N subunits of NADH:quinone oxidoreductase and their homologues among membrane-bound hydrogenases and bona fide antiporters, Biochim Biophys Acta 1556 (2002) 121-32.

[42] S.P. Albracht and R. Hedderich, Learning from hydrogenases: location of a proton pump and of a second FMN in bovine NADH--ubiquinone oxidoreductase (Complex I), FEBS Lett 485 (2000) 1-6.

[43] T. Ohnishi, Iron-sulfur clusters/semiquinones in complex I, Biochim Biophys Acta 1364 (1998) 186-206.

[44] T. Rasmussen, D. Scheide, B. Brors, L. Kintscher, H. Weiss and T. Friedrich, Identification of two tetranuclear FeS clusters on the ferredoxin-

type subunit of NADH:ubiquinone oxidoreductase (complex I), Biochemistry 40 (2001) 6124-31.

[45] E. Nakamaru-Ogiso, T. Yano, T. Yagi and T. Ohnishi, Characterization of the iron-sulfur cluster N7 (N1c) in the subunit NuoG of the proton-translocating NADH-quinone oxidoreductase from *Escherichia coli*, J Biol Chem 280 (2005) 301-7.

[46] V.D. Sled, T. Friedrich, H. Leif, H. Weiss, S.W. Meinhardt, Y. Fukumori, M.W. Calhoun, R.B. Gennis and T. Ohnishi, Bacterial NADH-quinone oxidoreductases: iron-sulfur clusters and related problems, J Bioenerg Biomembr 25 (1993) 347-56.

[47] M.L. Verkhovskaya, N. Belevich, L. Euro, M. Wikstrom and M.I. Verkhovsky, Real-time electron transfer in respiratory complex I, Proc Natl Acad Sci U S A 105 (2008) 3763-7.

[48] G. Yakovlev, T. Reda and J. Hirst, Reevaluating the relationship between EPR spectra and enzyme structure for the iron sulfur clusters in NADH:quinone oxidoreductase, Proc Natl Acad Sci U S A 104 (2007) 12720-5.

[49] M.M. Roessler, M.S. King, A.J. Robinson, F.A. Armstrong, J. Harmer and J. Hirst, Direct assignment of EPR spectra to structurally defined iron-sulfur clusters in complex I by double electron-electron resonance, Proc Natl Acad Sci U S A 107 1930-5.

[50] K. Shinzawa-Itoh, J. Seiyama, H. Terada, R. Nakatsubo, K. Naoki, Y. Nakashima and S. Yoshikawa, Bovine heart NADH-ubiquinone oxidoreductase contains one molecule of ubiquinone with ten isoprene units as one of the cofactors, Biochemistry 49 487-92.

[51] T. Yano, S. Magnitsky and T. Ohnishi, Characterization of the complex I-associated ubisemiquinone species: toward the understanding of their functional roles in the electron/proton transfer reaction, Biochim Biophys Acta 1459 (2000) 299-304.

[52] T. Yano, W.R. Dunham and T. Ohnishi, Characterization of the delta muH+-sensitive ubisemiquinone species (SQ(Nf)) and the interaction with cluster N2: new insight into the energy-coupled electron transfer in complex I, Biochemistry 44 (2005) 1744-54.

[53] M.M. Pereira, T.M. Bandeiras, A.S. Fernandes, R.S. Lemos, A.M. Melo and M. Teixeira, Respiratory chains from aerobic thermophilic prokaryotes, J Bioenerg Biomembr 36 (2004) 93-105.

[54] B. Soballe and R.K. Poole, Microbial ubiquinones: multiple roles in respiration, gene regulation and oxidative stress management, Microbiology 145 (Pt 8) (1999) 1817-30.

[55] H. Suzuki and T.E. King, Evidence of an ubisemiquinone radical(s) from the NADH-ubiquinone reductase of the mitochondrial respiratory chain, J Biol Chem 258 (1983) 352-8.

[56] S. Magnitsky, L. Toulokhonova, T. Yano, V.D. Sled, C. Hagerhall, V.G. Grivennikova, D.S. Burbaev, A.D. Vinogradov and T. Ohnishi, EPR characterization of ubisemiquinones and iron-sulfur cluster N2, central

components of the energy coupling in the NADH-ubiquinone oxidoreductase (complex I) in situ, J Bioenerg Biomembr 34 (2002) 193-208.
[57] A.D. Vinogradov, V.D. Sled, D.S. Burbaev, V.G. Grivennikova, I.A. Moroz and T. Ohnishi, Energy-dependent Complex I-associated ubisemiquinones in submitochondrial particles, FEBS Lett 370 (1995) 83-7.
[58] J.G. Okun, P. Lummen and U. Brandt, Three classes of inhibitors share a common binding domain in mitochondrial complex I (NADH:ubiquinone oxidoreductase), J Biol Chem 274 (1999) 2625-30.
[59] M.A. Tocilescu, U. Fendel, K. Zwicker, S. Drose, S. Kerscher and U. Brandt, The role of a conserved tyrosine in the 49-kDa subunit of complex I for ubiquinone binding and reduction, Biochim Biophys Acta.
[60] N. Kashani-Poor, K. Zwicker, S. Kerscher and U. Brandt, A central functional role for the 49-kDa subunit within the catalytic core of mitochondrial complex I, J Biol Chem 276 (2001) 24082-7.
[61] F. Schuler, T. Yano, S. Di Bernardo, T. Yagi, V. Yankovskaya, T.P. Singer and J.E. Casida, NADH-quinone oxidoreductase: PSST subunit couples electron transfer from iron-sulfur cluster N2 to quinone, Proc Natl Acad Sci U S A 96 (1999) 4149-53.
[62] P. Dimroth, Primary sodium ion translocating enzymes, Biochim Biophys Acta 1318 (1997) 11-51.
[63] N. Fisher and P.R. Rich, A motif for quinone binding sites in respiratory and photosynthetic systems, J Mol Biol 296 (2000) 1153-62.
[64] S. Sherwood and J. Hirst, Investigation of the mechanism of proton translocation by NADH:ubiquinone oxidoreductase (complex I) from bovine heart mitochondria: does the enzyme operate by a Q-cycle mechanism?, Biochem J 400 (2006) 541-50.
[65] M. Degli Esposti, Inhibitors of NADH-ubiquinone reductase: an overview, Biochim Biophys Acta 1364 (1998) 222-35.
[66] J.R. Tormo and E. Estornell, New evidence for the multiplicity of ubiquinone- and inhibitor-binding sites in the mitochondrial complex I, Arch Biochem Biophys 381 (2000) 241-6.
[67] U. Fendel, M.A. Tocilescu, S. Kerscher and U. Brandt, Exploring the inhibitor binding pocket of respiratory complex I, Biochim Biophys Acta 1777 (2008) 660-5.
[68] A. Vercesi, B. Reynafarje and A.L. Lehninger, Stoichiometry of H^+ ejection and Ca^{2+} uptake coupled to electron transport in rat heart mitochondria, J Biol Chem 253 (1978) 6379-85.
[69] T. Pozzan, F. Di Virgilio, M. Bragadin, V. Miconi and G.F. Azzone, H+/site, charge/site, and ATP/site ratios in mitochondrial electron transport, Proc Natl Acad Sci U S A 76 (1979) 2123-7.
[70] M.K. Al-Shawi and M.D. Brand, Steady-state H^+/O stoichiometry of liver mitochondria, Biochem J 200 (1981) 539-46.
[71] F. Di Virgilio and G.F. Azzone, Activation of site I redox-driven H^+ pump by exogenous quinones in intact mitochondria, J Biol Chem 257 (1982) 4106-13.

[72] M. Wikstrom, Two protons are pumped from the mitochondrial matrix per electron transferred between NADH and ubiquinone, FEBS Lett 169 (1984) 300-4.

[73] A.S. Galkin, V.G. Grivennikova and A.D. Vinogradov, -->$H^+/2e^-$ stoichiometry in NADH-quinone reductase reactions catalyzed by bovine heart submitochondrial particles, FEBS Lett 451 (1999) 157-61.

[74] A. Galkin, S. Drose and U. Brandt, The proton pumping stoichiometry of purified mitochondrial complex I reconstituted into proteoliposomes, Biochim Biophys Acta 1757 (2006) 1575-81.

[75] A.V. Bogachev, R.A. Murtazina and V.P. Skulachev, H^+/e^- stoichiometry for NADH dehydrogenase I and dimethyl sulfoxide reductase in anaerobically grown *Escherichia coli* cells, J Bacteriol 178 (1996) 6233-7.

[76] W. Krebs, J. Steuber, A.C. Gemperli and P. Dimroth, Na^+ translocation by the NADH:ubiquinone oxidoreductase (complex I) from *Klebsiella pneumoniae*, Mol Microbiol 33 (1999) 590-8.

[77] A.C. Gemperli, P. Dimroth and J. Steuber, The respiratory complex I (NDH I) from *Klebsiella pneumoniae*, a sodium pump, J Biol Chem 277 (2002) 33811-7.

[78] J. Steuber, C. Schmid, M. Rufibach and P. Dimroth, Na^+ translocation by complex I (NADH:quinone oxidoreductase) of *Escherichia coli*, Mol Microbiol 35 (2000) 428-34.

[79] P.C. Lin, A. Puhar and J. Steuber, NADH oxidation drives respiratory Na^+ transport in mitochondria from *Yarrowia lipolytica*, Arch Microbiol 190 (2008) 471-80.

[80] J. Steuber, The C-terminally truncated NuoL subunit (ND5 homologue) of the Na^+-dependent complex I from *Escherichia coli* transports Na^+, J Biol Chem 278 (2003) 26817-22.

[81] A.C. Gemperli, C. Schaffitzel, C. Jakob and J. Steuber, Transport of Na(+) and K (+) by an antiporter-related subunit from the *Escherichia coli* NADH dehydrogenase I produced in *Saccharomyces cerevisiae*, Arch Microbiol 188 (2007) 509-21.

[82] Y.V. Bertsova and A.V. Bogachev, The origin of the sodium-dependent NADH oxidation by the respiratory chain of *Klebsiella pneumoniae*, FEBS Lett 563 (2004) 207-12.

[83] S. Stolpe and T. Friedrich, The *Escherichia coli* NADH:ubiquinone oxidoreductase (complex I) is a primary proton pump but may be capable of secondary sodium antiport, J Biol Chem 279 (2004) 18377-83.

[84] C.C. Moser, T.A. Farid, S.E. Chobot and P.L. Dutton, Electron tunneling chains of mitochondria, Biochim Biophys Acta 1757 (2006) 1096-109.

[85] A.D. Vinogradov, Respiratory complex I: structure, redox components, and possible mechanisms of energy transduction, Biochemistry (Mosc) 66 (2001) 1086-97.

[86] K. Zwicker, A. Galkin, S. Drose, L. Grgic, S. Kerscher and U. Brandt, The Redox-Bohr group associated with iron-sulfur cluster N2 of complex I, J Biol Chem 281 (2006) 23013-7.

[87] L. Euro, G. Belevich, M.I. Verkhovsky, M. Wikstrom and M. Verkhovskaya, Conserved lysine residues of the membrane subunit NuoM are involved in energy conversion by the proton-pumping NADH:ubiquinone oxidoreductase (Complex I), Biochim Biophys Acta 1777 (2008) 1166-72.

[88] J. Steuber, Na(+) translocation by bacterial NADH:quinone oxidoreductases: an extension to the complex-I family of primary redox pumps, Biochim Biophys Acta 1505 (2001) 45-56.

[89] T. Friedrich, Complex I: a chimaera of a redox and conformation-driven proton pump?, J Bioenerg Biomembr 33 (2001) 169-77.

[90] L.A. Sazanov and J.E. Walker, Cryo-electron crystallography of two sub-complexes of bovine complex I reveals the relationship between the membrane and peripheral arms, J Mol Biol 302 (2000) 455-64.

[91] T. Pohl, D. Schneider, R. Hielscher, S. Stolpe, K. Dorner, M. Kohlstadt, B. Bottcher, P. Hellwig and T. Friedrich, Nucleotide-induced conformational changes in the *Escherichia coli* NADH:ubiquinone oxidoreductase (complex I), Biochem Soc Trans 36 (2008) 971-5.

[92] A.A. Mamedova, P.J. Holt, J. Carroll and L.A. Sazanov, Substrate-induced conformational change in bacterial complex I, J Biol Chem 279 (2004) 23830-6.

[93] A.S. Fernandes, M.M. Pereira and M. Teixeira, Purification and characterization of the complex I from the respiratory chain of *Rhodothermus marinus*, J Bioenerg Biomembr 34 (2002) 413-21.

[94] A.S. Fernandes, F.L. Sousa, M. Teixeira and M.M. Pereira, Electron paramagnetic resonance studies of the iron-sulfur centers from complex I of *Rhodothermus marinus*, Biochemistry 45 (2006) 1002-8.

[95] S.J. Kerscher, Diversity and origin of alternative NADH:ubiquinone oxidoreductases, Biochim Biophys Acta 1459 (2000) 274-83.

[96] C. Desplats, F. Mus, S. Cuine, E. Billon, L. Cournac and G. Peltier, Characterization of Nda2, a plastoquinone-reducing type II NAD(P)H dehydrogenase in chlamydomonas chloroplasts, J Biol Chem 284 (2009) 4148-57.

[97] J. Liu, T.A. Krulwich and D.B. Hicks, Purification of two putative type II NADH dehydrogenases with different substrate specificities from alkaliphilic *Bacillus pseudofirmus* OF4, Biochim Biophys Acta 1777 (2008) 453-61.

[98] F. Mus, L. Cournac, V. Cardettini, A. Caruana and G. Peltier, Inhibitor studies on non-photochemical plastoquinone reduction and H(2) photoproduction in *Chlamydomonas reinhardtii*, Biochim Biophys Acta 1708 (2005) 322-32.

[99] S.S. Lin, S. Kerscher, A. Saleh, U. Brandt, U. Gross and W. Bohne, The *Toxoplasma gondii* type-II NADH dehydrogenase TgNDH2-I is inhibited by 1-hydroxy-2-alkyl-4(1H)quinolones, Biochim Biophys Acta 1777 (2008) 1455-62.

[100] T. Yamashita, E. Nakamaru-Ogiso, H. Miyoshi, A. Matsuno-Yagi and T. Yagi, Roles of bound quinone in the single subunit NADH-quinone

oxidoreductase (Ndi1) from *Saccharomyces cerevisiae*, J Biol Chem 282 (2007) 6012-20.

[101] T. Yano, L.S. Li, E. Weinstein, J.S. Teh and H. Rubin, Steady-state kinetics and inhibitory action of antitubercular phenothiazines on mycobacterium tuberculosis type-II NADH-menaquinone oxidoreductase (NDH-2), J Biol Chem 281 (2006) 11456-63.

[102] A. Eschemann, A. Galkin, W. Oettmeier, U. Brandt and S. Kerscher, HDQ (1-hydroxy-2-dodecyl-4(1H)quinolone), a high affinity inhibitor for mitochondrial alternative NADH dehydrogenase: evidence for a ping-pong mechanism, J Biol Chem 280 (2005) 3138-42.

[103] R. Schmid and D.L. Gerloff, Functional properties of the alternative NADH:ubiquinone oxidoreductase from *E. coli* through comparative 3-D modelling, FEBS Lett 578 (2004) 163-8.

[104] C.K. Dong, V. Patel, J.C. Yang, J.D. Dvorin, M.T. Duraisingh, J. Clardy and D.F. Wirth, Type II NADH dehydrogenase of the respiratory chain of *Plasmodium falciparum* and its inhibitors, Bioorg Med Chem Lett 19 (2009) 972-5.

[105] J. Fang and D.S. Beattie, External alternative NADH dehydrogenase of *Saccharomyces cerevisiae*: a potential source of superoxide, Free Radic Biol Med 34 (2003) 478-88.

[106] T. Mogi, K. Matsushita, Y. Murase, K. Kawahara, H. Miyoshi, H. Ui, K. Shiomi, S. Omura and K. Kita, Identification of new inhibitors for alternative NADH dehydrogenase (NDH-II), FEMS Microbiol Lett 291 (2009) 157-61.

[107] S. Kerscher, S. Drose, V. Zickermann and U. Brandt, The three families of respiratory NADH dehydrogenases, Results Probl Cell Differ 45 (2008) 185-222.

[108] Y.V. Bertsova, A.V. Bogachev and V.P. Skulachev, Noncoupled NADH:ubiquinone oxidoreductase of *Azotobacter vinelandii* is required for diazotrophic growth at high oxygen concentrations, J Bacteriol 183 (2001) 6869-74.

[109] L. Rodriguez-Montelongo, S.I. Volentini, R.N. Farias, E.M. Massa and V.A. Rapisarda, The Cu(II)-reductase NADH dehydrogenase-2 of *Escherichia coli* improves the bacterial growth in extreme copper concentrations and increases the resistance to the damage caused by copper and hydroperoxide, Arch Biochem Biophys 451 (2006) 1-7.

[110] C.A. Howitt, P.K. Udall and W.F. Vermaas, Type 2 NADH dehydrogenases in the cyanobacterium *Synechocystis* sp. strain PCC 6803 are involved in regulation rather than respiration, J Bacteriol 181 (1999) 3994-4003.

[111] A.V. Bogachev and M.I. Verkhovsky, Na(+)-Translocating NADH:quinone oxidoreductase: progress achieved and prospects of investigations, Biochemistry (Mosc) 70 (2005) 143-9.

[112] B. Barquera, W. Zhou, J.E. Morgan and R.B. Gennis, Riboflavin is a component of the Na+-pumping NADH-quinone oxidoreductase from *Vibrio cholerae*, Proc Natl Acad Sci U S A 99 (2002) 10322-4.

[113] W. Zhou, Y.V. Bertsova, B. Feng, P. Tsatsos, M.L. Verkhovskaya, R.B. Gennis, A.V. Bogachev and B. Barquera, Sequencing and preliminary characterization of the Na^+-translocating NADH:ubiquinone oxidoreductase from *Vibrio harveyi*, Biochemistry 38 (1999) 16246-52.

[114] X.D. Pfenninger-Li, S.P. Albracht, R. van Belzen and P. Dimroth, NADH:ubiquinone oxidoreductase of *Vibrio alginolyticus*: purification, properties, and reconstitution of the Na^+ pump, Biochemistry 35 (1996) 6233-42.

[115] T. Unemoto and M. Hayashi, Sodium-transport NADH-quinone reductase of a marine *Vibrio alginolyticus*, J Bioenerg Biomembr 21 (1989) 649-62.

[116] O. Juarez, J.E. Morgan and B. Barquera, The Electron Transfer Pathway of the Na^+-pumping NADH:Quinone Oxidoreductase from *Vibrio cholerae*, J Biol Chem 284 (2009) 8963-72.

[117] A.V. Bogachev, Y.V. Bertsova, O. Aitio, P. Permi and M.I. Verkhovsky, Redox-dependent sodium binding by the Na(+)-translocating NADH:quinone oxidoreductase from *Vibrio harveyi*, Biochemistry 46 (2007) 10186-91.

[118] A.V. Bogachev, L.V. Kulik, D.A. Bloch, Y.V. Bertsova, M.S. Fadeeva and M.I. Verkhovsky, Redox properties of the prosthetic groups of Na(+)-translocating nadh:quinone oxidoreductase. 1. Electron paramagnetic resonance study of the enzyme, Biochemistry 48 (2009) 6291-8.

[119] A.V. Bogachev, R.A. Murtazina and V.P. Skulachev, The Na^+/e^- stoichiometry of the Na+-motive NADH:quinone oxidoreductase in *Vibrio alginolyticus*, FEBS Lett 409 (1997) 475-7.

1.3

Sodium/Proton Antiporters

Chapter 1: Energy Transduction in Biological Membranes

Section 1.3 – Sodium/proton antiporters

1.3.1 - INTRODUCTION

Sodium extrusion is important not only for the generation of a sodium gradient, which is used as the driving force for a variety of secondary Na^+-linked systems, but is also important for preventing the accumulation in the cytoplasm of sodium ions at toxic levels, which may inhibit protein synthesis [1]. Na^+/H^+ antiporters are membrane proteins that transport Na^+ and H^+ in opposite directions across the membrane. These proteins play a key role in pH and Na^+ homeostasis of prokaryotic and eukaryotic cells. Examples of such type of antiporters are the multiple resistance and pH related antiporter (Mrp). As described in the previous section, these antiporters are related to several membrane subunits of complex I and will be introduced in this section.

1.3.2 – MULTIPLE RESISTANCE AND pH RELATED ANTIPORTER (Mrp)

Mrp systems [4], also known as multisubunit Na^+/H^+ antiporter (Mnh) [5], as pH adaptation (Pha) system [6] and as sodium-hydrogen antiporter (Sha) [7], promote the transport of monovalent cations such as Na^+, K^+ and Li^+ in a coupled reaction that transports protons to the opposite direction. This type of antiporter has been found in many alkalophilic and mesophilic bacteria as well as in archaea [5, 6, 8-11]. Mrp antiporters are classified in their own family, the cation/proton antiporter-3 family due to their structural and functional properties. This type of antiporters was first identified in *Bacillus (B.) halodurans* C-125 being its presence crucial for cytoplasmatic pH homeostasis in this alkaliphilic bacterium [8, 12]. Besides the Na^+-dependent pH homeostasis function, other physiological roles have

been suggested for the Mrp system such as its requirement in symbiotic nitrogen fixation [6] and in the initial steps of sporulation [7], pathogenesis [10], arsenite oxidation [13], bile salt resistance [4, 14, 15] and photosynthesis [11].

Most of the Na^+/H^+ antiporters are encoded by single genes. However, the *mrp* gene cluster has typically seven genes encoding different integral membrane proteins, named MrpA to G, that are likely to be coordinately expressed as an operon [4-6, 14]. Two main groups of *mrp* operons are considered based on their gene organization (Figure 1.3.1). The major difference between the two groups lies in the arrangement of *mrpA* and *mrpB* genes that are separated in group 1 but fused in group 2 [2, 9]. In some cases, the operon can be organized in a different gene order and also gene duplications may occur [9]. Some organisms contain a second *mrp* operon suggested to have different products, whose physiological role is not known [9, 16].

mrp operons

Organism	Accession #
Group 1	
Bacillus pseudofirmus OF4	AAF21812 ~ AAF21818
Bacillus halodurans C-125	NP_242179 ~ NP_242185
Bacillus clausii KSM-K16	YP_174287 ~ YP_174293
Staphylococcus aureus subsp. aureus COL	YP_185818 ~ YP_185824
Bacillus subtilis subsp. subtilis str. 168	NP_391038 ~ NP_391044
Group 2	
Pseudomonas aeruginosa PAO1	NP_249745 ~ NP_249750
Vibrio cholerae O1 biovar eltor str. N16961	NP_232552 ~ NP_232557

Figure 1.3.1 - Examples of the different mrp operon types (Adapted from [2])

At the present, almost no biochemical information of the individual Mrp subunits exists. However, mutagenic studies reveal that the subunit MrpA should be the major responsible for the transport activity since its

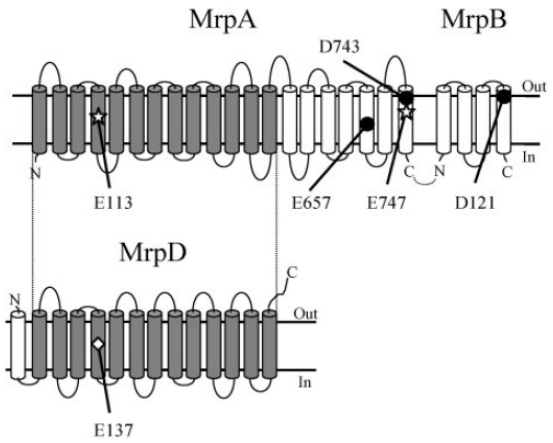

Figure 1.3.2 - Schematic representation of the secondary structure of Mrp A, B and D, highlighting the positions of the proposed amino acid residues important for the Mrp antiport activity. The two possible Na^+ binding residues Glu-113 and Glu747 of MrpA are indicated by stars. Glu-657, Asp743 of MrpA; Asp-121 of MrpB and Glu-137 of MrpD are indicated by dots or diamond (Adapted from [3]).

over-expression elevates the Na^+ resistance more than the over-expression of any of the other *mrp* genes [4, 14]. Also point mutations in the *mrpA* gene resulted in loss of the antiport activity [8, 10, 17]. Mutations in the predicted transmembrane amino acid residues Glu-113, Glu-657, Asp-743 and Glu-747 (*B. subtilis* MrpA numbering) abolish the antiport activity showing its importance in the ion transport process (Figure 1.3.2) [3, 17]. It was observed that the residues Glu-113 and Glu-747 are irreplaceable whereas in the case of Glu-657 and Asp-743 substitution by other amino acid containing a carboxyl group is sufficient to recover the activity [3]. It was shown that MrpD subunit is important at high pH but its over-expression does not increase the Na^+-resistance and thus it is unlikely that this subunit alone is an antiporter [14]. Nevertheless, mutations in Glu-137 of MrpD (*B. subtilis* MrpD numbering) abolish the antiport activity (Figure 1.3.2) [3]. This residue is localized at the corresponding position of MrpA Glu-113 but contrarily to it this residue is not totally irreplaceable because the presence of a carboxyl group is sufficient

to partially recover the antiport activity [3]. Interestingly, the complex I subunits homologous to the Mrp proteins, the subunits Nqo12 to 14, also have a glutamate localized at the corresponding position of MrpA Glu-133 (Noq12) and MrpD Glu-137 (Nqo13 and 14), which were also suggested to be involved in ion transport [18]. Apparently, MrpB has also an essential role in the ion transport process since a mutation in the residue Asp-121 (*B. subtilis* MrpB numbering) inhibits the antiport activity (Figure 1.3.2). However (and again) only the presence of a carboxyl group is demanded [3]. Based on these mutagenic studies, it was suggested that the subunits MrpA, MrpB and MrpD form the ion translocation pathway but no antiport activity was detected in an MrpA-to-MrpD sub-complex present in the *B. pseudofirmus* membranes [19]. Concerning other Mrp subunits, MrpF has been implicated in cholate and Na^+ efflux [4, 14] and a role as chaperone or assembler was hypothesized for MrpG and MrpE [4]. Nevertheless, all the Mrp subunits are, apparently, required for an optimal Na^+/H^+ antiport activity [5, 14, 19]. Based on this, the Mrp systems have been proposed to function as a multisubunit transporter [5]. This hypothesis was further supported by blue native electrophoresis and imunoblotting analyses whereas an active complex formation by the *mrpABCDEFG* gene products was showed [19, 20]. Other observation that reinforces the multisubunit form is the presence of MrpA, MrpD and MrpC homologous subunits in Complex I [21, 22].

The Mrp system operates as a typical secondary antiporter that is energized by respiration-dependent or artificially imposed $\Delta\tilde{\mu}_{H^+}$ [4, 5, 8, 14]. It has been shown that this type of antiporter is electrogenic as more than one H^+ is translocated per cation [15, 16]. The Mrp sytems in *Staphylococcus aureus*, in several *Bacillus* species and in *Vibrio cholerae* are $Na^+(Li^+)/H^+$ electrogenic antiporters with low (in the case of *V. cholera*) or no detected K^+ transport activity [15, 16]. On the contrary, the Mrp system of *Sinorhizobium melioti*

seems to be a K^+/H^+ antiporter with a low Na^+/H^+ transport activity [23]. The molecular mechanism for cation discrimination is still completely unknown.

1.3.3 – REFERENCES

[1] G. Speelmans, Na^+ and energy transduction in the thermophile *Clostridium fervidus*, Department of Microbiology, University of Groningen, Groningen, 1993.

[2] J. Liu, T.A. Krulwich and D.B. Hicks, Purification of two putative type II NADH dehydrogenases with different substrate specificities from alkaliphilic *Bacillus pseudofirmus* OF4, Biochim Biophys Acta 1777 (2008) 453-61.

[3] Y. Kajiyama, M. Otagiri, J. Sekiguchi, T. Kudo and S. Kosono, The MrpA, MrpB and MrpD subunits of the Mrp antiporter complex in *Bacillus subtilis* contain membrane-embedded and essential acidic residues, Microbiology 155 (2009) 2137-47.

[4] M. Ito, A.A. Guffanti, B. Oudega and T.A. Krulwich, mrp, a multigene, multifunctional locus in *Bacillus subtilis* with roles in resistance to cholate and to Na^+ and in pH homeostasis, J Bacteriol 181 (1999) 2394-402.

[5] T. Hiramatsu, K. Kodama, T. Kuroda, T. Mizushima and T. Tsuchiya, A putative multisubunit Na^+/H^+ antiporter from *Staphylococcus aureus*, J Bacteriol 180 (1998) 6642-8.

[6] P. Putnoky, A. Kereszt, T. Nakamura, G. Endre, E. Grosskopf, P. Kiss and A. Kondorosi, The pha gene cluster of *Rhizobium meliloti* involved in pH adaptation and symbiosis encodes a novel type of K^+ efflux system, Mol Microbiol 28 (1998) 1091-101.

[7] S. Kosono, Y. Ohashi, F. Kawamura, M. Kitada and T. Kudo, Function of a principal Na(+)/H(+) antiporter, ShaA, is required for initiation of sporulation in *Bacillus subtilis*, J Bacteriol 182 (2000) 898-904.

[8] T. Hamamoto, M. Hashimoto, M. Hino, M. Kitada, Y. Seto, T. Kudo and K. Horikoshi, Characterization of a gene responsible for the Na^+/H^+ antiporter system of alkalophilic *Bacillus* species strain C-125, Mol Microbiol 14 (1994) 939-46.

[9] T.H. Swartz, S. Ikewada, O. Ishikawa, M. Ito and T.A. Krulwich, The Mrp system: a giant among monovalent cation/proton antiporters?, Extremophiles 9 (2005) 345-54.

[10] S. Kosono, K. Haga, R. Tomizawa, Y. Kajiyama, K. Hatano, S. Takeda, Y. Wakai, M. Hino and T. Kudo, Characterization of a multigene-encoded sodium/hydrogen antiporter (sha) from *Pseudomonas aeruginosa*: its involvement in pathogenesis, J Bacteriol 187 (2005) 5242-8.

[11] A. Blanco-Rivero, F. Leganes, E. Fernandez-Valiente, P. Calle and F. Fernandez-Pinas, mrpA, a gene with roles in resistance to Na^+ and

adaptation to alkaline pH in the cyanobacterium *Anabaena* sp. PCC7120, Microbiology 151 (2005) 1671-82.

[12] T. Kudo, M. Hino, M. Kitada and K. Horikoshi, DNA sequences required for the alkalophily of *Bacillus* sp. strain C-125 are located close together on its chromosomal DNA, J Bacteriol 172 (1990) 7282-3.

[13] D.R. Kashyap, L.M. Botero, C. Lehr, D.J. Hassett and T.R. McDermott, A Na^+:H^+ antiporter and a molybdate transporter are essential for arsenite oxidation in *Agrobacterium tumefaciens*, J Bacteriol 188 (2006) 1577-84.

[14] K. Shinzawa-Itoh, J. Seiyama, H. Terada, R. Nakatsubo, K. Naoki, Y. Nakashima and S. Yoshikawa, Bovine heart NADH-ubiquinone oxidoreductase contains one molecule of ubiquinone with ten isoprene units as one of the cofactors, Biochemistry 49 487-92.

[15] J. Dzioba-Winogrodzki, O. Winogrodzki, T.A. Krulwich, M.A. Boin, C.C. Hase and P. Dibrov, The *Vibrio cholerae* Mrp system: cation/proton antiport properties and enhancement of bile salt resistance in a heterologous host, J Mol Microbiol Biotechnol 16 (2009) 176-86.

[16] T.H. Swartz, M. Ito, T. Ohira, S. Natsui, D.B. Hicks and T.A. Krulwich, Catalytic properties of *Staphylococcus aureus* and *Bacillus* members of the secondary cation/proton antiporter-3 (Mrp) family are revealed by an optimized assay in an *Escherichia coli* host, J Bacteriol 189 (2007) 3081-90.

[17] S. Kosono, Y. Kajiyama, S. Kawasaki, T. Yoshinaka, K. Haga and T. Kudo, Functional involvement of membrane-embedded and conserved acidic residues in the ShaA subunit of the multigene-encoded Na^+/H^+ antiporter in *Bacillus subtilis*, Biochim Biophys Acta 1758 (2006) 627-35.

[18] J. Torres-Bacete, E. Nakamaru-Ogiso, A. Matsuno-Yagi and T. Yagi, Characterization of the NuoM (ND4) subunit in *Escherichia coli* NDH-1: conserved charged residues essential for energy-coupled activities, J Biol Chem 282 (2007) 36914-22.

[19] M. Morino, S. Natsui, T.H. Swartz, T.A. Krulwich and M. Ito, Single gene deletions of mrpA to mrpG and mrpE point mutations affect activity of the Mrp Na^+/H^+ antiporter of alkaliphilic *Bacillus* and formation of hetero-oligomeric Mrp complexes, J Bacteriol 190 (2008) 4162-72.

[20] Y. Kajiyama, M. Otagiri, J. Sekiguchi, S. Kosono and T. Kudo, Complex formation by the mrpABCDEFG gene products, which constitute a principal Na^+/H^+ antiporter in *Bacillus subtilis*, J Bacteriol 189 (2007) 7511-4.

[21] C. Mathiesen and C. Hagerhall, The 'antiporter module' of respiratory chain complex I includes the MrpC/NuoK subunit -- a revision of the modular evolution scheme, FEBS Lett 549 (2003) 7-13.

[22] C. Mathiesen and C. Hagerhall, Transmembrane topology of the NuoL, M and N subunits of NADH:quinone oxidoreductase and their homologues among membrane-bound hydrogenases and bona fide antiporters, Biochim Biophys Acta 1556 (2002) 121-32.

[23] T. Yamaguchi, F. Tsutsumi, P. Putnoky, M. Fukuhara and T. Nakamura, pH-dependent regulation of the multi-subunit cation/proton antiporter Pha1 system from *Sinorhizobium meliloti*, Microbiology 155 (2009) 2750-6.

PART II

RESULTS

Chapter 2

Structural Studies of R. marinus complex I

Abbreviations

A.: *Aquifex*; *E.*: *Escherichia*; *R.*: *Rhodothermus*; *T.*: *Thermus*; *T.*: *Thermosynechococcus*; *Y.*: *Yarrowia.*

ACN: acetronitrile; BN: blue native; DDM: n-dodecyl-β-D-maltoside; DMN: 2, 3-dimethyl-1,4-naphthoquinone; EM: electron microscopy; ESI: electrospray ionization; HPLC: high-performance liquid chromatography; IR: infrared; K: lysine; LC: liquid chromatography; LILBID: laser-induced liquid bead ion desorption; MALDI: matrix assisted laser desorption ionization; MPD: methylpentanediol; MS: mass spectrometry; NBT: nitroblue tetrazolium: Nqo: complex I subunits; PAGE: polyacrilamide gel electrophoresis; PCD: pterin-4α-carbinolamine dehydratase; PMF: peptide mass fingerprinting; PMSF: phenylmethanesulfonyl fluoride; Q: quinone; R: arginine; SDS: sodium dodecylsulfate; TFA: trifluoroacetic acid; TOF: time of flight.

Chapter 2: Structural Studies of *R. marinus* complex I

2.1

MALDI-TOF MS and ESI MS/MS studies of *R. marinus* complex I

This section is published as:
A.P. Batista, C. Franco, M. Mendes, A.V. Coelho, M.M. Pereira, "Subunit composition of *Rhodothermus marinus* respiratory complex I." *Analytical Biochemistry* 407 (2010) 104-110.

These studies have been performed in collaboration with the Mass Spectrometry Laboratory (ITQB).

Chapter 2: Structural Studies of *R. marinus* complex I

Section 2.1 – MALDI-TOF MS and ESI MS/MS studies of *R. marinus* complex I

2.1.1 – SUMMARY

The basic structural characterization of complex I is still not trivial due to its complexity, not only in the number of its protein constituents, but especially because of the different properties of the several subunits. Bacterial complex I generally contains 14 subunits, seven hydrophilic proteins located in the peripheral arm and seven hydrophobic proteins present in the membrane arm. It is the identification of the hydrophobic proteins that makes the characterization of complex I and of membrane proteins in general very difficult. In this work we report the identification of the subunits of complex I from *Rhodothermus marinus*. The original approach, here presented, combined several protein and peptides separation strategies (different reversed phase materials, HPLC and gel electrophoresis) with different identification methods (ESI-MS/MS, MALDI-TOF MS and Edman degradation analysis) and represents a step forward in the characterization of membrane proteins which studies are still technically highly challenging. The combination of the different methodologies allowed the identification of complex I canonical subunits and also a possible novel subunit: a pterin-4α-carbinolamine dehydratase, PCD. This was the first time that a PCD is suggested to be part of complex I and its possible regulatory role is discussed.

2.1.2 - INTRODUCTION

Complex I from *R. marinus* was isolated with one FMN and six to eight iron-sulfur centres of the $[2Fe\text{-}2S]^{2+/1+}$ and $[4Fe\text{-}4S]^{2+/1+}$ types [1, 2]. It is sensitive to the complex I inhibitor rotenone and its reconstitution in liposomes showed proton translocation coupled to NADH:quinone oxidoreductase activity. The genes coding for the Nqo subunits are organized

in two clusters, *nqo*1-7 (nqoA) and *nqo*10-14 (nqoB) and two independent genes, *nqo*8 and *nqo*9. Among nqoB genes, and co-transcribed with them, two additional genes encoding a PCD and a putative Nha-type sodium/proton antiporter were identified [3].

The polypeptide composition of complex I and the specific assembly of its subunits into a large complex are fundamental aspects to understand its function. Because complex I is composed by proteins with very different hydrophobic properties the identification of all the subunits revealed to be highly challenging. There are several methods described in the literature for membrane protein identification, including the subunits of the complex I [4-11]. However, the identification process is still not straightforward.

In order to identify the subunits of *R. marinus* complex I different methods, such as mass spectrometry (MS), Edman degradation and reverse phase high-performance liquid chromatography (HPLC), were used. The originality of our approach was based on the combination of a sequential elution of the intact and digested complex in four differently packed RP-microcolumns (POROS R1, R2, R3 and graphite) with MS analysis. The identification of the canonical subunits, as well as the PCD, was only possible by integrating the different methodologies.

2.1.3 – MATERIAL AND METHODS

A. General procedures

Cell growth and Protein Purification: Bacterial growth, membrane preparation and solubilization were done as previously described [12], excepting the presence of 100 mM glutamate in the growth medium. Protein was purified according to an established procedure [2], optimized by introducing a further chromatographic step using a Mono Q column and 20

mM Tris-HCl pH8, 1 mM phenylmethanesulfonyl fluoride (PMSF), 0.1% n-dodecyl-β-D-maltoside (DDM) as buffer. The complex was eluted in a linear gradient of 0-1M NaCl.

Analytical procedures: Protein concentration was determined by the Bicinchoninic Acid method [13]. Flavin was extracted with trichloroacetic acid [14] and its content was determined by fluorescence spectroscopy. The iron content was determined by the 2,4,6-tripyridyl-1,3,5-triazine method [15].

Catalytic activity assays: NADH:quinone oxidoreductase activity was monitored at 55 ºC, following the NADH oxidation at 330 nm (ε = 5930 M^{-1} cm^{-1}). The reaction mixture contained 100 mM potassium phosphate pH 7.5, 0.1% DDM , 20 μM 2,3-dimethyl-1,4-naphthoquinone (DMN) and 50 μM NADH. The reaction was started by the addition of complex I. In the inhibition assays, the complex was pre-incubated with rotenone (50 μM) or piericidin A (100 μM), for 5 minutes, at room temperature.

Blue Native (BN) Electrophoresis: Molecular mass of the native complex was determined by BN-PAGE, using a gradient gel (5-13%) [16].

B. <u>Protein separation</u>

Electrophoresis: Separation of the subunits was performed by tricine SDS-PAGE 12.5% or by a tricine gradient gel (10-20%) [17, 18].

HPLC: Separation by reverse-phase HPLC was performed using a C4 column (150x3.9mm, 300 Å, 5 μm spherical silica, Delta-Pak, Waters), equilibrated with 0.1% trifluoroacetic acid (TFA) and eluting with 20-100% acetronitrile (ACN), at 1mL/min (System Gold Beckman HPLC).

C. Mass spectrometry analysis

Molecular mass of complex I subunits: Purified complex I was washed (see *in-solution digestion*) to remove the detergent, concentrated (15 mg/mL) and acidified with formic acid (5%). Prior to Matrix Assisted Laser Desorption Ionization-Time of Flight Mass Spectrometry (MALDI-TOF MS) analysis, the sample was desalted and concentrated using a GELoader tip packed with POROS R1 (poly(styrene-divinylbenzene), 10 μm bead size, Applied Biosystems). Elution of the retained proteins was done either with the matrix solution (sinapinic acid in 70% ACN, 0.1% TFA) or by 10% steps of 20-100% ACN, 0.1% TFA and directly applied onto the MALDI plate using the dry droplet method. External mass calibration was performed with ProMix3 (LaserBioLabs) and CalMix3 (Applied Biosystems).

In-gel digestion: Excised gel bands from tricine-SDS-PAG were washed with 50% ACN to remove the Coomassie dye. Gel pieces were then dehydrated by incubation with ACN, evaporated by centrifugation under vacuum, and digested with trypsin (Promega; 6.7 ng/μL in 50 mM NH_4HCO_3) [19].

In-solution digestion: The complex was first washed to remove the detergent and the PMSF by cycles of concentration/dilution steps with a DDM and PMSF free buffer. In-solution digestion of the R1 microcolumn fractions was performed as described elsewhere [20].

Purification and concentration of the peptides using reversed phase microcolumns: Desalting and concentration of the acidified supernatants (5% formic acid) containing the tryptic digested peptides was carried out with custom-made chromatographic microcolumns using GELoader tips packed with POROS R2 (poly(styrene-divinylbenzene), 20 μm bead size), POROS R3 (20 μm bead size) and graphite materials [21, 22]. Peptides were either directly eluted from

the microcolumns with the matrix solution (α-ciano-4-hydroxy-trans-cinnamic acid in 70% ACN, 5% of formic acid) or by 10% steps of 20-100% ACN, 5% formic acid .

Peptide Mass Fingerprinting (PMF): Monoisotopic peptide masses were determined using MALDI-TOF MS equipment and external mass calibration was performed with Pepmix1 (LaserBioLabs). Protein identification was performed using the MASCOT software online available version (Matrix Science, UK) [23]. Searches were done on MSDB non-redundant protein sequence database (version 20050929), having the following conditions: a minimum mass accuracy of 100 ppm, one missed cleavage in peptide masses, carbamidomethylation of cysteines and oxidation of methionines as fixed and variable amino acid modifications. To accept the identification the considered criteria were: significant homology scores achieved in MASCOT, significant sequence coverage values (above 15%), and distribution of the identified peptides over the sequence. An additional criterion, the ratio between Arginine (R)/Lysine (K) terminated peptides, was used in the case of the proteins identified via manual inspection of the mass spectra. Proteins were considered if the R/K ratio was >1 [24].

Tandem mass spectrometry experiments - Micro-RP HPLC-linear ion trap MS : Peptides were concentrated and desalted on a RP precolumn (silica, 0.18x30mm, BioBasic 18, Thermo Electron) and online eluted on an analytical RP column (silica, 0.18x150 mm, BioBasic 18, Thermo Electron), at 2 μL/min. Peptides were eluted using a gradient of 5-60% solvent B (solvent A: 0.1% formic acid, 5% ACN; solvent B: 0.1% formic acid, 80% ACN). Linear ion trap was operated in data-dependent ZoomScan and MS/MS switching mode using the three most intense precursors detected in a survey scan from 450 to 1600m/z (3 microscans). Singly charged ions were excluded for MS/MS analysis. ZoomScan settings were: maximum injection time, 200

ms; zoom target parameter, 3000 ions; and the number of microscans, 3. Normalized collision energy was set to 35%, and dynamic exclusion was applied during 10s periods to avoid fragmenting each ion from each chromatographic peak more than twice.

Peptide MS/MS data was evaluated using Bioworks™ 3.3.1 software. Searches were performed against an indexed UniRef100 database (Downloaded on April of 2008, 5.888.655 entries) and a specific database containing the sequences of the proteins from *R. marinus* complex I (NCBI, accession numbers: AY972100.1; AY972822.1; Q4QSC5.1; Q4QSC6.1). The following constraints were used for the searches: tryptic cleavage after Arginine and Lysine, up to two missed cleavage sites, and tolerances of 2 Da for precursor ions and 1 Da for MS/MS fragment ions. Modifications allowed were carbamidomethylation of cysteines and oxidation of methionines as fixed and variable amino acid modifications, respectively. Only protein identifications with two or more distinct peptides, a $p<0.01$ and *Xcorr* thresholds of at least 1.5/2.0/2.5 for singly/doubly/triply charged peptides were accepted. Protein identification was further validated by manual inspections of MS/MS spectra.

Instrumentation: Intact masses and PMF experiments were performed using MALDI-TOF MS Voyager DE-STR (PerSeptive Biosystems, Framingham, USA). Tandem mass experiments were performed using either microLC-ESI linear ion trap or a Surveyor LC system coupled to a linear ion trap mass spectrometer model LTQ (Thermo-Finnigan, San Jose, USA).

D. N-terminal sequence analysis

Western Blotting and Amino acid Sequencing: For N-terminal amino acid sequence analysis, proteins separated by tricine-SDS-PAGE were transferred to a poly(vinylidene difluoride) membrane and stained with Ponceau S dye.

Sequencing was performed by automated Edman degradation in an Applied Biosystems model 491HT sequencer [25].

2.1.4 – RESULTS AND DISCUSSION

Complex I integrity and purity

The integrity of *R. marinus* complex I was investigated by NADH:DMN oxidoreductase activity, and the value of 0.4μmol NADH.min^{-1}.mg^{-1}, in the range of other isolated bacterial enzymes [26], was obtained. Decreases of 50-70% in the specific activity were observed in the presence of complex I inhibitors (rotenone or piericidin A). A flavin/complex ratio of 1 and the iron content of the complex (≈27 iron/flavin) were in agreement with the presence of one flavin, six [4Fe-4S]$^{2+/1+}$ and two [2Fe-2S]$^{2+/1+}$ centres. These quantifications indicated the presence of all the expected prosthetic groups in the purified complex. BN-PAGE revealed that the complex has an apparent molecular mass of 450(±50)kDa, which is in agreement with the sum of the predicted molecular masses of the all *R. marinus* complex I subunits.

Identification of Complex I subunits

In order to be identified, the subunits of complex I had to be separated and isolated. The process of isolating at least 14 subunits with very different hydrophobic properties is not trivial. It required the optimization of several technical procedures such as SDS-PAGE and chromatographic fractioning (HPLC and POROS R1). To facilitate the reading of the description of complex I subunits separation and identification, a graphical representation of the strategy used was included as Figure 2.1.1.

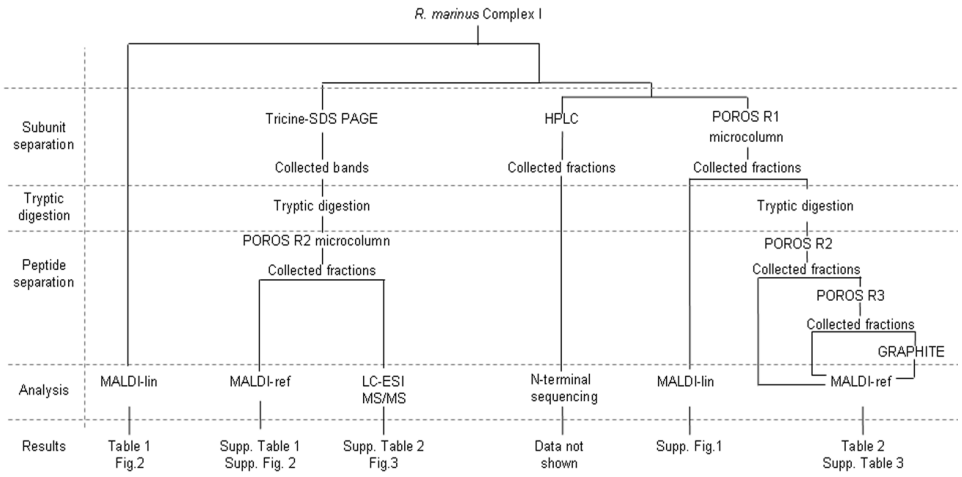

Figure 2.1.1 - Graphical representation of the strategy used for the separation and identification of complex I subunits**.** MALDI-lin: MS spectra collected using MALDI-TOF in linear mode; MALDI-ref: MS spectra collected using MALDI-TOF in reflector mode; POROS R1, R2, R3 and Graphite correspond to the different reverse phase materials used.

Determination of the intact masses of Complex I subunits

The mass spectrum of complex I in solution is shown in Figure 2.1.2. Almost all relevant m/z peaks observed in the spectrum could be assigned to the expected canonical subunits (Nqo1 to Nqo14) considering charges +1 (Table 2.1.1). The exceptions are subunits Nqo8, Nqo10, Nqo12 and Nqo14 whose predicted molecular mass could not be observed. It was shown previously that among complex I genes, and co-transcribed with them, two additional genes encoding for a PCD and a Nha-like antiporter were present [3]. The expected molecular mass for these two proteins are ~11.3 kDa and ~58.4 kDa, respectively. Peaks m/z corresponding to proteins with those compatible masses were observed in the mass spectrum. However, in the case of the antiporter, its assignment is questionable since Nqo13 has a close predicted molecular mass (58308 Da *versus* 58413 Da for the antiporter). The obtained identifications were further corroborated by elution of complex I

subunits through a POROS R1 microcolumn using a stepwise ACN gradient (Supplementary Figure 2.1.1).

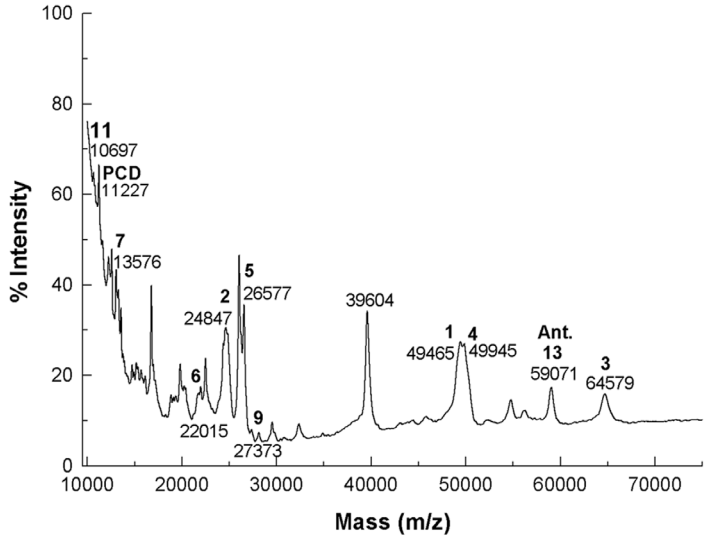

Figure 2.1.2 - MALDI mass spectrum of *R. marinus* complex I in solution. Matrix: sinapinic acid. Calibration mixture: ProMix3. The numbers refer to the respective subunit (for example, Nqo1 is represented by 1) with charge of +1. Ant: Antiporter.

Complex I subunits identified by peptide mass fingerprinting (in-gel digestion)

Subunits Nqo1 to 6 and Nqo9 were also identified by PMF after SDS-PAGE separation (Supplementary Figure 2.1.2, Supplementary Table 2.1.1). Interestingly, Nqo3, Nqo4, Nqo5 and Nqo9 subunits were identified at different positions, corresponding to the predicted molecular mass and also to higher or lower apparent molecular masses. For Nqo3, occurrence of proteolysis was excluded since the N- and C-terminal sequences were identified in all the respective bands.

Table 2.1.1 - Molecular masses of *R. marinus* complex I subunits: theoretical and determined by MALDI-TOF MS.

Subunit	Theoretical Molecular Mass (Da)[a]	Experimental Molecular Mass (Da)/MS resolution
Nqo1	49 299	49 464
Nqo2	25 042	24 846
Nqo3	64 724	64 578
Nqo4	50 186	49 944
Nqo5	26 622	26 576
Nqo6	18 676/ 21 593[b]	22 014
Nqo7	13 765	13 575
Nqo8	37 374	-
Nqo9	27 120	27 372
Nqo10	18 337	-
Nqo11	10 904	10 696
Nqo12	72 339	-
Nqo13	58 308	59 070
Nqo14	53 230	-
Antiporter	58 413	59 070
PCD	11 277	11 226

[a]Considering the gene sequences (and not considering the mass of the cofactors).
[b]Correct Molecular mass (determined after the reassignment of the N-terminal sequence).

Complex I proteins identified by LC-MS/MS (in-gel digestion)

Subunits separated by electrophoresis and subjected to trypsin digestion were also analysed by LC-ESI-MS/MS. In this way, the identification of the peripheral subunits (Nqo1-6 and Nqo9) was corroborated by sequence determination (MS/MS) (Supplementary Table 2.1.2). Furthermore, this procedure also allowed to correct the sequence of Nqo6 deposited at Uniref database. As shown in Figure 2.1.3, two of the fragmented peptides, $[MH]^+$ 2763.2 and 1099.6 helped to reassign the *N-terminal* region of Nqo6.

Complex I subunits identified by peptide mass fingerprinting (in-solution digestion)

There are several methods described in the literature for membrane proteins identification [4-11], most of which couple electrophoresis (native or

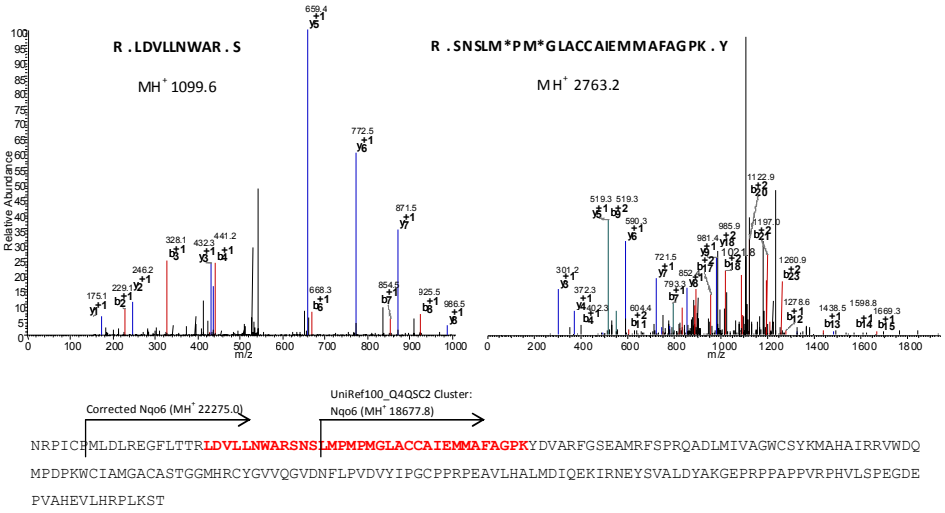

Figure 2.1.3 - MS/MS spectra of two Nqo6 peptides $[MH]^+$ of 2763.2 and 1099.6. These two peptides (highlighted) allowed to reassign the N-terminal sequence of Nqo6 in the protein database.

denaturant gels) techniques to MS analyses. In this study, this type of approach was undertaken, with success in the identification of the peripheral subunits but inefficient in the identification of the membrane subunits. The unsuccessful identification of the membrane subunits could be due to an incomplete extraction of peptides from the gel after digestion, thus a non-gel approach was undertaken. The R1 microcolumn fractions were tryptic digested and the obtained peptides were separated by sequential elution in the RP microcolumns POROS R2, POROS R3 and graphite and then analyzed by peptide mass fingerprinting. The sequential elution increased the number of peptides to be analyzed, minimizing a possible ion suppression effect, by which the best ionisable peptides mask the signal of the worst ionisable ones. The use of these three resins with different hydrophobic proprieties, allowed obtaining different peptides, which enhanced sequence coverage of the identified proteins. Subunit Nqo3 was identified in the first fractions (20-40% ACN) with sequence coverage of 60.9% (Table 2.1.2). Manual inspection of the spectra allowed the identification of other peptides with compatible

masses to other *R. marinus* complex I subunits, such as Nqo1, Nqo2, Nqo5, Nqo6 and Nqo9 (Table 2.1.2, Supplementary Table 2.1.3). The criteria used to validate the identification of a protein were amino acid sequence coverage higher than 15% and the distribution of identified peptides over the sequence. Based on these criteria the membrane subunits Nqo7, Nqo12, Nqo13, and Nqo14 were identified for the first time. Also the PCD was identified as a possible novel subunit with amino acid sequence coverage of 53%. The identification of Nqo8 or of the Nha-like antiporter were not considered since the obtained amino acid coverage were below 15% and/or the identified peptides were not well distributed in the sequence. Not surprisingly, the membrane subunits were observed in fractions that eluted at an ACN percentage higher than 40% (see also Supplementary Figure 2.1.1).

Trypsin cleaves peptide bonds specifically after the carboxyl group of arginine (R) and lysine (K) amino acid residues. It is known that the peptides that end with R are better ionized on MALDI than those that end with K [24]. This observation was used as an additional criterion to validate the results (see above Material and Methods section). The determined ratio R/K (Table 2.1.2) further supported the identification of the subunits Nqo7, Nqo12, Nqo13, Nqo14 and PCD.

Identification of the canonical subunits was expected since these proteins are necessary for a correct assemble of functional complex I. However, the identification of PCD as a possible complex I subunit was a new observation. This protein has been considered rare in prokaryotes. In fact, PCD is well characterized at the molecular-genetics level in mammals but only one bacterial example has been biochemically characterized (*Pseudomonas aeruginosa*) [27-29]. PCD is described as a bifunctional protein with catalytic and regulatory properties [27, 30]. It is involved in the regeneration of tetrahydrobiopterin, an essential cofactor of aromatic amino

Table 2.1.2 - Identification of *R. marinus* complex I subunits by PMF after sequential elution of the complex subunits with R1 and of their tryptic peptides by R2, R3 and graphite microcolumns.

% ACN for R1 elution	Subunit identified	Sequence coverage (%)	Nº of identified peptides[a]	R/K[b]
20 - 40%	Nqo1	66.14	32	3.4
20 - 30%	Nqo2	47.32	10	1.0
20 - 30%	Nqo3	60.94	38	2.4
40 - 50%	Nqo4	47.17	24	2.4
20 - 30%	Nqo5	76.96	16	4.0
20 - 60%	Nqo6	53.09	12	2.0
70 - 80%	Nqo7	17.50	3	2.0
20%	Nqo8	14.37	5	0.7
20 - 60%	Nqo9	66.09	18	1.1
-	Nqo10	-	-	-
-	Nqo11	-	-	-
60%	Nqo12	25.13	16	6.5
40 - 80%	Nqo13	19.66	9	3.0
40 - 80%	Nqo14	22.60	7	2.5
20 - 40%	Antiporter	17.27	7	0.8
60 - 70%	PCD	53.54	4	4.0

[a] considering 1 possible missed cleavage, and a peptide mass range between 720 and 5000.
[b] ratio between sequences that ends with arginine (R) or with lysine (K).

hydroxylase, and catalyses the conversion of 4α-hydroxytetrahydrobiopterin to quinoid-dihydrobiopterin. In mammals, this protein has also been shown to stabilize the dimeric homodomain transcription factor HNF1 and to enhance its activity. The relation between the enzymatic activity of PCD and its regulatory function as a dimerization cofactor of HNF1 is not understood [30]. Crystal structures showed that mammalian PCDs are tetramers (dimers of dimer configuration) whereas the bacterial ones are dimers [30]. It is believed that the regulatory function, as dimerization of transcription factor HNF1, is related with this tetramerization, having the bacterial PCD no role in transcription [27, 31]. Crystal structures, as well as site-directed mutagenesis studies and *in vivo* PCD activity assays, have shown that the motif [EDKH]-x(3)-H-[HN]-[PCS]-x(5,6)-[YWF]-x(9)-[HW]-x(8,15)-D is the signature for PCD activity [31]. This motif is present in *R. marinus* PCD

amino acid sequence (accession number: AAY42130.1); however no genes coding for a typical phenylalanine hydroxylase are present in the genome of this bacterium (www.genome.jp). This strongly suggests that the PCD may have a different function. An auxiliary role in the metabolism of molybdopterin cofactor was proposed [31]. Although no molybdopterin is present in complex I, it is believed that the Nqo3 C-terminal domain corresponded to a molybdopterin binding site of an ancestor protein [32]. Nqo3 structure revealed high flexibility and was suggested to be a possible regulatory site [33]. The presence, in *R. marinus* complex I, of a PCD may reinforce that suggestion and extend it to the involvement of PCD in a possible regulatory mechanism involving pterin like compounds. In *Salinibacter rubber* DSM 13855, a *R. marinus* closely related bacterium, the gene coding for a PCD protein is also present among complex I genes (www.genome.jp), suggesting that such protein could indeed be part of some complexes I including that of *R. marinus*. The presence of extra subunits in bacterial complex I has also been observed in the case of *T. thermophilus*, in which a frataxin-like protein has been shown to be part of its peripheral arm [33].

Complex I proteins identified by N-terminal sequencing

In parallel to mass spectrometry analyses, the proteins separated by electrophoresis and HPLC were subjected to Edman degradation allowing the identification for the first time of the membrane subunit Nqo11.

In conclusion, we have identified all the canonical subunits of complex I with the exception of Nqo8 and Nqo10 (Table 2.1.3). Nqo8 subunit has a predicted molecular mass of 37.4 kDa, which was not observed

Table 2.1.3 - Summary of the identification of complex I subunits by the different methodologies employed in this study.

Subunit	**Theoretical Molecular Mass (Da)**[a]	**MALDI Linear mode** (whole complex)	**LC-ESI-MS/MS** (in-gel trypsin digestion)	**MALDI-TOF** Peptide mass fingerprint (Subunit separated by sequential elution, and trypsin digestion)	**N-terminal sequencing** (Edman degradation)	**Subunits Identified**
Nqo1	49 299	+	+	+	+	+
Nqo2	25 042	+	+	+	+	+
Nqo3	64 724	+	+	+	+	+
Nqo4	50 186	+	+	+	+	+
Nqo5	26 622	+	+	+	+	+
Nqo6	21 593	+	+	+	-	+
Nqo7	13 765	+	-	+	-	+
Nqo8	37 374	-	-	-	-	-
Nqo9	27 120	+	+	+	-	+
Nqo10	18 337	-	-	-	-	-
Nqo11	10 904	+	-	-	+	+
Nqo12	72 339	-	-	+	-	+
Nqo13	58 308	+	-	+	-	+
Nqo14	53 230	-	-	+	-	+
Antiporter	58 413	[b]	-	-	-	-
PCD	11 277	+	-	+	-	+

[a]Considering the gene sequences.
[b]The presence of the antiporter is questionable since its predicted MM (58413 Da) is very close to that of Nqo13 (58308 Da).

in the *R. marinus* complex I mass spectrum (Figure 2.1.2). However, a peak with a m/z corresponding to a protein of 39.6 kDa was observed. This protein had eluted at an ACN percentage higher than 40% (Supplementary Figure 2.1.1), as all the identified membrane subunits. Given that N-terminal and C-terminal sequences of Nqo8 were not determined yet, a miss assignment of any of these cannot be excluded, as observed for Nqo6, which N-terminal sequence was reassigned in the present work (Figure 2.1.3). A PCD, which does not correspond to any previously known complex I subunit, was also identified and suggested as an additional protein of *R. marinus* complex I. To our knowledge, this study provides one of the few examples of detailed mass spectrometric analysis of bacterial complex I [10, 11]. Most of the reported studies addressed the mitochondrial enzyme [4-6]

and the identification of the membrane subunits is not always achieved [34]. In this work, the identification of the subunits, specially the membrane ones, was only possible establishing a new experimental protocol, which involved pre-separation of complex I subunits followed by their peptide digestion in solution. This approach is a step forward in the characterization of membrane proteins in general by MS, which studies are still technically highly challenging.

2.1.5 – ACKNOWLEDGEMENTS

I thank João Carita for cell growth and Manuela Regalla (Analytical Services Unit, ITQB) for N-terminal sequencing and reverse phase HPLC.

2.1.6 - REFERENCES

[1] A.S. Fernandes, M.M. Pereira, M. Teixeira, Purification and characterization of the complex I from the respiratory chain of *Rhodothermus marinus*, J Bioenerg Biomembr 34 (2002) 413-421.

[2] A.S. Fernandes, F.L. Sousa, M. Teixeira, M.M. Pereira, Electron paramagnetic resonance studies of the iron-sulfur centers from complex I of *Rhodothermus marinus*, Biochemistry 45 (2006) 1002-1008.

[3] A.M. Melo, S.A. Lobo, F.L. Sousa, A.S. Fernandes, M.M. Pereira, G.O. Hreggvidsson, J.K. Kristjansson, L.M. Saraiva, M. Teixeira, A nhaD Na^+/H^+ antiporter and a pcd homologues are among the *Rhodothermus marinus* complex I genes, Biochim Biophys Acta 1709 (2005) 95-103.

[4] J. Carroll, M.C. Altman, I.M. Fearnley, J.E. Walker, Identification of membrane proteins by tandem mass spectrometry of protein ions, Proc Natl Acad Sci U S A 104 (2007) 14330-14335.

[5] J. Carroll, I.M. Fearnley, J.M. Skehel, R.J. Shannon, J. Hirst, J.E. Walker, Bovine complex I is a complex of 45 different subunits, J Biol Chem 281 (2006) 32724-32727.

[6] J. Carroll, I.M. Fearnley, J.E. Walker, Definition of the mitochondrial proteome by measurement of molecular masses of membrane proteins, Proc Natl Acad Sci U S A 103 (2006) 16170-16175.

[7] C.C. Darie, M.L. Biniossek, V. Winter, B. Mutschler, W. Haehnel, Isolation and structural characterization of the Ndh complex from mesophyll and bundle sheath chloroplasts of *Zea mays*, Febs J 272 (2005) 2705-2716.

[8] A.S. Fandino, I. Rais, M. Vollmer, H. Elgass, H. Schagger, M. Karas, LC-nanospray-MS/MS analysis of hydrophobic proteins from membrane

protein complexes isolated by blue-native electrophoresis, J Mass Spectrom 40 (2005) 1223-1231.

[9] I.M. Fearnley, J. Carroll, R.J. Shannon, M.J. Runswick, J.E. Walker, J. Hirst, GRIM-19, a cell death regulatory gene product, is a subunit of bovine mitochondrial NADH:ubiquinone oxidoreductase (complex I), J Biol Chem 276 (2001) 38345-38348.

[10] P. Prommeenate, A.M. Lennon, C. Markert, M. Hippler, P.J. Nixon, Subunit composition of NDH-1 complexes of *Synechocystis* sp. PCC 6803: identification of two new ndh gene products with nuclear-encoded homologues in the chloroplast Ndh complex, J Biol Chem 279 (2004) 28165-28173.

[11] P. Zhang, N. Battchikova, V. Paakkarinen, H. Katoh, M. Iwai, M. Ikeuchi, H.B. Pakrasi, T. Ogawa, E.M. Aro, Isolation, subunit composition and interaction of the NDH-1 complexes from *Thermosynechococcus elongatus* BP-1, Biochem J 390 (2005) 513-520.

[12] M.M. Pereira, J.N. Carita, M. Teixeira, Membrane-bound electron transfer chain of the thermohalophilic bacterium *Rhodothermus marinus*: a novel multihemic cytochrome *bc*, a new complex III, Biochemistry 38 (1999) 1268-1275.

[13] P.K. Smith, R.I. Krohn, G.T. Hermanson, A.K. Mallia, F.H. Gartner, M.D. Provenzano, E.K. Fujimoto, N.M. Goeke, B.J. Olson, D.C. Klenk, Measurement of protein using bicinchoninic acid, Anal Biochem 150 (1985) 76-85.

[14] S. Susin, J. Abian, F. Sanchez-Baeza, M.L. Peleato, A. Abadia, E. Gelpi, J. Abadia, Riboflavin 3'- and 5'-sulfate, two novel flavins accumulating in the roots of iron-deficient sugar beet (Beta vulgaris), J Biol Chem 268 (1993) 20958-20965.

[15] D.S. Fischer, D.C. Price, A Simple Serum Iron Method Using the New Sensitive Chromogen Tripyridyl-S-Triazine, Clin Chem 10 (1964) 21-31.

[16] H. Schagger, Membrane Protein Purification and Crystallization 2/e: A Pratical Guide, Elsevier Science (USA) 2003.

[17] H. Schagger, G. von Jagow, Tricine-sodium dodecyl sulfate-polyacrylamide gel electrophoresis for the separation of proteins in the range from 1 to 100 kDa, Anal Biochem 166 (1987) 368-379.

[18] J.E. Walker, J.M. Skehel, S.K. Buchanan, Structural analysis of NADH: ubiquinone oxidoreductase from bovine heart mitochondria, Methods Enzymol 260 (1995) 14-34.

[19] B. Spenglen, Post-source decay analysis in matrix-assisted laser desorption/ionization mass spectrometry of biomolecules, J Mass Spectrom 32 (1997) 1019–1036

[20] S. Banuelos, M.J. Omaetxebarria, I. Ramos, M.R. Larsen, I. Arregi, O.N. Jensen, J.M. Arizmendi, A. Prado, A. Muga, Phosphorylation of both nucleoplasmin domains is required for activation of its chromatin decondensation activity, J Biol Chem 282 (2007) 21213-21221.

[21] J. Gobom, E. Nordhoff, E. Mirgorodskaya, R. Ekman, P. Roepstorff, Sample purification and preparation technique based on nano-scale

reversed-phase columns for the sensitive analysis of complex peptide mixtures by matrix-assisted laser desorption/ionization mass spectrometry, J Mass Spectrom 34 (1999) 105-116.

[22] M.R. Larsen, S.J. Cordwell, P. Roepstorff, Graphite powder as an alternative or supplement to reversed-phase material for desalting and concentration of peptide mixtures prior to matrix-assisted laser desorption/ionization-mass spectrometry, Proteomics 2 (2002) 1277-1287.

[23] D.N. Perkins, D.J. Pappin, D.M. Creasy, J.S. Cottrell, Probability-based protein identification by searching sequence databases using mass spectrometry data, Electrophoresis 20 (1999) 3551-3567.

[24] E. Krause, H. Wenschuh, P.R. Jungblut, The dominance of arginine-containing peptides in MALDI-derived tryptic mass fingerprints of proteins, Anal Chem 71 (1999) 4160-4165.

[25] P. Edman, G. Begg, A protein sequenator, Eur J Biochem 1 (1967) 80-91.

[26] S. Stolpe, T. Friedrich, The *Escherichia coli* NADH:ubiquinone oxidoreductase (complex I) is a primary proton pump but may be capable of secondary sodium antiport, J Biol Chem 279 (2004) 18377-18383.

[27] J. Song, T. Xia, R.A. Jensen, PhhB, a *Pseudomonas aeruginosa* homolog of mammalian pterin 4a-carbinolamine dehydratase/DCoH, does not regulate expression of phenylalanine hydroxylase at the transcriptional level, J Bacteriol 181 (1999) 2789-2796.

[28] G. Zhao, T. Xia, J. Song, R.A. Jensen, *Pseudomonas aeruginosa* possesses homologues of mammalian phenylalanine hydroxylase and 4 alpha-carbinolamine dehydratase/DCoH as part of a three-component gene cluster, Proc Natl Acad Sci U S A 91 (1994) 1366-1370.

[29] S. Koster, G. Stier, N. Kubasch, H.C. Curtius, S. Ghisla, Pterin-4a-carbinolamine dehydratase from *Pseudomonas aeruginosa*: characterization, catalytic mechanism and comparison to the human enzyme, Biological chemistry 379 (1998) 1427-1432.

[30] D. Suck, R. Ficner, Structure and function of PCD/DCoH, an enzyme with regulatory properties, FEBS Lett 389 (1996) 35-39.

[31] V. Naponelli, A. Noiriel, M.J. Ziemak, S.M. Beverley, L.F. Lye, A.M. Plume, J.R. Botella, K. Loizeau, S. Ravanel, F. Rebeille, V. de Crecy-Lagard, A.D. Hanson, Phylogenomic and functional analysis of pterin-4a-carbinolamine dehydratase family (COG2154) proteins in plants and microorganisms, Plant Physiol 146 (2008) 1515-1527.

[32] M.M. Pereira, P.N. Refojo, G.O. Hreggvidsson, S. Hjorleifsdottir, M. Teixeira, The alternative complex III from *Rhodothermus marinus* - a prototype of a new family of quinol:electron acceptor oxidoreductases, FEBS Lett 581 (2007) 4831-4835.

[33] L.A. Sazanov, P. Hinchliffe, Structure of the hydrophilic domain of respiratory complex I from *Thermus thermophilus*, Science 311 (2006) 1430-1436.

[34] H.R. Bridges, L. Grgic, M.E. Harbour, J. Hirst, The respiratory complexes I from the mitochondria of two *Pichia species*, Biochem J 422 (2009) 151-159.

2.1.7 – SUPPLEMENTARY MATERIAL

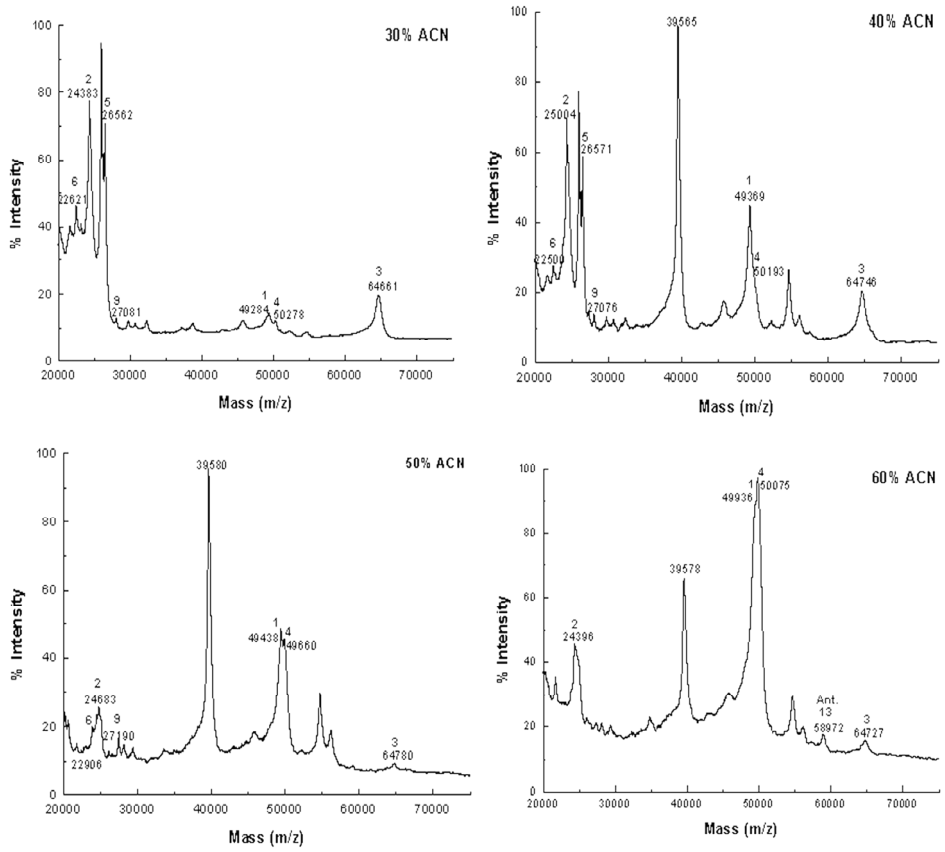

Supplementary Figure 2.1.1 - MALDI mass spectra of *R. marinus* complex I subunits separated by R1 microcolumn and eluted at different ACN concentrations (30 to 60 % in 0.1% TFA). Matrix: α-CHCA. Calibration mixture: ProMix3 and Calmix3. The numbers refer to the respective subunit (for example, Nqo1 is indicated by 1) with charge +1. Ant: Antiporter.

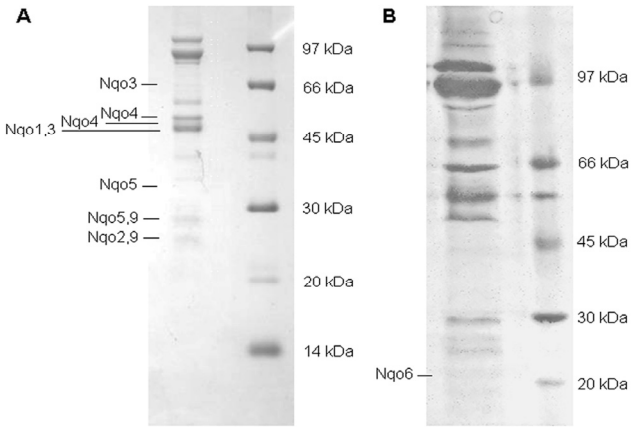

Supplementary Figure 2.1.2 - Electrophoretic profiles of *R .marinus* complex I obtained by tricine-SDS-PAGE. A) 12.5 %; B) 10- 20 % gradient after denaturing with 2-butanol. Positions corresponding to known subunits are labelled by the respective Nqo number.

Supplementary Table 2.1.1 - Identification by PMF of *R. marinus* complex I subunits after their separation by tricine-SDS-PAGE and *in gel-digestion*.

Gel	SwissProt Accession Number	Protein Name	Score	Pep	Sequence coverage (%)
12.5%	Q4QSB7_RHOMR	Nqo3	115	11/22	24
	Q4QSC0_RHOMR	Nqo4	176	16/29	22
	Q4QSC0_RHOMR	Nqo4	79	10/34	39
	Q4QSB8_RHOMR	Nqo1	112	11/28	29
	Q4QSB7_RHOMR	Nqo3	66	8/28	22
	Q4QSC1_RHOMR	Nqo5	157	10/15	46
	Q4QSC1_RHOMR	Nqo5	113	9/23	43
	Q4QSC5_RHOMR	Nqo9	88	8/23	26
	Q4QSB9_RHOMR	Nqo2	94	7/18	27
	Q4QSC5_RHOMR	Nqo9	81	7/18	27
10–20%	Q4QSC2_RHOMR	Nqo6	82	12/34	57

Score: The minimum MASCOT score for a probability less than 5% for the match to be a random event is 64.
Pep: Number of peptides submitted to search in protein databases/Number of peptides from experimental Peptide Mass Fingerprint whose masses match those from theoretical prediction determined from a known sequence.
Sequence coverage: percentage of identified protein sequences covered by matched peptides.

Supplementary Table 2.1.2 - LC-ESI-MS/MS identification of complex I subunits separated by tricine-SDS-PAGE (gradient gel).

Gel Piece[a]	Subunit identified	Sequence Coverage (%)	Number of Fragmented peptides (MS/MS)
1	Nqo9	46.5	13
	Nqo5	22.6	3
	Nqo3	13.9	5
	Nqo6	8.3	1
	Nqo1	6.3	2
2	Nqo9	46.5	16
	Nqo5	22.6	3
	Nqo6(+)[b]	17.0	2
	Nqo1	15.8	4
	Nqo3	8.3	4
	Nqo6	7.7	1
3	Nqo9	56.5	18
	Nqo5	30.4	5
	Nqo6	25.4	3
	Nqo6(+)[b]	17.0	4
	Nqo3	11.1	4
	Nqo1	10.2	3
	Nqo4	3.8	1
4	Nqo9	3.9	1
5	Nqo9	36.1	10
	Nqo5	27.8	6
6	Nqo5	50.9	9
	Nqo9	22.2	3
	Nqo2	21.9	3
7	Nqo5	57.4	10
	Nqo2	41.4	9
	Nqo9	15.2	2
8	Nqo9	22.2	4
	Nqo5	6.5	2
	Nqo4	3.8	2
9	Nqo1	34.1	11
	Nqo4	21.8	12
10	Nqo1	25.5	7
	Nqo3	17.7	5
	Nqo4	16.8	8
11	Nqo3	28.5	15
	Nqo1	22.6	7
	Nqo4	15.2	7
12	Nqo1	18.1	5
	Nqo4	17.0	8
	Nqo3	16.7	6
13	Nqo4	16.8	5
	Nqo3	9.4	4
	Nqo1	7.9	2
14	Nqo3	14.1	5
	Nqo5	7.8	1
	Nqo4	3.8	1
15	Nqo1	8.6	2

[a]From the higher apparent molecular mass to the lower one.
[b]Nqo6 with the correct N-terminal aminoacid sequence (full sequence).

Supplementary Table 2.1.3 - Identification by PMF (*in-solution digestion*) of *R. marinus* complex I subunits

Subunit	MM (Da)	$(M+H)^+$	Position	Sequence
Nqo1	49 299	904.4886	69-78	GGAGFPTGLK
		907.4302	1-9	MATNGAQSK
		917.4549	132-138	TCYLYVR
		1016.4618	144-150	WIEHMER
		1053.6203	204-212	IKPPFPAQR
		1058.5589	377-385	IEEGEGRLR
		1083.5217	420-427	FREEFEAR
		1345.6746	44-54	EVLTSDRWDPK
		1388.7168	365-376	EGTGWLENILTR
		1499.7311	144-154	WIEHMERELEK
		1500.7627	401-414	TVCALADAAAWPVR
		1508.6910	1-14	MATNGAQSKAGDWR
		1518.7158	79-90	WSFMPPVDDRPR
		1534.7471	132-143	TCYLYVRGEFAR
		1576.7325	139-150	GEFARWIEHMER
		1635.8125	30-43	LEVYEAHGGYQTLR
		1646.6825	91-105	FLCCNGDESEPGTFK
		1655.7251	307-321	ADMIDGVTMDAESLR
		1917.8105	91-107	FLCCNGDESEPGTFKDR
		2032.8837	179-198	GAGAYICGEESSLMESVEGK
		2064.8949	347-364	RVAHFYAHESCGQCTPCR
		2073.9103	179-198	GAGAYICGEESSLMESVEGK
		2079.8582	348-364	VAHFYAHESCGQCTPCR
		2090.1215	401-419	TVCALADAAAWPVRYTILR
		2147.1429	401-419	TVCALADAAAWPVRYTILR
		2157.0835	26-43	DLHRLEVYEAHGGYQTLR
		2172.9899	179-199	GAGAYICGEESSLMESVEGKR
		2230.0114	179-199	GAGAYICGEESSLMESVEGKR
		2235.9593	347-364	RVAHFYAHESCGQCTPCR
		2388.1917	69-90	GGAGFPTGLKWSFMPPVDDRPR
		2417.2016	422-443	EEFEARCKPSLVPTGIDLTPTG
		2554.4027	213-235	GLWGYPTTINNVETLANVPLILR
		2856.4229	294-321	AVIPGGSSTPPLRADMIDGVTMDAESLR
		2901.3426	322-347	EAGSMMGTAGLLVLDEDTDM VSWLRR

Subunit	MM(Da)	$(M+H)^+$	Position	Sequence
Nqo2	25 042	726.3491	1-6	MADFVK
		1015.5432	216-224	TPPVAHHTR
		1072.5884	173-181	VDQLLEDLK
		1126.5011	206-215	SDAEAVESYR
		1282.6022	205-215	RSDAEAVESYR
		1626.8196	39-52	FKEQYLEPAGAVMK
		2123.0264	206-224	SDAEAVESYRTPPVAHHTR
		2153.1236	185-204	LPPFVSLTLPQDEAELGGNR
		2321.1845	41-60	EQYLEPAGAVMKTLWLAQEK
		3326.7670	7-35	KPVVPLPELHPEPQIPADQLFFTEEEKAK

Subunit	MM (Da)	$(M+H)^+$	Position	Sequence
		773.4264	305-310	DDRLVR
		790.4417	99-105	TSEKVAR
		823.3549	171-176	CINCTR
		859.5108	481-487	TIRTVNR
		940.6050	476-483	VRPAKTIR
		983.5785	531-538	LGHPLRYK
		1031.4687	381-389	TPNAQGCQR
		1063.5605	131-139	CPLQIQAYK
		1067.4907	171-179	CINCTRCVR
		1096.6109	187-195	SHQLTIIER
		1154.5112	311-319	VSWEEAYDR
		1197.5932	177-186	CVRFTDEISK
		1201.5596	498-507	LDQHGTPYDR
		1204.5204	253-261	GSNCYYWVR
		1294.7729	390-401	LGILPVDEALVR
		1429.7110	140-151	YGPEGSRFEFLK
		1458.7443	47-59	QCLVEVGMPVIDR
		1461.6499	377-389	TDDRTPNAQGCQR
		1474.7392	47-59	QCLVEVGMPVIDR
		1518.6714	377-389	TDDRTPNAQGCQR
		1539.7076	164-176	VMLDAERCINCTR
Nqo3	64 724	1729.7805	80-95	LQTSCSLDMADGMVVK
		1866.9167	131-146	CPLQIQAYKYGPEGSR
		1917.0076	180-195	FTDEISKSHQLTIIER
		1974.0113	235-252	ARPWEMSATPSITITNAK
		2030.0844	332-349	ILFLGSAYATVEDNYLLK
		2099.0987	47-65	QCLVEVGMPVIDRETGKPK
		2123.9882	80-98	LQTSCSLDMADGMVVKTHR
		2136.0542	513-530	HQVDCKPSWEILPEVAER
		2149.0198	80-98	LQTSCSLDMADGMVVKTHR
		2156.1202	47-65	QCLVEVGMPVIDRETGKPK
		2186.1855	332-350	ILFLGSAYATVEDNYLLKR
		2193.0757	513-530	HQVDCKPSWEILPEVAER
		2307.2237	381-401	TPNAQGCQRLGILPVDEALVR
		2329.1393	253-271	GSNCYYWVRDNLIVEITAR
		2468.1948	109-130	DNLEFLLINHPLDCPICDQAGK
		2770.3946	351-376	LAEALGADTPVYIPHVEPGHGDGWLR
		2856.3773	508-530	WYNEKHQVDCKPSWEILPEVAER
		2931.4266	542-568	YIMQEIAETIPAFAGATYEAMGLEGVR
		3257.5973	351-380	LAEALGADTPVYIPHVEPGHGDGWLRTDDR
		3294.5877	66-95	LDENGQPVIQFMPKLQTSCSLDMADGMVVK
		3351.6091	66-95	LDENGQPVIQFMPKLQTSCSLDMADGMVVK
		3745.8338	542-576	YIMQEIAETIPAFAGATYEAMGLEGVRLAEIGAEV

Subunit	MM (Da)	$(M+H)^+$	Position	Sequence
		757.4679	238-243	IINRNK
		848.4108	299-306	TEGDSLAR
		936.4342	78-85	LDGEVMEK
		940.4635	34-40	HAWLEER
		952.5250	281-287	RFEPYLK
		998.4468	149-156	MIMCELAR
		1010.5629	96-104	GLEKVAEHK
		1058.5490	22-29	HNEAIYRR
		1138.5231	311-319	MEEMKESVR
		1173.5952	13-21	HGLFNFWPR
		1188.6194	86-95	CVLDLGYLHR
		1230.6147	1-12	MSTAPSLVGPDR
		1232.5802	307-315	YFVRMEEMK
		1245.6408	86-95	CVLDLGYLHR
Nqo4	50 186	1246.6096	1-12	MSTAPSLVGPDR
		1264.5700	307-315	YFVRMEEMK
		1413.7121	299-310	TEGDSLARYFVR
		1652.8069	144-156	AQWIRMIMCELAR
		1672.8839	86-99	CVLDLGYLHRGLEK
		1677.8386	144-156	AQWIRMIMCELAR
		1687.7632	185-198	EEIYSIFDEVCGAR
		1865.9068	223-237	RFVEEFPEELAGWEK
		2006.9276	183-198	YREEIYSIFDEVCGAR
		2030.9276	100-115	VAEHKTYQEFMPYTDR
		2090.0408	78-95	LDGEVMEKCVLDLGYLHR
		2147.0623	78-95	LDGEVMEKCVLDLGYLHR
		2385.1920	1-21	MSTAPSLVGPDRHGLFNFWPR
		3035.6159	244-271	IWIDRNEGIGVLTAEEAIELGVTGPNLR
		3152.6753	157-184	ISSHLLWLGVGLMDAGAVSVFLWAFKYR

Subunit	MM (Da)	$(M+H)^+$	Position	Sequence
		775.4131	72-77	IVEVCR
		860.4009	140-146	AANWNER
		980.4795	25-33	GDELNPHAK
		1032.5506	69-77	ADKIVEVCR
		1106.6390	72-80	IVEVCRFLK
		1126.5752	156-164	FEGHPDLRR
		1133.4754	147-155	ECYDMFGIR
		1190.4969	147-155	ECYDMFGIR
Nqo5	26 622	1883.8567	164-177	RMYMPEDFEYHPLR
		1915.8465	164-177	RMYMPEDFEYHPLR
		1917.9857	9-24	THEALKFYFTPVDPPR
		2045.0661	122-139	VRVEEDNPVVPSVTSVYR
		2063.0079	49-66	FGDVIEEVELYAGEHTVR
		2141.9531	147-163	ECYDMFGIRFEGHPDLR
		2185.0923	78-96	FLKEEQGFNYLADLGGIDR
		2200.0821	15-33	FYFTPVDPPRGDELNPHAK
		2519.0997	208-230	AHGYVPPPGFEEPPAEDEEVSEH
		3047.6240	179-207	EFPLLGIPGSLPLPPQTPGGPLTYDPFAR

Subunit	MM (Da)	$(M+H)^+$	Position	Sequence
Nqo6	21 593	797.3610	52-58	FGSEAMR
		823.4308	6-12	EGFLTTR
		854.4777	77-83	MAHAIRR
		870.4726	77-83	MAHAIRR
		1099.6258	13-21	LDVLLNWAR
		1131.5139	84-92	VWDQMPDPK
		1271.6201	83-92	RVWDQMPDPK
		1284.6153	52-62	FGSEAMRFSPR
		1300.6102	52-62	FGSEAMRFSPR
		1417.6528	47-58	YDVARFGSEAMR
		1683.6858	93-108	WCIAMGACASTGGMHR
		1765.7389	93-108	WCIAMGACASTGGMHR
		2088.0041	59-76	FSPRQADLMIVAGWCSYK
		2129.0306	59-76	FSPRQADLMIVAGWCSYK
		2264.1137	63-82	QADLMIVAGWCSYKMAHAIR
		2601.1534	22-46	SNSLMPMPMGLACCAIEMMAFAGPK

Subunit	MM (Da)	$(M+H)^+$	Position	Sequence
Nqo7	13 765	795.4359	54-59	ERYTVK
		1528.6406	40-53	MPYESGMDPVGSAR
		1652.7519	39-53	RMPYESGMDPVGSAR
		1684.7417	39-53	RMPYESGMDPVGSAR

Subunit	MM (Da)	$(M+H)^+$	Position	Sequence
Nqo8	37 374	1126.5851	65-74	EDIIPAQANR
		1269.6296	311-320	YNQLMTLGWK
		1528.7981	309-320	FKYNQLMTLGWK
		1544.8471	46-60	VGPAGFLQPFADVVK
		1565.7973	292-303	TCFFAFLYIWVR

Subunit	MM (Da)	$(M+H)^+$	Position	Sequence
Nqo9	27 120	775.4461	190-195	DRPFLK
		797.4879	151-157	LLVPAER
		918.4428	222-230	SWGGVRAEG
		992.5312	15-21	KLNFWER
		1021.5200	142-150	DEAIFGLEK
		1158.5426	133-141	EYDLTFQSR
		1245.6330	82-93	ACPPLAISMQAK
		1286.6595	82-93	ACPPLAISMQAK
		1478.8186	60-72	GRPVLVEENGRPR
		1505.7192	196-207	WLLEEEGMEELK
		1509.7842	1-14	MPGKPVNLASPNER
		1521.7141	196-207	WLLEEEGMEELK
		1525.7791	1-14	MPGKPVNLASPNER
		1590.7448	170-181	DPQYGQHWEFRK
		1706.8319	100-112	EREPAWFEINMLR
		2122.0098	73-93	CVACGLCARACPPLAISMQAK
		2239.9971	43-59	YTFQYPDELWYPPDSYR
		2278.1423	190-207	DRPFLKWLLEEEGMEELK
		2355.1954	60-81	GRPVLVEENGRPRCVACGLCAR
		2526.2598	60-81	GRPVLVEENGRPRCVACGLCAR
		2580.1830	40-59	SPRYTFQYPDELWYPPDSYR

Subunit	MM (Da)	$(M+H)^+$	Position	Sequence
Nqo12	72 339	738.3603	388-393	FMPATR
		760.3777	574-579	FGAFYR
		917.4873	625-632	LMAELGQR
		933.4822	625-632	LMAELGQR
		1045.5214	572-579	ERFGAFYR
		1172.6568	625-634	LMAELGQRVR
		1188.6517	625-634	LMAELGQRVR
		1190.5622	562-571	HGLAYDDMLR
		1269.6473	454-464	SYVLTFEGTPR
		1337.6960	602-613	FARNGLAAFDQK
		1356.5310	585-593	YYWDEFYDR
		1433.7495	168-180	NSEAANKAFIVNR
		1475.7059	562-573	HGLAYDDMLRER
		1683.9290	181-195	VGDAAFLLAMFLLFR
		1699.9239	181-195	VGDAAFLLAMFLLFR
		2062.0432	69-85	FFTWIAAGELELAFQYR
		2384.3311	175-195	AFIVNRVGDAAFLLAMFLLFR
		2903.6612	635-662	RVQTGVVQAYAMAIVLGVALVLALMLFG
		3048.6695	394-421	TTYLIATLAIAGFPLTAGFFSKDEILFK

Subunit	MM (Da)	$(M+H)^+$	Position	Sequence
Nqo13	58 308	830.4479	487-493	RTEPTAR
		896.4658	262-269	MGTYGLVR
		912.4607	262-269	MGTYGLVR
		1106.6092	494-502	FLLETVEQK
		1138.5561	366-375	LMEEFGGIAR
		1397.7495	451-462	EVNRTLPDLNAR
		1513.7856	521-534	LEVSEGETVRIANP
		1532.7638	363-375	HTRLMEEFGGIAR
		2783.5686	206-230	LLAYNVPLAAQGWLFFVFALAFAIK
		2822.4530	504-530	LAALEEAEQPVPAASARLEVSEGETVR

Subunit	MM (Da)	$(M+H)^+$	Position	Sequence
Nqo14	53 230	1010.4975	1-8	MDLLEAYR
		1026.4924	1-8	MDLLEAYR
		1059.5316	155-165	EDVGAGEAALK
		1096.5269	438-447	SPDEAPEPVR
		1882.0796	254-272	AAAFAALVLVLDAALPAER
		2149.0786	430-447	VVYVFWMKSPDEAPEPVR
		2931.5663	438-458	SPDEAPEPVRQQTFPVPLAPR
		3167.5328	224-253	VGAVPFHMWTPDVYQGAPTTLTGYMAAASK

Subunit	MM (Da)	$(M+H)^+$	Position	Sequence
Antiporter	58 413	911.4767	196-202	SYMRLNK
		1499.8178	328-340	EIIMFSVAVLAYK
		1939.0721	328-344	EIIMFSVAVLAYKLADR
		2033.0661	271-288	NKIESPDPDPSQPLVQIR
		2047.0818	273-291	IESPDPDPSQPLVQIRGAK
		2162.0144	474-492	AIAEENKVDMPSFMGYVTK
		3326.8115	169-199	NNAILLFVGSLVANLIATTGAAMLFVRSYMR

Subunit	MM (Da)	$(M+H)^+$	Position	Sequence
PCD	11 277	1074.5724	1-9	MSRVEPLSR
		1090.5673	1-9	MSRVEPLSR
		1324.7331	68-80	VTLALTTHAAGNR
		1347.7055	29-39	LQKTYTFGSFR
		2431.1901	48-67	IAFEAEQLNHHPELHNVYNR

2.2

LILBID MS of *R. marinus* complex I

These studies have been performed in collaboration with Lucie Sokova and Prof. Bernhard Brutschy (Institute of Physical and Theoretical Chemistry, Johann Wolfgang Goethe-Universität, Frankfurt am Main, Germany).

Chapter 2: Structural Studies of *R. marinus* complex I

Section 2.2 – LILBID MS studies of *R. marinus* complex I

2.2.1 - SUMMARY

The total molecular mass of *Rhodothermus marinus* complex I was estimated by combining blue native electrophoresis and laser-induced liquid bead ion desorption mass spectrometry (LILBID MS). An apparent molecular mass of ≈ 550 kDa is suggested for this bacterial enzyme. Under soft laser conditions, two sub-complexes of 337 kDa and 367 kDa could also be detected and their compositions are compatible with different complex I subunits combinations. Under high laser conditions most of the individual subunits were not observed which indicates that these two sub-complexes are probably high stable.

The total molecular mass of ≈ 550 kDa is compatible with the sum of the molecular masses of the fifteen subunits previously identified by peptide mass fingerprinting. Furthermore, it also indicates the absence of the Nha-like antiporter in the composition of complex I.

2.2.2 - INTRODUCTION

Respiratory complex I from *R. marinus* has been shown to be composed by at least fifteen subunits (section 2.1). Fourteen of those are the canonical proteins (Nqo1 to 14) present in all known complexes I, while the additional protein is a pterin-4α-carbinolamine dehydratase (PCD). As mentioned before (see section 1.2.2.8 and section 2.1), the gene that codifies for the PCD is among the other *R. marinus* complex I genes and is co-transcribed with them [1]. This situation is also observed for the gene that codifies for a putative Nha-type Na^+/H^+ antiporter (see figure 1.2.11 in section 1.2.2.8) [1]; however, this protein was never identified in any preparation of *R. marinus* complex I.

In order to investigate whether the Nha-like antiporter is part of *R. marinus* complex I, studies to determine the total mass of the complex were performed. These included laser induced liquid bead ion desorption mass spectrometry (LILBID MS) and native electrophoresis. LILBID MS is a recently developed method that is tolerant to various buffers and detergents allowing the detection of multisubunit complexes under conditions which closely mimic the native environment. This technique allows not only the determination of the total molecular mass of a multisubunit complex but also the individual masses of its components in a single setup by the stepwise disintegration of the complex via infrared (IR) laser thermolysis [2]. This method has been applied to respiratory enzymes including mitochondrial complex I [2-4].

Combining LILBID MS with blue native electrophoresis (BN-PAGE), it was possible to estimate a total molecular mass of ≈550 kDa for *R. marinus* complex I. This mass is compatible with the sum of the molecular masses of the fifteen subunits (Nqo1 to 14 and PCD), considering a single copy of each protein, and suggests that the Nha-type Na^+/H^+ antiporter is not part of this complex.

2.2.3 – MATERIAL AND METHODS

A. General procedures

Cell growth and Protein Purification: Bacterial growth, membrane preparation and solubilization and protein purification were done as previously described in section 2.1.

Activity assays: NADH:nitroblue tetrazolium (NBT) oxidoreductase activity was detected in blue native gel. The gel was incubated in 50 mM potassium phosphate buffer pH 7 containing 0.2 mg/mL NBT and 0.1

mg/mL NADH for 15-20 min at room temperature. After this incubation period, the formation of colored bands was observed.

Electrophoresis: BN-PAGE and isolation of complex I from the gel by electroelution (at 100 V overnight) were carried out as described [5]. After electroelution, buffer exchange to 30 mM ammonium hydrogen carbonate and 0.05% DDM was performed by repeated dilution/concentration cycles using spin concentrators (Microcon YM100).

B. LILBID MS

The detailed experimental setup for LILBID MS has been published elsewhere [6]. The droplet of analyte is injected into vacuum, exploded by IR laser and the ions are detected by TOF MS. Spectra at different laser intensities and in the anion mode were measured and calibrated using the spectra of bovine serum albumin (67 kDa) recorded under identical experimental conditions.

2.2.4 – RESULTS AND DISCUSSION

R. marinus complex I was submitted to BN-PAGE gel and the NADH oxidation activity was tested *in situ*. Two stained bands were observed: one with ≈ 520 kDa and another with ≈ 270 kDa. The band with the higher molecular mass is compatible with the intact complex I while the other is compatible with the peripheral part of the enzyme. Considering that *R. marinus* complex I is composed by a single copy of each subunit, it is expected that the total molecular mass of the complex is ≈ 540 kDa in the absence or ≈ 600 kDa in the presence of the Nha-like antiporter. The associated error of BN-PAGE is ± 50 kDa [7] and thus the presence of the Nha-like antiporter cannot be completely excluded. Since LILBID MS has a much smaller

associated error (± 5-10 kDa) we opt to use this method to address our problem.

LILBID spectra of the entire R. marinus complex I (≈520 kDa)

Under soft laser conditions, charge distributions of complexes of mass 337 kDa (shown as blue bars) and 367 kDa (shown as orange bars) were observed (Figure 2.2.1). These two complexes are probably due to the dissociation of *R. marinus* enzyme into sub-complexes, with different subunits compositions. Two of these possible compositions combine the membrane subunits *plus* Nqo6 and Nqo4 for 337 kDa; and membrane subunits *plus*

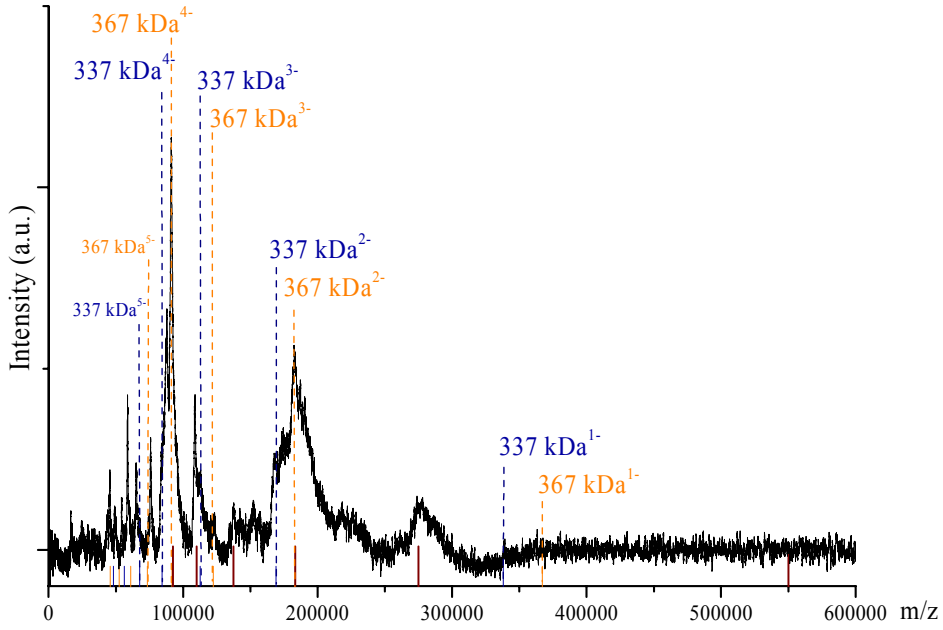

Figure 2.2.1 – LILBID spectrum, obtained in anion mode under low laser intensity, of the BN-PAGE band of ≈520 kDa. The blue bars correspond to the charge distribution of a complex of a 337 kDa size and the orange bars to a complex of a 367 kDa size. The brown bars could also correspond to a charge distribution of a 550 kDa complex, but as this charge distribution partially overlaps with the orange and blue ones its presence is not totally certain.

Table 2.2.1 - Molecular masses of *R. marinus* complex I subunits

Subunit	Theoretical Molecular Mass (Da) [a]	Prosthetic groups [b]
Nqo1	49 299	FMN; [4Fe-4S]
Nqo2	25 042	[2Fe-2S]
Nqo3	64 724	[2Fe-2S]; 2x [4Fe-4S]
Nqo4	50 186	-
Nqo5	26 622	-
Nqo6	21 593	[4Fe-4S]
Nqo7	13 765	-
Nqo8	37 374	-
Nqo9	27 120	2x [4Fe-4S]
Nqo10	18 337	-
Nqo11	10 904	-
Nqo12	72 339	-
Nqo13	58 308	-
Nqo14	53 230	-
Antiporter	58 413	-
PCD	11 277	-

[a]Considering the gene sequences (and not considering the mass of the cofactors).
[b]Molecular mass (Da): FMN: 456.4 ; [2Fe-2S]: 175.8; [4Fe-4S]: 351.7.

Nqo6, Nqo4 and Nqo5 for 367 kDa (see table 2.2.1 for subunit molecular masses). The reasoning for these proposed combinations took into account the available structural data (electron microscopy and X-ray data), specially the structures of *T. thermophilus* complex I, in which the subunits Nqo4, 5 and 6 are described as the ones closer to the membrane arm [8].

The spectrum also shows the presence of other proteins with molecular masses higher than 100 kDa which may also result from a combination(s) of subunits or contaminations. One of these, indicated by brown bars, may be assigned to a charge distribution of a complex of 550 kDa. Due to partial overlapping of the charge distribution of such possible complex with the ones of the 337 kDa and 367 kDa complexes, the presence of the 550 kDa complex is in this way not totally certain but it would be in complete agreement with the 520 kDa band eluted from the BN-PAGE and used as sample.

A total mass of 550 kDa agrees very well with a total mass of *R. marinus* complex I of 543 kDa, which can be calculated assuming the presence of one copy of each canonical subunit, one copy of the possible additional subunit (PCD) and including the masses of one FMN, six tetranuclear and two binuclear iron-sulfur centers. These results suggest, and also corroborate the previous MS analyses (section 2.1), that *R. marinus* complex I is composed by the fourteen canonical subunits *plus* an additional one, the PCD, while the Nha-type Na^+/H^+ antiporter is absent. Although a complex with ≈ 600 kDa cannot be completely excluded, its presence is unlikely, which also supports the existence of a fifteen subunits complex.

Further analysis of the LILBID spectrum was performed applying laser pulses with high energy to dissociate complex I into its subunits. The spectrum presented in Figure 2.2.2 was recorded under high laser intensity; however its analysis is difficult due to the presence of several peaks, which

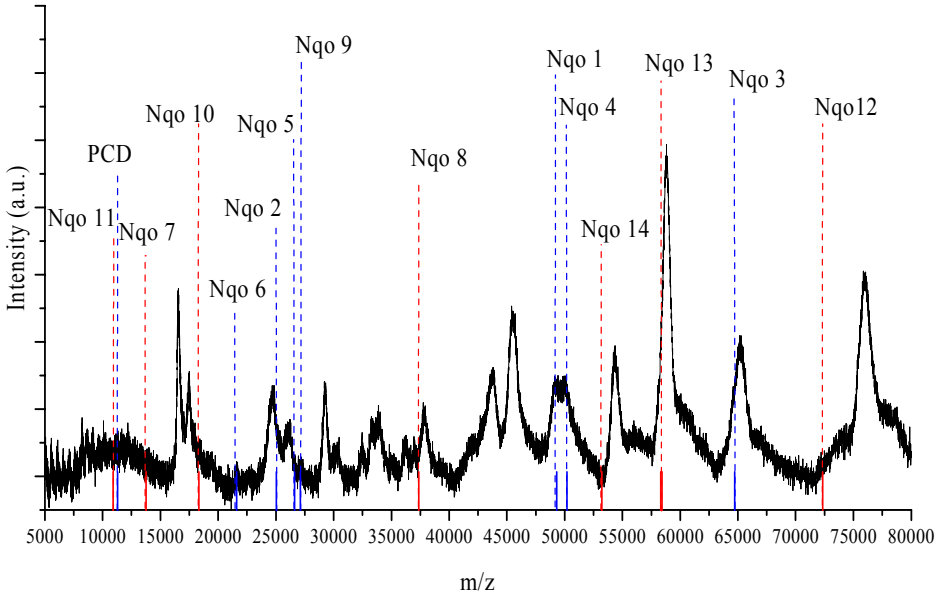

Figure 2.2.2 – LILBID spectrum, obtained in anion mode under high laser intensity, of the BN-PAGE band of ≈520 kDa. The bars in the spectrum represent expected masses of complex I subunits. The red bars refer to hydrophobic proteins and the blue bars to hydrophilic ones.

either do not belong to complex I or are combinations of different subunits. There are only three hydrophilic subunits where the peak is at the expected position: Nqo1, Nqo4 and Nqo9. Subunit Nqo3 contains two tetranuclear and one binuclear iron-sulfur centers which could still be associated with the subunit [2]. Considering that this protein has lost one tetranuclear center, the peak at 65.2 kDa could be assigned to it. There are no peaks at positions of hydrophilic subunits Nqo2, Nqo5 and Nqo6. There is a minor peak at a position corresponding to the mass of Nqo10 subunit. Mass peaks corresponding to other membrane subunits are not observed in this spectrum, which may indicate that these may form highly stable sub-complexes which were not separated under these intensities conditions, requiring very high energies to dissociate into theirs subunits. It may be suggested that the 337 kDa and 367 kDa complexes detected under soft laser conditions (Figure 2.2.1) may correspond to these stable membranar sub-complexes.

LILBID spectra of the peripheral part of R. *marinus complex I (≈270 kDa)*

The spectrum shown in Figure 2.2.3 was obtained under high laser conditions. Although the spectrum analysis is complex due to the presence of multiple peaks, almost all the peripheral subunits could be identified at the positions corresponding to the masses deduced from gene sequences, including Nqo1 which is the complex I subunit responsible for the NADH:NBT oxidoreductase actvity. This result supports our suggestion that the second stained band may correspond to the peripheral arm of complex I. Peaks of masses corresponding to the peripheral subunits Nqo5 and Nqo9 seem not to be present in the spectrum. The others peaks may correspond to proteins that do not belong to complex I (contaminations) or be combinations of different subunits.

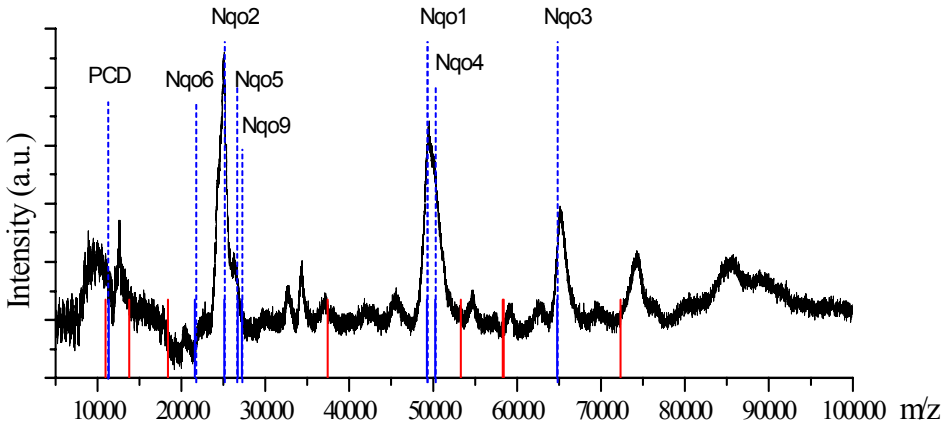

Figure 2.2.3 – LILBID spectrum, obtained in anion mode under high laser intensity, of the BN-PAGE band of ≈270 kDa. The bars in the spectrum represent expected masses of complex I subunits. The red bars refer to the hydrophobic proteins and the blue bars to hydrophilic ones

In conclusion, we have estimated the total molecular mass of complex I by combining BN-PAGE and LILBID MS. Although preliminary, the obtained results suggest that *R. marinus* complex I has a total mass of ≈ 550 kDa which agrees with the sum of the molecular masses of the fifteen subunits identified previously by peptide mass fingerprint, thus excluding the presence of the Nha-like antiporter in the composition of this complex I.

2.2.5 - ACKNOWLEDGEMENTS

I thank Dr. Guohong Peng and collaborators (Max-Planck Institute for Biophysics, Frankfurt am Main, Germany) for the help on the BN-PAGE and electroelution processes; João Carita (ITQB, Portugal) for cell growth.

2.2.6 - REFERENCES

[1] A.M. Melo, S.A. Lobo, F.L. Sousa, A.S. Fernandes, M.M. Pereira, G.O. Hreggvidsson, J.K. Kristjansson, L.M. Saraiva and M. Teixeira, A nhaD

Na^+/H^+ antiporter and a pcd homologues are among the *Rhodothermus marinus* complex I genes, Biochim Biophys Acta 1709 (2005) 95-103.

[2] N. Morgner, V. Zickermann, S. Kerscher, I. Wittig, A. Abdrakhmanova, H.D. Barth, B. Brutschy and U. Brandt, Subunit mass fingerprinting of mitochondrial complex I, Biochim Biophys Acta 1777 (2008) 1384-91.

[3] N. Morgner, T. Kleinschroth, H.D. Barth, B. Ludwig and B. Brutschy, A novel approach to analyze membrane proteins by laser mass spectrometry: from protein subunits to the integral complex, J Am Soc Mass Spectrom 18 (2007) 1429-38.

[4] L. Sokolova, I. Wittig, H.D. Barth, H. Schagger, B. Brutschy and U. Brandt, Laser-induced liquid bead ion desorption-MS of protein complexes from blue-native gels, a sensitive top-down proteomic approach, Proteomics 10 (2010) 1401-7.

[5] I. Wittig, H.P. Braun and H. Schagger, Blue native PAGE, Nat Protoc 1 (2006) 418-28.

[6] N. Morgner, H.D. Barth and B. Brutschy, A new way to detect noncovalently bonded complexes of biomolecules from liquid micro-droplets by laser mass spectrometry, Austral. J. Chem. 59 (2006) 109-114.

[7] E.H. Heuberger, L.M. Veenhoff, R.H. Duurkens, R.H. Friesen and B. Poolman, Oligomeric state of membrane transport proteins analyzed with blue native electrophoresis and analytical ultracentrifugation, J Mol Biol 317 (2002) 591-600.

[8] L.A. Sazanov and P. Hinchliffe, Structure of the hydrophilic domain of respiratory complex I from *Thermus thermophilus*, Science 311 (2006) 1430-6.

2.3

Crystallization and EM studies of *R. marinus* complex I

These studies have been performed in collaboration with Dr. Janet Vonck and Dr. Guohong Peng and collaborators (Max-Planck Institute for Biophysics, Frankfurt am Main, Germany).

Chapter 2: Structural Studies of *R. marinus* complex I

Section 2.3 – Crystallization and EM studies of *R. marinus* complex I

2.3.1 - SUMMARY

Rhodothermus marinus complex I was investigated by electron microscopy (EM) and the typical L-shaped form is suggested for this enzyme, which is in agreement with the several three dimensional structures available of bacterial and mitochondrial complexes I.

Crystallization studies of the complex were also performed. Two different types of crystals were obtained after the optimization of the protein purification process and of the crystallization conditions. One type of crystals was yellowish while the other was colourless and both diffracted to a resolution of 6-8 Å. Additional improvement of crystallization conditions is currently underway.

2.3.2 - INTRODUCTION

In contrast to the other respiratory enzymes, the atomic structure of the entire complex I is still not available making this enzyme the less understood of those that constitute the respiratory chain. A high-resolution structure is demanded as a basis for the understanding of the mechanism by which this enzyme couples electron transfer to charge translocation across the membrane, contributing in this way to the establishment of the transmembrane electrochemical potential difference. Large efforts have been undertaken to obtain a high resolution structure of this enzyme. Recently, the structure of the entire complex I from *T. thermophilus* was determined at 4.5 Å resolution [1]. Although the electron density of the crystal was not of sufficient quality to allow the build up of an atomic model of the entire enzyme, it was possible to observe that the complex has an L-shaped structure. Thus, this enzyme has two perpendicular sections, one peripheral

segment protruding into the bacterial cytoplasm or mitochondrial matrix and one membrane embedded segment, which serves as a membrane anchor. This L-shaped structure had already been obtained at low resolution by electron microscopy (EM) studies [2-8]. A horseshoe shape was also reported for the *E. coli* enzyme [9], however this result could not be reproduced and was later interpreted as a possible artifact [10].

Complex I from the bacterium *R. marinus* was investigated by negative staining EM and the typical L-shaped form is suggested. Crystallization studies on this enzyme have been performed and two different types of crystals were obtained (non-color and yellowish crystals), diffracting to a resolution of 6-8 Å.

2.3.3 – MATERIAL AND METHODS

A. General procedures

Cell growth and Protein Purification: Bacterial growth, membrane preparation and solubilization and protein purification were done as previously described in section 2.1.

Electrophoresis: BN-PAGE and isolation of complex I from the gel by electroelution (at 100V overnight) were carried out as described [11].

B. Crystallization conditions

Purified complex I was loaded on a Superdex 200 column and was eluted with 20 mM Tris-HCl pH 8, 1 mM PMSF, 150 mM NaCl and 0.1% DDM. The sample was concentrated to 8 mg/mL. Crystals were grown at 18°C under aerobic conditions by the hanging drop vapour diffusion method. An equal volume of protein and reservoir solution, containing 0.2 M di-ammoniumhydrogenphosphate and 40% methylpentanediol (MPD), was

mixed. Initial crystals were obtained after 6 days and flash frozen in liquid nitrogen stream after 2 to 3 weeks. Crystals with regular shapes were obtained in the reservoir solution of 0.1 M HEPES pH 7.0 and 40% MPD.

Crystal diffraction images were collected at 100 K on X10SA at the Swiss light source with a Mar 225 CCD detector.

C. Electron Microscopy

The samples were negatively stained with 1% (w/v) uranyl acetate. Electron micrographs were taken using a Philips CM120 electron microscope at 120 kV under low dose conditions. Data was collected on a 2048x2048 pixel Gatan CCD camera at a magnification of 59 000x.

2.3.4 – RESULTS AND DISCUSSION

Crystallization studies

Crystallization experiments of complex I from *R. marinus* have been performed since 2006 and some improvements have been achieved. One of the most important was the optimization of the protein purification protocol whereas an additional chromatographic step (Mono Q column) was introduced[1]. This extra step allowed the separation of complex I from a sugar kinase (a contamination that was always present in the complex preparation) and concomitantly a more homogeneous sample was obtained. The X-ray crystallographic structure of the sugar kinase was determined to 1.8 Å resolution (our unpublished data).

[1] Complex I, used for the mass spectrometry studies (sections 2.1 and 2.2), was purified according to this optimized purification protocol.

Yellowish crystals have been obtained from the complex I preparation without the sugar kinase (Figure 2.3.1 – A). After improving the crystallization conditions two other types of crystals with regular shapes were obtained, being one colorless (Figure 2.3.1 – B) while the other was yellowish (Figure 2.3.1 – C). Due to the different colors of the crystals, it is possible to hypothesize that the colorless crystals could correspond to the membrane arm of the complex while the yellowish to the peripheral arm or even to the entire complex I. These hypotheses could be tested, for example, by mass spectrometry analysis of the crystals; however, the crystal amount was insufficient to perform further studies. Both types of crystals were diffracting to a resolution of 6-8 Å. Additional improvements of the crystallization conditions are currently underway.

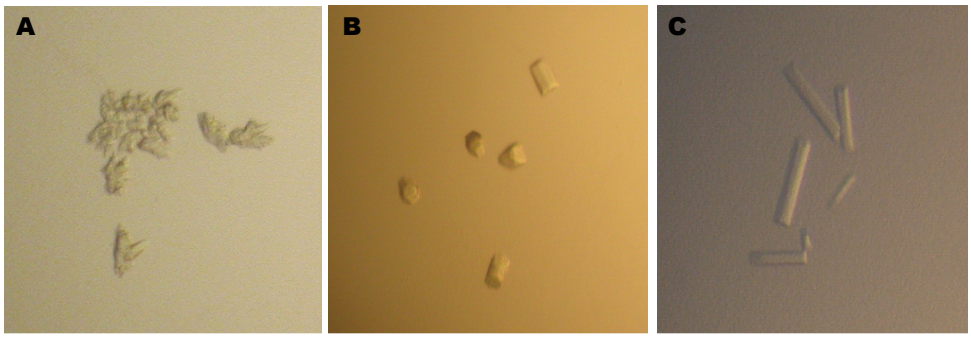

Figure 2.3.1 – Crystals of *R. marinus* complex I. (A) Initial yellowish crystals obtained after improving the protein purification process. (B) and (C) Crystals with regular shapes obtained after improving the crystallization conditions (B. non-color crystals; C. yellowish crystals). Both diffracted to a resolution of 6-8 Å.

Electron Microscopy Studies

In order to further improve the homogeneity of *R. marinus* complex I, the purified enzyme was applied into a BN-PAG and electroeluted. The molecular mass of the eluted sample was ≈ 480±50 kDa which agrees with

the sum of the predicted molecular mass of the all complex I subunits (see section 2.1 and 2.2).

After staining the sample with uranyl acetate, electron micrographs were obtained. Some L-shaped particles could be observed, in addition to other objects which could be assigned as detergent micelles (Figure 2.3.2). The L-shaped structure is in agreement with previous EM results obtained for other complexes I, such as *E. coli* [2], *Y. lipolytica* [6], *A. aeolicus* [3], bovine [7] and *T. elongatus* [5] enzymes. Also the size of the *R. marinus* particles is compatible with the size of other complexes I particles, reinforcing the EM data analysis. However, further EM studies are needed to corroborate these preliminary results. It is described, for *Y. lipolytica* complex I that the best results were obtained using phosphotungstic acid or ammonium molybdate as staining solutions instead of uranyl acetate [6, 8]. Changing the staining protocol could be an improved option for future EM studies of *R. marinus* complex I.

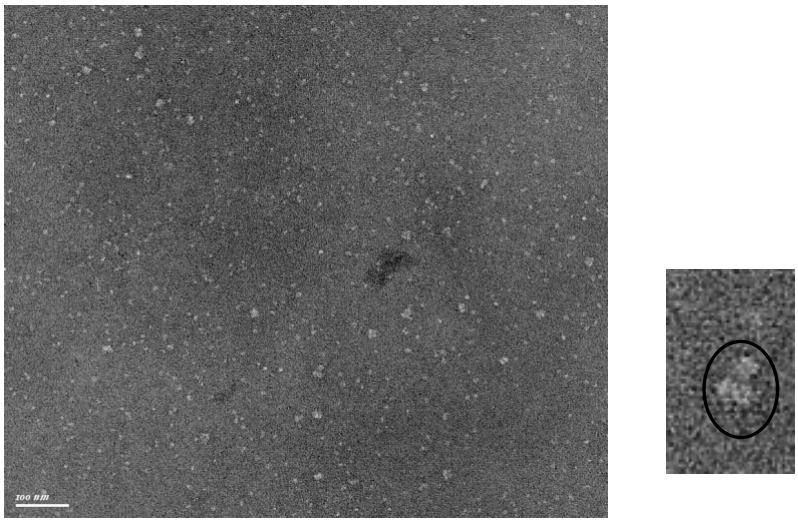

Figure 2.3.2- Electron micrograph of *R. marinus* complex I (negative stain). On the left: the complete micrograph. Scale bar 100nm. On the right: zoom of a particle showing a possible L-shape form.

2.3.5 – CONCLUSIONS

As other bacterial complexes I [6], purified *R. marinus* enzyme is apparently unstable and can be dissociated into different sub-complexes (see section 2.2) which makes its structural determination a great challenge. Nevertheless, at this stage data suggest that the complex I from this bacterium shows all the canonical characteristics of complex I (see section 2.1, 2.2 and [12, 13]) including the L-shaped structure. However, additional crystallographic and electron microscopy studies are required to obtain a deeper insight into the three dimensional structure of *R. marinus* enzyme.

2.3.6 - ACKNOWLEDGEMENTS

I thank João Carita (ITQB, Portugal) for cell growth.

2.3.7 - REFERENCES

[1] R.G. Efremov, R. Baradaran and L.A. Sazanov, The architecture of respiratory complex I, Nature 465 (2010) 441-5.

[2] V. Guenebaut, A. Schlitt, H. Weiss, K. Leonard and T. Friedrich, Consistent structure between bacterial and mitochondrial NADH:ubiquinone oxidoreductase (complex I), J Mol Biol 276 (1998) 105-12.

[3] G. Peng, G. Fritzsch, V. Zickermann, H. Schagger, R. Mentele, F. Lottspeich, M. Bostina, M. Radermacher, R. Huber, K.O. Stetter and H. Michel, Isolation, characterization and electron microscopic single particle analysis of the NADH:ubiquinone oxidoreductase (complex I) from the hyperthermophilic eubacterium *Aquifex aeolicus*, Biochemistry 42 (2003) 3032-9.

[4] E.A. Baranova, D.J. Morgan and L.A. Sazanov, Single particle analysis confirms distal location of subunits NuoL and NuoM in *Escherichia coli* complex I, J Struct Biol 159 (2007) 238-42.

[5] A.A. Arteni, P. Zhang, N. Battchikova, T. Ogawa, E.M. Aro and E.J. Boekema, Structural characterization of NDH-1 complexes of *Thermosynechococcus elongatus* by single particle electron microscopy, Biochim Biophys Acta 1757 (2006) 1469-75.

[6] M. Radermacher, T. Ruiz, T. Clason, S. Benjamin, U. Brandt and V. Zickermann, The three-dimensional structure of complex I from *Yarrowia lipolytica*: a highly dynamic enzyme, J Struct Biol 154 (2006) 269-79.

[7] N. Grigorieff, Three-dimensional structure of bovine NADH:ubiquinone oxidoreductase (complex I) at 22 A in ice, J Mol Biol 277 (1998) 1033-46.

[8] M. Radermacher, Chapter 1 Visualizing functional flexibility by three-dimensional electron microscopy reconstructing complex I of the mitochondrial respiratory chain, Methods Enzymol 456 (2009) 3-27.

[9] B. Bottcher, D. Scheide, M. Hesterberg, L. Nagel-Steger and T. Friedrich, A novel, enzymatically active conformation of the *Escherichia coli* NADH:ubiquinone oxidoreductase (complex I), J Biol Chem 277 (2002) 17970-7.

[10] L.A. Sazanov, J. Carroll, P. Holt, L. Toime and I.M. Fearnley, A role for native lipids in the stabilization and two-dimensional crystallization of the *Escherichia coli* NADH-ubiquinone oxidoreductase (complex I), J Biol Chem 278 (2003) 19483-91.

[11] I. Wittig, H.P. Braun and H. Schagger, Blue native PAGE, Nat Protoc 1 (2006) 418-28.

[12] A.S. Fernandes, M.M. Pereira and M. Teixeira, Purification and characterization of the complex I from the respiratory chain of *Rhodothermus marinus*, J Bioenerg Biomembr 34 (2002) 413-21.

[13] A.S. Fernandes, F.L. Sousa, M. Teixeira and M.M. Pereira, Electron paramagnetic resonance studies of the iron-sulfur centers from complex I of *Rhodothermus marinus*, Biochemistry 45 (2006) 1002-8.

Chapter 3

Energy conservation by R. marinus complex I

Abbreviations

E.: *Escherichia*; *P.*: *Paracoccus*; R.: R*hodothermus*; *T.*: *Thermus*.

ΔΨ: membrane potential; ΔpH: pH difference; ΔNa^+_{out}: external medium sodium concentration changes.

ACMA: 9-amino-6-chloro-2-methoxyacridine; CCCP: carbonyl cyanide *m*-chlorophenyl hydrazone; DDM: n-dodecyl-β-D-maltoside; DMN: 2, 3-dimethyl-1,4-naphthoquinone; $Dy(PPPi)_2^{7-}$: dysprosium (III) tripolyphosphate; EPR: electron paramagnetic resonance; Menadione: 2-methyl-1,4-naphthoquinone; Monen: monensine; Mrp: multiple resistance and pH related antiporter; Na^+-NQR: Na^+ translocating NADH:quinone oxidoreductase; NMR: nuclear magnetic resonance; NQ: 1,4-naphothoquinone; oxonol V: Bis (3-phenyl-5-oxoisoxazol-4 yl)pentamethine oxonol; Q: quinone; Rot: rotenone; Succ: succinate; TEMPO: 2,2,6,6-tetramethyl-1-piperidinyloxy; $Tm(DOTP)^{5-}$: thulium(III)1,4,7,10-tetraazacyclododecane-1,4,7,10-tetrakis(methylenephosphonate).

Chapter 3: Energy conservation by *R. marinus* complex I

3.1

Energy conservation by *R. marinus* complex I

This section is published as:

A.P. Batista, A.S. Fernandes, R.O. Louro, J. Steuber, M.M. Pereira, Energy conservation by *Rhodothermus marinus* respiratory complex I, Biochim Biophys Acta 1797 (2010) 509-515.

R. O. Louro helped with the NMR experiences; J. Steuber with the discussion and A. S. Fernandes with all the experimental work.

Chapter 3: Energy conservation by *R. marinus* complex I

Section 3.1 – Energy conservation by *R. marinus* complex I

3.1.1 - SUMMARY

A sodium ion efflux, together with a proton influx and an inside-positive $\Delta\Psi$, was observed during NADH-respiration by *Rhodothermus marinus* membrane vesicles. Proton translocation was monitored by fluorescence spectroscopy and sodium ion transport by ^{23}Na-NMR spectroscopy. Specific inhibitors of complex I (rotenone) and of the dioxygen reductase (KCN) inhibited the proton and the sodium ion transport, but the KCN effect was totally reverted by the addition of menaquinone analogues, indicating that both transports were catalyzed by complex I. We concluded that the coupling ion of the system is the proton and that neither the catalytic reaction nor the establishment of the ΔpH are dependent on sodium, but the presence of sodium increases proton transport. Moreover, studies of NADH oxidation at different sodium concentrations and of proton and sodium transport activities allowed us to propose a model for the mechanism of complex I in which the presence of two different energy coupling sites is suggested.

3.1.2 - INTRODUCTION

R. marinus is a halothermophilic bacterium isolated from shallow marine hot springs [1, 2] whose optimal growth conditions are 65 ºC, 2 % NaCl and pH 7. It was phylogenetically placed at the phylum Bacteroidetes [3]. It is considered to be an obligate aerobic organism, with menaquinone-7 being the main quinone in its membranes [4]. Respiratory chain complexes and electron carriers of *R. marinus* have been purified and biochemically characterized in recent years, namely complexes I and II [5-8], an alternative complex III [9, 10], three terminal oxygen reductases [11-13] and two soluble electron carriers: a cytochrome *c* and a high-potential iron-sulphur protein [10, 14, 15]. Additionally, a so-called type II NADH dehydrogenase coding gene is present in *R. marinus* genome, whereas genes coding for a Na^+-NQR are

absent [16]. One of the *R. marinus* oxygen reductases was shown to pump protons [17], contributing to the electrochemical potential difference that is the driving force for ATP synthesis.

Here, we report a study in which the nature of the charge(s) transported by *R. marinus* complex I was investigated. The 9-amino-6-chloro-2-methoxyacridine (ACMA) fluorescence quenching method was used to monitor proton transport by this complex. Furthermore, due to the possible relation between complex I and sodium ions, the Na^+ transport by this complex was also investigated. We used ^{23}Na-NMR spectroscopy, which has the advantage of directly monitoring changes in sodium concentration. To our knowledge, this is the first report on the use of the ^{23}Na-NMR to monitor substrate-driven Na^+ transport by membrane vesicles. The obtained findings have a significant impact on the general understanding of the coupling mechanisms of complex I.

3.1.3 – MATERIAL AND METHODS

A. Cell growth and membrane vesicles preparation

Rhodothermus marinus PRQ 62B was grown as described previously [10]. After harvesting, cells in 10 mM HEPES-Tris buffer pH 7.5 with 10, 25 or 50 mM Na_2SO_4, were broken in a French Pressure cell at 6 000 psi. For control experiments, Na_2SO_4 was replaced with 10 mM choline chloride or 50 mM K_2SO_4. The membrane vesicles were obtained by ultracentrifugation of the broken cells at 205 000 g, 2 h, 4 ºC followed by re-suspension in the same buffer. Integrity of vesicles was checked by the K^+/valinomycin assay using oxonol V as a $\Delta\Psi$ sensitive dye (see below $\Delta\Psi$ detection). Lipids were extracted from membrane preparations [18]. Protein concentration was determined by the Biuret method modified for membrane proteins [19].

B. ΔΨ detection

ΔΨ generation was detected following oxonol V absorption (A_{640} *minus* A_{612}) by an OLIS upgraded Aminco DW2 dual wavelength spectrophotometer, at 27 ºC [20]. Membrane vesicles (in HEPES-Tris buffer pH 7.5 and 50 mM Na_2SO_4) were added to 1.5 μM oxonol V in 10 mM HEPES-Tris pH 7.5 buffer with the appropriate salt. To demonstrate the membrane vesicles integrity, K^+ gradients were generated with K^+/valinomycin in an external buffer containing 50 mM K_2SO_4 (internal K^+ concentration was <10 μM). The assay was started adding 2 μM valinomycin, creating a positive-inside ΔΨ due to the influx of K^+. To detect the NADH-driven ΔΨ formation, the assay contained membrane vesicles in 10 mM HEPES-Tris buffer pH 7.5 with 50 mM Na_2SO_4. The reaction was started by adding 4 mM of NADH. When referred, 40 μM rotenone, 10 μM carbonyl cyanide *m*-chlorophenyl hydrazone (CCCP), 2.5 mM KCN and 100 μM DMN were added prior to the addition of NADH.

C. Determination of the internal volume of membrane vesicles

The internal volume of the membrane vesicles was determined by EPR spectroscopy, using 2,2,6,6-Tetramethyl-1-piperidinyloxy (TEMPO) [21]. The samples contained approximately 40 mg protein.mL^{-1} and 100 μM TEMPO oxidized with $K_3[Fe(CN)_6]$. TEMPO in the external medium was quenched with 100 mM of potassium chromium(III) oxalate trihydrate. Relative decrease of TEMPO concentration upon addition of the quencher was 96 % indicating that the internal volume is 4 % of the total volume. EPR measurements were performed at room temperature, with a microwave frequency of 9.39 GHz, microwave power 1 mW and modulation amplitude 0.04 mT.

D. Activity measurements

Oxygen consumption was measured with a Clark-type oxygen electrode YSI Model 5300 at 27 ºC and 45 ºC. The assay mixture contained membrane vesicles and 10 mM HEPES-Tris pH 7.5 with 10, 25 or 50 mM Na_2SO_4, or 10 mM choline chloride or 50 mM K_2SO_4. The reaction was started by adding 4 mM NADH. When used, ionophores or inhibitors were added prior to the addition of substrates.

NADH oxidation by membrane vesicles was monitored at 330 nm (ε = 5930 $M^{-1}cm^{-1}$) with a Shimadzu UV-1603 spectrophotometer. The reaction medium contained membrane vesicles in the presence or absence of 2.5 mM KCN and 100 μM DMN. The reaction was started by adding 100 μM NADH.

NADH:$K_3[Fe(CN)_6]$ oxidoreductase activity was monitored at 340 nm (ε = 6220 $M^{-1}cm^{-1}$). The reaction medium contained membrane vesicles or solubilized membranes (added to start the reaction) in 10 mM HEPES-Tris pH 7.5, 25 or 50 mM Na_2SO_4, 1 mM $K_3[Fe(CN)_6]$ and 200 μM NADH. Solubilized membranes were obtained by stirring an aliquot of membrane vesicles with 9 % of DDM for 1 h at 4 °C.

E. Fluorescence spectroscopy

The generation of pH difference (ΔpH) was determined by the quenching of the fluorescence of ACMA, recorded on a Varian Cary Eclipse spectrofluorimeter (excitation λ=410 nm, emission λ=480 nm). Membrane vesicles were incubated aerobically for 5 min at 27 ºC in the assay buffer (10 mM HEPES-Tris pH 7.5, 10 or 25 mM Na_2SO_4 or 10 mM choline chloride) containing 1 μM of ACMA. The reaction was started by adding 50 μM of

NADH or succinate. When referred, CCCP (10 μM), rotenone (40 μM), monensin (20 μM), KCN (5 mM) and DMN (50 μM) were added prior to the addition of NADH.

F. ^{23}Na-NMR spectroscopy

NMR spectra were recorded on a Bruker Avance II 500 MHz spectrometer at 27 °C, operating at 132 MHz for ^{23}Na, equipped with a 10 mm sodium selective probe and a vertical bore magnet. Experiments were performed using a 13.5 μs 90º pulse and 8k data points were recorded over a spectral width of 40 kHz. 1051 scans were accumulated for each experiment. The vesicles were prepared in 10 mM HEPES-Tris, pH 7.5 with 10, 25 or 50 mM Na_2SO_4 or 10 mM choline chloride without shift reagents and the intra-vesicle sodium signal was not shifted. Thulium (III) 1, 4, 7, 10 – tetraazacyclododecane - 1, 4, 7, 10 -tetrakis (methylenephosphate) ($Tm(DOTP)^{5-}$) at a concentration of 3, 4.5 or 6 mM (depending on the Na_2SO_4 concentration in the buffer) was added to prepared membrane vesicles and used as a shift reagent for the sodium signal of the suspension medium. Since 1 equivalent of $Tm(DOTP)^{5-}$ contains 5 equivalents of Na^+, the concentration of sodium in the external medium was always higher than inside the vesicles. In average, 400 μL of membrane vesicles containing 20 mg of membrane protein were used in each NMR experiment in a 5 mm diameter tube. A concentric capillary tube with 2 mm diameter, containing 50 μL of the shift reagent dysprosium (III) tripolyphosphate ($Dy(PPPi)_2^{7-}$) at a concentration of 22 mM, placed inside the NMR tube, was used in all experiments as external reference. The integral of the resonance frequency peak of Na^+ in the presence of $Dy(PPPi)_2^{7-}$ (this reagent contains 10 equivalents of Na^+) was used to calibrate the concentration of sodium in the suspension medium [22]. The sodium concentration in that medium was

measured by integration of the sodium shifted signal. The intra-vesicle concentration of sodium was not monitored due to its small signal to noise ratio. Spectra were recorded under the same conditions as above described, upon addition of 4 mM NADH (in the form of potassium salt) to membrane vesicles which were previously incubated with or without inhibitors, quinones or ionophores.

3.1.4 - RESULTS

Membrane vesicles preparation

The membrane preparations obtained by the procedure described above were found to be composed of tight vesicles which allowed formation of a $\Delta\Psi$ using K^+ and valinomycin, stable for at least 30 min, and detected by monitoring the change in the absorbance of oxonol V. If external potassium was replaced by sodium, no oxonol V response was observed. The positive oxonol V response could only be observed at a certain oxonol V to membrane ratio, typically 0.75 μmol oxonol per 1 μg of lipid, which was optimized by changing the membrane concentration at a fixed oxonol V concentration of 1.5 μM. Closed membrane vesicles were stable at temperatures up to 45 ºC. The internal membrane vesicles volume, determined by EPR spectroscopy, was found to be 1 μL per mg of protein. Since NADH is unable to cross lipid membranes, one way of determining the percentage of inside-out membrane vesicles is to compare NADH:$K_3[Fe(CN)_6]$ oxidoreductase activity in membrane vesicles before and after their solubilization by detergent. After solubilization of the membrane vesicles with the detergent DDM, the activity was increased at most 10%. Thus, it can be concluded that the membranes obtained by French press cell rupture are composed preferentially of inside-out vesicles.

NADH and dioxygen consumption by R. marinus respiratory chain

R. marinus membrane vesicles were able to reduce dioxygen to water in 10 mM HEPES-Tris buffer pH 7.5 with 50 mM Na_2SO_4, upon addition of NADH, with an approximate rate of 12 nmol O_2 min^{-1} mg^{-1} at 45 ºC. The same rate was observed in the presence of 10 mM Na_2SO_4, 25 mM Na_2SO_4 and also if Na_2SO_4 in the membrane preparation and in the assay buffers was replaced by K_2SO_4 or choline chloride ($[Na^+] < 10$ μM). Maximal NADH oxidase inhibition by rotenone was observed to be ~70 % at concentrations ≥ 10 μM of the inhibitor. KCN could inhibit the same activity at 95 % when present at ≥ 10 mM concentration.

When the NADH consumption was spectrophotometrically monitored, it was observed that KCN also completely inhibited NADH oxidation. This inhibition was totally overcome by the presence of 100 μM of the menaquinone analogue DMN.

NADH-driven ΔΨ generation by R. marinus membrane vesicles

To analyze the generation of a ΔΨ during NADH oxidation by the vesicles, the optimal oxonol V to membrane ratio (determined in control experiments performed with the K^+ /valinomycin assay) was chosen. A jump in absorbance (A_{640} *minus* A_{612}) of oxonol V was observed upon addition of NADH to membrane vesicles prepared in buffer containing 50 mM Na_2SO_4 (Figure 3.1.1.A-a), demonstrating the build-up of a ΔΨ (positive inside) across the vesicle membrane. If the membrane vesicles were preincubated with the respiratory chain inhibitors rotenone or KCN, the jump in A_{640} *minus* A_{612} observed upon NADH addition was much smaller (Figures 3.1.1.A-b and c), indicating that the observed ΔΨ was generated by the functioning of the respiratory chain. The ΔΨ was dissipated by the addition of the protonophore

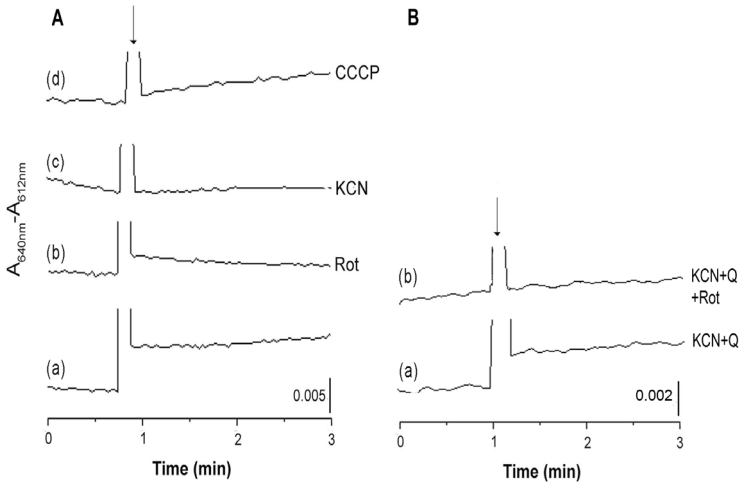

Figure 3.1.1 - Generation of a ΔΨ by *R. marinus* membrane vesicles. Absorbance difference A_{640} *minus* A_{612} of 1.5 μM oxonol V in membrane vesicles with 10 mM HEPES-Tris buffer pH 7.5, 50 mM Na_2SO_4 upon addition of 4 mM NADH (indicated by an arrow). Panel A) without preincubating the membrane vesicles (a), after preincubation with 40 μM rotenone (b), in the presence of 2.5 mM KCN (c), or 10 μM CCCP (d). Panel B) preincubating the membrane vesicles with 2.5 mM KCN *plus* 100 μM DMN (a), or with 2.5 mM KCN *plus* 100 μM DMN *plus* 40 μM rotenone (b).

CCCP (Figure 3.1.1.A-d). To focus on the NADH-menaquinone segment of this respiratory chain, a preincubation of the membrane vesicles with KCN and the menaquinone analogue DMN was performed. After NADH addition, changes in the oxonol absorbance were observed, showing the formation of a ΔΨ (Figure 3.1.1.B-a). This ΔΨ was assigned to complex I, since in the presence of rotenone no absorbance differences were detected (Figure 3.1.1.B-b). Average and standard deviation of the results represented in Figure 3.1.1 are given in Supplementary Figure 3.1.1.

Investigation of NADH-driven proton transport

NADH-driven proton transport by the membrane vesicles was monitored by fluorescence spectroscopy using ACMA as a ΔpH indicator

(Figure 3.1.2). After NADH addition, a quenching in the ACMA fluorescence intensity was observed, indicating proton transport to the inside of the vesicles (Figure 3.1.2.A-a). Prior incubation of the membrane vesicles with the complex I specific inhibitor rotenone led to a lower ACMA quenching (Figure 3.1.2.A-b). If the vesicles had been previously incubated with KCN, the protonophore CCCP, or the sodium/proton exchanger monensin, the ACMA fluorescence quenching was negligible upon addition of NADH (Figures 3.1.2.A-c to e). These observations reflect the NADH-driven proton

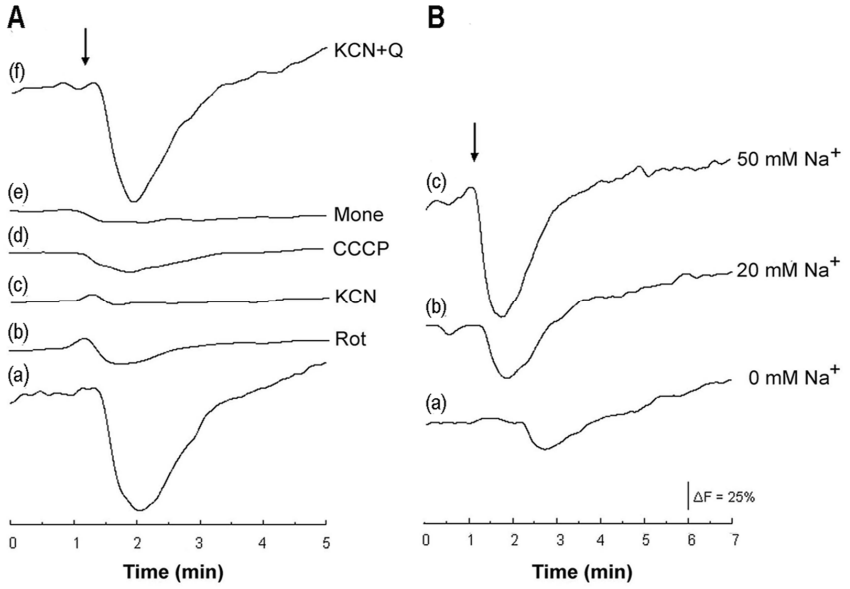

Figure 3.1.2 - Generation of a pH difference by the respiratory chain of *R. marinus* monitored by ACMA fluorescence. The ACMA fluorescence was detected using an excitation wavelength of 410 nm and an emission wavelength of 480 nm. Panel A) The assay contained membrane vesicles in 10 mM HEPES-Tris buffer pH 7.5 with 25 mM Na_2SO_4. The reaction was started by the addition of 50 μM NADH (indicated by an arrow) without preincubating the membrane vesicles (a), after preincubation with 40 μM rotenone (b), 5 mM KCN (c), 10 μM CCCP (d), 20 μM monensin (e) or 5 mM KCN *plus* 50 μM DMN (f). Panel B) The assay contained membrane vesicles in 10 mM HEPES-Tris buffer pH 7.5 with 10 mM choline chloride (a), with 10 mM Na_2SO_4 (b) and with 25 mM Na_2SO_4 (c). The reaction was started by the addition of 50 μM NADH (indicated by an arrow).

transport by the whole *R. marinus* respiratory chain. To focus on the NADH-menaquinone segment and using the same principle as in $\Delta\Psi$ generation the membrane vesicles were pre-incubated with KCN and the menaquinone analogue DMN. The absence of quenching of ACMA fluorescence upon addition of NADH in the presence of KCN was, similarly to NADH oxidation and $\Delta\Psi$ generation, totally reversed by the addition of DMN (Figure 3.1.2.A-f). The influence of the sodium concentration on ACMA fluorescence quenching was also investigated (Figures 3.1.2.B). Being maximal at 50 mM Na^+ (inside the vesicles and in the outside buffer) (Figure 3.1.2.B-c), the extent of ACMA fluorescence quenching was found to decrease to 43 % in the presence of 20 mM Na^+ (Figure 3.1.2.B-b) and to 30 % when Na_2SO_4 is substituted by choline chloride (Figure 3.1.2.B-a).

It was also observed the establishment of a ΔpH when the initial electron donor was succinate, instead of NADH. However, in this situation sodium ions did not influence the proton translocation process (Supplementary Figure 3.1.2), discarding any kind of influence by this ion on proton translocations mediated by complexes III and IV.

Investigation of NADH-driven sodium ion transport

The involvement of Na^+ in respiration was studied by following NADH-driven Na^+ transport by membrane vesicles. ^{23}Na-NMR spectroscopy was chosen to directly monitor changes of sodium ions concentration. By adding the shift reagent $Tm(DOTP)^{5-}$ to the external medium of the membrane vesicles, it is possible to distinguish between internal and external Na^+, since the resonance of the latter is shifted to higher frequency (Figure 3.1.3.). After NADH addition, the external Na^+ concentration increased, *i.e.*, sodium ion was transported from the inside to vesicles (Figure 3.1.4-filled circles). As described in Materials and Methods section, four different internal

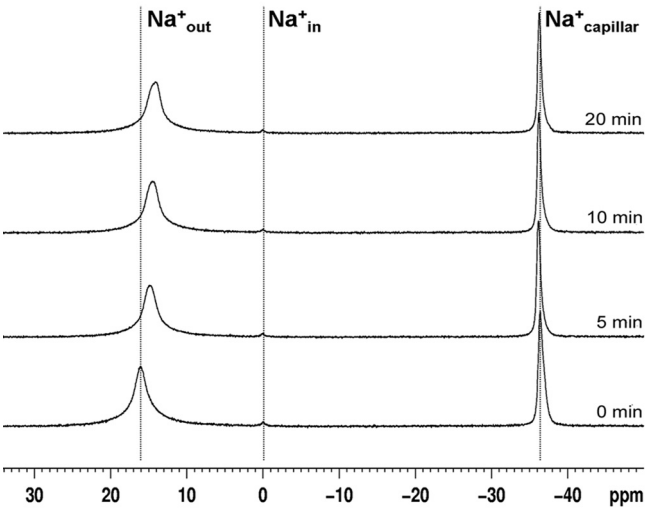

Figure 3.1.3 - ^{23}Na-NMR spectra of membrane vesicles in 10 mM HEPES-Tris buffer pH 7.5 with 10 mM Na_2SO_4 and containing 3 mM $Tm(DOTP)^{5-}$ in the suspension medium, obtained before addition of NADH and 5, 10 and 20 min after the addition. The signal at -36.17 ppm is due to the external reference present in the concentric capillary tube inside the NMR tube, which contained 22 mM $Dy(PPPi)_2^{7-}$. The weak signal at 0 ppm originates from the intravesicle Na^+ and the resonance at ~15 ppm is the signal from the Na^+ present in the suspension medium. This signal changes its resonance frequency because the equilibrium exchange of Na^+ ions between free and shift reagent bound states is in the fast-exchange-limit, and the concentration ratio of Na^+ and the shift reagent is increasing in the outside medium, together with other factors.

sodium concentrations were used: approximately 0 (Na_2SO_4 is substituted by choline chloride), 20, 50 and 100 mM. Knowing that the membrane vesicles internal volume is 1 μL mg^{-1} of protein, approximately 0, 20, 50 or 100 nmol of Na^+ per mg of protein, respectively, were available to be transported to the outside. No change was observed in the external sodium concentration when choline was present inside the vesicles. In the case of 20 mM Na^+ inside ($[Na_i^+]$), an increase of 20 nmol of Na^+ per mg of protein was observed in the external medium, while an increase of 25 nmol of Na^+ per mg of protein was observed for the conditions of 50 or 100 mM Na^+. Taken together, these

observations suggest that the system is operating under [Na_i^+]-limiting conditions for Na^+ transport in the presence of choline or 20 mM Na^+, but that it is under non-[Na_i^+]-limiting conditions for 50 or 100 mM Na^+, even considering that 10% of the vesicles are inside-in oriented and thus unable to react with NADH.

If membrane vesicles had been previously incubated with rotenone, the increase in external sodium ion concentration was much smaller (Figure 3.1.4-open diamonds). Furthermore, when incubated with KCN, no sodium ion transport from the inside to the outside was observed (Figure 3.1.4-filled diamonds). Thus, sodium ion transport through the membrane vesicles occurred during NADH consumption by the respiratory chain. As expected, a

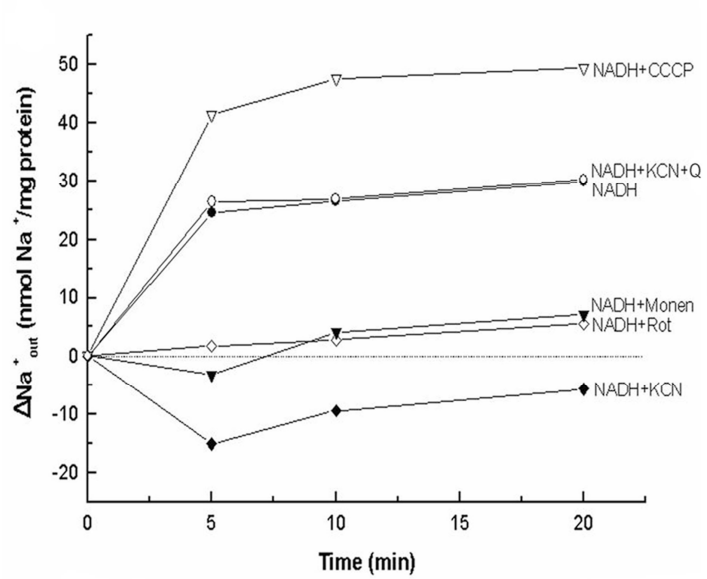

Figure 3.1.4- Sodium ion transport by *R. marinus* NADH-respiring membrane vesicles. Effect of 4 mM K_2-NADH on external Na^+ concentration at time zero to membrane vesicles containing 50 or 100 mM Na^+ without preincubations (filled circles) or after preincubation with 40 μM rotenone (open diamonds), 10 mM KCN (filled diamonds), 10 μM CCCP (open triangles), 20 μM monensin (filled triangles) or 10 mM KCN plus 200 μM of each menaquinone analogue DMN, NQ and menadione (open circles). The represented data are the average of at least three independent assays.

decrease in the ion transport was observed when the sodium/proton exchanger monensin was added (Figure 3.1.4-filled triangles). To distinguish between an active transport by some respiratory complex and a possible secondary sodium transport due to the proton gradient formed by respiration, the uncoupler and protonophore CCCP was added to the vesicles prior to the addition of NADH. Dissipation of the proton gradient with CCCP increased sodium transport (Figure 3.1.4-open triangles). The CCCP experiment shows that Na^+ transport to the outside of the membrane vesicles is not a secondary event that arises from a proton gradient formation, and thus it is actively performed by a component of the respiratory chain. Hypothesizing that this component is located at the NADH-menaquinone segment of the respiratory chain, and using the same rationale applied to NADH oxidation, $\Delta\Psi$ generation and proton transport, the addition of quinones to vesicles preincubated with KCN should restore sodium ion transport activity. Indeed, when adding NADH to KCN-treated membrane vesicles in the presence of the menaquinone analogues DMN, NQ (1,4-Naphthoquinone) and menadione (2-methyl-1,4-naphthoquinone), sodium ion transport was found to be similar to the one observed with non-inhibited vesicles in the absence of added quinones (Figure 3.1.4-open circles). Supplementary Figure 3.2.3 shows average and standard deviation of the results from Figure 3.2.4.

Sodium ion transport and NADH consumption ratio

Measuring the amount of dioxygen consumed in the first 5 min after NADH addition to membrane vesicles under the same conditions used in the NMR experiments, allowed the calculation of the amount of NADH oxidized during this period. By comparing this result with the sodium ion transported by the membrane vesicles, under non-$[Na_i^+]$-limiting conditions, during the first 5 min after NADH addition, we estimated that 0.3 to 1 Na^+ was

transported upon consumption of 1 NADH molecule. This nearly 1 to 1 stoichiometry supports the hypothesis that the observed sodium ion transport is a primary event caused by NADH consumption. It should be noted that if the Na^+ transport observed after the first 5 min had occurred in a shorter period of time, and/or if the Na^+ flux observed in the reverse direction when the respiratory chain is inhibited by KCN (Figure 3.1.4) can be taken as a baseline, the indicated Na^+/NADH values appear underestimated.

3.1.5 - DISCUSSION

The membrane vesicles prepared as described, were active with respect to NADH oxidation and dioxygen reduction, and could create and maintain an NADH-driven ΔΨ positive inside. This ΔΨ was fully sensitive to the protonophore CCCP, indicating a ΔpH contribution to the ΔΨ, as confirmed by monitoring the ΔpH using the indicator ACMA. The ACMA fluorescence quenched after the addition of NADH, and did not change when the membrane vesicles were incubated with rotenone, CCCP, monensin or KCN. A proton translocation site in the respiratory chain of *R. marinus* could be attributed to the NADH:menaquinone electron transfer segment, since proton transport was observed upon short cutting KCN inhibited membrane vesicles with the menaquinone analogue DMN. Due to the fact that only the inside-out membrane vesicles contribute to the observed results, it can be concluded that H^+ transport into the vesicles corresponds to the proton transport from the cytoplasm to the periplasm, in agreement with the ΔΨ (positive inside) detected with oxonol V. These results show that the coupling ion between NADH:quinone oxidoreductase activity and the establishment of the ΔΨ is H^+.

^{23}Na-NMR spectroscopy showed that NADH consumption was accompanied by a net sodium ion transport from the inside to the outside of

the membrane vesicles. The long time scale of this process (Figure 3.1.4) is due to the temperature of the assays, 27 ºC, which is much lower than the physiological *R. marinus* growth temperature (65 ºC). It was shown that the sodium ion transport is actively performed by a respiratory chain component since it was stimulated by the protonophore CCCP, excluding a transport by a secondary event dependent on a proton gradient. Na^+ transport was also prevented by KCN, the inhibitor of terminal dioxygen reductases which hampers the electron transfer from NADH to dioxygen by 95 %. The site of sodium ion transport could undoubtedly be identified at the NADH to menaquinone electron transfer segment, since the sodium ion transport activity was recovered upon providing a shortcut for electrons by the presence of menaquinone analogues to KCN inhibited membranes. Moreover, because the specific complex I inhibitor rotenone also inhibited sodium ion transport, we assign the Na^+ translocation activity of the respiratory chain of *R. marinus* to complex I. So far, neither an experimental evidence for the presence of a Na^+-NQR (Na^+ -translocating NADH dehydrogenases) (eg. [23]) in this respiratory chain exists, nor genes coding for such a complex were found in *R. marinus* genome [16]. Furthermore, Na^+ -NQRs are not inhibited by rotenone, excluding a contribution of this enzyme to the observed activity. It was also observed that in the conditions in which Na^+ transport is limited (≤ 20 mM -Na_i^+), the NADH consumption by the respiratory chain is the same as the one observed in non-[Na_i^+]-limiting conditions, implying that Na^+ does not influence the NADH oxidase activity of *R. marinus* complex I.

The observed Na^+ efflux corresponds to a transport from the periplasm to the cytoplasm in the living organism, whereas H^+ influx corresponds to a transport from the cytoplasm to the periplasm. Consequently, the transport of H^+ is higher than that of Na^+, since it

accompanies the positive establishment of the ΔΨ. How these transport activities are processed is still not known. Na^+ is not required for NADH oxidation nor for the establishment of ΔpH. Considering these observations, we propose a possible mechanism of *R. marinus* complex I schematized in Figure 3.1.5. NADH oxidation drives electrogenic proton translocation (represented by 1) to the periplasm and sodium import (represented by 2). It was observed that sodium is not necessary for proton transport but its presence increases the NADH-driven proton transport, possibly indicating the presence of another site for proton transport. Thus, we suggest that there is an export of H^+, associated with sodium import (represented by 2 in Figure 3.1.5), possibly performed by the action of an antiporter. The involvement of a Na^+/H^+ antiporter is the most attractive scenario since complexes I, including the one from *R. marinus*, possess the so called Mrp like subunits, related to these types of antiporters. In the case of complex I from *R. marinus*, there is a second candidate, a Nha like sodium/proton antiporter. Namely, its gene was found among *R. marinus* complex I genes, and is co-transcribed with the canonical ones [24]. Whether this Na^+/H^+ exchange contributes to the

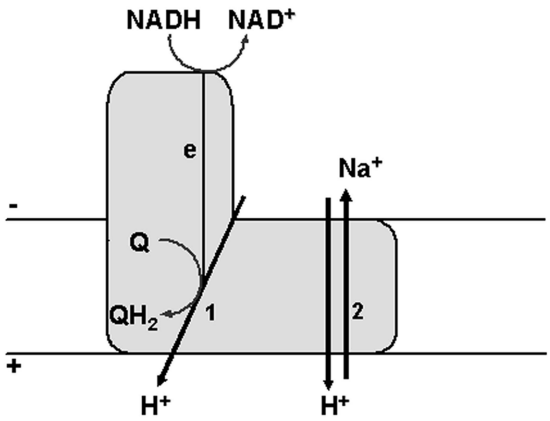

Figure 3.1.5 - Schematic representation of a proposed mechanism for *R. marinus* complex I, considering the H^+ and Na^+ transport observed in this study. 1- Represents the coupling event between NADH oxidation and the translocation of electrogenic charge, H^+. 2- Represents the coupling between NADH oxidation and the gating mechanism that allows the observed Na^+ transport.

increase of the electrochemical potential difference created by the respiratory chain depends on the sodium/proton stoichiometry of this module: a simple exchange of 1 H^+ per 1 Na^+ would not contribute to an increase of the electrochemical potential difference, but could benefit ATP synthesis by ATP synthase if it is H^+-dependent.

The mechanism that we propose here can be further applied to other prokaryotic complexes I. All known complexes I have the so-called Mrp like subunits. Moreover, in the case of *E. coli* an increase in the proton transport was observed upon a Na^+ gradient [25]. Thus, we suggest that the complex I may have two coupling sites, one at the quinone reduction site and a second at the level of the Na^+/H^+ antiporter, whose gating would be dependent on conformational changes originating from electron transport from NADH to the quinone.

In summary, our study indicates that complex I from *R. marinus* is electrogenic involving the transport of protons and sodium ions. It has been already demonstrated that complex I from different organisms contribute, by proton translocation to the periplasm, to the establishment of a electrochemical potential difference. In addition, *R. marinus* complex I translocates Na^+ in the opposite direction, ie, to the cytoplasm. This finding opens new perspectives for the investigation of the electron transfer/charge transport mechanism in complexes I in general, which may be more versatile than one could anticipate.

3.1.6 – ACKNOWLEDGEMENTS

I thank João Carita for cell growth and Dr. Julia Steuber, Prof. Carlos Geraldes, Prof. Alexander Konstatinov and Dr. Smilja Todorovic for numerous suggestions, experimental discussions and advices. A special thank

to Dr. Andreia S. Fernandes, who did all this work with me, and Dr. Ricardo O. Louro for NMR technical training and for all the helpful discussions.

3.1.7 - REFERENCES

[1] G.A. Alfredsson, J.K. Kristjansson, S. Hjorleifsdottir, K.O. Steiter, *Rhodothermus marinus*, gen. nov., sp. nov., a Thermophilic, Halophilic Bacterium from Submarine Hot Springs in Iceland, J of Gen Microbiol 134 (1988) 299-306.

[2] O.C. Nunes, M.M. Donato, M.S. da Costa, Isolation and Characterization of *Rhodothermus* Strains from S. Miguel, Azores, System. Appl. Microbiol 15 (1992) 92-97.

[3] S.H. Bjornsdottir, T. Blondal, G.O. Hreggvidsson, G. Eggertsson, S. Petursdottir, S. Hjorleifsdottir, S.H. Thorbjarnardottir, J.K. Kristjansson, *Rhodothermus marinus*: physiology and molecular biology, Extremophiles 10 (2006) 1-16.

[4] B.J. Tindall, Lipid composition of *Rhodothermus marinus*, FEMS Microbiol Lett 80 (1991) 65-68.

[5] A.S. Fernandes, M.M. Pereira, M. Teixeira, Purification and characterization of the complex I from the respiratory chain of *Rhodothermus marinus*, J Bioenerg Biomembr 34 (2002) 413-421.

[6] A.S. Fernandes, M.M. Pereira, M. Teixeira, The succinate dehydrogenase from the thermohalophilic bacterium *Rhodothermus marinus*: redox-Bohr effect on heme b_L, J Bioenerg Biomembr 33 (2001) 343-352.

[7] A.S. Fernandes, A.A. Konstantinov, M. Teixeira, M.M. Pereira, Quinone reduction by *Rhodothermus marinus* succinate:menaquinone oxidoreductase is not stimulated by the membrane potential, Biochem Biophys Res Commun 330 (2005) 565-570.

[8] A.S. Fernandes, F.L. Sousa, M. Teixeira, M.M. Pereira, Electron paramagnetic resonance studies of the iron-sulfur centers from complex I of *Rhodothermus marinus*, Biochemistry 45 (2006) 1002-1008.

[9] M.M. Pereira, P.N. Refojo, G.O. Hreggvidsson, S. Hjorleifsdottir, M. Teixeira, The alternative complex III from *Rhodothermus marinus* - a prototype of a new family of quinol:electron acceptor oxidoreductases, FEBS Lett 581 (2007) 4831-4835.

[10] M.M. Pereira, J.N. Carita, M. Teixeira, Membrane-bound electron transfer chain of the thermohalophilic bacterium *Rhodothermus marinus*: a novel multihemic cytochrome *bc*, a new complex III, Biochemistry 38 (1999) 1268-1275.

[11] M.M. Pereira, M. Santana, C.M. Soares, J. Mendes, J.N. Carita, A.S. Fernandes, M. Saraste, M.A. Carrondo, M. Teixeira, The caa_3 terminal oxidase of the thermohalophilic bacterium *Rhodothermus marinus*: a HiPIP:oxygen oxidoreductase lacking the key glutamate of the D-channel, Biochim Biophys Acta 1413 (1999) 1-13.

[12] M.M. Pereira, J.N. Carita, R. Anglin, M. Saraste, M. Teixeira, Heme centers of *Rhodothermus marinus* respiratory chain. Characterization of its cbb_3 oxidase, J Bioenerg Biomembr 32 (2000) 143-152.

[13] A.F. Verissimo, M.M. Pereira, A.M. Melo, G.O. Hreggvidsson, J.K. Kristjansson, M. Teixeira, A ba_3 oxygen reductase from the thermohalophilic bacterium *Rhodothermus marinus*, FEMS Microbiol Lett 269 (2007) 41-47.

[14] M.M. Pereira, A.M. Antunes, O.C. Nunes, M.S. da Costa, M. Teixeira, A membrane-bound HIPIP type center in the thermohalophile *Rhodothermus marinus*, FEBS Lett 352 (1994) 327-330.

[15] M. Stelter, A.M. Melo, L.M. Saraiva, M. Teixeira, M. Archer, Crystallization and X-ray analysis of *Rhodothermus marinus* cytochrome *c* at 1.23 A resolution, Protein Pept Lett 14 (2007) 1038-1040.

[16] *Rhodothermus marinus* DSM 4252, whole genome shotgun sequencing project, 2009.

[17] M.M. Pereira, M.L. Verkhovskaya, M. Teixeira, M.I. Verkhovsky, The *caa*(3) terminal oxidase of *Rhodothermus marinus* lacking the key glutamate of the D-channel is a proton pump, Biochemistry 39 (2000) 6336-6340.

[18] G.F. Ames, Lipids of *Salmonella typhimurium* and *Escherichia coli*: structure and metabolism, J Bacteriol 95 (1968) 833-843.

[19] C. Watters, A one-step biuret assay for protein in the presence of detergent, Anal Biochem 88 (1978) 695-698.

[20] J.C. Smith, P. Russ, B.S. Cooperman, B. Chance, Synthesis, structure determination, spectral properties, and energy-linked spectral responses of the extrinsic probe oxonol V in membranes, Biochemistry 15 (1976) 5094-5105.

[21] D.P. Briskin, I. Reynolds-Niesman, Determination of H/ATP Stoichiometry for the Plasma Membrane H-ATPase from Red Beet (*Beta vulgaris* L.) Storage Tissue, Plant Physiol 95 (1991) 242-250.

[22] A.M. Delort, G. Gaudet, E. Forano, ^{23}Na NMR study of *Fibrobacter succinogenes* S85: comparison of three chemical shift reagents and calculation of sodium concentration using ionophores, Anal Biochem 306 (2002) 171-180.

[23] M. Hayashi, Y. Nakayama, T. Unemoto, Recent progress in the Na(+)-translocating NADH-quinone reductase from the marine *Vibrio alginolyticus*, Biochim Biophys Acta 1505 (2001) 37-44.

[24] A.M. Melo, S.A. Lobo, F.L. Sousa, A.S. Fernandes, M.M. Pereira, G.O. Hreggvidsson, J.K. Kristjansson, L.M. Saraiva, M. Teixeira, A nhaD Na^+/H^+ antiporter and a pcd homologues are among the *Rhodothermus marinus* complex I genes, Biochim Biophys Acta 1709 (2005) 95-103.

[25] S. Stolpe, T. Friedrich, The Escherichia coli NADH:ubiquinone oxidoreductase (complex I) is a primary proton pump but may be capable of secondary sodium antiport, J Biol Chem 279 (2004) 18377-18383.

3.1.8 – SUPPLEMENTARY MATERIAL

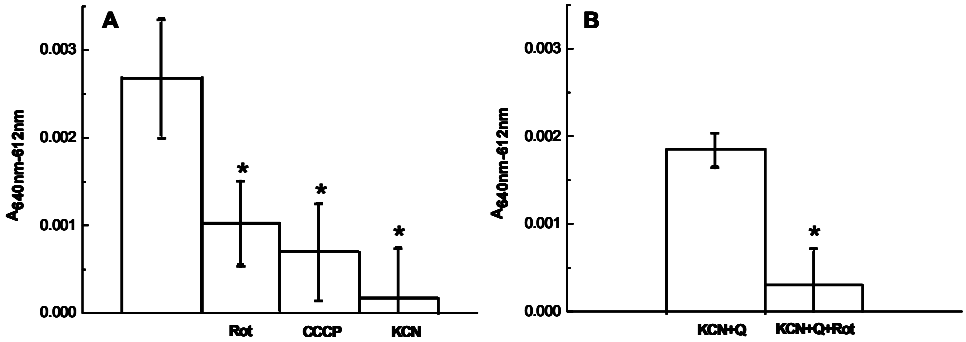

Supplementary Figure 3.1.1 - Generation of a ΔΨ by *R. marinus* membrane vesicles. Change in A_{640} *minus* A_{612} of 1.5 μM oxonol V in membrane vesicles with 10 mM HEPES-Tris buffer pH 7.5, 50 mM Na_2SO_4 after addition of 4 mM NADH. Panel A) When indicated, membrane vesicles were pre-incubated with 40 μM rotenone (Rot), 10 μM CCCP or 2 mM KCN (*, $p<0.05$, *versus* membranes without pre-incubations). Panel B) Membrane vesicles were pre-incubated with 2 mM KCN *plus* 100 μM DMN (KCN+Q) or with 2 mM KCN *plus* 100 μM DMN *plus* 40 μM Rot (KCN+Q+Rot) (*, $p<0.05$, *versus* membranes pre-incubated with 2 mM KCN *plus* 100 μM DMN). The represented data is the average ± standard deviation of at least three separate assays.

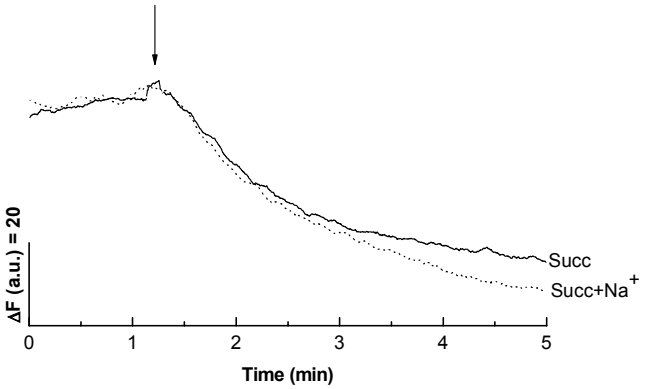

Supplementary Figure 3.1.2 - Generation of a pH difference by the respiratory chain of *R. marinus* monitored by ACMA fluorescence. The assay contained membrane vesicles in 10 mM HEPES-Tris buffer pH 7.5 with 0 or 25 mM Na_2SO_4. The reaction was started by the addition of 50 μM succinate (indicated by an arrow).

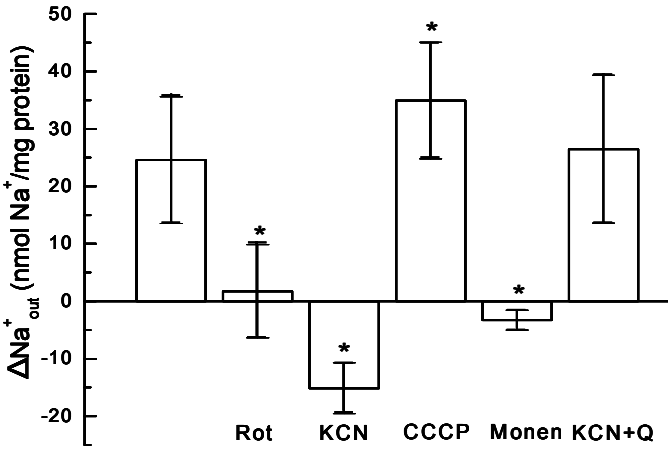

Supplementary Figure 3.1.3 - Sodium ion transport by *R. marinus* NADH-respiring membrane vesicles. Representation of the effect on external Na^+ after 5 min upon addition of 4 mM K_2NADH to membrane vesicles containing 50 or 100 mM Na^+. When indicated, membrane vesicles were preincubated with 40 μM rotenone (Rot), 10 mM KCN, 10 μM CCCP, 20 μM monensin (Monen) or 10 mM KCN plus 200 μM of each menaquinone analogue DMN, NQ and menadione (KCN+Q) (*, $p<0.05$, *versus* membranes without pre-incubations). The represented data is the average ± standard deviation of at least three separate assays.

3.2

^{23}Na-NMR spectroscopy: Data Analysis

Chapter 3: Energy conservation by *R. marinus* complex I

Section 3.2 – ^{23}Na-NMR spectroscopy: Data Analysis

3.2.1 – SUMMARY

In this section, methodological aspects concerning the use of ^{23}Na-NMR spectroscopy to measure accurately sodium transport in *R. marinus* membrane vesicles are discussed. External-vesicle sodium concentrations were determined by two different methods, one based on $Tm(DOTP)^{5-}$ induced resonance frequency shift and a second on peak area changes. Although the resonance frequency shift is a suitable way to determine sodium concentration changes under conditions of fast exchange, it was shown to be not applicable to the *R. marinus* membrane vesicles system. In this case, the measurement of the peak area is the most appropriate analysis for the determination of the changes on the external sodium concentration.

3.2.2 – INTRODUCTION

NMR spectroscopy is one of the most suitable, nondestructive and relatively sensitive techniques for the study of sodium ions in biological systems, with the strong advantage of allowing a direct observation of the nuclei via their own resonance frequency. Sodium concentration differences across a biological membrane can be measured by the use of the so-called shifts reagents which make possible to distinguish the resonance of the sodium ions in the internal and external media of the membrane vesicles [1-4]. These reagents are anionic complexes of lanthanides whose paramagnetic proprieties induce a shift on the sodium resonance frequency. As the shift reagent cannot cross the membrane, the resonance frequency of the sodium inside the vesicle is not shifted (see figure 3.1.3 in section 3.1). Compared with other shift reagents, $Tm(DOTP)^{5-}$ requires a lower dosage to achieve resolution of internal and external sodium signals [2, 5], has a more favorable geometry for sodium binding [6] and has the advantage of having a lower

paramagnetic susceptibility (allowing that both the shifted and unshifted peak are sharp and well resolved) [2].

Respiratory complex I couples the electron transfer from NADH to quinone with charge translocation across the membrane. The nature of this charge is still a controversial issue being the proton [7, 8] and the sodium ion [9, 10] the possible candidates. In the previous section, it was shown that the *R. marinus* complex I coupling ion is the proton; however this enzyme is also capable of sodium translocation but in an opposite direction. Sodium transport was measured using ^{23}Na-NMR spectroscopy and the sodium concentration was quantified by integration of the sodium signal. In principle, the sodium concentration could have also been determined using calibration curves for the shift of the sodium resonance frequency. The measurement of the resonance frequency is considered to be more precise than the measurement of the peak area [3, 11]. Thus the NMR data presented on section 3.1, were also analyzed in this manner to determine sodium concentration. Although the same conclusions were obtained for sodium transport directionality, the analysis based on the peak area revealed to be the most suitable approach for the determination of the concentration of the external sodium in the case of *R. marinus* membrane vesicles.

3.2.3 – MATERIAL AND METHODS

A. Cell growth, membrane vesicles preparation and characterization

Cell growth, membrane vesicles preparation and characterization were performed as described in section 3.1 (parts A, B and C).

B. ^{23}Na-NMR spectroscopy

NMR measurements were performed in the same conditions as described in section 3.1 for the following samples: i) 4.5 mM $Na_5Tm(DOTP)$

in 10 mM HEPES-Tris buffer pH 7.5; ii) 25 mM Na_2SO_4 + 4.5 mM $Na_5Tm(DOTP)$ in 10 mM HEPES-Tris buffer pH 7.5; and iii) 25 mM Na_2SO_4 + 4.5 mM $Na_5Tm(DOTP)$ + membrane vesicles in 10 mM HEPES-Tris buffer pH 7.5. In experiments ii) and iii), the NMR sample was left non-perturbed in the spectrometer and data were collected over time. In experiment i), known amounts of sodium were added consecutively to the NMR tube and data were collected after each addition. Sodium concentration was measured by peak integral and resonance frequency changes.

The NMR data presented in section 3.1 were carefully re-analyzed taking into account the resonance frequency (in addition to the analysis of the peak area presented before). Sodium titration curves for all the experiments (membrane vesicles and membrane vesicles in the presence of KCN, KCN+quinones, monensine, CCCP and rotenone) were performed in the presence and absence of 4 mM of K_2SO_4. A total of 12 different titration curves were obtained. NMR data collection was performed as described in section 3.1.

3.2.4 – RESULTS AND DISCUSSION

Resonance Frequency versus Peak Area

Under fast exchange conditions, the sodium resonance frequency is inversely proportional to the ratio $[Na^+]/[Tm(DOTP)^{5-}]$, meaning that if the sodium concentration increases its resonance frequency decreases [11]. This frequency/concentration ratio is not linear reaching a limiting value when the sodium concentration is much higher than the shift reagent concentration. Figure 3.2.1 presents a titration of $Tm(DOTP)^{5-}$ with Na^+ and the frequency/concentration ratio is well described. This type of behavior is consistent with multiple sodium binding sites on the shift reagent [12]. At low $[Na^+]/[Tm(DOTP)^{5-}]$ ratio most of the sodium ions are suggested to be

bound as 1/1 complex while at high ratios the sodium ions bind at different positions on the shift reagent with a lower bound shift [12].

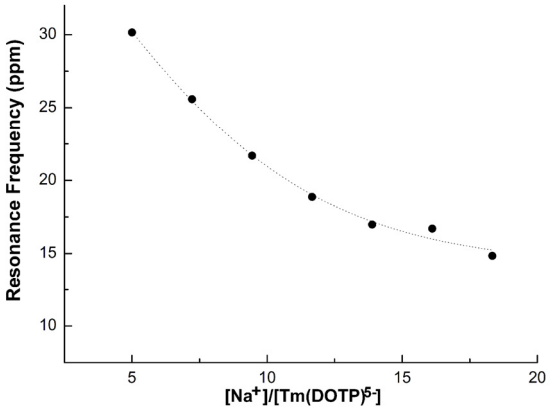

Figure 3.2.1 – Dependence of $Tm(DOTP)^{5-}$ induced sodium resonance frequency on the ratio $[Na^+]/[Tm(DOTP)^{5-}]$. Small amount of sodium were added consecutively to 10 mM HEPES-Tris buffer pH 7.5, 4.5 mM $Na_5Tm(DOTP)$.

Six different NMR samples were measured in the previous section 3.1: membrane vesicles and membrane vesicles pre-incubated with CCCP, KCN, KCN+Q, rotenone and monensine. The presence of other ions in solution and changes in the ionic strength also influence the $Tm(DOTP)^{5-}$ induced sodium resonance frequency [1, 3, 11-13]. Thus, for each individual sample, titration curves similar to the one shown in Figure 3.2.1 were obtained. Because the reactions were initiated by the addition of 4 mM of K_2NADH, calibration curves in the presence of potassium ions were also performed. One example of such a titration is illustrated in Figure 3.2.2 which shows the dependence of the $Tm(DOTP)^{5-}$ induced sodium resonance frequency on the ratio $[Na^+]/[Tm(DOTP]^{5-}$ for *R. marinus* membrane vesicles (in the absence of any inhibitor or uncoupler).

For the analysis of sodium transport based on these curves, the first point (prior to the addition of NADH) was analyzed using the curves

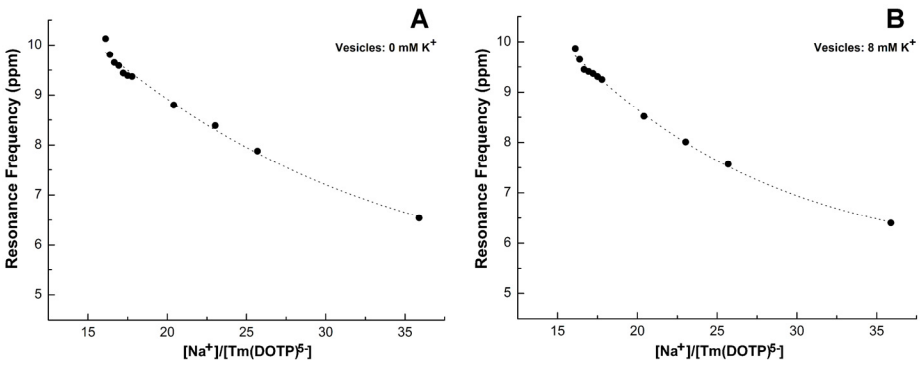

Figure 3.2.2 – Dependence of $Tm(DOTP)^{5-}$ induced sodium resonance frequency on the ratio $[Na^+]/[Tm(DOTP)^{5-}]$ for *R. marinus* membrane vesicles in 10 mM HEPES-Tris buffer pH 7.5, 4.5 mM $Na_5Tm(DOTP)$ and initially 25 mM Na_2SO_4, in the absence (A) and presence (B) of 8 mM K^+.

determined without potassium ions and the following points were analyzed with the curves obtained in the presence of these ions. Table 3.2.1 shows some of the external-vesicle sodium concentration quantified by this method as well as by peak area integration.

Knowing that the internal sodium concentration was 50 mM and that the *R. marinus* membrane vesicles internal volume is 1 μL/mg of protein, the transport of 60 to 500 nmol Na^+/mg of protein is certainly overestimated since the *R. marinus* vesicles contained a maximum of 50 nmol Na^+/mg of protein inside the vesicles. This clearly indicates that the $Tm(DOTP)^{5-}$ induced sodium resonance frequency was affected by other factors besides

Table 3.2.1 – Sodium ion transport by *R. marinus* NADH-respiring membrane vesicles. The amount of sodium translocated, during the first 5 min after NADH addition, was determined by two different methods: $Tm(DOTP)^{5-}$ induced sodium resonance frequency and by peak area integration.

	ΔNa^+_{out} (nmol Na^+/mg protein)	
	Resonance Frequency	Peak Area
Vesicles	57	24.5
Vesicles + CCCP	533	40.5
Vesicles + KCN	-329	-15

the amount of sodium that was translocated and/or the presence of potassium ions.

The analysis based on the peak area was, apparently, not affected by external factors. The changes in sodium concentrations were always in agreement with the available amount of sodium, even considering the inherent uncertainty of this quantification method (see Supplementary Figure 3.1.3 of section 3.1). This observation was reinforced by the experiments performed under sodium-limiting conditions (0 or 20 mM Na^+ inside vesicles) whereas an increase in the external vesicle medium of 0 or 20 nmol of Na^+ was determined by peak area integration, which were in complete agreement with the total available sodium amount inside the vesicles (see section 3.1).

It is worth mentioning that the experimental set up described in this section had the advantage of having well determined internal and external sodium concentration, which allowed a critical estimation of the available amount of sodium to be transport. On the contrary, in many of the studies described in literature the sodium transport is determined in conditions in which the sodium concentrations in the different compartments are not known and thus a critical evaluation of the amount of transported sodium is not possible [1-3, 11].

$Tm(DOTP)^{5-}$ versus R. marinus membrane vesicles

In order to investigate the problem with the $Tm(DOTP)^{5-}$ induced sodium resonance frequency shift analysis, NMR measurements were performed in the presence and absence of the vesicles. In both experiments, the sample was left non-perturbed in the spectrometer and data were collected over time. A capillary containing $Dy(PPPi)_2^{7-}$ was used for position calibration and for area calibration in the case of peak area measurements (Supplementary Figure 3.2.1). As it can be observed in Figure 3.2.3A and B,

both the $Tm(DOTP)^{5-}$ induced resonance frequency and the peak area remained unchanged over time when only sodium and the shift reagent were present in the sample. However, in the presence of the vesicles, the $Tm(DOTP)^{5-}$ induced sodium resonance frequency drifts over time whereas the peak area remained stable (Figure 3.2.3 C and D).

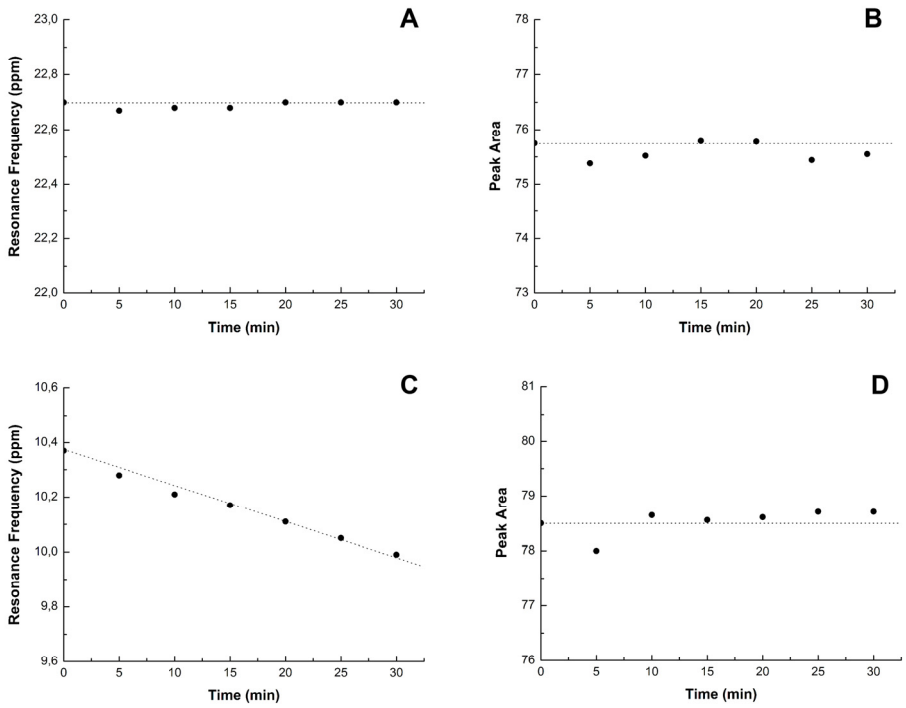

Figure 3.2.3 – Time dependency of the $Tm(DOTP)^{5-}$ induced sodium resonance frequency (A and C) and peak area (B and D). In panels A and B the shift reagent (4.5 mM $Na_5Tm(DOTP)$) and sodium ions (25 mM Na_2SO_4) were present in 10 mM HEPES-Tris pH 7.5, while in panels C and D also *R. marinus* membrane vesicles were present together with shift reagent and sodium ions.

The data presented on Figure 3.2.3 shows that changes on the $Tm(DOTP)^{5-}$ induced sodium resonance frequency do not reflect solely changes in the $[Na^+]/[Tm(DOTP)^{5-}]$ ratio and several factors may contribute to it. As mentioned above, it is described that the presence of competitive

cations such as calcium, magnesium, potassium and protons affects the sodium resonance frequency shift caused by $Tm(DOTP)^{5-}$ [1, 3, 11-13]. It was also reported that $Tm(DOTP)^{5-}$ can form aggregates for concentrations of reagent of the same order of magnitude as those used in the present study [14]. These factors decrease the effective availability of the shift reagent for the sodium and can contribute to the drift in resonance frequency observed in Supplementary Figure 3.2.1. These factors can also contribute to the overestimated values of external sodium calculated taking into account the $Tm(DOTP)^{5-}$ induced sodium resonance frequency shift (Table 3.2.1).

We have hypothesized that an additional factor contributing for the drift in resonance frequency was an unspecific association of the shift reagent with the membrane vesicles. This suggestion was supported by the studies performed using other bacterial membrane vesicles (*E. coli* and *P. denitrificans* vesicles) in which the $Tm(DOTP)^{5-}$ induced sodium resonance position drifted in a similar way as in the case of *R. marinus* vesicles, although *P. denitrificans* complex I was not able to perform sodium translocation (see chapter 5).

$Dy(PPPi)_2^{7-}$ was also used as the shift reagent for the external sodium in *R. marinus* membrane vesicle studies; however it was shown that the $Dy(PPPi)_2^{7-}$ induced sodium resonance frequency shift, when measured in cell suspension, is not stable with time, drifting to higher frequency at approximately 1.5-3 ppm h^{-1} [15]. The analogue behavior of these two shift reagents, $Tm(DOTP)^{5-}$ and $Dy(PPPi)_2^{7-}$, was also detected after showing that the presence of other cations, such as calcium, affects the sodium resonance frequency shift caused by $Dy(PPPi)_2^{7-}$ [1].

In conclusion, the analysis based on the peak area is, for the *R. marinus* system, the most suitable approach for determining the external sodium concentration. In order to perform the same type of studies using other

systems, the establishment of a methodology which should be straightforward to implement is mandatory. Data analysis based on area integration fulfils this aim and it will be applied in subsequent studies (see chapters 4 and 5).

3.3.5 – ACKNOWLEDGEMENTS

I thank to Dr. Ricardo O. Louro, Prof. Carlos Geraldes and Prof. Charles Springer Jr for numerous suggestions, advices and stimulating discussions regarding ^{23}Na-NMR data analysis.

3.3.6 – REFERENCES

[1] D.C. Buster, M.M. Castro, C.F. Geraldes, C.R. Malloy, A.D. Sherry, T.C. Siemers, Tm(DOTP)$^{5-}$: a $^{23}Na^{+}$ shift agent for perfused rat hearts, Magn Reson Med 15 (1990) 25-32.

[2] N. Bansal, M.J. Germann, V. Seshan, G.T. Shires, 3rd, C.R. Malloy, A.D. Sherry, Thulium 1,4,7,10-tetraazacyclododecane-1,4,7,10-tetrakis(methylene phosphonate) as a ^{23}Na shift reagent for the in vivo rat liver, Biochemistry 32 (1993) 5638-5643.

[3] J.A. Balschi, J.A. Bittl, C.S. Springer, Jr., J.S. Ingwall, ^{31}P and ^{23}Na NMR spectroscopy of normal and ischemic rat skeletal muscle. Use of a shift reagent in vivo, NMR Biomed 3 (1990) 47-58.

[4] A.D. Sherry, C.R. Malloy, F.M. Jeffrey, W.P. Cacheris, C.F. Geraldes, Dy(DOTP)$^{5-}$: A new, Stable ^{23}Na Shift Reagent, Journal of Magnetic Resonance 76 (1988) 528-533.

[5] A.M. Delort, G. Gaudet, E. Forano, ^{23}Na NMR study of *Fibrobacter succinogenes* S85: comparison of three chemical shift reagents and calculation of sodium concentration using ionophores, Anal Biochem 306 (2002) 171-180.

[6] P.M. Winter, N. Bansal, TmDOTP($^{5-}$) as a (^{23})Na shift reagent for the subcutaneously implanted 9L gliosarcoma in rats, Magn Reson Med 45 (2001) 436-442.

[7] A.V. Bogachev, R.A. Murtazina, V.P. Skulachev, H^{+}/e^{-} stoichiometry for NADH dehydrogenase I and dimethyl sulfoxide reductase in anaerobically grown *Escherichia coli* cells, J Bacteriol 178 (1996) 6233-6237.

[8] A.S. Galkin, V.G. Grivennikova, A.D. Vinogradov, -->$H^{+}/2e^{-}$ stoichiometry in NADH-quinone reductase reactions catalyzed by bovine heart submitochondrial particles, FEBS Lett 451 (1999) 157-161.

[9] J. Steuber, C. Schmid, M. Rufibach, P. Dimroth, Na^+ translocation by complex I (NADH:quinone oxidoreductase) of *Escherichia coli*, Mol Microbiol 35 (2000) 428-434.

[10] A.C. Gemperli, P. Dimroth, J. Steuber, The respiratory complex I (NDH I) from *Klebsiella pneumoniae*, a sodium pump, J Biol Chem 277 (2002) 33811-33817.

[11] M.S. Albert, W. Huang, J.H. Lee, J.A. Balschi, C.S. Springer, Jr., Aqueous shift reagents for high-resolution cation NMR. VI. Titration curves for in vivo ^{23}Na and $^{1}H_2O$ MRS obtained from rat blood, NMR Biomed 6 (1993) 7-20.

[12] A.D. Sherry, J. Ren, J. Huskens, E. Brucher, É. Tóth, C.F. Geraldes, M.M. Castro, W.P. Cacheris, Characterization of Lanthanide(III) DOTP Complexes: Thermodynamics, Protonation and Coordination to Alkali Metal Ions, Inorg Chem 35 (1996) 4604-4612.

[13] J. Ren, A.D. Sherry, ^{7}Li, ^{6}Li, ^{23}Na and ^{133}Cs multinuclear NMR studies of adducts formed with shift reagent, $TmDOTP^{5}$, Inorganica Chimica Acta 246 (1996) 331-341.

[14] E.S. Henriques, M. Bastos, C.F. Geraldes, M.J. Ramos, Studies of inclusion complexes between cyclodextrines and polyazamacrocyclic chelates of lanthanide (III) ions, J Chem Thermodynamics 35 (2003) 1717-1735.

[15] A.M. Castle, R.M. Macnab, R.G. Shulman, Measurement of intracellular sodium concentration and sodium transport in *Escherichia coli* by ^{23}Na nuclear magnetic resonance, J Biol Chem 261 (1986) 3288-3294.

3.3.7 – SUPPLEMENTARY MATERIAL

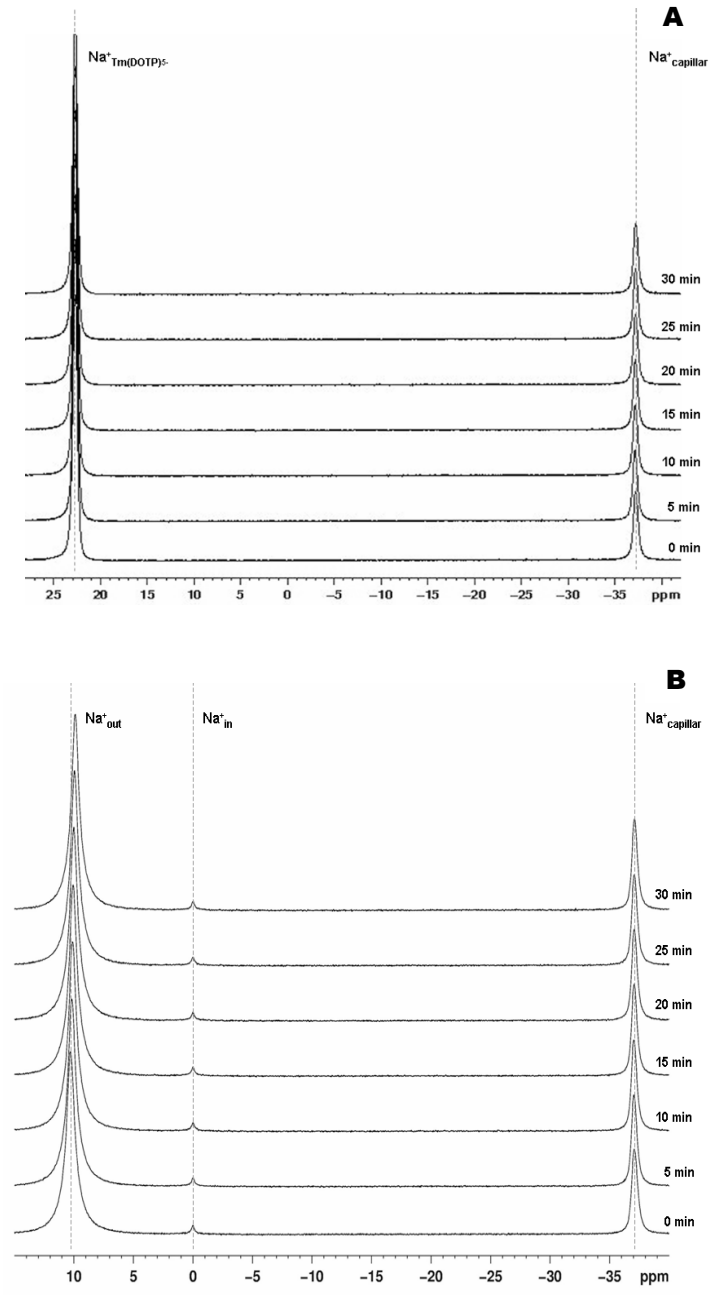

Supplementary Figure 3.2.1 – Time evolution of ^{23}Na-NMR spectra of 25 mM Na_2SO_4 and 4.5 mM $Na_5Tm(DOTP)$ in 10 mM HEPES-Tris pH 7.5 in the absence (A) and in the presence (B) of *R. marinus* membrane vesicles.

Chapter 4

Decoupling of R. marinus complex I

Abbreviations

E.: *Escherichia*; *P.*: *Paracoccus;* R.: *Rhodothermus*; *T.*: *Thermus*.

ΔΨ: membrane potential; ΔpH: pH difference; ΔpH_{out}: external medium pH difference; ΔpNa^{+}_{out}: external medium sodium concentration changes.

ACMA: 9-amino-6-chloro-2-methoxyacridine; CCCP: carbonyl cyanide *m*-chlorophenyl hydrazone; DDM: n-dodecyl-β-D-maltoside; DMN: 2, 3-dimethyl-1,4-naphthoquinone; $Dy(PPPi)_2^{7-}$: dysprosium (III) tripolyphosphate; EIPA: 5-(*N*-ethyl-*N*-isopropyl)-amiloride; EPR: electron paramagnetic resonance; Mrp: multiple resistance and pH related antiporter; NMR: nuclear magnetic resonance; oxonol VI: 1,5-Bis(5-oxo-3-propylisoxazol-4yl)pentamethine oxonol; PMSF: phenylmethane sulfonyl fluoride; Q: quinone; Rot: rotenone; TEMPO: 2,2,6,6-tetramethyl-1-piperidinyloxy; $Tm(DOTP)^{5-}$: thulium(III)1,4,7,10-tetraazacyclododecane-1,4,7,10-tetrakis(methylenephosphonate); Val: valinomycin.

This chapter is under review as:
A.P. Batista and M.M. Pereira, "Decoupling of the catalytic and transport activities of complex I from *Rhodothermus marinus* by a sodium/proton antiporter inhibitor."

Chapter 4: Decoupling of *R. marinus* complex I

4.1 - SUMMARY

The energy transduction by *R. marinus* complex I was addressed studying the influence of 5-(*N*-ethyl-*N*-isopropyl)-amiloride (EIPA) on its activities. EIPA is an inhibitor of Na^+/H^+ antiporters and is also described to inhibit complex I NADH:quinone oxidoreductase activity. We performed studies on *R. marinus* complex I NADH:quinone oxidoreductase activity and H^+ and Na^+ transports at different concentrations of EIPA, using inside-out membrane vesicles. We observed that the oxidoreductase activity and both H^+ and Na^+ transports are inhibited by EIPA. Most interestingly, the catalytic and the two transport activities showed different inhibition profiles, being the transports differently inhibited at concentrations of EIPA at which the catalytic activity is not affected. In this way the catalytic and transports activities were decoupled. Moreover, we also observed that the inhibition of the catalytic activity was not influenced by the presence of Na^+, whereas the H^+ transport presented different inhibition behaviors in the presence and absence of Na^+. Taking together our observations, we concluded that *R. marinus* complex I performs energy transduction by two different processes: proton pumping and Na^+/H^+ antiporting. The decoupling of the catalytic and transports activities suggests the involvement of an indirect coupling mechanism, possibly through conformational changes.

4.2 – INTRODUCTION

R. marinus complex I is capable of H^+ and Na^+ translocations, although to opposite directions. The coupling ion of the system is the H^+ and neither the catalytic reaction nor the establishment of the ΔpH required the presence of Na^+, but the presence of these ions increased proton transport [1]. A model for the functional mechanism of complex I was then proposed, suggesting the presence of two different energy coupling sites, both coupled

to menaquinone reduction. One of the sites is Na^+ independent, while the other needs Na^+ to promote H^+ translocation. It was suggested that this second site might work as a Na^+/H^+ antiporter [1]. Our model is here further investigated by studying the effect of 5-(*N*-ethyl-*N*-isopropyl)-amiloride (EIPA) on the catalytic activity and on the ion translocation processes of *R. marinus* complex I.

EIPA, as other amiloride derivatives, has been known to be an inhibitor for Na^+/H^+ antiporters [2-4]. As mentioned before, some subunits of complex I are related to Mrp type Na^+/H^+ antiporters [5, 6] and thus amiloride derivatives have also been applied in studies of this respiratory complex. Nakamaru-Ogiso and coworkers have shown that the electron transfer of mitochondrial and bacterial complex I is inhibited by amiloride derivatives [7] and that these compounds prevent labeling of the ND5 (homologue of NuoL/Nqo12) subunit in bovine complex I with a fenpyroximate analogue, a potent complex I inhibitor [8]. The inhibitory effect on the catalytic activity was also observed for the *E. coli* enzyme [9]. The expressed C-terminally truncated NuoL subunit of the *E. coli* complex I was shown to mediate sodium uptake when reconstituted into liposomes and this transport was inhibited by the addition of EIPA [10]. Inhibition of complex I proton pumping by EIPA was suggested by studies with isolated rat liver mitochondria [11].

The results now obtained reinforce our previous model, in which we proposed the existence of two energy coupling sites and suggest that *R. marinus* complex I transduces energy by two processes: proton pumping and Na^+/H^+ antiporting. Moreover, our findings suggest the involvement of an indirect mechanism for energy transduction, possibly through conformational changes.

4.3 – MATERIAL AND METHODS

A. Cell growth and membrane vesicles preparation

R. marinus PRQ 62B was grown as described previously [12], with the exception that the growth medium contained 100 mM glutamate. After harvesting, cells were suspended in 2.5 mM HEPES-Tris pH 7.5, 5 mM K_2SO_4, 25 mM Na_2SO_4 (buffer A) or 2.5 mM HEPES-Tris pH 7.5, 5 mM K_2SO_4, 50 mM choline chloride (buffer B) and broken in a French Pressure cell at 19 000 psi. The membrane vesicles were obtained by ultracentrifugation of the broken cells at 200 000 g, 2 h at 4 ºC followed by re-suspension in buffer A or buffer B. Integrity of vesicles was checked by the K^+/valinomycin assay using 1,5-Bis (5-oxo-3-propylisoxazol-4-yl) pentamethine oxonol (oxonol VI) as a $\Delta\Psi$ sensitive dye (see below). Protein concentration was determined by the Biuret method modified for membrane proteins [13].

B. Protein purification

Protein was purified as described before [14], introducing a further chromatographic step using a Mono Q column and 20 mM Tris-HCl pH 8, 1 mM PMSF, 0.1% DDM as buffer. The complex was eluted in a linear gradient of 0 to 100% NaCl (1 M). Protein concentration was determined by the Bicinchoninic Acid Method as described before [15].

C. $\Delta\Psi$ detection

$\Delta\Psi$ generation was detected following oxonol VI absorption (A_{628} *minus* A_{587}) at 27 ºC, on an OLIS upgraded Aminco DW2 dual wavelength spectrophotometer [16]. The vesicles integrity was checked generating K^+ gradients with K^+/valinomycin in an external buffer containing 50 mM

K_2SO_4 (internal $[K^+]$=10 mM). The assay was started adding 2 μM valinomycin. To detect the NADH-driven ΔΨ formation, 4 mM K_2-NADH was added to vesicles in buffer A or buffer B. When referred, EIPA (0 to 100 μM), CCCP (10 μM), rotenone (10 μM) and KCN (5 mM) were added prior to the addition of NADH.

D. Determination of the internal volume of membrane vesicles

The internal volume of the vesicles was determined by EPR spectroscopy, using TEMPO oxidized with $K_3[Fe(CN)_6]$ [17]. TEMPO in the external medium was quenched with 100 mM of potassium chromium(III) oxalate. EPR measurements were performed at room temperature, with a microwave frequency of 9.39 GHz, microwave power 1 mW and modulation amplitude 0.04 mT.

E. Activity measurements

Oxygen consumption was measured with a Clark-type oxygen electrode YSI Model 5300. The assay mixture contained vesicles in buffer A or buffer B. The reaction was started by adding K_2-NADH. When used, EIPA (0 to 100 μM), valinomycin (2 μM) or CCCP (10 μM) were added prior to the addition of substrate. NADH:quinone oxidoreductase activity was monitored on an OLIS upgraded Aminco DW2 dual wavelength spectrophotometer, at 55 ºC, following the NADH oxidation at 330 nm (ε= 5930 $M^{-1}cm^{-1}$). The reaction mixture contained 200 mM KPi pH 7.5, 0.1% DDM and 0 or 25 mM Na_2SO_4, 50 μM DMN and 50 μM NADH. The reaction was started by the addition of complex I. When used, NaCl (0 to 200 mM) or EIPA (0 to 250 μM) were added prior to the addition of substrate. NADH:$K_3[Fe(CN)_6]$ oxidoreductase activity was monitored at 420 nm (ε= 1020 $M^{-1}cm^{-1}$). The reaction medium contained membrane vesicles or

solubilized membranes in buffer A or buffer B, 250 μM $K_3[Fe(CN)_6]$ and 250 μM NADH. Solubilized membranes were obtained by stirring an aliquot of membrane vesicles with 10% of DDM for 4 h at 4 °C.

F. Fluorescence spectroscopy

Fluorescence spectroscopy was performed on a Varian Cary Eclipse spectrofluorimeter. The generation of ΔpH was determined by the quenching of the fluorescence of ACMA ($\lambda_{excitation}$=410 nm, $\lambda_{emission}$=480 nm). Vesicles were incubated aerobically for 5 min at 27 ºC in buffer A or buffer B containing 1 μM of ACMA. The reaction was started by adding 100 μM of NADH. When referred, valimonycin (2 μM) and EIPA (0 to 100 μM) were added prior to the addition of NADH.

The extra-vesicle pH (pH_{out}) was monitored using the hydrophilic and membrane impermeable pH indicator, pyranine ($\lambda_{emission}$=508 nm). Fluorescence spectra ($\lambda_{excitation}$=458 nm) were obtained before and after NADH addition (at 5, 10 and 15 min). Vesicles were incubated in buffer A or buffer B containing 2 μM pyranine. The reaction was started by adding 4 mM NADH. When referred, valimonycin (2 μM), rotenone (10 μM), KCN (5 mM), DMN (200 μM) or EIPA (0 to 20 μM) were added prior to the addition of NADH.

G. ^{23}Na-NMR spectroscopy

NMR spectra were recorded on a Bruker Avance II 500 MHz spectrometer at 27 °C, operating at 132 MHz for ^{23}Na (see chapter 3, section 3.1) [1]. $Tm(DOTP)^{5-}$ (4.5 mM) was used as a shift reagent for the Na^+ signal of the suspension medium. A capillary tube containing the shift reagent $Dy(PPPi)_2^{7-}$ (22 mM), was used in all experiments as external reference [18].

Spectra were recorded upon addition of 4 mM K_2-NADH to vesicles which were previously incubated with KCN (10 mM), DMN (200 μM), valinomycin (2 μM) or EIPA (0 to 20 μM).

4.4 – RESULTS

Membrane vesicles characterization

R. marinus vesicles, with an internal volume of 1 μL per mg of protein, allowed the formation of a membrane potential using K^+ and valinomycin, which was stable for at least 20 min. This observation indicated that the vesicles were tight. The orientation of the vesicles was determined comparing the NADH:$K_3[Fe(CN)_6]$ oxidoreductase activity of vesicles before and after their solubilization with DDM. The activity was, approximately, the same in both situations. It can be concluded that the *R. marinus* membrane vesicles obtained by French press cell rupture had an inside-out orientation.

Effect of EIPA on NADH-driven ΔΨ generation

The addition of the substrate NADH to the vesicles originated a jump in the absorbance of the oxonol VI, indicating the establishment of a ΔΨ (positive inside) (Figure 4.1). If the vesicles were pre-incubated with the terminal dioxygen reductases inhibitor, KCN, the jump in A_{628nm}-A_{587nm} observed upon substrate addition was negligible, indicating that the observed ΔΨ was created by the functioning of the respiratory chain (trace b, Figure 4.1A). A similar behavior was observed in the presence of rotenone (complex I inhibitor) or in the presence of the protonophore CCCP (traces c and d, Figure 4.1A). These observations are in agreement with the results obtained before (see chapter 3, section 3.1) [1]. In the absence of the amiloride derivative, EIPA, approximately the same absorbance difference was detected

in the presence of 25 mM Na_2SO_4 or 50 mM choline chloride ($[Na^+]$ < 10 μM) (traces a, Figures 4.1B and 4.1C and Figure 4.1D).

The effect of EIPA, on the NADH-driven ΔΨ formation was tested in the presence and absence of Na^+ (Figures 4.1B, 4.1C and 4.1D). Different EIPA concentrations were added to the reaction mixture before NADH addition. For EIPA concentrations up to 20 μM, no clear effect was observed, independently of the presence of Na^+ (traces a and b, Figures 4.1B,

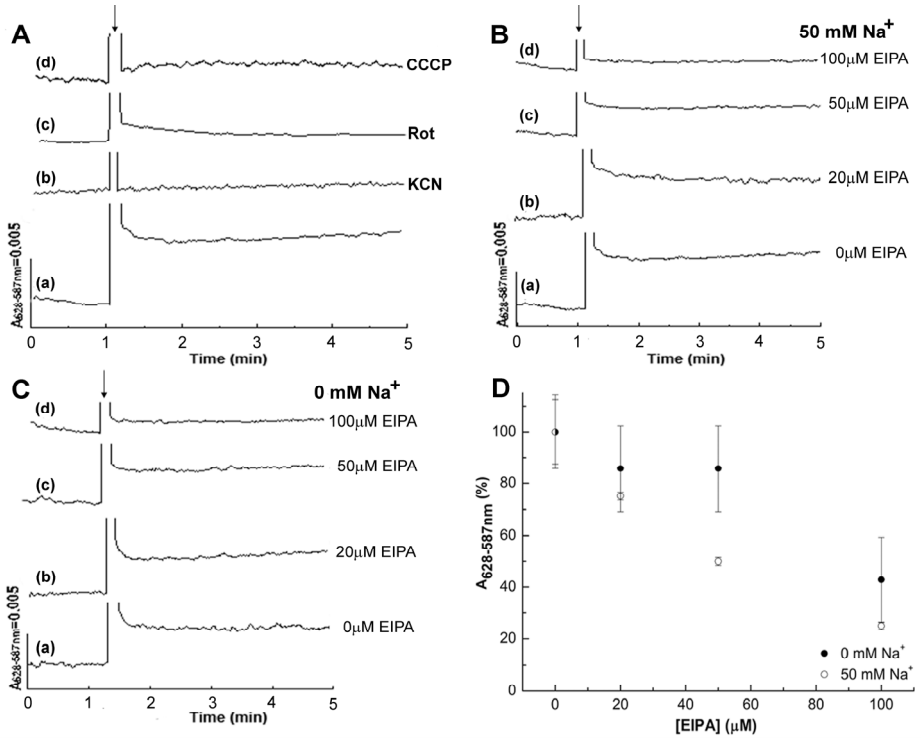

Figure 4.1 - Generation of a ΔΨ by the functioning of *R. marinus* respiratory chain, monitored by the absorbance difference ($A_{628\text{-}587nm}$) of oxonol VI. Membrane vesicles were prepared in buffer A or buffer B. The reaction was started by the addition of 4 mM NADH (indicated by an arrow). Panel A: Absorbance difference of oxonol VI, in the presence of Na^+, upon the addition of NADH to vesicles (a) and pre-incubated vesicles with 5 mM KCN (b), 10 μM rotenone (Rot) (c) or 10 μM CCCP (d). Panels B, C and D: Influence of EIPA on the NADH-driven ΔΨ in the presence (panel B, open circles panel D) or the absence (panel C, filled circles panel D) of Na^+. The represented data are the average ± standard deviation of at least three separated assays (panel D).

4.1C and 4.1D). A 40-60% inhibition of ΔΨ formation is observed at 100 μM of EIPA in the absence of Na^+ (trace d, Figures 4.1C, 4.1D), whereas in the presence of this ion approximately 50% of inhibition is already observed at 50 μM EIPA (trace c, Figures 4.1B, 4.1D).

Effect of EIPA on the NADH:dioxygen oxidoreductase activity

R. marinus vesicles were able to consume dioxygen upon addition of NADH, with an approximate rate of 23 nmol $O_2.mg^{-1}.min^{-1}$ at 27 ºC. As previously observed (see chapter 3, section 3.1) [1], this activity was not dependent or stimulated by the presence of Na^+ . In the presence of valinomycin and CCCP the dioxygen consumption increased (~38 nmol $O_2.mg^{-1}.min^{-1}$). The NADH:dioxygen oxidoreductase activity was affected by EIPA and an inhibition of 10-20% was observed at 50 μM EIPA (Figure 4.2). The inhibition increased with the increase of the concentration of EIPA at

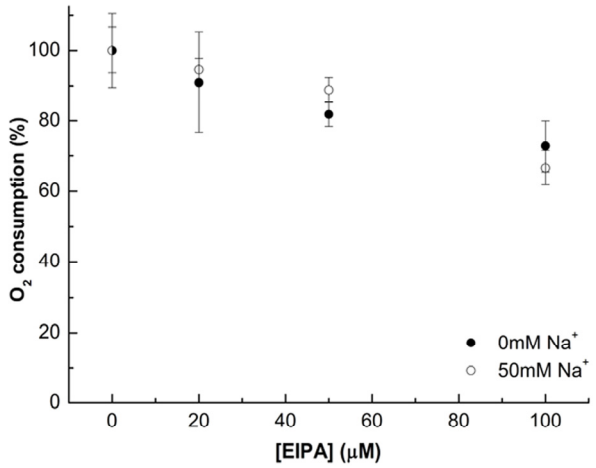

Figure 4.2 - Effect of EIPA inhibition on the NADH:O_2 oxidoreductase activity of *R. marinus* membrane vesicles. The activity was measured in the presence (open circles) or absence (filled circles) of Na^+. The reaction was started by the addition of 4 mM NADH. NADH:O_2 oxidoreduction in the presence of Na^+ and 0 μM of EIPA was used as reference (100%). The represented data are the average ± standard deviation of at least three separated assays.

least up to 100 μM. The effect of EIPA on the NADH:dioxygen oxidoreductase activity was approximately the same in the presence and absence of Na^+ (Figure 4.2).

Effect of EIPA on the NADH:DMN oxidoreductase activity

NADH:quinone oxidoreductase activity by purified *R. marinus* complex I was determined using the menaquinone analogue, DMN, at different Na^+ concentrations (0 to 200 mM). The specific activity was 0.8 μmol of NADH.min^{-1}.mg^{-1} in the absence of Na^+, a value in the range of those determined for other isolated bacterial enzymes in the presence of detergent [9]. NADH:DMN oxidoreductase activity was not stimulated by the presence of Na^+; on the contrary, a slight decrease in activity was observed upon increasing [Na^+] (Figure 4.3A). It is worth mentioning that such a

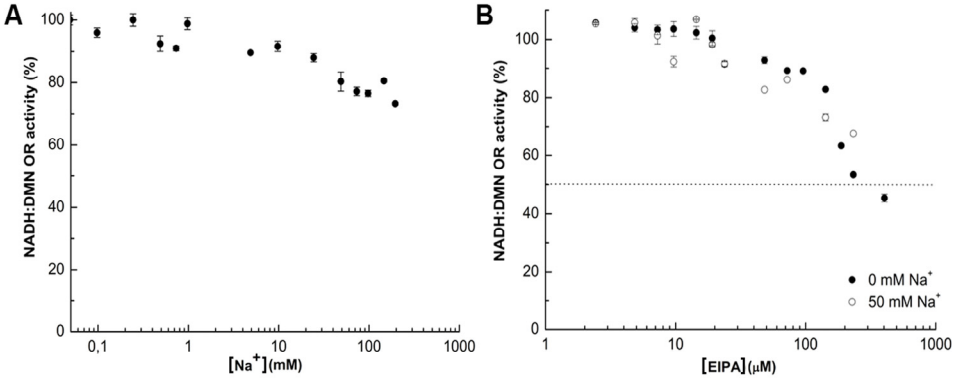

Figure 4.3 - NADH:DMN oxidoreductase activity profiles of purified *R. marinus* complex I. The assay mixture contained 24 μg of purified complex I in 200 mM KPi pH 7.5 with 0.1% DDM, 50 μM NADH and 50 μM DMN. The reaction was started by the addition of complex I and was monitored at 330 nm. The represented data are the average ± standard deviation of at least three separated assays. Panel A: Influence of the Na^+ concentration on the catalytic activity. NADH:DMN oxidoreduction in the absence of Na^+ was used as reference (100%). Panel B: Effect of EIPA on the catalytic activity in the presence (open circles) and absence (filled circles) of Na^+. NADH:DMN oxidoreduction in the absence of EIPA was used as reference (100%).

decrease was not observed in the case of vesicles.

No inhibition of NADH:quinone oxidoreductase activity was observed at least up to 20 μM EIPA, and a half maximal inhibition (IC_{50}) for EIPA of approximately 230 μM was estimated. The inhibitory effect was not affected by the presence or absence of Na^+ (Figure 4.3B).

Effect of EIPA on ⊿pH generation

It was previously shown that the functioning of *R. marinus* complex I allowed the establishment of a ΔpH, which was completely sensitive to the protonophore CCCP and to the Na^+/H^+ exchanger monensin. Although the presence of Na^+ was not a requisite for the establishment of ΔpH, the ΔpH increased in the presence of this type of ions (see chapter 3, section 3.1) [1]. In the current study, the effect of EIPA on the NADH-driven ΔpH was monitored using ACMA in the presence and absence of Na^+ (Figure 4.4). Since we have observed an NADH-driven ΔpH increase of 20-30% in the

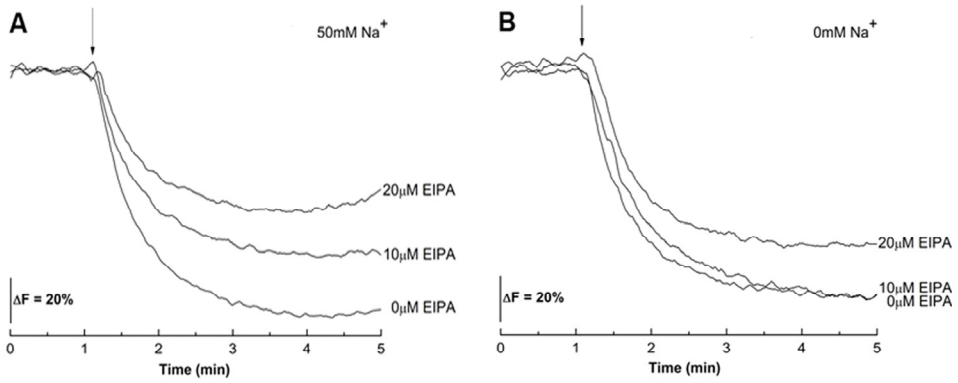

Figure 4.4 - Effect of EIPA on NADH-driven ΔpH generation by the respiratory chain of *R. marinus*. The ACMA fluorescence was detected using an $\lambda_{excitation}$=410 nm and an $\lambda_{emission}$=480 nm. The reaction was started by the addition of 100 μM NADH (indicated by an arrow). NADH-driven ΔpH generation, in absence of EIPA was used as reference (100%). Panel A and B: Influence of EIPA (0, 10 and 20 μM) on NADH-driven ΔpH generation by vesicles prepared in the presence (panel A) or absence (panel B) of Na^+.

absence of ΔΨ (Supplementary Figure 4.1), these assays were performed in the presence of valinomycin and K^+, so that the establishment of ΔpH was not limited by ΔΨ. In the presence of Na^+, a decrease of ~30% and ~45% of the ΔpH amplitude were measured at 10 and 20 μM of EIPA, respectively (Figure 4.4A). When Na_2SO_4 was replaced by choline chloride, only ~20% of inhibition on ΔpH amplitude was observed at 20 μM EIPA. In the absence of Na^+, 10 μM EIPA had no effect on the NADH-driven ΔpH (Figure 4.4B).

Effect of EIPA on NADH-driven external-vesicle pH (pH_{out}) change

Changes on the pH_{out} due to the activity of complex I were measured using the pyranine fluorescence probe. Pyranine is a hydrophilic and membrane impermeable pH indicator that responds rapidly to changes in pH in the physiological range [19]. To focus on the NADH-quinone segment of the *R. marinus* respiratory chain, the vesicles were pre-incubated with KCN and DMN. Upon addition of NADH, an increase in the pyranine fluorescence intensity is observed, indicating an increase in the pH_{out} due to the functioning of complex I. In the presence of valinomycin more than a two-fold increase of the pH_{out} change was observed indicating that NADH:DMN oxidoreductase activity was previously limited by ΔΨ (Figure 4.5A). If the vesicles were pre-incubated with KCN (without DMN) or rotenone the alkalinization upon NADH addition was considerably impaired (filled and open squares, Figure 4.5B). The observed increase in the presence of valinomycin, was the same in the presence or absence of Na^+. However, the change in pH_{out} is more pronounced in the presence of Na^+ than in its absence (filled circles, Figures 4.5C and 4.5D).

The NADH-driven pH_{out} change was also investigated using different EIPA concentrations (0, 10 and 20 μM), in the presence or absence of Na^+ (Figures 4.5C and 4.5D). These assays were also performed in the presence of

valinomycin in order to overcome the limitation of activity by ΔΨ. In the absence of Na^+, ~46% of inhibition was reached at 20 μM EIPA and no inhibition was detected at 10 μM (open and filled triangles, Figure 4.5C). An IC_{50} of ~22 μM was estimated for the NADH-driven pH_{out} change in the

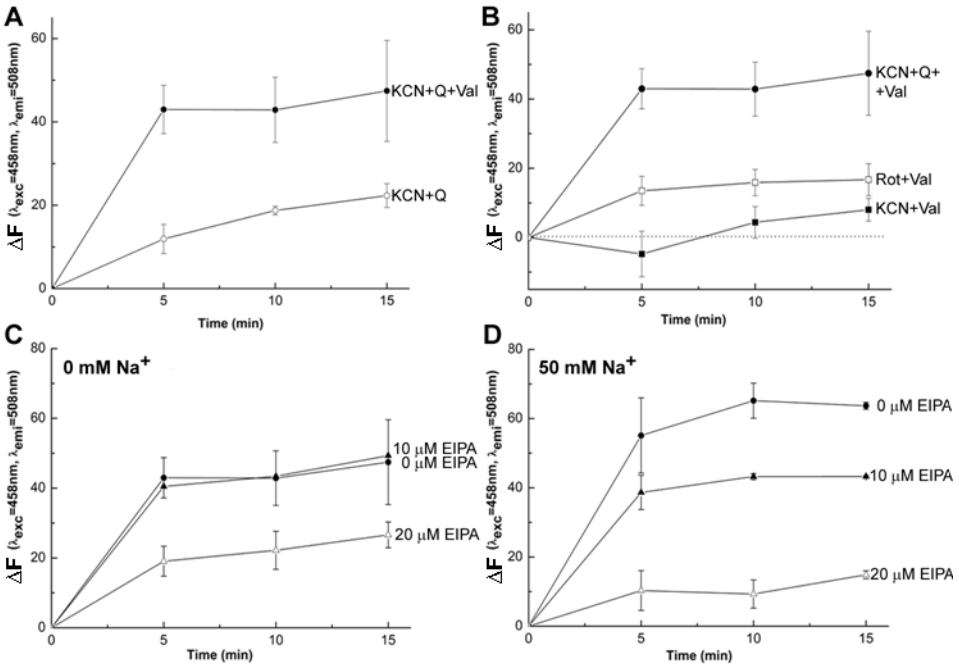

Figure 4.5 - Effect of ΔΨ, inhibitors and EIPA on NADH-driven pH_{out} variation by *R. marinus* complex I. The pyranine fluorescence was detected using an $\lambda_{excitation}$=458 nm and an $\lambda_{emission}$=508 nm. The reaction was started by the addition of 4 mM NADH. The represented data are the average ± standard deviation of at least three separated assays. Panel A: Influence of ΔΨ on NADH-driven pH_{out} variation. The assay mixture contained vesicles pre-incubated with KCN (5 mM) and DMN (200 μM) in the absence (open circles) or presence of valinomycin (2 μM) (filled circles). Panel B: Influence of inhibitors on NADH-driven pH_{out} variation. The assay mixture contained vesicles pre-incubated with KCN (5 mM) *plus* valinomycin (2 μM) (filled squares), rotenone (10 μM) *plus* valinomycin (2 μM) (open squares) and KCN (5 mM) *plus* DMN (200 μM) *plus* valinomycin (2 μM) (filled circles). Panel C and D: Influence of EIPA (0, 10 and 20 μM) on NADH-driven pH_{out} variation. The assay mixture contained vesicles, prepared in the absence (panel C) or presence of Na^+ (panel D), pre-incubated with KCN (5 mM), DMN (200 μM) and valinomycin (2 μM).

absence of Na^+. In the presence of Na^+, at 10 μM EIPA a decrease in the change of the pyranine fluorescence intensity of ~32% was observed and at 20 μM EIPA the decrease in that change was ~80% (filled and open triangles, Figure 4.5D). In this case, an IC_{50} of ~14 μM was estimated. EIPA concentrations responsible for a complete inhibition of the ions transports were not possible to determine since at higher EIPA concentrations the catalytic reaction was inhibited.

Effect of EIPA on Na^+- transport

It was previously shown using ^{23}Na-NMR spectroscopy that NADH consumption was accompanied by Na^+ transport from the inside to the outside of *R. marinus* vesicles, which was completely sensitive to KCN, monensin and rotenone. This transport was actively performed since it was stimulated by the protonophore CCCP, excluding a transport by a secondary event dependent on a proton gradient or simply by a charge compensation effect (see chapter 3, section 3.1) [1]. The influence of EIPA on Na^+ transport by *R. marinus* complex I was also investigated using pre-incubated vesicles with KCN and DMN. After NADH addition, an increase in the external medium of, approximately, 20 to 25 nmol of Na^+ per mg of protein was observed (open circles, Figure 4.6A) and an increase of 35 to 45% was observed in the presence of valinomycin (filled circles, Figure 4.6A), showing that Na^+ transport was limited by $\Delta\Psi$. EIPA, used in the presence of valinomycin, was shown to inhibit the external increase of $[Na^+]$ by ~50% and ~80% at 10 and 20 μM, respectively (filled and open triangles Figure 4.6B). An IC_{50} of ~10 μM was estimated.

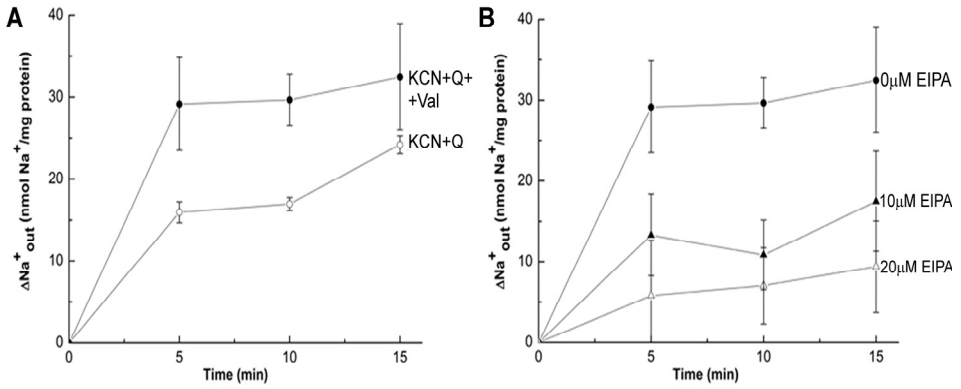

Figure 4.6 - Effect of ΔΨ and EIPA on NADH-driven $\Delta[Na^+]_{out}$ by *R. marinus* complex I monitored by ^{23}Na-NMR. The reaction was started by the addition of 4 mM NADH. The represented data are the average ± standard deviation of at least three separated assays. Panel A: Influence of ΔΨ on NADH-driven $[Na^+]_{out}$ variation. The assay mixture contained vesicles pre-incubated with KCN (5 mM) and DMN (200 μM) in the absence (open circles) or presence of valinomycin (2 μM) (filled circles). Panel B: Influence of EIPA (0, 10 and 20 μM) on NADH-driven $[Na^+]_{out}$ variation. The assay mixture contained vesicles pre-incubated with KCN (5 mM), DMN (200 μM) and valinomycin (2 μM).

4.5 – DISCUSSION

We have shown previously that *R. marinus* complex I performs three activities: 1) the catalytic activity NADH:quinone oxidoreductase, 2) H^+ translocation in the same direction of the established ΔΨ and 3) Na^+ transport to the opposite direction of 2) (see chapter 3, section 3.1) [1]. In this work we studied the influence of a Na^+/H^+ antiporter inhibitor, EIPA, on those activities, using inside-out membrane vesicles.

It has been reported for *E. coli* and sub-mitochondrial particles that EIPA inhibited complex I NADH:quinone oxidoreductase activity [7, 9]. In the case of *R. marinus* 10% inhibition was also observed at 25 μM EIPA and the concentration of half maximal inhibition was calculated to be approximately 230 μM. This value is in the range of those determined for

reconstituted *E. coli* complex I (IC_{50}=100 μM) [9], for complex I activity in bacterial membrane vesicles (*E. coli*, *P. denitrificans*) and in sub-mitochondrial particles [7].

Considering the EIPA inhibitory profile of the catalytic reaction, EIPA concentrations between 0 to 20 μM (a range in which the catalytic reaction is not affected) were chosen for the ion translocations studies. We observed different inhibitory behaviors for complex I proton transport by EIPA in the presence and absence of Na^+ (Table 4.1 and Figure 4.5). In its absence, 20 μM EIPA was responsible for a decrease of ~46% in ΔpH_{out}. At this EIPA concentration, the NADH:quinone oxidoreduction was not affected (Table 4.1), which indicated that the observed decrease in ΔpH_{out} was not due to a decrease in proton consumption for quinone reduction, but only due to a decrease in proton uptake for translocation. It could thus be concluded that in those conditions EIPA inhibited H^+ translocation and that the oxidoreductase and H^+ translocating activities were decoupled. In the presence of Na^+, 10 μM EIPA was sufficient to inhibit both H^+ and Na^+ transports, but to different extensions (Table 4.1). In these conditions, decreases of ~32% and ~50% were observed for NADH-driven pH_{out} change and NADH-driven $[Na^+]_{out}$ change, respectively. At 20 μM EIPA, the pH_{out} and $[Na^+]_{out}$ changes decreased both to ~80%. Since NADH:quinone oxidoreductase activity was not affected at these concentrations of EIPA, we

Table 4.1 - Inhibition of *R. marinus* complex I activities: NADH:quinone oxidoreductase activity (NADH:Q OR), proton transport (ΔpH_{out}) and sodium transport (ΔpNa^+_{out}), by different EIPA concentrations.

	% of inhibition				
	0 mM Na^+		50 mM Na^+		
[EIPA] (μM)	NADH:Q OR	ΔpH_{out}	NADH:Q OR	ΔpH_{out}	ΔpNa^+_{out}
10	0	0	0	32	50
20	0	46	0	80	80
230	50	-[a]	50	-[a]	-[a]

[a] At 230 μM EIPA, NADH:quinone oxidoredutase activity is already 50% inhibited thus ΔpH_{out} and ΔpNa^+_{out} are also directly affected by that inhibition.

could again conclude that H^+ and Na^+ transports were both decoupled from the oxidoreductase activity. The decoupling of H^+ transport from the catalytic activity was corroborated by the studies performed with the overall *R. marinus* respiratory chain, in which an inhibition of the proton transport was observed at EIPA concentrations at which the catalytic activity was not inhibited (Figure 4.4). Our observations are in agreement with the results obtained by Dlasková and coworkers, who using rat liver mitochondria, observed H^+ transport inhibition by EIPA using glutamate and malate as substrates without affecting respiration [11] . An apparent IC_{50} for EIPA inhibition of that transport, when added before the substrates was estimated to be 27 μM. The observed decoupling effect was assigned to decoupling of complex I. The authors also observed no inhibition of mitochondrial respiration of the mentioned substrates until EIPA concentration reached 250-500 μM [11].

We have previously proposed a model for energy transduction by *R. marinus* complex I, in which we suggested the presence of two energy transducing sites, one involving Na^+ independent H^+ translocation and the other processing Na^+ dependent H^+ translocation (see chapter 3, section 3.1) [1]. This model was based on the observations that *R. marinus* complex I performs NADH:quinone oxidoreductase activity and H^+ and Na^+ transports and that Na^+ does not influence the catalytic activity nor it is necessary for H^+ transport, but the presence of Na^+ increases H^+ transport. The studies here described not only corroborate the presence of two proton translocation sites, but also showed that the two sites have different inhibition profiles for EIPA. In the absence of EIPA, the two H^+ translocations sites (Na^+ dependent and independent) are perfectly able to operate and a NADH-driven H^+ transport occurs, as well as NADH-driven Na^+ transport in the opposite direction. In the presence of 10 μM EIPA, the antiporter site is partially inhibited (50%) whereas the sodium independent H^+ translocating site is not affected;

explaining why, in these conditions, the $\Delta[Na^+]_{out}$ decreases in a higher amplitude when compared to ΔpH (30% for ΔpH_{out} and 50% for ΔpNa^+ – Table 4.1). 20 μM EIPA, in the presence of Na^+, causes 80% of inhibition of H^+ and Na^+ transports. However, in the absence of Na^+, the H^+ transport is only 50% inhibited at that same EIPA concentration. This effect of EIPA on H^+ transport in the absence of Na^+ reflects the inhibition profile of the Na^+ independent H^+ translocating site. The two different inhibition profiles for H^+ translocation, in a concentration range, in which the oxidoreduction activity is not affected, reinforce the hypothesis for the presence of two H^+ translocating sites. Taking into account all the observations it could be assigned the IC_{50} value of ~22 μM to the Na^+ independent proton translocating site and the IC_{50} value of ~10 μM to the Na^+ dependent H^+ translocating site, the same value of the Na^+ transport. The estimated IC_{50} value of ~14 μM for H^+ transport in the presence of Na^+ is thus interpreted as a combination of the different inhibition profiles of the two H^+ translocating sites. The obtained IC_{50} values are in the range of that observed for the inhibition of rat liver mitochondrial H^+ transport (see above) [11].

It was reported that in some situations, EIPA could also act as a protonophore, even stronger than CCCP [2, 20, 21]. This effect is completely absent in our studies. EIPA did not influence NADH-driven $\Delta\Psi$ formation in the concentration range used for the translocation studies (0 to 20 μM), meaning that, in this system, EIPA does not act as a protonophore as CCCP does. This conclusion was further reinforced by the ^{23}Na-NMR experiments, in which the presence of EIPA did not increase Na^+ translocation, as expected for a protonophore (see chapter 3, section 3.1) [1]; on the contrary it worked as a Na^+ transport inhibitor.

Strong clues for the coupling mechanism for energy transduction in complex I have recently been provided by the α-helical structure of the

membrane domain of complex I from *E. coli* and by the entire structure of complex I from *T. thermophilus* at 3.9 Å and 4.5 Å resolutions, respectively. The structures suggest that 3 protons may be translocated by an indirect coupling mechanism, involving conformational changes from near the quinone binding site to the antiporter subunits, with the participation of a long amphipatic helix, which spans almost the entire membrane domain [22]. In order to achieve the stoichiometry of 4 translocated H^+ per NADH, proposed for complex I [23], an additional H^+ translocating site was considered. This was previously proposed to operate through a redox-driven mechanism, representing a direct coupling mechanism in which H^+ uptake would occur upon reduction of cluster N2 [24]. This proposal also suggested that the process for H^+ uptake would be the same for H^+ translocation and for quinone reduction. Such a possibility is not supported in the case of *R. marinus* complex I since the catalytic reaction and H^+ translocation, whether Na^+ independent or dependent, could be completely decoupled, i.e. catalytic activity was not affected at certain conditions that inhibited H^+ translocation. The new structural data [22] do not exclude the possibility that the translocation of the fourth proton may also be conformational driven.

In conclusion, we propose that *R. marinus* complex I has two energy transducing sites, both dependent on menaquinone reduction and both promoting H^+ translocation. However, one of the sites requires Na^+ for its operation. *R. marinus* complex I also promotes Na^+ transport in the opposite direction to that of H^+ transport. Furthermore, different EIPA inhibition profiles were observed for the two coupling sites. Taken together all data, we can hypothesize that one coupling site may work as a proton pump, while the other may operate by a Na^+/H^+ antiporter mechanism. In both cases energy transduction occurs through indirect coupling, most probably by conformational changes. These conclusions are in agreement with the recently

obtained complex I structural data and strengthen the clarification of the coupling mechanisms for energy transduction by complex I.

4.6 – ACKNOWLEDGEMENTS

I thank Dr. Andreia S. Fernandes, Prof. Alexander Konstatinov and Dr. Smilja Todorovic for the helpful discussions and numerous advices and João Carita cell growth.

4.7 – REFERENCES

[1] A.P. Batista, A.S. Fernandes, R.O. Louro, J. Steuber and M.M. Pereira, Energy conservation by *Rhodothermus marinus* respiratory complex I, Biochim Biophys Acta 1797 (2010) 509-515.

[2] T.R. Kleyman and E.J. Cragoe, Jr., Amiloride and its analogs as tools in the study of ion transport, J Membr Biol 105 (1988) 1-21.

[3] T. Kuroda, T. Shimamoto, T. Mizushima and T. Tsuchiya, Mutational analysis of amiloride sensitivity of the NhaA Na^+/H^+ antiporter from *Vibrio parahaemolyticus*, J Bacteriol 179 (1997) 7600-2.

[4] N. Mochizuki-Oda and F. Oosawa, Amiloride-sensitive Na^+-H^+ antiporter in *Escherichia coli*, J Bacteriol 163 (1985) 395-7.

[5] C. Mathiesen and C. Hagerhall, The 'antiporter module' of respiratory chain complex I includes the MrpC/NuoK subunit -- a revision of the modular evolution scheme, FEBS Lett 549 (2003) 7-13.

[6] C. Mathiesen and C. Hagerhall, Transmembrane topology of the NuoL, M and N subunits of NADH:quinone oxidoreductase and their homologues among membrane-bound hydrogenases and bona fide antiporters, Biochim Biophys Acta 1556 (2002) 121-32.

[7] E. Nakamaru-Ogiso, B.B. Seo, T. Yagi and A. Matsuno-Yagi, Amiloride inhibition of the proton-translocating NADH-quinone oxidoreductase of mammals and bacteria, FEBS Lett 549 (2003) 43-6.

[8] E. Nakamaru-Ogiso, K. Sakamoto, A. Matsuno-Yagi, H. Miyoshi and T. Yagi, The ND5 subunit was labeled by a photoaffinity analogue of fenpyroximate in bovine mitochondrial complex I, Biochemistry 42 (2003) 746-54.

[9] S. Stolpe and T. Friedrich, The *Escherichia coli* NADH:ubiquinone oxidoreductase (complex I) is a primary proton pump but may be capable of secondary sodium antiport, J Biol Chem 279 (2004) 18377-83.

[10] J. Steuber, The C-terminally truncated NuoL subunit (ND5 homologue) of the Na^+-dependent complex I from *Escherichia coli* transports Na^+, J Biol Chem 278 (2003) 26817-22.

[11] A. Dlaskova, L. Hlavata, J. Jezek and P. Jezek, Mitochondrial Complex I superoxide production is attenuated by uncoupling, Int J Biochem Cell Biol 40 (2008) 2098-109.

[12] M.M. Pereira, A.M. Antunes, O.C. Nunes, M.S. da Costa and M. Teixeira, A membrane-bound HIPIP type center in the thermohalophile *Rhodothermus marinus*, FEBS Lett 352 (1994) 327-30.

[13] C. Watters, A one-step biuret assay for protein in the presence of detergent, Anal Biochem 88 (1978) 695-8.

[14] A.S. Fernandes, F.L. Sousa, M. Teixeira and M.M. Pereira, Electron paramagnetic resonance studies of the iron-sulfur centers from complex I of *Rhodothermus marinus*, Biochemistry 45 (2006) 1002-8.

[15] P.K. Smith, R.I. Krohn, G.T. Hermanson, A.K. Mallia, F.H. Gartner, M.D. Provenzano, E.K. Fujimoto, N.M. Goeke, B.J. Olson and D.C. Klenk, Measurement of protein using bicinchoninic acid, Anal Biochem 150 (1985) 76-85.

[16] H.J. Apell and B. Bersch, Oxonol VI as an optical indicator for membrane potentials in lipid vesicles, Biochim Biophys Acta 903 (1987) 480-94.

[17] D.P. Briskin and I. Reynolds-Niesman, Determination of H/ATP Stoichiometry for the Plasma Membrane H-ATPase from Red Beet (*Beta vulgaris* L.) Storage Tissue, Plant Physiol 95 (1991) 242-250.

[18] A.M. Delort, G. Gaudet and E. Forano, ^{23}Na NMR study of *Fibrobacter succinogenes* S85: comparison of three chemical shift reagents and calculation of sodium concentration using ionophores, Anal Biochem 306 (2002) 171-80.

[19] E. Damiano, M. Bassilana, J.L. Rigaud and G. Leblanc, Use of the pH sensitive fluorescence probe pyranine to monitor internal pH changes in *Escherichia coli* membrane vesicles, FEBS Lett 166 (1984) 120-4.

[20] K. Davies and M. Solioz, Assessment of uncoupling by amiloride analogs, Biochemistry 31 (1992) 8055-8.

[21] W.P. Dubinsky, Jr. and R.A. Frizzell, A novel effect of amiloride on H^+-dependent Na^+ transport, Am J Physiol 245 (1983) C157-9.

[22] R.G. Efremov, R. Baradaran and L.A. Sazanov, The architecture of respiratory complex I, Nature 465 (2010) 441-445.

[23] A.S. Galkin, V.G. Grivennikova and A.D. Vinogradov, -->$H^+/2e^-$ stoichiometry in NADH-quinone reductase reactions catalyzed by bovine heart submitochondrial particles, FEBS Lett 451 (1999) 157-61.

[24] J.M. Berrisford and L.A. Sazanov, Structural basis for the mechanism of respiratory complex I, J Biol Chem 284 (2009) 29773-83.

4.8 – SUPPLEMENTARY MATERIAL

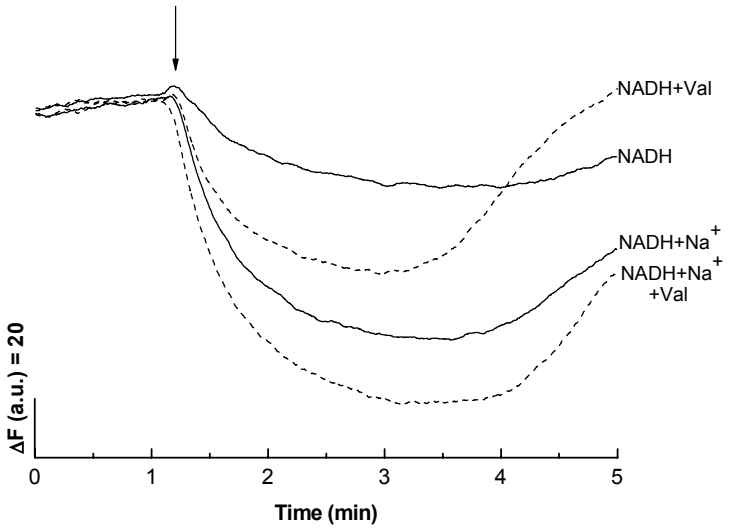

Supplementary Figure 4.1 - Effect of ΔΨ on NADH-driven ΔpH generation by the respiratory chain of *R. marinus*. NADH-driven ΔpH in absence or in the presence of sodium ions (Na^+) and/or valinomycin (Val). The ACMA fluorescence was detected using a $\lambda_{excitation}$=410 nm and a $\lambda_{emission}$=480 nm. The reaction was started by the addition of 100 μM NADH (indicated by an arrow).

Chapter 5

Energy transduction by complexes I from E. coli and P. denitrificans

Abbreviations

E.: *Escherichia*; *P.*: *Paracoccus;* R.: *Rhodothermus*.

ΔΨ: membrane potential; ΔpH: pH difference; ΔpH_{out}: external medium pH difference; ΔNa^{+}_{out}: external medium sodium concentration changes; pH_{out}: external medium pH.

ACMA: 9-amino-6-chloro-2-methoxyacridine; CCCP: carbonyl cyanide *m*-chlorophenyl hydrazone; DDM: n-dodecyl-β-D-maltoside; DMN: 2, 3-dimethyl-1,4-naphthoquinone; DUQ: decylubiquinone; $Dy(PPPi)_2^{7-}$: dysprosium (III) tripolyphosphate; EPR: electron paramagnetic resonance; FCCP: carbonylcyanide *p*-trifluoromethoxy-phenylhydrazone; Monen: monensine; NMR: nuclear magnetic resonance; oxonol VI: 1,5-Bis(5-oxo-3-propylisoxazol-4yl)pentamethine oxonol; Pier.A: piericidin A; Q: quinone; Rot: rotenone; TEMPO: 2,2,6,6-tetramethyl-1-piperidinyloxy; $Tm(DOTP)^{5-}$: thulium(III)1,4,7,10-tetraazacyclododecane-1,4,7,10-tetrakis(methylenephosphonate); Val: valinomycin.

This chapter is under review as:
A.P. Batista and M.M. Pereira, "Sodium influence on energy transduction by complexes I from *Escherichia coli* and *Paracoccus denitrificans*."

Chapter 5: Energy transduction by complexes I from *E. coli* and *P. denitrificans*

5.1 - SUMMARY

The nature of the ions that are translocated by *E. coli* and *P. denitrificans* complexes I was investigated and a different energy conservation mechanism was detected for the two enzymes. We observed that *E. coli* complex I was capable of proton translocation in the same direction to the established $\Delta\Psi$, showing that in the tested conditions the coupling ion is the H^+. Furthermore, Na^+ transport to the opposite direction was also observed and, although Na^+ was not necessary for the catalytic or proton transport activities, its presence increased the latter one. We also observed H^+ translocation by *P. denitrificans* complex I, but in this case H^+ transport was not influenced by Na^+ and also Na^+ transport was not observed. We concluded that *E. coli* complex I has two energy coupling sites (one Na^+ independent and the other Na^+ dependent), as previously observed for *Rhodothermus marinus* complex I, whereas the coupling mechanism of *P. denitrificans* enzyme is completely Na^+ independent. This work thus shows that complex I energy transduction by proton pumping and Na^+/H^+ antiporting is not exclusive of the *R. marinus* enzyme. Nevertheless the Na^+/H^+ antiport activity seems not to be a general property of complex I, which may be correlated with the metabolic characteristics of the organisms.

5.2 – INTRODUCTION

R. marinus complex I is capable of proton and sodium translocation but in opposite directions, being the proton the coupling ion. A model for the functional mechanism of complex I was proposed, suggesting the presence of two different energy coupling sites. One coupling site may work as a proton pump and the other as a Na^+/H^+ antiporter (see chapter 3, section 3.1) [1]. A

possible relation of complex I with antiporters has also been suggested based on sequence analyses of the hydrophobic subunits Nqo11, 12, 13 and 14, which are related to subunits of the Mrp type family of Na^+/H^+ antiporters [2, 3]. In order to address whether the observed Na^+ transport by complex I was not exclusive of *R. marinus* complex I we have investigated H^+ and Na^+ translocations by two canonical complexes I, from *E. coli* and *P. denitrificans*.

P. denitrificans respiratory enzymes are commonly used as model systems due to their close relation to the mitochondrial respiratory enzymes. Complex I is not an exception and it has been used in a large number of studies [4-11]. As mitochondrial complex I, *P. denitrificans* enzyme is described as a proton pump and a H^+/e^- ratio of 1.5 to 2 was estimated [12, 13]. The proton transport capacity was observed in comparative studies whereas ratios of 8 H^+:O and 3-4 H^+:O were determined in cells, using different electron donors and inhibitors [12-14]. Complex I from *E. coli* is one of the most studied complexes I at genetic and molecular levels [15-22]. It has been proposed that the coupling ion is the H^+ [17, 23] and a stoichiometry of 1.5 H^+/e was indirectly determined in cells, using DMSO as an electron donor [23]. However, also Na^+ has been suggested to be the coupling ion of *E. coli* complex I [16]. Additionally, Stolpe and Friedrich observed an increase in proton transport by liposome-incorporated *E. coli* complex I when a sodium gradient was imposed, and a Na^+/H^+ antiport activity coupled to quinone reduction was suggested [17]. It was also shown that the over-expressed C-terminally truncated NuoL (Nqo12) subunit of the *E. coli* complex I mediates sodium uptake when reconstituted into liposomes and this transport was inhibited by the addition of amiloride derivatives, known as Na^+/H^+ antiporter inhibitors [15].

The present work allowed us to further investigate our previous model for energy conservation in *R. marinus* complex I in which we proposed

the existence of two energy coupling sites and suggest that this complex I transduces energy by two processes: proton pumping and Na^+/H^+ antiporting (see chapter 3, section 3.1) [1]. We extended our studies to the canonical complexes I from *E. coli* and *P. denitrificans* and we observed that the Na^+/H^+ antiport activity is not exclusive of *R. marinus* but is not a general property. We suggest that due to thermodynamic constrains, this property may be correlated with the type of quinone used as substrate. In this way our findings open new perspectives in the discussion of energy transduction by complex I, in general.

5.3 – MATERIAL AND METHODS

A. Cell growth and membrane vesicles preparation

E. coli was grown anaerobically (pO_2=0%) in LB medium at 37 ºC until OD_{600nm}=0.7. *P. denitrificans* Pd1222 was grown aerobically in succinate medium at 30 ºC, as previously described [24], until OD_{600nm}=6. After harvesting, cells in 2.5 mM HEPES-Tris pH 7.5 with 5 mM K_2SO_4 and 10 mM Na_2SO_4 (buffer A), 25 mM Na_2SO_4 (buffer B) or 50 mM choline chloride (buffer C), were broken in a French Pressure cell at 19 000 psi. The membrane vesicles were obtained by ultracentrifugation of the broken cells at 200 000 g, 2 hours, 4 ºC. Integrity of vesicles was checked by K^+/valinomycin assays using oxonol VI as a $\Delta\Psi$ indicator (see below). Protein concentration was determined by the Biuret method modified for membrane proteins [25].

B. Internal volume determination

The internal volume of the membrane vesicles was determined by EPR spectroscopy, using TEMPO [26]. TEMPO (oxidized with $K_3[Fe(CN)_6]$) in the external medium was quenched with 100 mM of potassium

chromium(III) oxalate. EPR measurements were performed at room temperature, with a microwave frequency of 9.39 GHz, microwave power 1 mW and modulation amplitude 0.04 mT.

C. ΔΨ detection

ΔΨ generation was detected following oxonol VI absorption (A_{628} *minus* A_{587}) at 18 ºC [27]. The vesicles integrity was checked generating K^+ gradients with K^+/valinomycin in an external buffer containing 250 mM K_2SO_4 (internal $[K^+]$=10 mM). The assays were started by the addition of 2 μM of valinomycin. To detect the NADH-driven ΔΨ formation, the assay contained membrane vesicles in buffer B or buffer C. The reaction was started by adding 4 mM of K_2NADH. When referred, CCCP (10 μM), rotenone (10 μM), piericidin A (30 μM) or KCN (5 mM) were added prior to the addition of NADH. Measurements were obtained on an OLIS upgraded Aminco DW2 dual wavelength spectrophotometer.

D. Activity measurements

Oxygen consumption was measured with a Clark-type oxygen electrode YSI Model 5300. The assay mixture contained membrane vesicles in buffer B or buffer C. The reaction was started by adding 4 mM NADH. When used, KCN (10 mM), CCCP (10 μM), rotenone (10 μM) and piericidin A (30 μM) were added prior to the addition of the substrate. NADH:$K_3[Fe(CN)_6]$ oxidoreductase activity was monitored at 420 nm (ε = 1020 $M^{-1}cm^{-1}$) on an OLIS upgraded Aminco DW2 dual wavelength spectrophotometer. The reaction medium contained membrane vesicles or solubilized membranes in buffer B and C, 250 μM $K_3[Fe(CN)_6]$ and 250 μM NADH. Solubilized membranes were obtained by stirring an aliquot of membrane vesicles with 2 % of DDM for 2 hour at 4 °C.

NADH oxidation by membrane vesicles was monitored at 330 nm (ε = 5930 $M^{-1}cm^{-1}$). The reaction medium contained membrane vesicles in the presence of 2.5 mM KCN and 150 μM of quinone analogues. The reaction was started by adding 150 μM of NADH. When used, CCCP (10 μM) was added prior to the addition of the substrate.

E. Fluorescence spectroscopy

The generation of ΔpH was determined by the quenching of the fluorescence of ACMA ($\lambda_{excitation}$=410 nm, $\lambda_{emission}$=480 nm). *P. denitrificans* membrane vesicles were incubated aerobically for 5 minutes at 18 ºC in the assay buffer A, buffer B and buffer C containing 1 μM of ACMA. The reaction was started by adding 50 μM of NADH. When referred, KCN (5 mM), rotenone (10 μM), CCCP (10 μM), monensine (20 μM) were added prior to the addition of NADH. The external medium pH (pH_{out}) was followed using the hydrophilic and membrane impermeable pH indicator, pyranine ($\lambda_{emission}$=508 nm). The excitation wavelength, 458 nm, was monitored before and after NADH addition (at 0, 5, 10 and 15 min) [28]. *E. coli* membrane vesicles, when indicated, were incubated in the assay buffer B or buffer C containing 2 μM of pyranine, 5 mM KCN, 200 μM DMN, 200 μM decylubiquinone (DUQ) and 2 μM valinomycin. The reaction was started by adding 4 mM of NADH. When referred CCCP (20 μM) was added prior to the addition of NADH. Fluorescence spectra and kinetics were recorded on a Varian Cary Eclipse spectrofluorimeter.

F. ^{23}Na-NMR spectroscopy

NMR spectra were recorded on a Bruker Avance II 500 MHz spectrometer at 18 °C, operating at 132 MHz for ^{23}Na. Experiments were

performed as described in chapter 3, section 3.1 [1]. Spectra were recorded upon addition of 4 mM K_2NADH to membrane vesicles (prepared in buffer B) or to membrane vesicles which were previously incubated with CCCP (10 μM), rotenone (10 μM), piericidin A (30 μM), KCN (10 mM), DMN (200 μM) and DUQ (200 μM).

G. Sequence analysis tools

Searches for amino acid sequences in databases were performed at NCBI using the BLAST network service. Multiple alignments and dendrograms were obtained using CLUSTALX version 2.0.

5.4 – RESULTS

Membrane vesicles characterization

The membrane vesicles preparations of *E. coli* and *P. denitrificans* were composed by tight vesicles which allowed the formation of a $\Delta\Psi$ using K^+ and valinomycin, stable for at least 30 minutes. The orientation of *E. coli* and *P. denitrificans* membrane vesicles was determined comparing the NADH:K_3[Fe(CN)$_6$] oxidoreductase activity in membrane vesicles before and after their solubilization with DDM. The activity was, approximately, the same in both situations and for both organisms, meaning that *E. coli* and *P. denitrificans* membrane vesicles were ~100% inside-out orientated. For both organisms, the internal membrane vesicles volume, determined by EPR spectroscopy, was found to be 1 μL.mg^{-1} of protein.

NADH-driven ⊿Ψ generation

E. coli and *P. denitrificans* membrane vesicles were capable of create and maintain a membrane potential after the addition of NADH, one of the

electron donors of aerobic respiratory chains (Figure 5.1A-a and 5.1B-a). The membrane potential was detected by monitoring the change in the absorbance of oxonol VI, showing the build-up of a ΔΨ (positive inside). If the membrane vesicles were pre-incubated with KCN (terminal dioxygen reductases inhibitor), rotenone or piericidin A (complex I inhibitors), the jump in A_{628nm}-A_{587nm} observed upon NADH addition was negligible, indicating that the observed ΔΨ was generated by the functioning of the respiratory chain and showing the contribution of complex I to the generated ΔΨ (Figure 5.1A-b,c and 5.1B-b,c). NADH-driven ΔΨ was also sensitive to the protonophore CCCP, indicating the contribution of a ΔpH for that ΔΨ (Figure 5.1A-d and 5.1B-d).

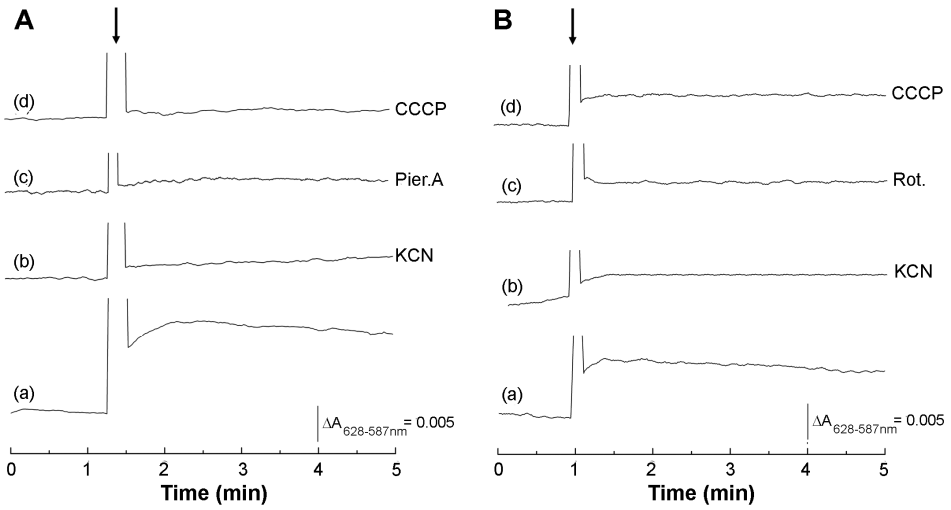

Figure 5.1 - Generation of a ΔΨ by the functioning of *E. coli* and *P. denitrificans* respiratory chains, monitored by the absorbance difference of oxonol VI. The reaction was started by the addition of 4 mM of NADH (indicated by an arrow). Panel A: Absorbance difference of oxonol VI upon addition of NADH to *E. coli* membrane vesicles (a) and pre-incubated vesicles with 5 mM KCN (b), 30 μM piericidin A (Pier.A) (c) or 10 μM CCCP (d). Panel B: Absorbance difference of oxonol VI upon addition of NADH to *P. denitrificans* membrane vesicles (a) and pre-incubated vesicles with 5 mM KCN (b), 10 μM rotenone (Rot.) (c) or 10 μM CCCP (d).

Effect of sodium on the NADH:dioxygen oxidoreductase activity

The effect of sodium ions on the dioxygen reduction by *E. coli* and *P. denitrificans* respiratory chains was monitored following the NADH:dioxygen oxidoreductase activity. *E. coli* membrane vesicles, prepared in 0 and 50 mM Na^+, were able to consume dioxygen with similar rates (33 ± 3 nmol NADH mg^{-1} min^{-1} and 36 ± 3 nmol NADH mg^{-1} min^{-1}, respectively). In *P. denitrificans* membrane vesicles a decrease of approximately 20% on the NADH oxidation was observed when Na_2SO_4 was replaced by choline (54 ± 2 nmol NADH mg^{-1} min^{-1} *versus* 44 ± 2 nmol NADH mg^{-1} min^{-1}, respectively). In all the four cases, NADH oxidation was almost completely inhibited by KCN and by piericidin A or rotenone. An increase of up to 30% on the dioxygen consumption was observed in the presence of the protonophore, CCCP. Focusing on the NADH:quinone segment of the *E. coli* respiratory chain, a pre-incubation of membrane vesicles with KCN and quinone analogues was performed and the NADH consumption was spectrophotometrically monitored. An increase of up to 20% on the NADH:quinone oxidoreduction was observed in the presence of CCCP, indicating that this activity was limited by ΔpH.

NADH-driven ΔpH generation

Upon NADH addition to *P. denitrificans* membrane vesicles, a quenching in ACMA fluorescence intensity (used as a ΔpH indicator) was observed, indicating the establishment of a ΔpH (Figure 5.2A-a). If the vesicles had been previously incubated with rotenone, KCN, the protonophore CCCP or the Na^+/H^+ exchanger monensine, the ACMA fluorescence quenching was negligible upon addition of the electron donor (Figure 5.2A-b to e). It was previously shown, that the NADH-driven ΔpH generation by complex I from *R. marinus* was not dependent on sodium, but

the presence of this ion increases proton transport (see chapter 3, section 3.1) [1]. A similar behaviour was not observed for *P. denitrificans* complex I. Membrane vesicles prepared in the presence of 0, 20 and 50 mM Na^+ showed the same ΔpH amplitude upon NADH addition (Figure 5.2B-a to c). Thus, in the case of *P. denitrificans* the presence of sodium was not necessary for the establishment of a ΔpH neither influenced it.

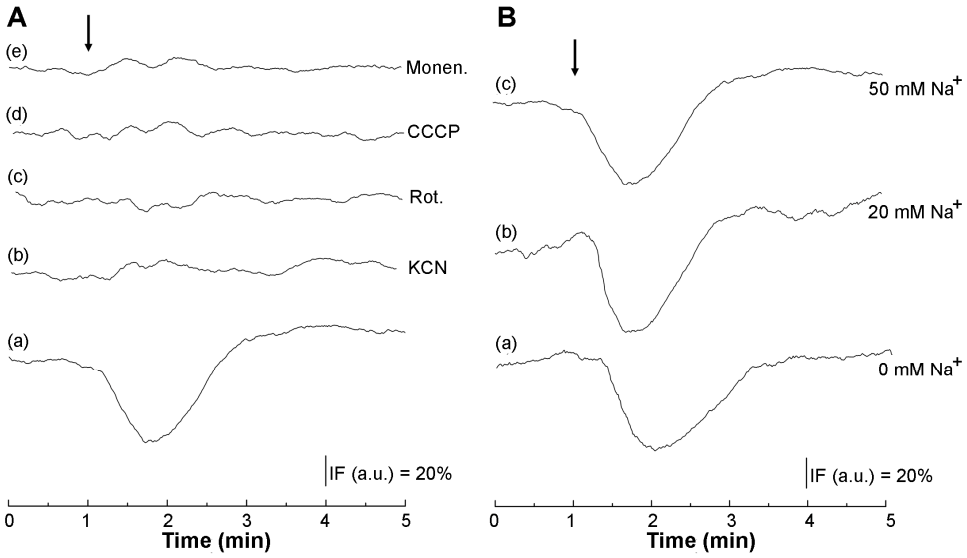

Figure 5.2 - Generation of a ΔpH by the respiratory chain of *P. denitrificans* monitored by ACMA fluorescence. The ACMA fluorescence was detected using an excitation wavelength of 410 nm and an emission wavelength of 480 nm. Panel A: The assay contained membrane vesicles in 2.5 mM HEPES-Tris pH 7.5, 5 mM K_2SO_4, 25 mM Na_2SO_4. The reaction was started by the addition of 50 μM NADH (indicated by an arrow) without preincubating the membrane vesicles (a), after preincubation with 5 mM KCN (b), 10 μM rotenone (c), 10 μM CCCP (d), 20 μM monensin (e). Panel B: The assay contained membrane vesicles in 2.5 mM HEPES-Tris pH 7.5 with 50 mM choline chloride (a), with 10 mM Na_2SO_4 (b) and with 25 mM Na_2SO_4 (c). The reaction was started by the addition of 50 μM NADH (indicated by an arrow).

NADH-driven external vesicles pH (pH_{out}) variation

The use of the ACMA as a ΔpH indicator is not a straightforward procedure in the case of *E. coli* membrane vesicles [17]. Thus, in this case we

opt to monitor the change in pH outside the membrane vesicles upon NADH addition. This was performed by monitoring the changes on the pyranine fluorescence intensity. To focus on the NADH:quinone segment of the *E. coli* respiratory chain, a pre-incubation of membrane vesicles with KCN, DMN and DUQ was performed. Addition of NADH (in the presence and absence of sodium), promoted an increase in the pyranine fluorescence

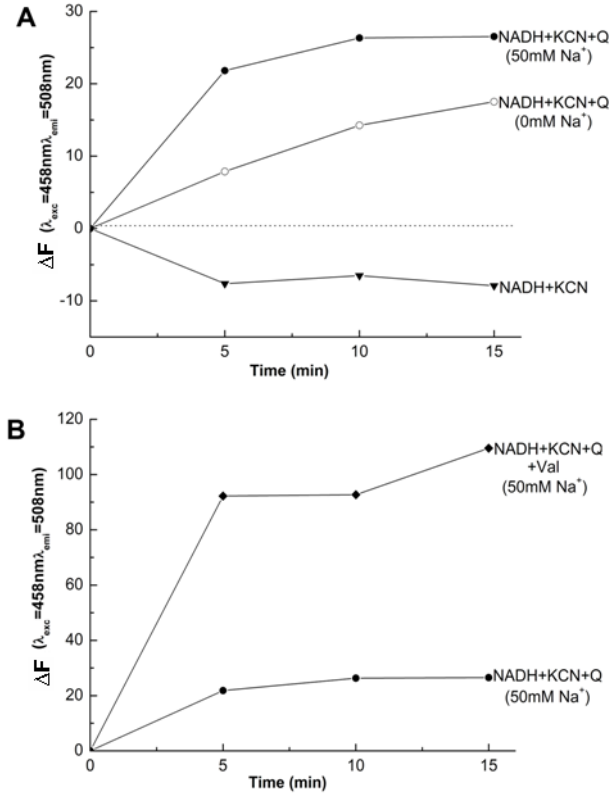

Figure 5.3 - Effect of sodium ions and ΔΨ on NADH-driven pH_{out} variation by *E. coli* complex I. The pyranine fluorescence was detected using an excitation wavelength of 458 nm and an emission wavelength of 508 nm. The vesicles were pre-incubated with KCN (5 mM), DMN (200 μM) and DQU (200 μM). The reaction was started by the addition of 4 mM NADH. Panel A: Influence of Na^+ on NADH-driven pH_{out} variation. The assays contained membrane vesicles in 2.5 mM HEPES-Tris pH 7.5, 5 mM K_2SO_4 with 25 mM Na_2SO_4 or 50 mM choline chloride. Panel B: Influence of ΔΨ on NADH-driven pH_{out} variation. The assays contained membrane vesicles in the presence and absence of valinomycin. The represented data are the average of at least three independent assays.

intensity at 458 nm, indicating an increase in the pH_{out}. A decrease of this pyranine fluorescence intensity occurs upon addition of CCCP, which indicates a dissipation of ΔpH established by the operation of *E. coli* complex I. The pH difference was due to the proton translocation, from the outside to the inside of the vesicles, in addition to the proton uptake upon quinone reduction. The change in the pH_{out} was higher for membrane vesicles prepared with 50 mM Na^+ (Figure 5.3A). For this membrane vesicles preparation, a more than four-fold increase of the pH_{out} change was observed in the presence of valinomycin, indicating that NADH:quinone oxidoreductase activity was limited by ΔΨ (Figure 5.3B). This observation excluded the possibility that the observed increase in H^+ uptake in the presence of Na^+ was due to a simple charge compensation effect.

NADH-driven ⊿Na^+_{out} generation

^{23}Na-NMR spectroscopy was chosen to directly monitor changes in Na^+ concentration ([Na^+]). In the case of *E. coli* membrane vesicles (prepared in buffer B), an increase on the external [Na^+] of approximately 30 nmol of Na^+ per mg of protein was observed after NADH addition, meaning that sodium ions were transported from the inside to the outside of the membrane vesicles (Figure 5.4A – filled circles). Identical directionality of sodium ions transport was observed for *P. denitrificans*, however the amount of translocated sodium was smaller (10 nmol $Na^+.mg^{-1}$ of protein) (Figure 5.4B – filled circles). If membrane vesicles had been previously incubated with KCN or with a complex I inhibitor (piericidine A or rotenone), no Na^+ transport from the inside to the outside was observed (Figure 5.4A and 5.4B– filled and open triangles). Thus, Na^+ transport through the membrane vesicles occurred during NADH consumption by the *E. coli* and *P. denitrificans* respiratory chains. To distinguish between an active Na^+ transport by some respiratory

enzyme and a possible secondary effect due to the proton gradient formed by respiration, the protonophore CCCP was added to the vesicles prior to the addition of NADH. Dissipation of the proton gradient, and concomitantly of the $\Delta\Psi$, with CCCP increased Na^+ transport by *E. coli* membrane vesicles,

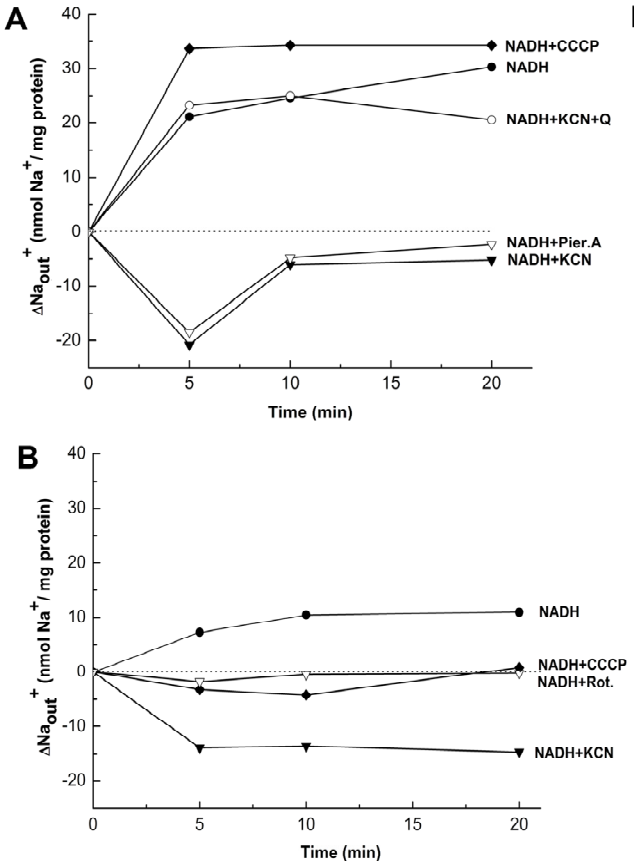

Figure 5.4 - Sodium ion transport by *E. coli* and *P. denitrificans* NADH-respiring membrane vesicles. Panel A: Sodium ion transport by *E. coli* membrane vesicles. Effect of 4 mM K_2-NADH on external Na^+ concentration of membrane vesicles containing 50 mM Na^+ without pre-incubations (filled circles) or after pre-incubation with 30 μM piericidin A (open triangles), 10 mM KCN (filled triangles), 10 μM CCCP (filled lozenges) or 10 mM KCN plus 200 μM of menaquinone analogue DMN and ubiquinone analogue, DUQ (filled circles). Panel B: Sodium ion transport by *P. denitrificans* membrane vesicles. Effect of 4 mM K_2-NADH on external Na^+ concentration of membrane vesicles containing 50 mM Na^+ without preincubations (filled circles) or after preincubation with 10 μM rotenone (open triangles), 10 mM KCN (filled triangles) or 10 μM CCCP (filled lozenges).

meaning that Na^+ transport to the outside of the membrane vesicles was actively performed by the *E. coli* respiratory chain (Figure 5.4A – filled lozenges). This active Na^+ transport was not observed in *P. denitrificans*. In this case the NADH-driven ΔpNa^+ was completely dissipated by the presence of CCCP (Figure 5.4B – filled lozenges), indicating most probably that the observed Na^+ transport was a secondary event established by the action of the respiratory chain. Hypothesizing that the respiratory enzyme responsible for the *E. coli* active Na^+ transport was complex I, as in the case of *R. marinus* (see chapter 3, section 3.1) [1], the membrane vesicles from *E. coli* were pre-incubated with KCN and with ubiquinone and menaquinone analogues, DUQ and DMN. In these conditions, Na^+ transport was found to be similar to the one observed with non-inhibited vesicles in the absence of added quinones (Figure 5.4A – open circles).

Amino acid sequence analyses of subunits Nqo11, 12, 13 and 14

Subunits Nqo11, 12, 13 and 14, due to their relation to the Mrp Na^+/H^+ antiporter subunits are the strongest candidates to be involved in Na^+ transport. Taking in consideration that complexes I from *E. coli* and *R. marinus* are able to translocate Na^+, whereas *P. denitrificans* complex I is not, we performed amino acid sequence alignments of the mentioned subunits in order to identify possible features that could be correlated to Na^+ transport. From the obtained dendrograms we observed that the sequences of Nqo12 and Nqo14 subunits from *E. coli* and *R. marinus* are closer to each other than to the sequences from *P. denitrificans*. Inspection of the sequence alignments did not reveal any particular difference between the groups of sequences including those from *E. coli*, *R. marinus* and closest ones and the groups containing *P. denitrificans* sequence and its closest ones.

5.5 – DISCUSSION

In order to investigate whether the presence of two coupling sites was a specific characteristic of *R. marinus* complex I or if the proposed mechanism could be extended to other complexes I, H^+ and Na^+ transports were studied using *E. coli* and *P. denitrificans* complexes I. Inside-out membrane vesicles from these two organisms were prepared and were active towards NADH oxidation. These vesicles were capable to create and maintain a $\Delta\Psi$, positive inside. The abolishment of the $\Delta\Psi$ in the presence of the protonophore CCCP indicated the existence of a proton gradient generated by NADH oxidation. This effect was observed in membrane vesicles from the two organisms, showing that the functioning of each respiratory chain was responsible for the formation of a ΔpH.

The nature of the charge that is translocated by *E. coli* complex I has been determined to be H^+ [23, 29] or Na^+ [16]. To focus on the NADH-quinone segment of the *E. coli* respiratory chain, the membrane vesicles were pre-incubated with KCN and quinone analogues, and H^+ and Na^+ translocations studies were performed. The change on the pH_{out} was followed using the pH indicator, pyranine. Upon NADH addition, an increase on the fluorescence intensity was observed being this change more pronounced when Na^+ was present. Since NADH oxidase activity is not stimulated by Na^+, we concluded that the ΔpH_{out} observed in these conditions was due to an increase in H^+ translocation and not to a higher H^+ consumption by quinone reduction. Thus, our results showed that *E. coli* complex I promoted H^+ translocation, and corroborated the previous results obtained by Stolpe and Friedrich, who observed an increase in proton transport by liposome-incorporated *E. coli* complex I when a sodium gradient was imposed [17]. By ^{23}Na-NMR spectroscopy, Na^+ translocation from the inside to the outside of *E. coli* membrane vesicles was observed. This NADH-driven Na^+ transport

was inhibited by KCN and piericidin A, specific inhibitors of heme-copper oxygen reductases and complex I, respectively, showing that Na^+ transport was performed by the functioning of the respiratory chain. The Na^+ transport was actively performed by a respiratory complex since it was not impaired by the presence of the protonophore CCCP. The site of Na^+ transport could be identified at the NADH-quinone segment because the Na^+ transport was recovered in membrane vesicles pre-incubated with KCN and DMN+DUQ. The possible contribution of the alternative NADH dehydrogenase to the observed results was excluded since this enzyme is not electrogenic neither it is inhibited by complex I specific inhibitors at the concentrations ranges used in the present work [30, 31]. Also, the participation of a Na^+-dependent NADH dehydrogenase was not considered because the observed NADH:quinone oxidoreductase activity was not dependent on the presence of Na^+. Furthermore *E. coli* does not contain genes coding for a Na^+-dependent NADH dehydrogenase (www.genome.jp). In this way the observed Na^+ transport was assigned to the functioning of *E. coli* complex I.

The addition of NADH to *P. denitrificans* membrane vesicles resulted in the generation of a ΔpH, as indicated by the quenching of ACMA. The ACMA fluorescence did not change when the membrane vesicles were incubated with rotenone, KCN, CCCP or monensin, showing a NADH-driven ΔpH formation by the functioning of the respiratory chain. These observations suggested that in *P. denitrificans* the coupling ion between NADH oxidation and the establishment of the $\Delta\Psi$ is the proton. This result is in perfect agreement with previous studies performed in *P. denitrificans* cells in which a H^+/e^- stoichiometry of 1.5 to 2 was estimated [12]. It was also observed that the rate of NADH oxidation by *P. denitrificans* membrane vesicles increased in the presence of the protonophore carbonylcyanide *p*-trifluoromethoxy-phenylhydrazone (FCCP), which corroborates the existence

of a proton gradient [14]. We also performed Na^+ transport experiments with *P. denitrificans* membrane vesicles, using ^{23}Na-NMR spectroscopy and a slight increase in Na^+ concentration in the outside of the membrane vesicles upon NADH addition was observed. However, this increase upon NADH oxidation collapsed in the presence of the protonophore CCCP, indicating that the Na^+ transport was a secondary event. Thus, we concluded that *P. denitrificans* complex I was not able to perform Na^+ translocation, at least under the tested conditions. This is in agreement with the absence of any effect of Na^+ on NADH-driven ΔpH.

The observations that *R. marinus* and *E. coli* complexes I are able to transport Na^+, whereas *P. denitrificans* complex I is not raise one essential question: What is/are the main difference(s) between these complexes? All the three enzymes have the typical features of canonical complexes I [17, 22, 32-34]. Assuming that the responsible for Na^+ transport are the Mrp-like subunits (Nqo11 to Nqo14), the difference(s) between *E. coli* and *R. marinus* complexes I and that from *P. denitrificans* should reside on those subunits and thus we addressed this issue performing amino acid sequence analysis. These showed that Nqo12 and Nqo14 subunits from *P. denitrificans* complex I are more related to those of the mitochondrial complex I, than to those of complex I from *E. coli* and *R. marinus*. However, no relevant difference in the amino acid sequences could be observed between the cluster including *P. denitrificans* and the mitochondrial sequences and the cluster containing the sequences from *R. marinus* and *E. coli*. A common aspect to *E. coli* and *R. marinus* complexes I is that these reduce menaquinone, whereas complex I from *P. denitrificans* uses ubiquinone as substrate. The difference in the reduction potentials of the two different types of quinones ($E_{m,7}$≈-80 mV for menaquinone *versus* $E_{m,7}$≈+120 mV for ubiquinone) [35] has strong thermodynamic implications. Considering the reduction potential of NADH,

-320 mV, the free energy obtained by its oxidation by menaquinone can be ~240 mV, whereas in the case of oxidation by ubiquinone the free energy obtained can be ~440 mV. Thus, considering a membrane potential usually of ~120 mV, in the first situation the $H^+/2e^-$ cannot exceed 2 while in the latter it can be up to 4. Although completely speculative, these observations may suggest that complexes I using ubiquinone as the electron acceptor, transduce energy just by a proton pumping process (as in the case of *P. denitrificans*) while those that use menaquinone (as in the case of *E. coli* and *R. marinus*) transduce energy by proton pumping *plus* sodium/proton antiporting. In this case the additional Na^+ transport may occur in order to guaranty the high efficiency of complex I in the overall energy transduction process. The situation created by the operation of complexes I from *E.coli* and *R. marinus* could result in sodium accumulation inside the cells, which in turn should be removed by the action of Na^+/H^+ antiporters. Such a scenario could create a sodium futile cycle. In fact such sodium futile cycle has been proposed before for *E. coli* cells, based on the observation of global H^+ and Na^+ transports [36, 37]. It cannot be anticipated whether this futile cycle will be energetically unfavorable. A futile cycle of a specific ion may in fact contribute to a global energy yield. The overall process will depend on the different stoichiometries of the individual transporting processes, and the overall energy yield results from a combination of multiple factors.

In summary, our study indicates that complex I from *E. coli* transduces energy by proton pumping and by Na^+/H^+ antiporting, showing that these properties are not exclusive of *R. marinus* complex I. However, the Na^+/H^+ antiporting seems not to be a general property of complexes I since it was not observed for *P. denitrificans* complex I. Whether complex I from *P. denitrificans* does not contain a second coupling site or if the second coupling site lost its Na^+ dependency is still an open question. The findings here

reported open new perspectives in the studies of the process of energy transduction by complex I.

5.6 – ACKNOWLEDGEMENTS

I thank João Carita for cell growth.

5.7 - REFERENCES

[1] A.P. Batista, A.S. Fernandes, R.O. Louro, J. Steuber and M.M. Pereira, Energy conservation by *Rhodothermus marinus* respiratory complex I, Biochim Biophys Acta 1797 (2010) 509-515.

[2] C. Mathiesen and C. Hagerhall, Transmembrane topology of the NuoL, M and N subunits of NADH:quinone oxidoreductase and their homologues among membrane-bound hydrogenases and bona fide antiporters, Biochim Biophys Acta 1556 (2002) 121-32.

[3] C. Mathiesen and C. Hagerhall, The 'antiporter module' of respiratory chain complex I includes the MrpC/NuoK subunit -- a revision of the modular evolution scheme, FEBS Lett 549 (2003) 7-13.

[4] X.M. Xu, A. Matsuno-Yagi and T. Yagi, Characterization of the 25-kilodalton subunit of the energy-transducing NADH-ubiquinone oxidoreductase of *Paracoccus denitrificans*: sequence similarity to the 24-kilodalton subunit of the flavoprotein fraction of mammalian complex I, Biochemistry 30 (1991) 8678-84.

[5] X.M. Xu, A. Matsuno-Yagi and T. Yagi, The NADH-binding subunit of the energy-transducing NADH-ubiquinone oxidoreductase of *Paracoccus denitrificans*: gene cloning and deduced primary structure, Biochemistry 30 (1991) 6422-8.

[6] X. Xu, A. Matsuno-Yagi and T. Yagi, Gene cluster of the energy-transducing NADH-quinone oxidoreductase of *Paracoccus denitrificans*: characterization of four structural gene products, Biochemistry 31 (1992) 6925-32.

[7] T. Yano, T. Yagi, V.D. Sled and T. Ohnishi, Expression and characterization of the 66-kilodalton (NQO3) iron-sulfur subunit of the proton-translocating NADH-quinone oxidoreductase of *Paracoccus denitrificans*, J Biol Chem 270 (1995) 18264-70.

[8] M.C. Kao, S. Di Bernardo, A. Matsuno-Yagi and T. Yagi, Characterization of the membrane domain Nqo11 subunit of the proton-translocating NADH-quinone oxidoreductase of *Paracoccus denitrificans*, Biochemistry 41 (2002) 4377-84.

[9] M.C. Kao, S. Di Bernardo, A. Matsuno-Yagi and T. Yagi, Characterization and topology of the membrane domain Nqo10 subunit of the proton-translocating NADH-quinone oxidoreductase of *Paracoccus denitrificans*, Biochemistry 42 (2003) 4534-43.

[10] T. Yano, S. Magnitsky, V.D. Sled, T. Ohnishi and T. Yagi, Characterization of the putative 2x[4Fe-4S]-binding NQO9 subunit of the proton-translocating NADH-quinone oxidoreductase (NDH-1) of *Paracoccus denitrificans*. Expression, reconstitution, and EPR characterization, J Biol Chem 274 (1999) 28598-605.

[11] T. Yano and T. Yagi, H(+)-translocating NADH-quinone oxidoreductase (NDH-1) of *Paracoccus denitrificans*. Studies on topology and stoichiometry of the peripheral subunits, J Biol Chem 274 (1999) 28606-11.

[12] E.M. Meijer, H.W. van Verseveld, E.G. van der Beek and A.H. Stouthamer, Energy conservation during aerobic growth in *Paracoccus denitrificans*, Arch Microbiol 112 (1977) 25-34.

[13] H.W. van Verseveld, E.M. Meijer and A.H. Stouthamer, Energy conservation during nitrate respiration in *Paracoccus denitrificans*, Arch Microbiol 112 (1977) 17-23.

[14] P. John and F.R. Whatley, The bioenergetics of *Paracoccus denitrificans*, Biochim Biophys Acta 463 (1977) 129-53.

[15] J. Steuber, The C-terminally truncated NuoL subunit (ND5 homologue) of the Na^+-dependent complex I from *Escherichia coli* transports Na^+, J Biol Chem 278 (2003) 26817-22.

[16] J. Steuber, C. Schmid, M. Rufibach and P. Dimroth, Na^+ translocation by complex I (NADH:quinone oxidoreductase) of *Escherichia coli*, Mol Microbiol 35 (2000) 428-34.

[17] S. Stolpe and T. Friedrich, The *Escherichia coli* NADH:ubiquinone oxidoreductase (complex I) is a primary proton pump but may be capable of secondary sodium antiport, J Biol Chem 279 (2004) 18377-83.

[18] T. Pohl, J. Walter, S. Stolpe, J.H. Soufo, P.L. Grauman and T. Friedrich, Effects of the deletion of the *Escherichia coli* frataxin homologue CyaY on the respiratory NADH:ubiquinone oxidoreductase, BMC Biochem 8 (2007) 13.

[19] M.C. Kao, S. Di Bernardo, M. Perego, E. Nakamaru-Ogiso, A. Matsuno-Yagi and T. Yagi, Functional roles of four conserved charged residues in the membrane domain subunit NuoA of the proton-translocating NADH-quinone oxidoreductase from *Escherichia coli*, J Biol Chem 279 (2004) 32360-6.

[20] D. Flemming, P. Hellwig and T. Friedrich, Involvement of tyrosines 114 and 139 of subunit NuoB in the proton pathway around cluster N2 in *Escherichia coli* NADH:ubiquinone oxidoreductase, J Biol Chem 278 (2003) 3055-62.

[21] X. Gong, T. Xie, L. Yu, M. Hesterberg, D. Scheide, T. Friedrich and C.A. Yu, The ubiquinone-binding site in NADH:ubiquinone oxidoreductase from *Escherichia coli*, J Biol Chem 278 (2003) 25731-7.

[22] K. Matsushita, T. Ohnishi and H.R. Kaback, NADH-ubiquinone oxidoreductases of the *Escherichia coli* aerobic respiratory chain, Biochemistry 26 (1987) 7732-7.

[23] A.V. Bogachev, R.A. Murtazina and V.P. Skulachev, H^+/e^- stoichiometry for NADH dehydrogenase I and dimethyl sulfoxide reductase in anaerobically grown *Escherichia coli* cells, J Bacteriol 178 (1996) 6233-7.

[24] B. Ludwig, Terminal oxidases in *Paracoccus denitrificans*, Biochim Biophys Acta 1101 (1992) 195-7.
[25] C. Watters, A one-step biuret assay for protein in the presence of detergent, Anal Biochem 88 (1978) 695-8.
[26] D.P. Briskin and I. Reynolds-Niesman, Determination of H/ATP Stoichiometry for the Plasma Membrane H-ATPase from Red Beet (*Beta vulgaris* L.) Storage Tissue, Plant Physiol 95 (1991) 242-250.
[27] H.J. Apell and B. Bersch, Oxonol VI as an optical indicator for membrane potentials in lipid vesicles, Biochim Biophys Acta 903 (1987) 480-94.
[28] E. Damiano, M. Bassilana, J.L. Rigaud and G. Leblanc, Use of the pH sensitive fluorescence probe pyranine to monitor internal pH changes in *Escherichia coli* membrane vesicles, FEBS Lett 166 (1984) 120-4.
[29] T. Friedrich, Complex I: a chimaera of a redox and conformation-driven proton pump?, J Bioenerg Biomembr 33 (2001) 169-77.
[30] S. Kerscher, S. Drose, V. Zickermann and U. Brandt, The three families of respiratory NADH dehydrogenases, Results Probl Cell Differ 45 (2008) 185-222.
[31] T. Yagi, Bacterial NADH-quinone oxidoreductases, J Bioenerg Biomembr 23 (1991) 211-25.
[32] T. Yagi, Purification and characterization of NADH dehydrogenase complex from *Paracoccus denitrificans*, Arch Biochem Biophys 250 (1986) 302-11.
[33] A.S. Fernandes, F.L. Sousa, M. Teixeira and M.M. Pereira, Electron paramagnetic resonance studies of the iron-sulfur centers from complex I of *Rhodothermus marinus*, Biochemistry 45 (2006) 1002-8.
[34] A.S. Fernandes, M.M. Pereira and M. Teixeira, Purification and characterization of the complex I from the respiratory chain of *Rhodothermus marinus*, J Bioenerg Biomembr 34 (2002) 413-21.
[35] B. Soballe and R.K. Poole, Microbial ubiquinones: multiple roles in respiration, gene regulation and oxidative stress management, Microbiology 145 (Pt 8) (1999) 1817-30.
[36] A.M. Castle, R.M. Macnab and R.G. Shulman, Coupling between the sodium and proton gradients in respiring *Escherichia coli* cells measured by ^{23}Na and ^{31}P nuclear magnetic resonance, J Biol Chem 261 (1986) 7797-806.
[37] J.W. Pan and R.M. Macnab, Steady-state measurements of *Escherichia coli* sodium and proton potentials at alkaline pH support the hypothesis of electrogenic antiport, J Biol Chem 265 (1990) 9247-50.

PART III

CONCLUSIONS

Chapter 6

Final Discussion

Chapter 6: Final Discussion

6.1– ENERGY TRANSDUCTION BY RESPIRATORY COMPLEX I

In order to obtain a deeper insight into the overall function of respiratory complex I, the energy conservation mechanism of this enzyme from three different prokaryotic organisms (*R. marinus*, *E. coli* and *P. denitrificans*) was investigated. All the three enzymes have the typical features of canonical complexes I such as, a non-covalently bound flavin (FMN), a series of iron-sulfur centers and quinone reduction inhibited by specific complex I inhibitors and coupled to charge translocation across the membrane [1-5].

The main model system used in this work was *R. marinus* complex I which, as other bacterial complexes I, has a L-shaped structure and a total molecular mass of ≈ 550 kDa, compatible with the sum of the predicted molecular masses of the canonical 14 subunits *plus* an additional one (PCD). Previous studies performed on the *R. marinus* enzyme, reconstituted in liposomes, have shown that the NADH:quinone oxidoreductase activity was stimulated up to 54% in the presence of the protonophore CCCP [5]. This indicates that the energy release by the redox reaction was transduced to the form of $\Delta\tilde{\mu}_{X^{m+}}$, being the proton the coupling ion, which is in agreement with several studies performed in other bacterial and mitochondrial complexes I. Due to the presence of Mrp like subunits in the composition of complex I [6, 7], the proposal that sodium ion could be the coupling ion of this enzyme [8-11], and given that *R. marinus* is a halophile [12, 13], it could be hypothesized that complex I from this organism could also be capable of sodium translocation. Thus, sodium transport by *R. marinus* complex I was addressed and indeed it was observed that the enzyme is electrogenic involving the transport of protons and sodium ions. The coupling ion

between NADH:quinone oxidoreductase activity and the establishment of the $\Delta\tilde{\mu}_{X^{m+}}$ is the H^+, meaning that this ion is transported from the cytoplasm to the periplasm (positive side of the membrane). On the contrary, sodium ions are translocated from the periplasm to the cytoplasm. Since it was observed that sodium is not necessary for proton translocation but its presence increases the NADH-driven proton transport, it is proposed that *R. marinus* complex I performs energy transduction by two different processes (Figure 6.1, panel A), proton pumping (represented by *1*) and Na^+/H^+ antiporting (represented by *2*), suggesting the presence of two different energy coupling sites both coupled to menaquinone reduction.

It could be hypothesized that complex I has only one energy coupling site that works exclusively as a proton pump, in the absence of sodium ions, and as a Na^+/H^+ antiporter in the presence of this ion. However, this hypothesis was refuted by studies performed in the presence of a Na^+/H^+ antiporter inhibitor (EIPA). It was observed that, in the presence of sodium

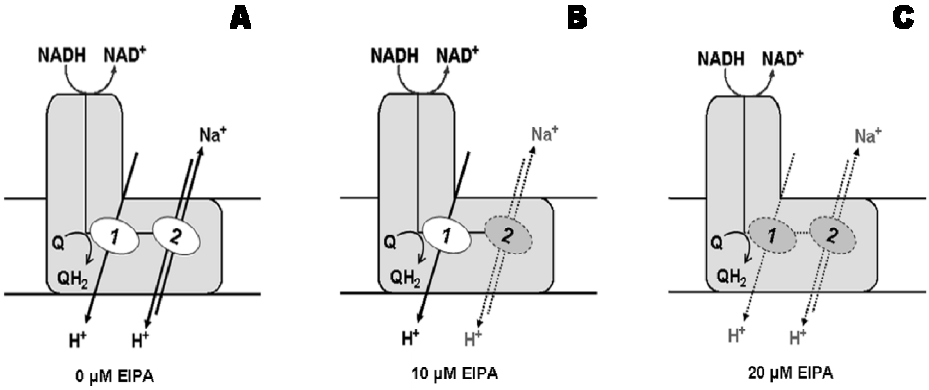

Figure 6.1 – Schematic representation of the proposed mechanism for *R. marinus* complex I, showing the two different energy transduction processes. *1*- Represents the proton pumping process. *2*- Represents the Na^+/H^+ antiporting process. Panels A to C show the different behavior of the two coupling sites in the presence of increased amounts of an antiporter inhibitor. Site *2* is affected in the presence of 10 µM of EIPA (Panel B) while site *1* is only affected at higher EIPA concentrations (Panel C).

ions, both H^+ and Na^+ transports are inhibited by EIPA but have different inhibition profiles, what excludes the existence of only one common transport site (Figure 6.1, panel B and C). Moreover, the H^+ transport had different inhibition behaviors in the presence and absence of Na^+, which reinforced the hypothesis for the presence of two H^+ translocating sites.

The presence of two types of energy conservation sites in complex I is since a long time proposed on the basis of the stoichiometry of 4 translocated H^+ per NADH and on amino acid sequence analysis. It has been assumed that the subunits homologous to hydrogenases (Nqo8) and to Mrp antiporters (Nqo12-14) would be responsible for the translocation process. The work described in this dissertation provides one of the strongest experimental evidences for the existence of such two coupling sites. In order to address whether these two different energy conservation sites can also be present in other complexes I and that the coupling mechanism proposed for the *R. marinus* enzyme can be further considered, the process of energy transduction of *E. coli* and *P. denitrificans* complexes I was also investigated. It was observed that the Na^+/H^+ antiport activity is not exclusive of *R. marinus*, since the *E. coli* enzyme is also capable of such a transport, but is not a general property given that the *P. denitrificans* enzyme does not performed sodium translocation.

The observation that the *E. coli* enzyme can also perform sodium transport completely excluded the possible participation of the Nha-type Na^+/H^+ antiporter which, although it was never identified as a *R. marinus* complex I subunit, could also be considered as a candidate for performing sodium translocation. The involvement of the so-called Mrp like subunits (Nqo 12-14) is currently the most attractive scenario. The fact that the over-expressed C-terminally truncated NuoL (Nqo12) subunit of the *E. coli* complex mediates sodium uptake when reconstituted into lipossomes [14]

corroborates the involvement of these subunits in the sodium transport process.

The presence of this Na^+/H^+ antiporter device operating on complex I may explain part of the controversy related with the nature of its coupling ion. Assuming that this module is able of changing its transports directionality, sodium ions could be transported to the positive side of the membrane contributing in this sense for the establishment of the $\Delta\tilde{\mu}_{X^{m+}}$.

The possibility of having two coupling ions instead of one may increase the robustness and adaptation of some organisms to different environments.

Other important aspects of this Na^+/H^+ antiporter module on the overall cell bioenergetics should be its Na^+/H^+ stoichiometry and the establishment of a sodium futile cycle. A simple exchange of 1 H^+ per 1 Na^+ would not contribute to an increase of the $\Delta\tilde{\mu}_{X^{m+}}$ but could benefit the ATP synthesis by ATP synthase if the latter is H^+-dependent. A sodium futile cycle could be established by sodium transport to the cytoplasm since this ion would be then transported on the opposite direction, most likely by the action of other antiporters. In fact, such a sodium futile cycle has been proposed before for *E. coli* cells, based on the observation of global H^+ and Na^+ transports [15, 16]. It cannot be anticipated whether this futile cycle will be energetically unfavorable. The overall process will depend on the different stoichiometries of the individual transporting processes, thus the overall energy yielding is a combination of multiple factors, and at the end the referred futile cycle may indeed contribute to energy conservation.

As mentioned above, Na^+/H^+ antiporting is not a characteristic of all complexes I. A possible explanation for the *R. marinus* and *E. coli* enzymes being able to transport sodium ions, whereas *P. denitrificans* complex I is not

can reside on the type of quinone used as substrate. *E. coli* and *R. marinus* complexes I reduce menaquinone ($E_{m,7}$≈ -80 mV), whereas complex I from *P. denitrificans* uses ubiquinone as substrate ($E_{m,7}$≈ +120 mV) [17]. Taking into consideration the reduction potential of NADH ($E_{m,7}$≈ -320 mV), the free energy obtained by NADH oxidation by menaquinone can be ~ 240 mV, whereas in the case of oxidation by ubiquinone the free energy obtained can be ~440 mV. These different ΔG´s clearly show that more energy can be transduced into the form of $\Delta\tilde{\mu}_{H^+}$ when the electron acceptor is ubiquinone, meaning that a higher H^+/2e stoichiometry is possible to be achieved with this type of quinone then using menaquinone. One thermodynamic explanation for a possible equal H^+/2e stoichiometry of menaquinone and ubiquinone reducing enzymes could invoke the use of a ΔpNa by menaquinone reducing enzymes in order to achieve that same stoichiometry.

Studies performed with *Methanosarcina mazei* complex I may support the suggestion that the different coupling efficiencies are related with the electron acceptor. It was observed that the complex I from this archaeon is capable of proton translocation exhibiting a maximum H^+/2e stoichiometry of 1.8 [18]. This stoichiometry is lower than the one suggested for bacterial and mitochondrial complexes I (H^+/2e ≈ 3 or 4) and a possible reason is the fact that the electron acceptor in this case is methanophenazine instead of ubiquinone or menaquinone. Assuming that the methanophenazine has a reduction potential of -255 mV and the $F_{420}H_2$ (electron donor of archaeal complexes I) has a reduction potential of -360 mV, the maximum free energy available is only ~ 105 mV compared with a ΔG of ~ 440 mV or of -240 mV for the NADH-dependent reduction of ubiquinone or menaquinone, which may explain the different coupling efficiencies of the enzymes.

In evolutionary terms, it was suggested that the menaquinone represents the ancestral type of quinone in bioenergetics systems and thus, the only type of quinone in early branching archaeal and bacterial phyla [19]. Therefore, menaquinone reducing complexes (as *E. coli* and *R. marinus*) may be considered ancestor enzymes. On the other hand, the ubiquinone reducing complexes (as *P. denitrificans* enzyme) belong to organisms located in the upper part of the Woese´s tree and their catalytic reaction became energetically more efficient. Thus, the ubiquinone reducing enzymes may have lost the need of ΔpNa to promote additional proton translocation and thus, transducing energy only by a proton pumping process.

In summary, it can be suggested that complexes I using ubiquinone as the electron acceptor, transduce energy only by a proton pumping process while those that use menaquinone transduce energy by proton pumping *plus* Na^+/H^+ antiporting (Figure 6.2). The additional Na^+ transport may occur in order to guaranty the high efficiency of complex I in the overall energy transduction process.

A deeper insight into the overall coupling mechanism of this respiratory enzyme was obtained by studying the influence of EIPA on the *R. marinus* complex I NADH:quinone oxidoreduction and on the H^+ and Na^+ transports. Interestingly, the catalytic and the two transports activities showed different inhibition profiles, being the transports inhibited at concentrations of EIPA at which the catalytic activity is not affected. This means that the activities can be completely decoupled and suggests the involvement of strictly indirect coupling mechanisms for complex I, possibly through conformational changes. This possibility is strongly supported by the recently solved structure of the entire complex I from *T. thermophilus* [20]. The structure suggest that 3 protons may be translocated by an indirect coupling

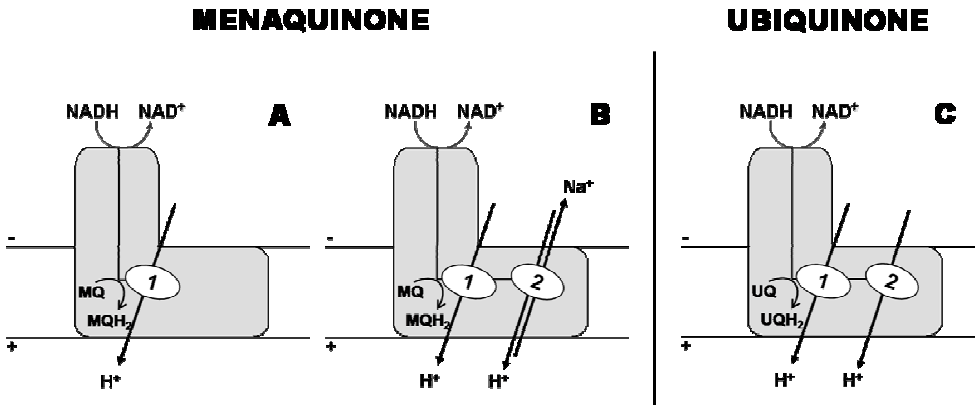

Figure 6.2 – Schematic representation of the possible mechanisms for complex I. Panels A and B represent the transducing process of complex I considering menaquinone as the electron acceptor. In the absence of Na^+ the enzyme is only a proton pump (Panel A) while in the presence of Na^+ transduces energy by proton pumping and Na^+/H^+ antiporting (Panel B). Panel C represents the coupling mechanism when ubiquinone is the electron acceptor (the mechanism is the same in the presence and absence of Na^+).

mechanism, involving conformational changes from near the quinone binding site (Nqo8 and Nqo7, 10 and 11) to the antiporter subunits (Nqo12-14), with the participation of a long amphipatic helix of the Nqo12 subunit, which spans almost the entire membrane domain [20]. In order to achieve the stoichiometry of $4H^+/2e$ an additional H^+ translocating site was considered, being the fourth proton suggested to be translocated at the interface of the peripheral and membrane domain (via the Nqo7, 10 and 11 or Nqo8) through a redox-driven mechanism, representing a direct coupling mechanism in which H^+ uptake would occur upon reduction of cluster N2 [21]. This proposal also suggested that the process for H^+ uptake would be the same for H^+ translocation and for quinone reduction. Such hypothesis is not compatible with the data obtained for complex I from *R. marinus* since the catalytic reaction and H^+ transport could be completely decoupled. Thus, our observations are a step forward showing that the coupling mechanism

operating at this site is also indirect. Supporting completely the experimental data reported in this dissertation, are the new structural data that do not exclude the possibility that the translocation of this fourth proton be also conformational driven[20].

To understand a conformation mechanism it is necessary to identify the precise trigger that drives the conformational change, the parts of the complex that transmit the conformational energy and the pumping devices. The latter two aspects can be mostly explained by the structure of complex I from *T. thermophilus*. However, the structure does not elucidate which redox component is directly involved in the coupling process. The electron transfer between NADH and the center N2 occurs with an apparent time constant of ≈ 90 μs and is unlikely to be coupled to other reactions [22]. The direct involvement of the center N2 is also unlikely, not only because its role on the translocation process due to its redox-Bohr proprieties could be excluded [23] but also due to its distance of 20-25 Å from the surface of lipid bilayer [20]. This means that most likely quinone reduction provides an essential contribution for trigger the pump. This corroborates the hypothesis that the existence of distinct mechanisms for complex I charge translocation may be correlated with the type of quinone used as substrate.

A respiratory enzyme working exclusively by an indirect mechanism is not a unique characteristic of complex I since it is for long assumed that ATP synthase works also by such a mechanism. Interestingly, "ATP synthase has been compared to a turbine while complex I is now compared with a steam engine, where the energy of the electron transfer is used to move a piston, which then drives, instead of wheels, a set of discontinuous helices" [20].

6.2– FINAL REMARKS

In summary, the results presented in this work allowed to elucidate some important mechanistic aspects of respiratory complex I, namely the observation that this enzyme performs energy transduction by indirect coupling mechanisms. It enables also the comparison of two distinct types of charge translocation mechanisms operating in complex I, proton pumping and Na^+/H^+ antiporting, being the latter type not a general property of the enzyme. It is suggested that the Na^+/H^+ antiport activity may be correlated with the type of quinone used as substrate.

6.3 – REFERENCES

[1] J. Torres-Bacete, E. Nakamaru-Ogiso, A. Matsuno-Yagi and T. Yagi, Characterization of the NuoM (ND4) subunit in *Escherichia coli* NDH-1: conserved charged residues essential for energy-coupled activities, J Biol Chem 282 (2007) 36914-22.

[2] S. Stolpe and T. Friedrich, The *Escherichia coli* NADH:ubiquinone oxidoreductase (complex I) is a primary proton pump but may be capable of secondary sodium antiport, J Biol Chem 279 (2004) 18377-83.

[3] A.S. Fernandes, F.L. Sousa, M. Teixeira and M.M. Pereira, Electron paramagnetic resonance studies of the iron-sulfur centers from complex I of *Rhodothermus marinus*, Biochemistry 45 (2006) 1002-8.

[4] K. Matsushita, T. Ohnishi and H.R. Kaback, NADH-ubiquinone oxidoreductases of the *Escherichia coli* aerobic respiratory chain, Biochemistry 26 (1987) 7732-7.

[5] A.S. Fernandes, M.M. Pereira and M. Teixeira, Purification and characterization of the complex I from the respiratory chain of *Rhodothermus marinus*, J Bioenerg Biomembr 34 (2002) 413-21.

[6] C. Mathiesen and C. Hagerhall, Transmembrane topology of the NuoL, M and N subunits of NADH:quinone oxidoreductase and their homologues among membrane-bound hydrogenases and bona fide antiporters, Biochim Biophys Acta 1556 (2002) 121-32.

[7] C. Mathiesen and C. Hagerhall, The 'antiporter module' of respiratory chain complex I includes the MrpC/NuoK subunit -- a revision of the modular evolution scheme, FEBS Lett 549 (2003) 7-13.

[8] A.C. Gemperli, P. Dimroth and J. Steuber, The respiratory complex I (NDH I) from *Klebsiella pneumoniae*, a sodium pump, J Biol Chem 277 (2002) 33811-7.

[9] W. Krebs, J. Steuber, A.C. Gemperli and P. Dimroth, Na^+ translocation by the NADH:ubiquinone oxidoreductase (complex I) from *Klebsiella pneumoniae*, Mol Microbiol 33 (1999) 590-8.

[10] P.C. Lin, A. Puhar and J. Steuber, NADH oxidation drives respiratory Na^+ transport in mitochondria from *Yarrowia lipolytica*, Arch Microbiol 190 (2008) 471-80.

[11] J. Steuber, C. Schmid, M. Rufibach and P. Dimroth, Na^+ translocation by complex I (NADH:quinone oxidoreductase) of *Escherichia coli*, Mol Microbiol 35 (2000) 428-34.

[12] G.A. Alfredsson, J.K. Kristjansson, S. Hjorleifsdottir and K.O. Steiter, *Rhodothermus marinus*, gen. nov., sp. nov., a Thermophilic, Halophilic Bacterium from Submarine Hot Springs in Iceland, J of Gen Microbiol 134 (1988) 299-306.

[13] M.M. Pereira, A.M. Antunes, O.C. Nunes, M.S. da Costa and M. Teixeira, A membrane-bound HIPIP type center in the thermohalophile *Rhodothermus marinus*, FEBS Lett 352 (1994) 327-30.

[14] J. Steuber, The C-terminally truncated NuoL subunit (ND5 homologue) of the Na^+-dependent complex I from *Escherichia coli* transports Na^+, J Biol Chem 278 (2003) 26817-22.

[15] A.M. Castle, R.M. Macnab and R.G. Shulman, Coupling between the sodium and proton gradients in respiring *Escherichia coli* cells measured by ^{23}Na and ^{31}P nuclear magnetic resonance, J Biol Chem 261 (1986) 7797-806.

[16] J.W. Pan and R.M. Macnab, Steady-state measurements of *Escherichia coli* sodium and proton potentials at alkaline pH support the hypothesis of electrogenic antiport, J Biol Chem 265 (1990) 9247-50.

[17] B. Soballe and R.K. Poole, Microbial ubiquinones: multiple roles in respiration, gene regulation and oxidative stress management, Microbiology 145 (Pt 8) (1999) 1817-30.

[18] S. Baumer, T. Ide, C. Jacobi, A. Johann, G. Gottschalk and U. Deppenmeier, The $F_{420}H_2$ dehydrogenase from *Methanosarcina mazei* is a Redox-driven proton pump closely related to NADH dehydrogenases, J Biol Chem 275 (2000) 17968-73.

[19] B. Schoepp-Cothenet, C. Lieutaud, F. Baymann, A. Vermeglio, T. Friedrich, D.M. Kramer and W. Nitschke, Menaquinone as pool quinone in a purple bacterium, Proc Natl Acad Sci U S A 106 (2009) 8549-54.

[20] R.G. Efremov, R. Baradaran and L.A. Sazanov, The architecture of respiratory complex I, Nature 465 (2010) 441-5.

[21] J.M. Berrisford and L.A. Sazanov, Structural basis for the mechanism of respiratory complex I, J Biol Chem 284 (2009) 29773-83.

[22] M.L. Verkhovskaya, N. Belevich, L. Euro, M. Wikstrom and M.I. Verkhovsky, Real-time electron transfer in respiratory complex I, Proc Natl Acad Sci U S A 105 (2008) 3763-7.

[23] K. Zwicker, A. Galkin, S. Drose, L. Grgic, S. Kerscher and U. Brandt, The Redox-Bohr group associated with iron-sulfur cluster N2 of complex I, J Biol Chem 281 (2006) 23013-7.